Department of Chemical Engineering

Division of Science and Engineering

Crystallisation and Dissolution Studies of Struvite in Aqueous Solutions

Eko Ariyanto

This thesis is presented for the Degree of
Doctor of Philosophy
of
Curtin University

October, 2013

DECLARATION

To the best of my knowledge and belief this thesis contains no material previously published by any other person except where due acknowledgment has been made.

This thesis contains no material which has been accepted for the award of any other degree or diploma in any university.

Signature : ……..

Date : ……..……...

ACNOWLDGEMENTS

I would like to express my sincere gratitude and indebtedness to a number of people who have contributed to this work. I am particulary grateful to my supervisor: Professor Ming Ang and DR. Tushar Kanti Sen for their tremendous support, encouragement and inspiring guidance throughout the course of this project.

My appreciation also goes to:

1. The analytical laboratory staff at the Department of Chemical Engineering, especially Mrs Karen Haynes, Ms Ann Carrol and Mr Jason Wright for their help.
2. The analytical laboratory staff at Curtin Centre for Advanced Energy Science and Engineering (CCAESE), especially Ms Angelina Jane Rossiter, for setting up the solubility rig, helping me with pump problems and teaching me to use microscope.
3. Thanks to DR. Alf Larcher from the Curtin Centre for Advanced Energy Science and Engineering (CCAESE) for help in TGA work
4. The staff at the Applied Physics Department, especially Elaine Miller, for help in SEM work
5. The administrative staff and postgraduates at the Department of Chemical Engineering for the co-operation and friendship.
6. Directorate Higher Education of Indonesia (DIKTI) for financial support of my project
7. Last but not least, special thanks to my wife Denilah, my son Ahamd Alif Muflih and my parents for their love, support and encouragement and unconditional sacrifices.

PUBLICATION

Journal Papers

Eko Ariyanto, H. M. Ang, Tushar Kanti Sen. (2013), Impact of various physico-chemical parameters on spontaneous nucleation of struvite (MgNH4PO4.6H2O) formation in a wastewater treatment plant: kinetic and nucleation mechanism, *Desalination and Water Treatment* (accepted for publication)

Eko Ariyanto, Tushar Kanti Sen, Ha Ming Ang (2013), The influence of various physico-chemical process parameters on kinetics and growth mechanism of struvite crystallisation in wastewater treatment plant, *Advanced Powder Technology* (accepted for publication)

Eko Ariyanto, Ha-Ming Ang, Tushar Kanti Sen, (2013), Effect of Various Process Parameters on the Dissolution Kinetics of Struvite Crystals Formation, (Submitted and under review in *Korean Journal of Chemical Engineering*)

Conference Papers

E. Ariyanto, H. M. Ang, and T. K. Sen. (2011), *Effect of initial solution pH on solubility and morphology of struvite crystals*, paper presented at CHEMECA Conference, Sep 18-21 2011. Sydney: Australia

Eko Ariyanto, H. M. Ang, Tushar Kanti Sen. (2012), *Effect of Agitation on the Metastable Zone, Nucleation and Growth of Struvite Crystals in a Batch Crystallizer*, paper presented at 19th Regional Symposium of Chemical Engineering RSCE 2012, *November 7-8, 2012*, Bali, Indonesia

Eko Ariyanto, H. M. Ang, Tushar Kanti Sen. (2012), *Effect of NaCl and Seed Crystal on Induction Time for Struvite Precipitation*, paper presented at 19th Regional Symposium of Chemical Engineering RSCE 2012, *November 7-8, 2012*, Bali, Indonesia

ABSTRACT

Magnesium, ammonium and phosphate ions are present during anaerobic digestion of sewage sludge and also during dewatering operations. Under certain conditions, these dissolved wastewater constituents can combine to form struvite. In response to struvite formation problems in wastewater treatment plants (WWTP), this kinetic study of struvite ($MgNH_4PO_4.6H_2O$) crystallisation was undertaken to provide a comprehensive understanding of the process and thereby will assist in better control of struvite in wastewater treatment plants.

The solubility of struvite was determined at different initial solution pH, temperature and in the presence of chloride salt solutions (NaCl, KCl, and $CaCl_2$). The solubility of struvite decreases slightly with increase in initial solution pH from 3 to 7 while solubility of struvite increases with increasing solution from pH 9 – 11. The solubility of struvite reached a minimum point at initial solution pH 7 – 9. The minimum Ksp value was found to range 2.89×10^{-13} – 3.26×10^{-13} at pH 7 – 9. The effect of temperature on solubility of struvite between 20 – 50^{O}C showed that increasing Ksp value was found between 20 – 35^{O}C. The Ksp value decreased subsequently with increase in temperature 35 – 50^{O}C. Maximum solubility occurred at 35^{O}C with K_{SP} 7.99×10^{-13}. A phase transition occurred at 35^{O}C. Based on the K_{SP} value and temperature, the dissolution energy of struvite crystal was found to be 100.9 kJ/mol in temperature range of 35 – 50^{O}C and 85.5 kJ/mol for temperature range of 20 – 35^{O}C. The solubility of struvite was determined in the presence of excess chloride salt (KCl, NaCl and $CaCl_2$) solutions at 25^{O}C and pH 7. It was observed that solubility, in pure water and in aqueous chloride salts solution, increased with increase in chloride salt concentrations. The standard molar Gibbs energies of transfer of struvite from pure water to the chloride salts solution have been calculated from the solubility data. The chloride salts effect can be correlated to a ΔG decreasing order at 25^{O}C, i.e., KCl > NaCl > $CaCl_2$. A study was also made to investigate how the morphology of the struvite crystals was affected when they were exposed to solutions at different initial pH values. The original struvite crystals and other residual crystals after the solubility test were examined by both SEM and EDS. It

was found that the shapes of crystals were amorphous, rhombohedral, and hexagonal for initial pH 3, 7, and 11, respectively and for pH 5 and 9 platelets and spherical resulted, respectively.

The effect of various physico-chemical parameters such as supersaturation, temperature, pH and presence of foreign ion on the nucleation of struvite formation were studied experimentally. Mechanism of nucleation kinetics of struvite ($MgNH_4PO_4.6H_2O$) formation has been identified by thermodynamic parameters study. The time taken for nucleation to occur (often indicated by the induction time) is a measure of struvite nucleation. It was found that induction time decreased with an increase in supersaturation, temperature, pH but increased with presence of excess chloride (Cl^-) ion. Interfacial energy of two nucleation mechanisms ($\gamma_{s,hom}$ and $\gamma_{s,het}$), homogeneous and heterogeneous, increased with an increase in solution pH for all temperatures whereas interfacial energy of crystals increased with decrease in temperature. Thermodynamic parameters such as activation energy and interfacial energy were calculated based on rate of nucleation for both homogeneous and heterogeneous crystallisation. The activation energy for struvite nucleation was calculated as 30.1 $kJ.mol^{-1}$ and 24.9 $kJ.mol^{-1}$ at pH 8 and 8.5, respectively. The activation energies in the presence of NaCl and KCl were higher (64.5 and 51.7 kJ/mol, respectively) at pH 8. The interfacial energy between struvite crystals and supersaturated solution decreased with increase in pH but increased in the presence of either NaCl or KCl.

Struvite crystal growth kinetics were studied under different physico-chemical process parameters such as supersaturation ($Mg^{2+}, NH_4^+, PO_4^{3-}$), solution pH, stirrer speed, temperature, impurities and presence of seeds. To measure the growth rate of struvite crystals and to identify its various dependencies on system parameters, laboratory measurements were conducted in an isothermal batch 1 L stirred seeded crystalliser.

The pseudo-first and pseudo-second order kinetic models were employed to analyse the rate of decay of supersaturation data of solution pH, temperature and stirrer speed and much useful kinetic information are revealed. The experimental results agreed with the first-order kinetic model prediction. The obtained rate constant, *k*, can be used to explain the struvite precipitation behaviour.

Supersaturation and pH were found to be most influential parameters for struvite crystallisation. The rate of change of supersaturation in the bulk solution increases with increasing supersaturation. It was also found that growth rate increased with an increase in solution pH in the pH range of 8 to 9. The fitted rate constants (k_1) for first-order kinetic model were 3.0, 4.3 and 5.8 hr^{-1} for a solution pH of 8.0, 8.5 and 9.0, respectively. The increasing stirred speeds influenced growth rate of struvite crystal. The rate constants resulting from different stirrer speeds at supersaturation 2.04 are 2.6, 3.7 and 5.8 h^{-1} for 50, 100, and 120 rpm, respectively. The constants, K_G and K_L increased with higher stirrer speed. The growth rate increased with increase in temperature. The growth rate constant increased between 2×10^{-9} and 5.2×10^{-9} m/s with increase in temperature from 20 to 30^{O}C. The value of activation energy of growth of struvite crystals of 55.42 $kJ.mol^{-1}$ were obtained by fitting the data to the Arrhenius equation. The presence of impurities (NaCl) in the solution was also investigated on growth of struvite crystal. It was found that NaCl addition in a system can have a significant effect on the growth of struvite crystals. The growth constant (K_G) and overall mass transfer coefficient (K_L) increased with increasing NaCl addition. However, at NaCl concentration exceeding 100 ppm, the growth rate of struvite remained constant.

The dissolution kinetics of struvite crystals ($MgNH_4PO_4.6H_2O$) in deionized water was investigated in a batch crystallizer. The effects of stirrer speeds, temperature and crystals size on the dissolution rate were determined. The results showed an increase of struvite dissolution rate with increasing stirring speed. Struvite dissolution occurred via a diffusion-controlled mechanism in the range of stirrer speeds 120 – 400 rpm but became interfacial-reaction-controlling at over 400 rpm. The influence of temperature on dissolution kinetic of struvite crystals was investigated at stirrer speeds of 200 and 500 rpm. The overall mass transfer coefficient increased from 1.6×10^{-5} to 5.4×10^{-5}m/s with increase in stirrer speeds 120 – 400 rpm and remained relatively constant above 400 rpm. The dissolution rates increased with an increase in the temperature for both stirrer speeds (200 and 500 rpm). The activation energies derived from these curves were found as 17.92 kJ/mol and 54.56 kJ/mol for the stirrer speed of 200 and 500 rpm,

respectively. The change in activation energies as a function of stirrer speeds confirms the change of dissolution mechanism from a diffusion-controlled mechanism under low stirrer speeds to an interfacial-reaction-controlled mechanism at higher stirrer speeds. The dissolution rate of struvite crystals increased with smaller crystal sizes. The values of volumetric mass transfer coefficient ($K_L a$) are given as follows; 3.0×10^{-3}, 2.3×10^{-3} and $2.0 \times 10^{-3}$for initial size of 24.3, 43.5, and 84.5 μm, respectively. The values of $K_L a$ decreased with increase in crystal size, indicating that smaller crystals dissolve more rapidly than large crystals. However, the K_L values are almost the same within a margin of error of 2 %. This result indicates that the rate of dissolution of struvite from the crystal surface does not depend on the size of crystals, at least for those crystals with L in the range from 24 to 85 μm.

TABLE OF CONTENTS

LIST OF FIGURES

LIST OF TABLES

CHAPTER 1
INTRODUCTION

1.1 Background Information

Crystallization is an important unit operation in chemical industries for separating mixture or solution by forming solids with the desired physical properties. The applications of crystallization techniques are used in a wide range of industries such as pharmaceuticals, fertilizers, catalysts, sugar, and specialty chemicals. The definition of crystallization is a phase change in which a crystalline product is obtained from a solution. In general, crystalline product from solution can be produced through a two-step process. The first step is the nucleation process in which birth of new crystals appears in the solution, and the crystals grow to larger crystals as a second-step process. The second-step of crystal growth process can be simply produced in a supersaturated solution in which seed crystals are placed, and the solution will eventually reach equilibrium. The decreasing concentration mechanism of the solution reaching the equilibrium point can be quantitatively calculated based on the rate of crystallisation kinetics. Crystallization kinetics is the fundamental information which governs the performance of a crystallization process, together with the governing conservation laws of mass, energy, and population balance (Nývlt, 1992)

Crystallisation involves the separation of a solid component from a homogeneous liquid or gas phase. However, in most system of interest it is the separation of a soluble salt from its aqueous solution. Typically, the term solution has come to mean a liquid, and a solute, which is the dissolve solid, at the condition of interest. The solution for crystallisation must be supersaturated. A solution in which the solute concentration exceeds the equilibrium (saturated) solute concentration at a given temperature is known as a supersaturated solution. An appreciable supersaturated solution may be achieved for many solutions by proper manipulation of operating conditions. There are four main methods to generate supersaturation in solution (Myerson, 2002):

1. Temperature change
2. Evaporation of solvent
3. Chemical reaction
4. Changing the solvent composition.

A solute dissolves in solution until a sufficiently high level of supersaturation has been developed to induce spontaneous nucleation. The extent of this supersaturation is referred to as the metastable zone width. The metastable zone width depends on many process parameters such as temperature, rate of supersaturation generation, impurities, mixing, and solution history (Nyvlt et al., 1985).

The method of generating supersaturation through chemical reaction is called precipitation. In this case, two or more reactants are added together to form a solid product insoluble in the reaction mixture. For a compound with a very high solubility, it is possible to create a high supersaturation with chemical reaction methods (Giulietti et al., 2001). Moreover, concentration of reactants can be varied to obtain any desirable supersaturation and manipulating the pH may also create the same outcome (Myerson, 2002). Crystalline produced by chemical reaction methods can generally be controlled for increasing crystal size, shape, yield and purity with lower energy consumption compared to either evaporation or cooling methods. The shape and size of crystals often are influenced by both growth and nucleation processes interacting in a crystallizer. Control of the quality and physical form of the product is primarily concerned with control of the crystal size distribution (CSD). A good quality of CSD can be influenced by properties of the solution and operating mode such as supersaturation, temperature, impurities, ionic strength, pH and stirrer speed (Mullin, 2001).

Reactive crystallisation is often called a "precipitation" process because it is a combination of both crystallisation and chemical reaction mechanisms. The driving force for reactive crystallisation is different from traditional crystallisation. In a reactive crystallisation, supersaturation is caused not only by changes to the physical properties of a solution, but it is also influenced by a chemical reaction between two soluble components leading to a less soluble

product which then crystallises. Reactive crystallisation is more difficult to study than classical crystallisation because the crystal generation depends on various factors, all of which have their own kinetics, such as chemical reaction kinetics, crystallisation kinetics, and mixing mechanisms.

1.2 Research Direction and Overall Objectives

Magnesium, ammonium, and phosphate ions are released as the result of solids degradation in an anaerobic digestion of wastewater treatment plant. Under certain physico-chemical conditions, these dissolved wastewater constituents can combine to form struvite which causes scale deposition on pipe walls, pump and equipment surfaces of anaerobic digestion and post-digestion processes. The blockage of pipes leads to an increase of pumping cost and also reduces plant capacity. It is not only pipes that are affected by struvite deposits, centrifuges, pumps, heat exchanger and aerators are also prone to fouling by struvite. Due to a problem to eliminate or inhibit struvite formation (Doyle and Parsons, 2002), struvite also offers itself as a fertilizer which encourages wastewater treatment companies to study its possible recovery (Le Corre et al., 2007). Predicting struvite precipitation potential is critical to designer and operators for anticipating potential struvite formation. Struvite precipitation can be separated into two basic stages: nucleation and growth. Nucleation occurs when ions combine to form crystal embryos that can act as the foundation for growth into detectable crystals (Ohlinger et al., 1999). Crystal growth continues until equilibrium is reached (Doyle and Parsons, 2002). Predicting and controlling of these two stages are complex as they are controlled by a combination of factors including thermodynamics of liquid-solid equilibrium, phenomena of mass transfer between solid and liquid phases and kinetics of reaction (Myerson, 2002). There are also various physico-chemical parameters such as solution pH, supersaturation (i.e. combined concentrations of Mg^{2+}, NH_4^+, and PO_4^{3-} exceeding the struvite solubility limit), temperature, interfacial energy, agitation energy and presence of other interfering ions (Uludag-Demirer et al., 2005, Ohlinger et al., 1998, Le Corre et al., 2005, Bhuiyan et al., 2008) strongly influence the mechanism of crystal nucleation of struvite. Increases in temperature or supersaturation, or a

decrease in the interfacial energy are expected to produce an increased nucleation rate (Mullin, 2001, Judge et al., 1999). For those reasons, it has become important to study the principles of solubility, nucleation, growth and dissolution of struvite crystal to assess the various controlling physico-chemical parameters on struvite crystallisation.

1.3 Thesis Overview

This thesis contains eight chapters, in which the four chapters of the experimental work are successively presented in Chapters 4 to 7. Each chapter opens with a brief introduction section which conveys the motivation and structure of individual chapters. The main points and findings are captured in a summary section at the end of each chapter.

Chapter 1: Introduction

In this chapter the background and purpose of the present study, the contribution of previous researchers in this area of research, the presence state of knowledge about the study topic, and the sequence of approach taken for this study are all discussed.

Chapter 2: Literature review

This chapter describes the general background of this study including the basic processes of struvite crystallization, such as the mechanism of nucleation, crystal growth and solubility of crystals. The discussion of this chapter starts with the fundamental theory of crystallization in solution, the effect of solution pH, the effect of foreign ions, the effect of temperature on the nucleation and crystal growth. A detailed description of solubility, nucleation and growth of struvite is clearly described in this chapter.

Chapter 3: Experimental studies of struvite solubility, nucleation, growth, and dissolution in aqueous solution

To reduce the errors in the results from crystallization experiment, accurate, and reliable analytical techniques must be established. The various analytical

laboratory techniques adopted in this study are detailed in this chapter. The details of the experiment studies are presented, which includes the preparation of the crystallising solutions and seed preparation, followed by techniques employed the determining the solution concentration and particle size distribution.

Chapter 4: Effect of initial solution pH, temperature and salts on solubility of struvite crystals

This chapter discusses systematically some of the research data on the solubility of struvite crystals. This study investigates some valuable issues on solubility of struvite, such as the effect of initial solution pH, temperature, and foreign ions. The effect of initial solution pH is investigated in detail on crystal morphology. The results show that the initial solution pH can affect a change in crystal morphology, which is not available in the literature.

Chapter 5: Impact of various physico-chemical parameters on spontaneous nucleation of struvite ($MgNH_4PO_4.6H_2O$) in water: kinetics and nucleation mechanism

This chapter demonstrates the operation of the batch crystallization system. Batch crystallization system is used to observe nucleation of struvite crystals. This study was undertaken to estimate nucleation rate parameters of struvite formation in a stirred batch crystalliser while examining the influence of pH, temperature, supersaturation, and salt (NaCl and KCl) impurities on nucleation. From the experimental results, the activation and interfacial energies during struvite formation could be determined so that a better understanding of the phenomenon can be obtained.

Chapter 6: The influence of various physico-chemical process parameters on struvite crystallization in water: crystal growth kinetics

This chapter demonstrates the operation of the batch crystallization system. Batch crystallization system is used to observe metastable zone width and growth of struvite crystals. Observation of metastable zone width uses three variable hydrodynamic condition (50, 100 and 200 rpm). Furthermore, a detailed study on

the effect of hydrodynamic condition on kinetics and growth of struvite crystals are discussed in this chapter. The effect of foreign ions, pH and temperature on the growth of crystals are also studied and discussed in this chapter. This chapter also describes in detail the effect of temperature, supersaturation, NaCl addition and pH on growth study. From this growth study, the activation energy of struvite crystals is calculated.

Chapter 7: Effect of various process parameters on the dissolution kinetics of struvite crystals in wastewater treatment plant

This chapter demonstrate the operation of the batch crystallisation system. This chapter focus on the dissolution kinetics of struvite crystals in deionized water (pH 7). An analytical equation describing the relationship between the solute concentration and the dissolution time was obtained. Therefore, this study was attempted to explore the effect of stirrer speeds, temperature and crystal size on the struvite dissolution. Moreover, activation energies from either diffusion-controlled or interfacial-reaction-controlled were accounted by using dissolution rate equations.

Chapter 8: Conclusions and recommendations

In this Chapter, the conclusions from this research study, the practical implication from the results and the recommendations for future directions for research in this area are summarised.

CHAPTER 2
LITERATURE REVIEW

2.1 Introduction

This chapter provides a brief literature review relevant to this study. It includes some of the theoretical aspects of crystallisation including basic crystallisation, solubility, crystal growth mechanisms, effect of impurities on nucleation and growth, and a review on struvite crystals growth rate, nucleation and dissolution available in the literature.

The chapter ends with a conclusion section, which captures the essence and gaps of the literature review resulting in the proposed study.

2.2 Fundamentals of Crystallisation from Solution

Crystallisation from solution is widely utilized in the chemical and process industry (Jancic and Grootscholten, 1984, Söhnel and Garside, 1992). Crystallisation techniques are widely employed in the separation and purification of solid to produce a variety of materials of high purity at low cost (De Jong, 1984, Myerson and Toyokura, 1990). A crystallisation process, furthermore, results in a particulate product which is usually easy to handle, store, transport and apply. Crystals are produced in varying sizes ranging from as small as a few tens nanometres to several millimetres or more, both as discrete particles and as structured agglomerates. Crystallisation products include bulk and fine chemicals and their intermediates, such as sugar, sodium chloride, sodium carbonate, zeolite catalysts, adsorbents, detergents, fertilizers, pharmaceuticals and pigments (Jones, 2002).

Crystallisation from supersaturated solution can be considered as a two-step process, namely nucleation and crystal growth. Nucleation is the formation of the solid phase or “birth” of new crystals and crystal growth is the growth of the crystallisation phase into larger sizes. These two processes continue to occur simultaneously only if the solution is supersaturated; hence the rate of nucleation and growth is governed by the level of supersaturation. The following sections will discuss the supersaturation and the crystallisation kinetics in detail.

2.3 Solubility and Supersaturation

Crystallisation may be defined as a phase change in which a crystalline product is obtained from a solution. Crystallisation occurs through two basic steps, namely formation of nuclei and growth of crystals. A solution is a mixture of two or more species that form a homogeneous single liquid phase.

Three characteristics of solutions in crystallisation are saturated, supersaturated, and undersaturated solution. The solution that attains constant concentration after prolonged contact with the solid solute in a system which is at constant temperature or pressure is called a saturated solution. Saturated solution can be represented by curve D – G called solubility curve in Figure 2.1 and for the majority of cases solubility increases with increasing temperature. For some solutes, their solubilities can also decrease with increasing temperature (Myerson, 2002). If a solution is capable of dissolving more solids it is considered to be undersaturated with respect to that solute. Such solutions are represented in Figure 2.1 by the area below the solubility curve.

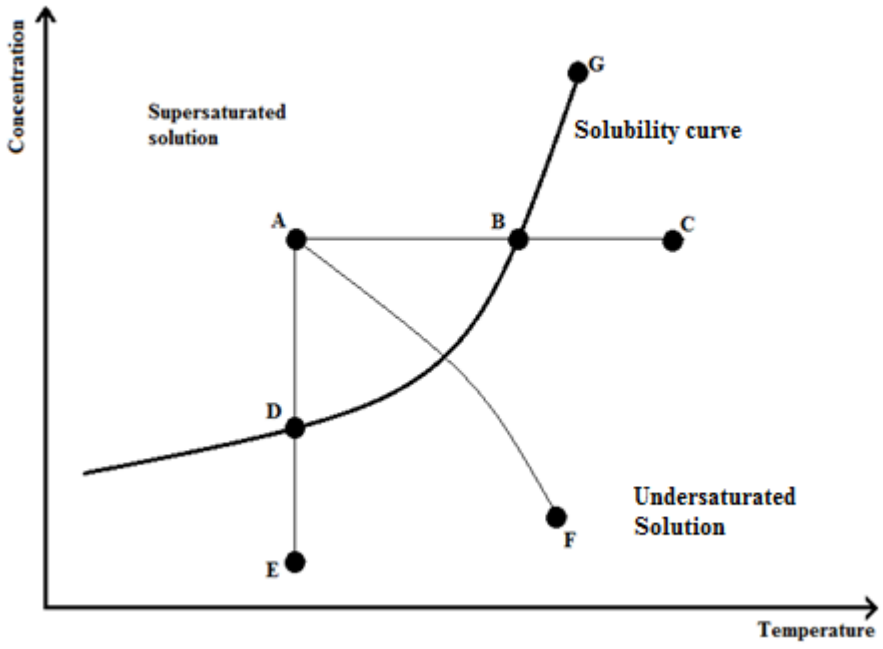

Figure 2.1 Solubility curve for a typical substance

If the solution happens to contain solute in excess of that prescribed by the equilibrium condition, then the solution is supersaturated and it can be represented by point A in Figure 2.1. Such a solution may adjust to its equilibrium value by

releasing the excess solute partly through the deposition on crystals that are already formed, and partly through the formation of new crystals. The level of supersaturation may be expressed in term of temperature, by the difference between A and B, or in term of concentration, by difference between A and D. The supersaturation, A, as indicated in Figure 2.1, can be achieved by cooling the solution at constant composition along CA; or by concentrating the solution by isothermal evaporation along EA. The intermediate path FA corresponds to adiabatic evaporation.

2.3.1 Solubility

Solubility is a measure of the amount of a solid chemical substance called solute that dissolves in a liquid to form a homogeneous solution of the solute in the solvent at a certain temperature. The solubility of a substance fundamentally depends on the solvent as well as on temperature and pressure. The extent of the solubility of a substance in a specific solvent is measured as the saturation concentration, where adding more solute does not increase the concentration of the solution.

The solubility is measured in terms of concentration of ion that is present in a smaller ratio in solution. On the other hand, solubility equilibrium refers to the equilibrium between the dissolved salt (ions) and undissolved salt that usually exists in a saturated solution or a solution of a sparingly soluble salt. The solubility of a sparingly soluble electrolyte in water is called solubility product. The solute (i.e; M_xA_y) dissolves in the solvent and dissociates into cations (M^{z+}) and anions (A^{z-}) according to the reaction,

$$\boldsymbol{M_xA_y \rightleftharpoons xM^{z+} + yA^{z-}} \quad (2.1)$$

where z^+ and z^- are the valencies of the ions.

So, solubility product in term of concentration is

$$\boldsymbol{K_c = [M^{z+}]^x.[A^{z-}]^y} \quad (2.1)$$

And the solubility product in term of ion activity can be written as follows;

$$\boldsymbol{K_{sp} = \gamma_{M^{z+}}[M^{z+}]^x.\gamma_{A^{z-}}[A^{z-}]^y} \quad (2.2)$$

Therefore,

$$\boldsymbol{\prod_{i=1}^{n}\gamma_i = \frac{K_{sp}}{K_c}} \quad (2.3)$$

2.3.2 Supersaturation

Supersaturation is the key variable in any crystallisation. The supersaturation evaluated in term of solution concentration influences the kinetic rate of crystallisation. The kinetic rate of crystal growth and nucleation depends on the thermodynamic driving force for transferring solute in the supersaturated solution (state 1) to the crystalline form (state 2) (Loehe and Donohue, 1997). The difference between the chemical potential of the given substance in the transferring and transferred states can be written as follows;

$$\Delta\boldsymbol{\mu} = \boldsymbol{\mu_1} - \boldsymbol{\mu_2} \tag{2.4}$$

where $\mu_1$is chemical potential in solution, $\mu_2$is chemical potential in the crystal

The chemical potential, μ, is defined in terms of the standard potential, μ_0, and the activity, a, by

$$\Delta\boldsymbol{\mu} = \boldsymbol{\mu_0} + \boldsymbol{RT}\ln\boldsymbol{a} \tag{2.5}$$

where *R* is the gas constant and *T* is the absolute temperature.

The fundamental dimensionless driving force for crystallisation may therefore be expressed as

$$\frac{\Delta\boldsymbol{\mu}}{\boldsymbol{RT}} = \ln\left(\frac{\boldsymbol{a}}{\boldsymbol{a^*}}\right) = \ln\boldsymbol{S} \tag{2.6}$$

Where a^* is the activity of a saturated solution and S is the fundamental supersaturation.

Since the solute activity is somewhat difficult to measure, concentration can be used. Supersaturation in term of concentration is defined as a difference between the concentration c of a supersaturated solution and c^*, the concentration of a saturated solution at the given temperature,

$$\boldsymbol{S} = \frac{\boldsymbol{a}}{\boldsymbol{a^*}} = \frac{\boldsymbol{c}}{\boldsymbol{c^*}} \tag{2.7}$$

The most common expressions of supersaturation are the concentration driving force,

$$\Delta\boldsymbol{c} = \boldsymbol{c} - \boldsymbol{c^*} \tag{2.8}$$

Alternatively, supersaturation can be expressed by the relative supersaturation, σ:

$$\boldsymbol{\sigma} = (\boldsymbol{c} - \boldsymbol{c^*})/\boldsymbol{c^*} = \Delta\boldsymbol{c}/\boldsymbol{c^*} \tag{2.9}$$

So, the supersaturation ratio, S:

$$\boldsymbol{S = \frac{c}{c^*} = \sigma + 1} \quad (2.10)$$

Therefore, for a saturated solution S = 1, an undersaturated solution is denoted by S<1 and S>1 indicates a state of supersaturation.

Supersaturation in aqueous solution of sparingly soluble electrolytes is best expressed in term of the solubility product, so,

$$\boldsymbol{S = \left(\frac{IAP}{K_{sp}}\right)} \quad (2.11)$$

where *IAP* is the ion activity product of the lattice ions in solution and K_{sp} is the activity solubility product of salts.

The logarithmic of Eq. (2.12) can results saturation index correlation,

$$\boldsymbol{SI = \log\left(\frac{IAP}{K_{sp}}\right)} \quad (2.12)$$

2.4 Metastable Zone Width

The Metastable Zone Width is defined as the zone between the solubility curve and the metastable limit curve (Figure 2.2) and provides essential information for developing well-controlled crystallisation processes. Solubility and Metastable Zone Width curves are critical parameters for the definition of the operational and optimal design space for a crystallisation process. The illustration of Figure 2.2 describes supersaturation in metastable zone, which constitutes the allowable supersaturation level during crystallisation process.

From Figure 2.2, the diagram can be distinguished in terms of three distinct zones:

1. The stable zone is the undersaturated zone, where no nucleation or crystal growth is possible. In this zone, existing crystals can still be dissolved into solution until the solubility of solute is reached.
2. The supersaturated metastable zone, between the solubility and supersolubility curve, where growth may occur but spontaneous nucleation does not occur. However, if a seed crystal was placed in such a metastable solution, growth would occur on it.
3. The labile zone is where spontaneous and rapid nucleation can occur

Point A on Figure 2.2 represents a solution which is undersaturated. If this solution is cooled without loss of solvent to point B the solution will be saturated and if the solution is cooled further past point C into the labile zone crystallisation may take

place rapidly in order to relieve the highly supersaturated conditions so it can return back to equilibrium or it may be induced by seeding, agitation or mechanical shock. Further cooling to point D may be necessary before crystallisation can be induced, especially with very soluble substances since the solution may have become highly viscous and could even set to glass preventing crystallisation. As previously mentioned, supersaturation can also be achieved by solvent evaporation, which is represented by the path AB'C' at constant temperature. In practice, a combination of cooling and evaporation is employed which is represented by the path AB"C". All the above conditions only apply to homogeneous solutions since if a crystal of the solute was placed in the metastable region, growth would occur on it (Mullin, 2001).

The metastable zone width is an essential parameter in the design, control and optimization of crystallisation processes, such as for the growth of large size crystals from solution. The metastable zone width is affected by various process parameters, such as supersaturation generation rate (Barrett and Glennon, 2002), agitation speed (O'Grady et al., 2007) and the presence of impurities (Myerson and Jang, 1995, Sayan and Ulrich, 2001).

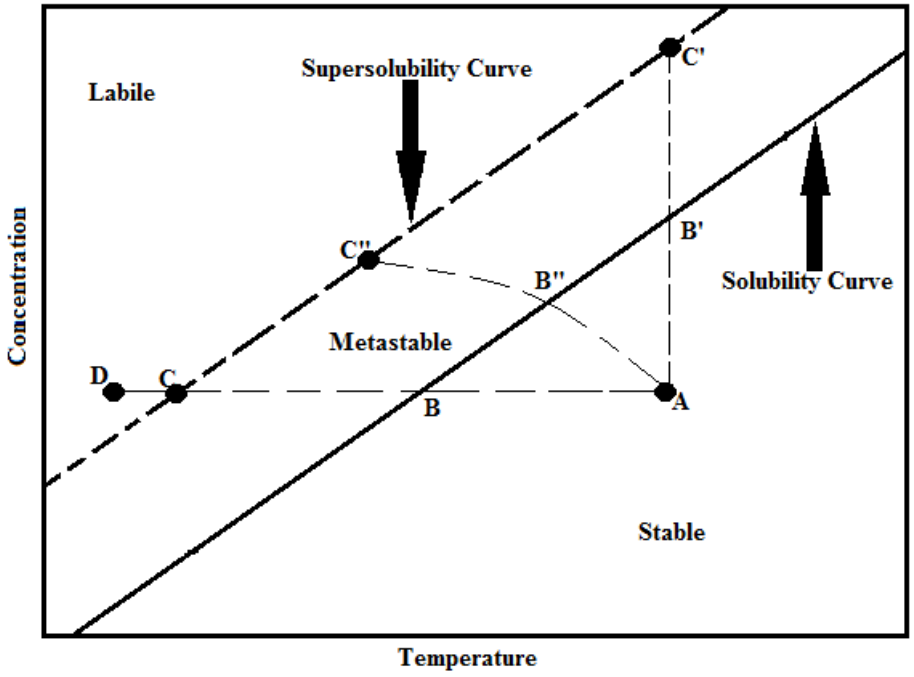

Figure 2.2 The solubility – supersolubility diagram (Mullin, 2001)

Metastable zone width in primary nucleation is important in crystallisation of unseeded and highly supersaturated solutions. The unseeded crystallizers are commonly used in the chemical industry to control product qualities like crystal

size, crystal size distribution and crystal shape. It is, however, very difficult to estimate the qualities for product crystals obtained from unseeded crystallizers. In spite of this, unseeded crystallisation is applied widely in chemical production such as explosive materials (Kim and Ryu, 1997), emulsion latex (Hansen and Ugelstad, 1978), nano particle production (Song et al., 1997), etc. In the case of unseeded batch crystallizer spontaneous nucleation must be considered.

2.5 Nucleation Study

Nucleation occurs when solid crystals, called nuclei, are produced in specific supersaturated solution. There are different mechanisms that produce nuclei. Nucleation that involves either homogeneous or heterogeneous is primary nucleation. Secondary nucleation occurs in the presence of crystals of the same material being crystallized. Possibilities of secondary nucleation can be caused by dust on dry seeds (initial breeding type), breakage of dendritic growth on parent crystals (Dendritic type), breakage of agglomerates (polycrystalline breeding type), fluids shear on crystal face (shear nucleation type), and collision breeding (contact type) (Wilsenach et al., 2007).

Generally, the difference between primary and secondary nucleation is that primary nucleation is the initial formation of crystals in the absence of other similar crystals, whereas secondary nucleation occurs in the presence of crystals of the same material. Primary nucleation needs higher supersaturation while secondary nucleation needs much lower supersaturations (Wilsenach et al., 2007, Jones, 2002)

2.5.1 Primary nucleation

Primary nucleation can be classified into homogenous and heterogeneous nucleation. The formation of a crystal that is not influenced by other crystals is called homogenous nucleation. Heterogeneous nucleation occurs when solid particle of any substance cause an increase in the rate of nucleation that would otherwise not be seen without the existence of these foreign particles. Heterogeneous nucleation occurs more often than homogeneous nucleation since it is not easy to prepare systems free from impurities, and physical equipment

such as vessel walls, stirrer and baffles (Kim et al., 2009) are required for crystallisation process. Homogeneous nucleation requires a much higher level of supersaturation and in most situations heterogeneous nucleation takes place before reaching conditions suitable for homogeneous nucleation.

2.5.1.1 Homogeneous nucleation

The classical theory of nucleation assumes that clusters are formed in solution according to following scheme;

$$\boldsymbol{A + A \rightleftarrows A_2} \quad (2.13)$$

$$\boldsymbol{A_2 + A \leftrightarrows A_3} \quad (2.14)$$

$$\boldsymbol{A_{n-1} + A \rightleftarrows A_n}\text{(Critical cluster)} \quad (2.15)$$

Homogeneous nucleation occurs purely due to supersaturation. High supersaturation provides ions or molecule to produces nuclei that is called embryo. If the embryos grow to exceed a particle size, called critical nuclei, then thermodynamics predicts that this aggregate would be stable and grow in size spontaneously. Further molecular addition to the critical size reached would result in nucleation and subsequent growth into crystals. Similarly, ions or molecules in a solution can interact to form short-lived clusters. Short chains may be formed initially or flat monolayer, and eventually a crystalline lattice structure is built up. The construction process, which occurs very rapidly, can only continue in local regions of very high supersaturation, and many embryos or 'sub-nuclei' fail to achieve maturity; they simply redissolve because they are extremely unstable. If, however, the nucleus grows beyond a certain critical size, as explained below, it becomes stable under the average condition of supersaturation obtaining in the bulk of the fluid.

The structure of assembly of molecule or ions which we call a critical nucleus is not known, and it is too small to observe directly. It could be a miniature crystal, nearly perfect in form. On the other hand, it could be a rather diffuse body with molecules or solvated ions in a state not too different from that in the bulk fluid, with no clearly defined surface.

The classical nucleation theory is based on the condensation of a vapour to a liquid; these phenomena can be applied to crystallisation from melts and solution

(Mersmann, 2001). The thermodynamic consideration for homogeneous nucleation may be predicted as follows:

The change in overall free energy of formation is the sum of the surface free energy ΔG_S and the volume free energy (ΔG_V) (see in Figure 2.3). The change in positive free-surface energy increases with the interfacial tension (γ) between the surface of the particle and the surrounding solution, and the change in free-volume energy is proportional to the volume of particle ($r = \infty$) and increases energy of solute in solution.

$$\Delta \boldsymbol{G} = \Delta \boldsymbol{G_S} + \Delta \boldsymbol{G_V} \tag{2.16}$$

$$\Delta \boldsymbol{G} = \boldsymbol{\beta L^2 \gamma} + \boldsymbol{\alpha L^3 \Delta G_v} \tag{2.17}$$

Here, γ is the interfacial tension, β and α are the area and volume shape factor, respectively, L is characteristic length. Under the assumption that these clusters or nuclei are spherical, the equation becomes

$$\Delta \boldsymbol{G} = \boldsymbol{4\pi r^2 \gamma} + \boldsymbol{\frac{4}{3}\pi r^3 \Delta G_v} \tag{2.18}$$

According to Figure 2.3, in which the free-surface energy ΔG_S and the free-volume energy ΔG_V and total free energy ΔG are plotted against the nucleus radius. The change in overall free energy of formation with respect to the nucleus size r passes through a maximum value. The critical size result in decrease in free energy of the particle and will participate in the nucleation process.

Differentiation of overall free-energy formation against size of nucleus (Eq. 2.19) and equating to zero will result in a thermodynamically stable nucleus. The critical size can be calculated by minimizing the free energy function with respect to the radius.

$$\boldsymbol{\frac{d(\Delta G)}{dr} = 8\pi r_c \gamma + 4\pi r_c^2 \Delta G_v = 0} \tag{2.19}$$

$$\boldsymbol{r_c = -\frac{2\gamma}{\Delta G_v}} \tag{2.20}$$

Substituting for ΔG_v from Eq. (2.21) in Eq. (2.20) we get

$$\Delta \boldsymbol{G_{crit}} = \boldsymbol{\frac{4\pi r_c^2 \gamma}{3}} \tag{2.21}$$

The behaviour of newly created crystalline lattice structure in a supersaturated solution depends on its size where the crystalline lattice can either grow or

redissolve. The crystalline lattice can continue to grow if critical size of lattice becomes bigger than its critical size, r_c.

The Gibbs-Thompson equation can be used to calculate growth of clusters

$$\boldsymbol{ln\frac{c}{c^*} = \ln S = \frac{2\gamma v}{kTr_c}} \quad (2.22)$$

where c is the solution concentration, c^* is the equilibrium saturation at given temperature T and v is molecular volume. Substituting for r_c from Eq. 2.23 into Eq. 2.22 we get

$$\boldsymbol{\Delta G_{crit} = \frac{16\pi\gamma^3 v^2}{3(kT\ln S)^2}} \quad (2.23)$$

The rate of nucleation, *J*, e.g. the number of nuclei formed per unit time per unit volume, by primary homogeneous nucleation mechanism can be expressed in the form of the Arrhenius reaction equation (Kim et al., 2009, Wilsenach et al., 2007, Jones, 2002)

$$\boldsymbol{J = A\ exp\left(\frac{-\Delta G}{kT}\right)} \quad (2.24)$$

where *A* is the pre-exponential factor and has a theoretical value of 10^{30} nuclei/cm^{3}s (Jones, 2002), *k* is the Boltzmann constant, ΔG is the free energy change between a small particle of solute and solute in solution, and *T* is the temperature in Kelvin.

The nucleation rate can now be obtained from Eq. 2.25

$$\boldsymbol{J = A\ exp\left[\frac{-16\pi\gamma^3 v^2}{3k^3T^3(\ln S)^2}\right]} \quad (2.25)$$

$$\boldsymbol{B = \frac{-16\pi\gamma^3 v^2}{3k^3T^3}} \quad (2.26)$$

$$\boldsymbol{v = \frac{M}{\rho_c N_A}} \quad (2.27)$$

where *M* is the molar mass, ρ_C is the crystal density and N_A is the Avogadro number.

$$\boldsymbol{J = A\ exp\left[\frac{-B}{(\ln S)^2}\right]} \quad (2.28)$$

where *B* is a constant.

It is clear that increasing supersaturated solution and temperature can increase nucleation rate. And nucleation rate decreases with an increase in surface energy.

As discussed by Nielsen (2010), Nyvlt (2012), and Shonel and Garside (2003), over limited ranges of supersaturation, Eq. (2.29) may be simplified to

$$J = k_N S^n \tag{2.29}$$

where k_N is the nucleation rate constant and n is the kinetic order of nucleation.

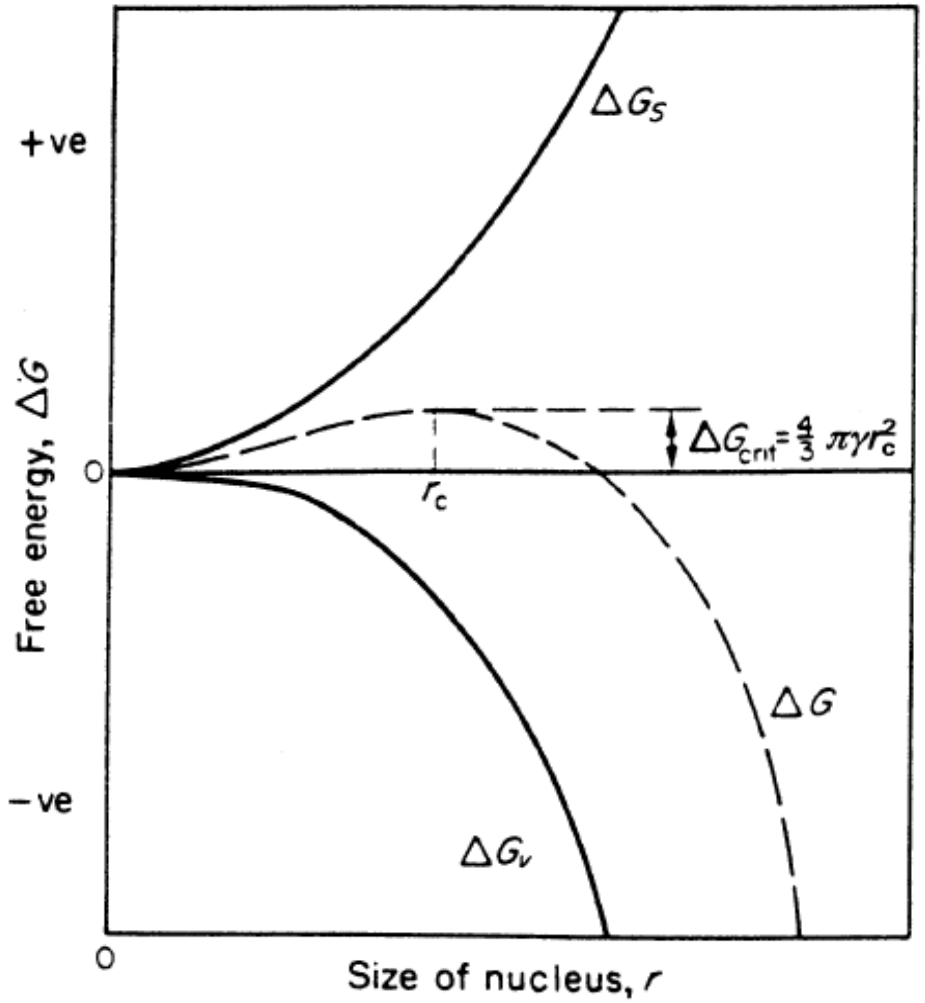

Figure 2.3 Free energy diagrams for nucleation explanation against clusters size (Mullin, 2001).

2.5.1.2 Heterogeneous nucleation

As mentioned previously homogeneous nucleation is thought to occur quite rarely in real life situation since the presence of foreign particles are difficult to avoid in the supersaturated solution. Generally, heterogeneous nucleation takes place more quickly since the foreign particles act as a catalyst for the crystal growth (Figure 2.4), thus eliminating the necessity of creating a new surface and the incipient surface energy requirements. The decrease in free energy depends on the contact

(or wetting) angle between the crystalline deposits and the foreign solid surface. The relationship is formulated in Eq. (2.31)

$$\Delta \boldsymbol{G_{hom}} = \emptyset\, \Delta \boldsymbol{G_{het}} \tag{2.30}$$

$$\emptyset = \frac{\mathbf{1}}{\mathbf{4}}(\mathbf{2} + \mathbf{cos}\,\emptyset)(\mathbf{1} - \mathbf{cos}\,\emptyset)^{\mathbf{2}} \tag{2.31}$$

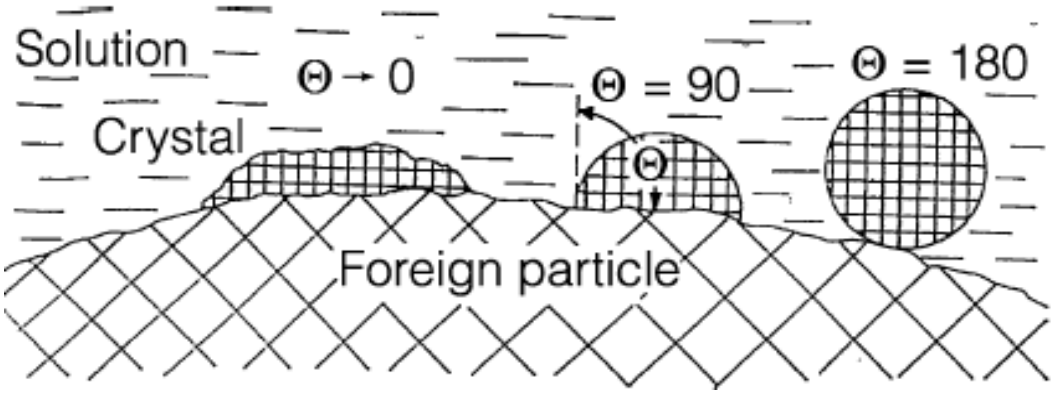

Figure 2.4 Nucleation on a foreign particle for different wetting angles (Mersmann et al., 2002)

The contact angle equals to zero (Eq. (2.32)), complete wetting, and the energy consideration show that spontaneous nucleation would occur for the system.

2.5.1.3 Induction time

The rate of nucleation can be determined by observing induction time. Induction time is defined as the amount of time elapsed between the creation of supersaturation and the point at which crystals are first detected. The appearance of the first visible crystals can be observed by changing in properties of the solution (for example, an increase in turbidity, a decrease in conductivity, a change in pH solution, and a concentration decrease).

The induction time is divided into three periods as shown in Figure 2.5. At the beginning, the solution requires a time to achieve a quasi-steady state distribution of molecules. This period is called a certain 'relaxation time', t_r. Then time is required for the formation of a stable nucleus, t_n, and then for the nucleus to grow to a detectable size, t_g. So the induction time, t_{ind}, may be written as

$$\boldsymbol{t_{ind}} = \boldsymbol{t_r} + \boldsymbol{t_n} + \boldsymbol{t_g} \tag{2.32}$$

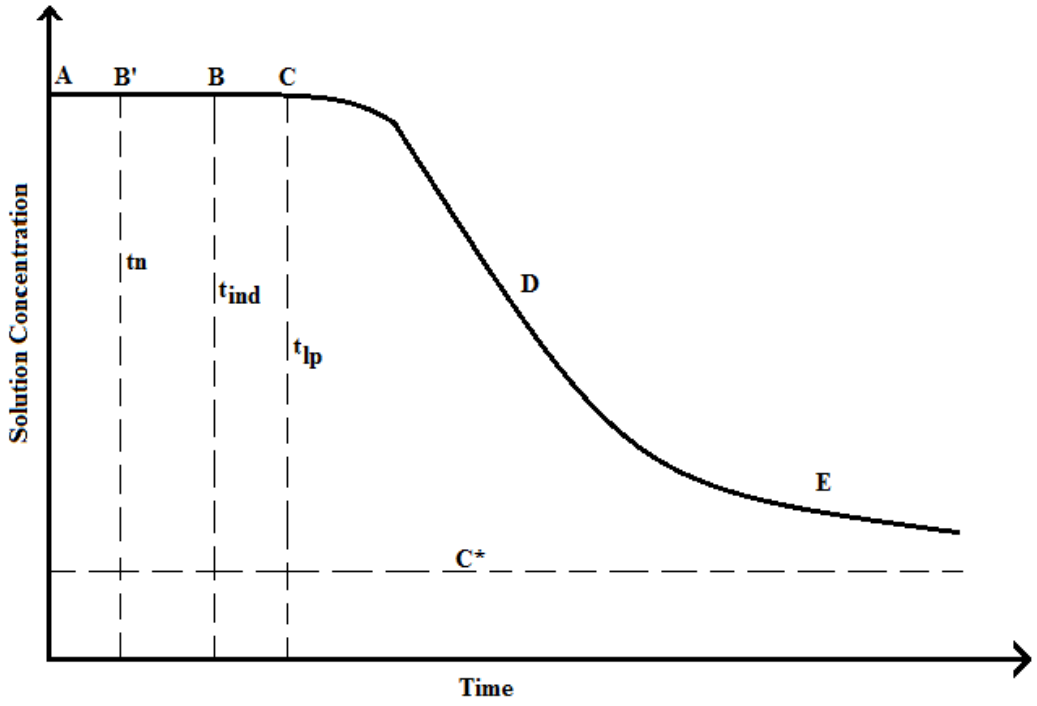

Figure 2.5 A desupersaturation curve (Mullin, 2001)

It is difficult to isolate these separate quantities. The relaxation time depends to great extent on the system viscosity and hence diffusivity. The nucleation time depends on the supersaturation which affects the size of the critical nucleus. The growth time depends on the size at which nuclei are detectable and the growth rate applicable to this early stage of development.

Figure 2.5 shows a typical desupersaturation curve. At point *A*, the initial supersaturation is created when time is zero and after a certain time, at point *B*', the solution form critical sized nuclei at which crystals can not be visually detected. This point is called the critical nuclei time (t_n). At point *B*, a certain induction time t_{ind} elapses and crystals are first detected. However, at point *B*, no significant changes in the solution may be detected until, at point *C*, sometimes referred to as the end of the latent period, t_{lp}, followed by rapid decay of supersaturation (*D*). Crystal growth in predominant during the decay of supersaturation region. Growth will slow down near equilibrium concentration at point *E*. At very high supersaturation, the induction time and latent period can be extremely short and virtually indistinguishable.

The presence of seed crystals generally reduces the induction time. A measurable of induction time when seed crystal is introduced in the system is defined as secondary nucleation. Factors that can influence the induction time, latent periods, and rate of desupersaturation are temperature, agitation, heat effect during crystallisation, seed size, seed surface area, and the presence of impurities (Mullin, 2001)

Based on the assumption that nucleation time is much greater than growth time during the induction period ($t_n \gg t_g$), and using the statistical concept of nucleation (Ohlinger et al., 1999), the induction time has frequently been used as a measure of the nucleation rate. It can be considered to be inversely proportional to the rate of nucleation (Mullin, 2001, Sohnel and Graside, 1992):

$$\boldsymbol{t_{ind} = \frac{1}{J}} \tag{2.33}$$

Combining Eq. (2.34) and (2.29) provides an expression for homogenous nucleation induction time.

$$\mathbf{\log} \boldsymbol{t_{ind}} \mathbf{= \log A + \log}\left[\frac{\boldsymbol{B}}{\mathbf{2.303\ (\ln} \boldsymbol{S}\mathbf{)^2}}\right] \tag{2.34}$$

Plotting data between $log(t_{ind})$ and $log(S)^{-2}$ should result in a straight line but two straight lines having different slopes are usually obtained, illustrating the change of nucleation mechanism at specific supersaturations (Figure 2.6). At lower supersaturation, heterogeneous nucleation is effective while at higher supersaturation homogeneous nucleation dominates.

The Eq. (2.35) can be used to estimate the mechanism of nucleation. The empirical dependence of $log\ t_{ind}$ versus $(log\ S)^{-2}$ results in different slopes which has two distinctive regions (Figure 2.6): Region I is for low supersaturation, characteristic of heterogeneous nucleation mechanism; Region II for high supersaturation where homogeneous nucleation mechanism dominates (Stumm and Morgan, 1995).

The induction period t_{ind} has become an experimental basis to determine the nucleation rate *J*, using a simple relationship.

$$\boldsymbol{J = \frac{1}{t_{ind}}} \tag{2.35}$$

By combining Eq. (2.30) and (2.36) one obtains

$$\boldsymbol{t_{ind} = (1/k_N)S^{-n}} \tag{2.36}$$

$$\boldsymbol{K = \frac{1}{k_n}} \tag{2.37}$$

Or,

$$\boldsymbol{t_{ind} = K.S^{-n}} \tag{2.38}$$

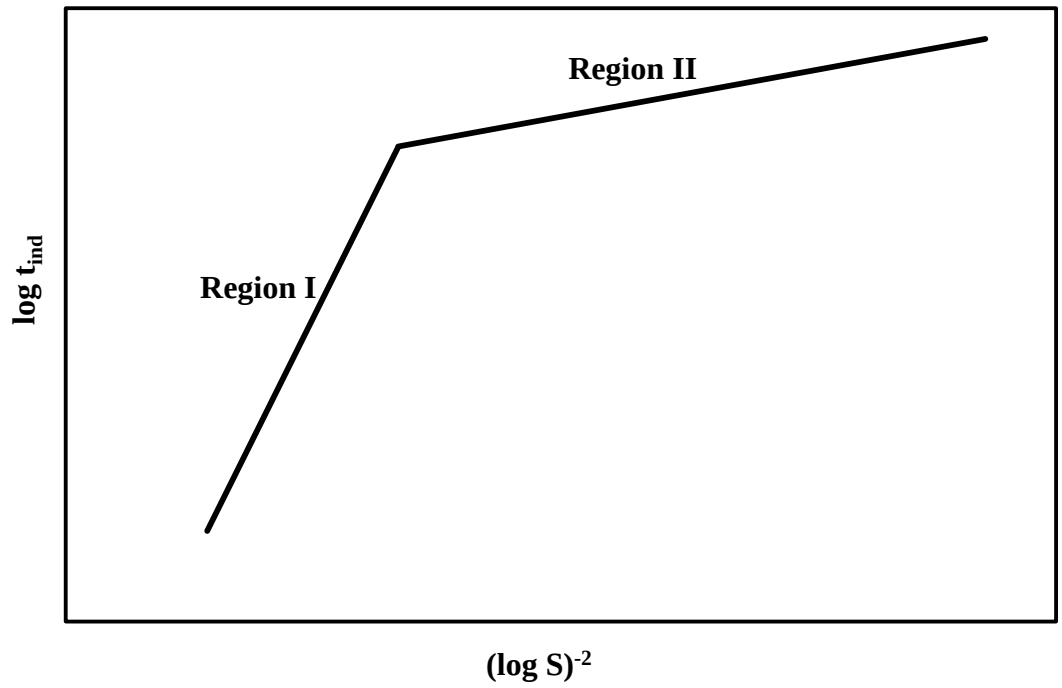

Figure 2.6 Empirical dependence of induction period on supersaturated solution.

In similar manner, the activation energy is calculated in terms of induction time by combining Eq. (2.34) and Eq. (2.25):

$$\boldsymbol{t_{ind} = A \exp\left(\frac{\Delta G}{kT}\right)} \tag{2.39}$$

Or

$$\boldsymbol{t_{ind} = A \exp\left(\frac{E_{act}}{RT}\right)} \tag{2.40}$$

$$\boldsymbol{\log \frac{1}{t_{ind}} = \log A - \frac{E_{act}}{2.303\ R\ T}} \tag{2.41}$$

where A is a constant, E_{act} is the activation energy (J mol^{-1}) for the process, and R is the gas constant (8.314 J/K.mol).

The slope of a straight line plot of $log(1/t_{ind})$ versus T^{-1} can evaluate the activation energy of system. Activation energy represents the minimum energy that is required for change of phase to take place.

2.5.2 Secondary nucleation

Secondary nucleation is a nucleation process resulting from the presence of seed crystals in the solution. The size of seed crystals influences secondary nucleation. For example, large seed crystals generate more secondary nuclei in agitation system than do small seed crystals because of their greater contact probabilities and collision energies. Furthermore, the small crystals (less than about 10 μm) probably grow much more slowly than do macrocrystals. And the small crystals may breakup in agitation system and it may not be capable of growing at all. The secondary nucleation phenomena can be caused by several different mechanisms (Söhnel and Garside, 1992).

1. Apparent secondary nucleation when the nuclei are brought into the system along with inoculating crystals. The type of apparent nucleation are:
   - *Seeding with crystal dust (dust breeding),* which occurs when a supersaturated solution is seeded with untreated crystals. The seed crystals are covered with tiny crystallites formed during drying of the adhering mother liquor after their preparation, or electrostatically captured crystalline dust formed by rubbing together of the crystals during storage (Jancic and Grootscholten, 1984, Myerson, 2002, Rousseau et al., 1976). When introduced into the solution, the crystallites act as nucleation sites (Ting and McCabe, 1934, Strickland-Constable and Mason, 1963). Thus these nucleation sites are not formed in situ but were introduced into the solution.
   - *Polycrystalline breeding*, here, at high supersaturations crystals do not grow regularly but form polycrystalline aggregates.
   - *Macroabrasion*, it can become important during intense stirring of suspensions, probably together with other mechanism of secondary nucleation (Denk Jr and Botsaris, 1972). The rate of nucleation does not depend on the supersaturation (Asselbergs and De Jong, 1972). The rate of nucleation of this type is dependent on the number nuclei formed by macrobrasion, the mean retention time of the solution and the rate constant of macrobrasion (Nyvlt et al., 1985).

2. True secondary nucleation where new nuclei are formed by interaction between the crystal and solution. The type of true secondary nucleation is shear nucleation caused by fluid shear. This type can be divided into three groups;
    - Formation of nuclei from the solid phase, i.e. from a seed crystal;
    - Formation of nuclei from a dissolved substance in solution;
    - Formation of nuclei from a transition phase at the crystal surface
3. Contact nucleation, this mechanism is probably most predominant in any stirred crystallizer. Nucleation is caused by;
    - crystal-crystal collision
    - crystal-stirrer collision
    - crystal-crystallizer wall collision

    Collisions in a liquid medium can initiate complex behaviour. Break-up of the crystals is difficult to predict and it is hard to avoid, but substantial hydrodynamic forces can operate over the surface in the vicinity of the point of contact, giving rise to plastic and elastic deformation in the parent crystal. Due to energy adsorption, a small fragment broken off a crystal by collision could be in a considerably disordered state, with many dislocations and mismatch surfaces.

The rate of secondary nucleation is governed by three processes; (1) the generation of secondary nuclei on or near a solid phase; (2) removal of the clusters, and (3) growth to form a new solid phase (Myerson, 2002). Several factors influencing these processes are supersaturation, rate of cooling, agitation, temperature and presence of impurities.

The degree of supersaturation is the critical parameter to control the rate of nucleation. At higher supersaturation, the adsorbed layer is thicker and results in a large number of nuclei. The size of the critical nucleus decreases with increase in supersaturation. Thus, the probability of the nuclei surviving to form crystals is higher. As the supersaturation increased, the microroughness of the crystals surface also increase, resulting in a larger nuclei population.

For several systems, the nucleation rate declined with increasing temperature for a given supersaturation (Söhnel and Garside, 1992). This could be attributed to the

faster rate of incorporation of the absorbed layer on to the crystal surface at higher temperatures. Since the thickness of the absorbed layer was reduced, the nucleation rates also decline with increasing temperature. A few contradictory results exist where an increase was found with increasing temperature for a potassium nitrate system and increasing rates with increasing temperature for a potassium chloride system (Genk and Larson, 1972).

Intuitively, the crystals in a solution will require agitation to keep them suspended, which generate crystal-crystal and crystal-impeller contacts. These contacts are most likely to influence the extent of secondary nucleation and increase nucleation rate (Sikdar and Randolph, 1976). Stirring the solution leads to a thinning of the absorbed layer and hence should lead to lower nucleation rate. The relative hardness of the contacting bodies is also a factor to consider, for example a metal impeller gives a much higher nucleation rate than one coated with a soft material such as polyethylene (Shah et al., 1973, Randolph and Sikdar, 1974). The numbers of blade impeller are also a factor that must be considered in secondary nucleation. At the same rotation speed, 6-blade impeller causes higher axial velocity than 4-blade impeller (Liri et al., 2002). Increasing axial velocity decreases impact velocity in collisions of crystals with pitched blade impeller. Decrease in impact velocity decreases secondary nucleation rate.

Small amounts of impurity can profoundly affect the nucleation rate. The presence of additive can either enhance or inhibit the solubility of a substance. Enhanced solubilities would lead to lower supersaturation and lower nucleation rate. If it is postulated that the impurity adsorbs on the surface crystals then two opposing effects come into play. The presence of additive would lower the surface tension and lead to higher nucleation rate, however, the impurity adsorption blocks potential growth sites and lower nucleation rate. Thus, the effect of impurities is complex and unpredictable.

2.6 Crystal Growth Study

The birth of new crystals which is formed from nucleation process refers to the starting point of solid formation from the solution. The next stage of the crystallisation process is for these nuclei to grow larger by the addition of solute

molecules from the supersaturated solution. This part of crystallisation process is known as crystal growth. Crystal growth, along with nucleation, controls the final particle size distribution obtained in the system. In addition, the conditions and rate of crystal growth have a significant impact on the product purity and crystal habit (Nývlt, 1992). An understanding of the crystal growth theory and experimental techniques for examining crystal growth from solution are important and very useful in the development of industrial crystallisation processes.

Various crystal growth theories have evolved spanning from atomic to microscopic scale(Myerson, 2002). Crystal growth theoretically involves either diffusion controlled or surface integration controlled (Mullin, 2001). The basic mechanisms of crystal growth can be seen in Figure 2.7. A possible mechanism for growth of a crystal from a liquid phase involves the following stages: (i) adsorption of growth unit (depicted as a cube) onto the crystal surface (*A*), (ii) surface diffusion of the molecules from the surface of the crystal towards a step, (*B*), and (iii) incorporation of the molecules absorbed onto the step to the kink site, (*C*). The most favourable energetically is called a kink site and is depicted by *C*. *A* less favourable energetically is simply a step and is depicted by *B*. As growth rate increases, the growth units fit into less energetically favourable sites and the crystal typically grows imperfectly. Thus, slow growth generally leads to perfect crystals, while fast growth leads to crystals with many more imperfections (Mullin, 2001, Myerson, 2002, Nyvlt et al., 1985, Hartel, 2001)

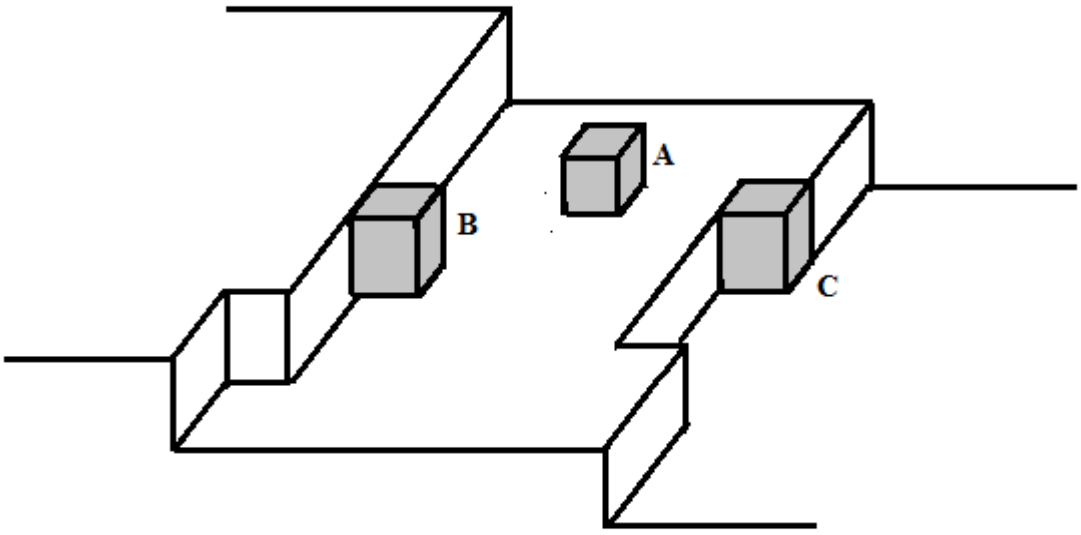

Figure 2.7 Idealization of a growing crystal surface (Myerson, 2002)

The growth rate of a crystal is often described by the change in some dimension of the crystals with time. The change of crystal dimension can be indicated by increasing mass of a crystal and the change in size. The increase in mass and size with time is often used and can be directly related to the overall linear growth velocity through the relation.

$$\boldsymbol{G = \frac{dL}{dt}} \tag{2.42}$$

where *G* is a linear crystal growth velocity (length/time); *dL* is changing size of crystal; and *dt* is time.

For engineering purpose in crystallizer design and assessment, the simple empirical power-law relationship expressing specific rate of mass deposition as given by

$$\mathbf{G = K_G S^g} \tag{2.43}$$

where K_G is overall growth rate constant, *g* is the order of the overall growth process, and *S* is supersaturation.

The overall growth rate constant depends on temperature, crystals size, hydrodynamic situation, and presence of impurities (Mayerson, 2002, Mullin, 1992, and Mersmann, 2001). The effect of temperature on the overall growth rate constant may generally be expressed by an Arrhenius relation. So, the overall growth rate constant on Eq. (2.44) is function of temperature, size, stirrer speed and impurities, or;

$$\mathbf{K_g = f(T, L, N, I, \dots)} \tag{2.44}$$

The growth of crystals from solution consist of least three stages (Jancic and Grootscholten, 1984);

1. The transport of solute from the bulk of the solution to the crystal surface by volume, or convection or a combination of both mechanisms.
2. Some process at the crystal surface, probably involving adsorption into the surface layer followed by orientation of the molecules into the crystal lattice. This stage is often referred to as the surface integration process.
3. Dissipation of the heat of crystallisation liberated at the crystal surface.

The three stage process can be seen in Figure 2.8 which illustrates a crystal face growing in a supersaturated solution of concentration, C. The transport of solute

from the bulk to the crystal surface is affected by diffusion and convection across the thickness of the mass transfer boundary layer, δ_{EM}. The thickness of boundary layer would obviously depend on the relative solid-liquid velocity, i.e. on the degree of agitation of the system. The driving forces will rarely be of equal magnitude, and the concentration drop across the thickness of boundary layer is not necessary linear. The concentration drop by diffusional transfer is followed by a second-order reaction at the crystal solution interface. Hence, the corresponding driving forces will be for transport to the interface, $(C - C_i)$, and for the surface integration process, $(C_i - C^*)$.

After the solution molecule has been incorporated into the crystals lattice, the heat of crystallisation will be liberated and must be conducted through the surface film to the bulk of solution. Generally, therefore, the surface temperature, T_i, and hence the equilibrium saturation concentration at the crystal surface will be slightly higher than bulk of solution (Figure 2.8). This effect will decrease the driving forces available for crystallisation. However, the rate of heat removed from the crystal surface to the bulk of the solution is usually neglected as an overall crystallisation rate controlling factor. Consequently, transport of solute to the interface and surface integration stage, govern the crystallisation rate and therefore requires careful consideration.

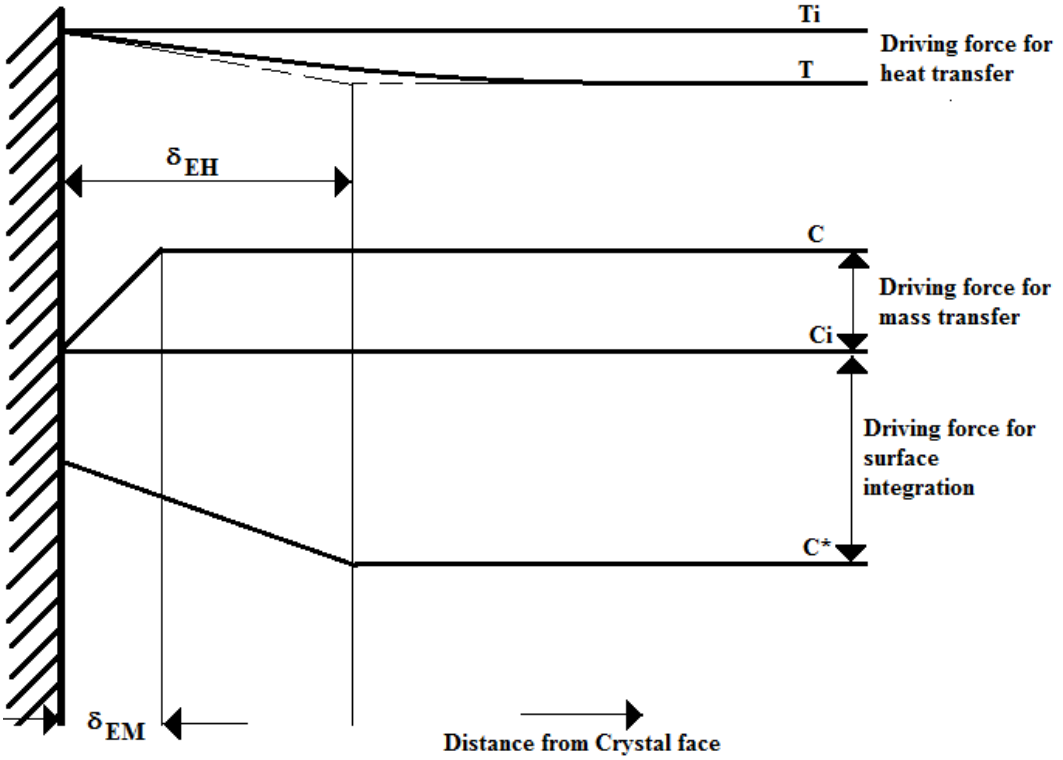

Figure 2.8 Concentration and temperature profile adjacent to crystal surfaces (Myerson, 2002)

These two stages, occurring under the influence of different concentration driving forces, can be represented by the equation;

a) Solute molecules diffuse from bulk liquid to the solid surface

$$\boldsymbol{G = k_d(C - C_i)} \qquad \text{(diffusion step)} \qquad (2.45)$$

b) Solute molecules are integrated into the crystal surface

$$\boldsymbol{G = k_r(C_i - C^*)^r} \qquad \text{(reaction or integration step)} \qquad (2.46)$$

where k_d is coefficient of mass transfer by diffusion, k_r is rate constant for surface reaction (integration) process, r is order of reaction, C_i is solute concentration in the solution at crystal-solution interface, C^* is equilibrium saturation concentration, and C is bulk solute concentration.

A general equation for crystallisation based on this overall driving force can be written as

$$\boldsymbol{G = K_G(C - C^*)^g} \qquad \text{(Overall growth)} \qquad (2.47)$$

Equation 2.46 and 2.47 are not easy to apply in practice because they involve interfacial concentration that is difficult to measure. The term C_i is usually

eliminated by considering an overall concentration driving force, $C - C^*$, which is quite easy to measured. From Eq. (2.46), C_i can be simplified,

$$\boldsymbol{C_i = C - G/k_d} \tag{2.48}$$

so equation 2.47 representing the surface integration step, may be written

$$\boldsymbol{G = k_r(\Delta C - G/k_d)^r} \tag{2.49}$$

where $\Delta C = C - C^* = S$ and $r \geq 1$, If $r = 1$ Eq. (2.50) is simplified to be

$$\boldsymbol{G = \frac{S}{1/k_d + 1/k_r}} \tag{2.50}$$

Many inorganic salts crystallizing from aqueous solution give an overall growth rate order, g, in the range 1 to 2. If g = 1, and Eq. (2.48) is substituted with Eq. (2.51), so

$$\boldsymbol{\frac{1}{K_G} = \frac{1}{k_d} + \frac{1}{k_r}} \tag{2.51}$$

or

$$\boldsymbol{K_G = \frac{k_d k_r}{k_d + k_r}} \tag{2.52}$$

Looking at Eq. (2.48) and (2.50), the crystal growth rate will be diffusion controlled, if coefficient of mass transfer is higher than rate constant of reaction step ($k_d >> k_r$) and overall rate constant is equal coefficient of mass transfer ($k_g = k_d$). And if rate constant of reaction step is higher than coefficient of mass transfer ($k_r >> k_d$), the crystal growth rate will be controlled by the reaction or integration step.

If r =2 in Eq. (2.47), Eq. (2.50) is written as follows

$$\boldsymbol{\frac{S}{\sqrt{R_G}} = \frac{1}{\sqrt{k_r}} + \frac{\sqrt{R_G}}{\sqrt{k_d}}} \tag{2.53}$$

Thus, the mass-transfer coefficient, k_d, and surface-reaction coefficient, k_r, are calculated from the slope of the plot, $S/\sqrt{R_G}$ versus $\sqrt{R_G}$.

However, for a surface-reaction order $r = 2$, the following expression of crystal growth rate can be used (Mullin, 2001).

$$\boldsymbol{R_G = k_d\left[\left(1 + \frac{k_d}{2k_r\Delta C}\right) - \sqrt{\left(1 + \frac{k_d}{2k_r\Delta C}\right)^2 - 1}\right]S} \tag{2.54}$$

2.6.1 Crystal growth theories

Crystal growth is a major stage of a crystallisation process. The successive growth of the critical nuclei of microscopic size leads to the formation of a crystal. In order to understand the mechanism and the kinetics of growth, several theories have been developed, which includes surface energy theory, adsorption theory, kinematic theory, diffusion-reaction theory and birth and spread theory (Mullin, 2001).

2.6.1.1 Surface energy theory

The surface energy theories are based on the thermodynamic treatment of equilibrium (Gibbs, 1948). This experiment compared the growth of crystals with the formation of water droplets in mist. The principles of surface energy theory are: the total free energy of a crystal in equilibrium with its surrounding at constant temperature and pressure would be a minimum for a given volume (Gibbs, 1948).

A liquid droplet is very different from a crystalline particle; in the former the constituent atoms or molecules are randomly dispersed, whereas in the latter they are regularly located in a lattice structure (Mullin, 2001).

The velocity of growth of a crystal face can be described in Figure 2.9. The velocity of growth will vary from face to face depending on faster or slower growing each faces. Figure 2.9(a) shows the growth of a crystal on each face with maintaining the same geometry of every face. Such a crystal is called “invariant”. Invariant crystal has three *A* faces with the same growth rate resulting from the same surface energy. The growth rate of *B* faces is smaller than *A* faces. And *C* face grows fastest of all. The differences of the growth rate of each face are caused by random deployment of atoms or molecules forming a crystal face.

In practice, a crystal does not always maintain geometric similarity during growth; the smaller, fastest-growing faces are often eliminated, and this mode of crystal growth is known as “overlapping”. Figure 2.9(b) shows the various stages of growth of such a crystal. The smaller *B* faces, which grow much faster than the *A* faces, gradually disappear from the pattern.

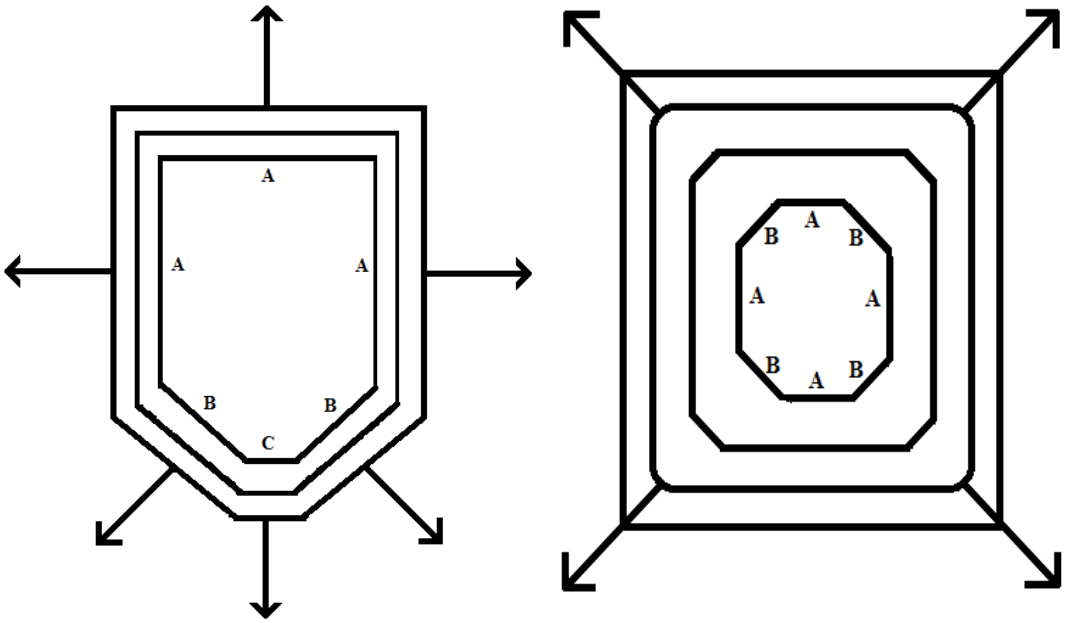

(a) (b)

Figure 2.9 Velocity of crystal growth faces: (a) invariant; (b) overlapping (Mullin, 2001)

2.6.1.2 Adsorption theory

The concept of a crystal growth mechanism based on the existence of an adsorbed layer of solute atoms or molecule on a crystal face was first suggested by Volmer (1939). The thermodynamic treatment suggested by Volmer was later extended and modified by a number of researchers. A brief description of the adsorption layer theory developments will be described below.

Volmer's theory describes how ions or molecules of a substance arrive at crystal face where they are not immediately integrated into lattice, but merely lose one degree of freedom and it continues to migrate over the crystal face (surface diffusion) (Mullin, 2001). The greatest of the attractive forces will act as a link between the crystallizing substance and the lattice to be placed in a position, and under ideal conditions this step-wise build-up will continue until the whole layer is completed (Figure 2.10(a) and (b)). Before a new layer can begin to grow on the surface a "centre of crystallisation" must be created, and Volmer theory suggested that monolayer island nucleus is formed on the surface, often called a two-dimensional nucleus.

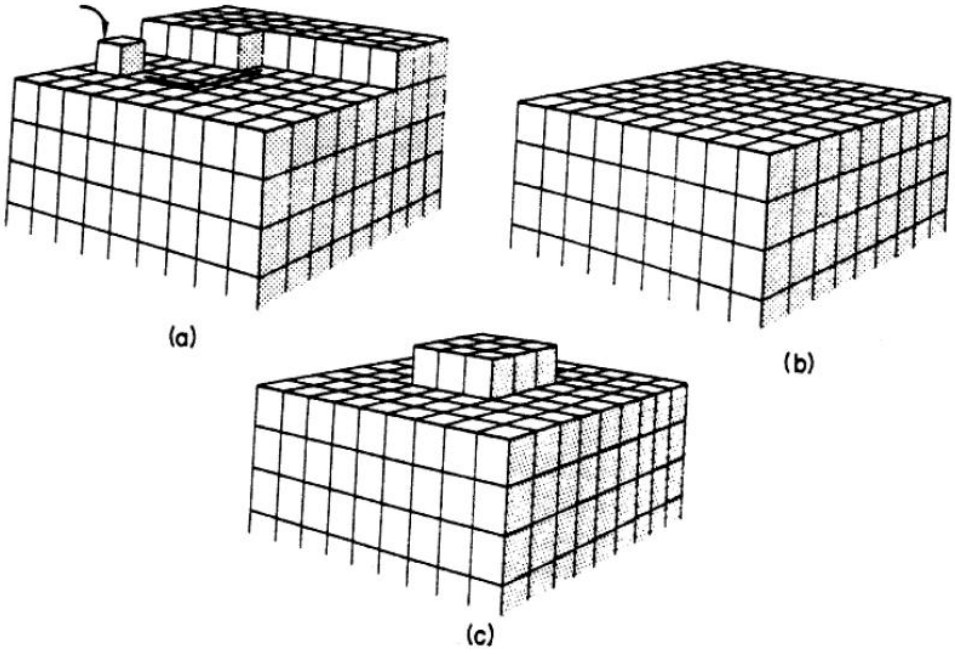

Figure 2.10 Two-dimensional nucleus; (a) migration toward desired location; (b) completed layer; (c) surface nucleation (Mullin, 2001)

Kossel (1934) also developed a model based on the theory that an apparently flat crystal surface actually consists of moving layer of monatomic height which may contain one or more kinks. On the crystal surface there will also be loosely adsorbed growth unit (atoms, molecule, or ions) which can easily be incorporated into the crystal at the kink. The kink will move along the surface until the layer is complete. A new step can be created by surface nucleation. One flaw associated with this model due to the dependence on high level of supersaturation for surface nucleation since it is known that many crystal faces can grow at quite high rates at low supersaturation levels (Mullin, 2001).

A solution to this problem was presented by Frank (1949). Frank (1949) argued that few crystals grow in the ideal layer-by-layer fashion without developing imperfections. During crystal growth in the solution, molecules adsorb on the crystal surface and diffuse to the top step of the planes of dislocation. The most common type of dislocation is screw dislocation. The screw dislocation can be seen in Figure 2.11. Furthermore, a screw dislocation continuously grows on the surface of crystal and it could be a spiral staircase formation. The interesting of Frank's idea was that these dislocations promote the growth of crystals without

depending on surface nucleation and that growth could occur at a fine rate at low supersaturation.

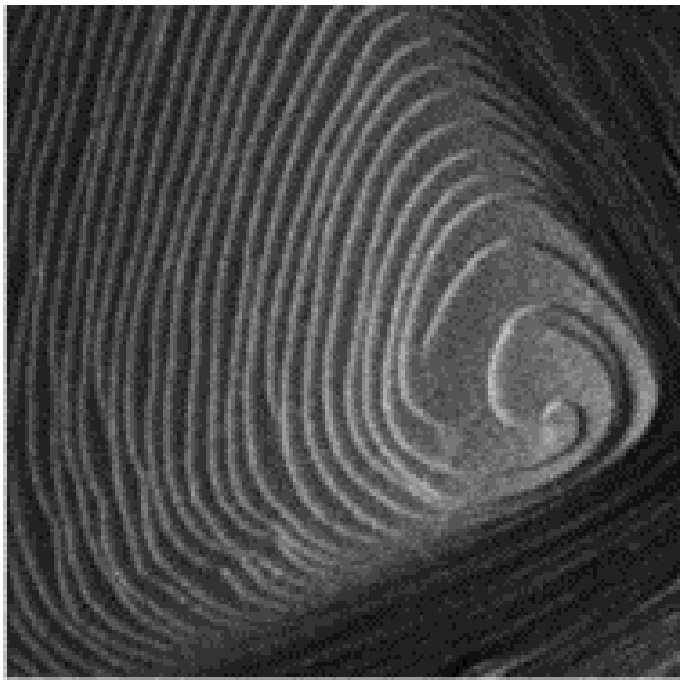

Figure 2.11 Screw dislocation during crystal growth (De Yoreo et al., 1996)

Another theory of adsorption theory is Burton-Cabera-Frank (BCF) theory. The concept of BCF's theory was when atoms or molecules or ions of crystallizing substance transfer to crystal surface and diffuse along the surface. Then they are joined into the sites of the crystal (such as, ledge site, step site, or kink site).

The BCF theory offers a concept in a growth model in which surface diffusion was considered to be the rate-controlling step so the model is called the *BCF surface diffusion model*. The BCF theory predicts that the growth rate is proportional to the second power of the supersaturation for low supersaturation, changing to a linear dependence at higher supersaturations.

2.6.1.3 Kinematic theory

The kinematic theory, developed by Frank (1958), involves two processes of crystal growth on the crystal surface in which the generation of step on the surface followed movement of surfaces across the face. The step velocity, *u*, depends on the closeness of other step since all steps are competing units (Figure 2.12).

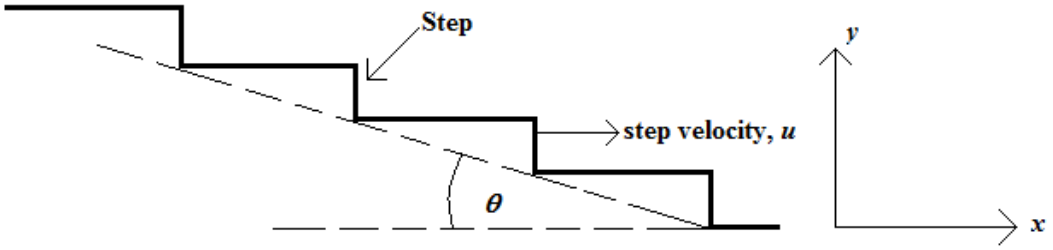

Figure 2.12 Two-dimensional nucleus of steps on a crystal face (Frank, 1958)

2.6.1.4 Diffusion-reaction theory

Diffusion theory was first proposed by Noyes and Whitney (1897) and Nernst (Nernst, 1904). The diffusion-reaction theory considers that the deposition of solid on the face of a growing crystal is essentially a diffusion process. Noyes and Whitney (1897) assumed that crystallisation was reverse of dissolution, and that the rates of both processes were calculated by the difference between concentration at the solid surface, C, and in the bulk of the solution, C^*. They proposed an equation as below;

$$\frac{dm}{dt} = k_m A(C - C^*) \tag{2.55}$$

where m is mass of solid deposited in time t, k_m is diffusion-reaction coefficient and A is surface area of the crystals.

Nernst (1904) modified equation 2.56, with an assumption that a thin stagnant film on the growing crystal face in which molecules of the solute would have to diffuse:

$$\frac{dm}{dt} = \frac{D}{\delta} A(C - C^*) \tag{2.56}$$

where dm is the mass of the solute deposited over the crystal surface of area A during time dt, D is coefficient of diffusion of the solute, and δ is the thickness of the stagnant layer adjacent to the crystal surface.

The theory proposed by both the above authors fails to be consistent with experimental observations. In agitation system, the concept of diffusion film would not clarify the rate of crystal growth because of the thickness of the stagnant film depending on the degree of agitation. In addition, crystallisation is not necessarily the reverse of dissolution (Mullin, 2001).

2.6.1.5 Birth and spread theory

Birth and spread theory was first observed by Keller (1986). The surface diffusion on birth and spread theory may be described by three different models shown schematically in Figure 2.13. The mechanism of crystal growth based on birth and spread theory is when the newly formed nuclei, formed by ions, atom, or molecules, located on the crystal surface (Figure 2.13(a)). The nucleus is called two-dimensional nucleus. Before the previous layer is completed the new nuclei will form on the surface crystal (Figure 2.13 (b)). In Figure 2.13(c) the new crystal layer is formed by linking of many two-dimensional nuclei which spread on the crystal surface. New nuclei and further layers begin to form on previously formed incomplete layers.

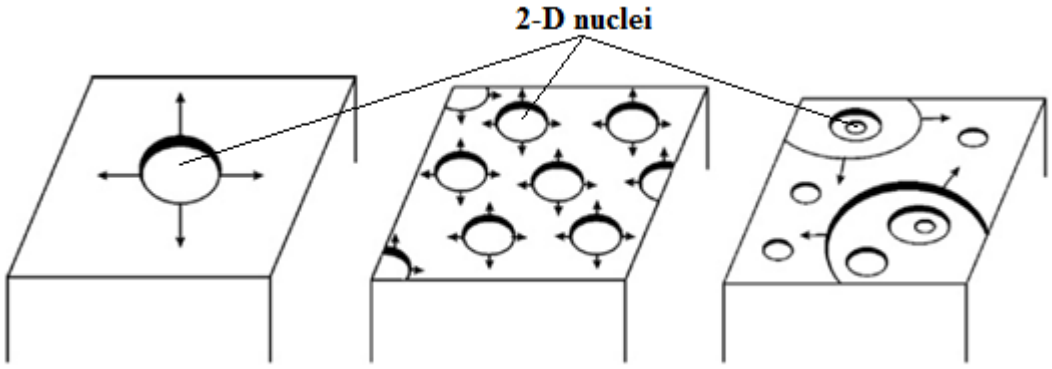

(a) (b) (c)

Figure 2.13 Crystal growth develops from crystal surface; (a) mononuclear model, (B) Polynuclear in one crystal step, (C) Polynuclear in multi steps (Ehrlich et al., 2009).

2.6.2 Factors influencing crystal growth

The crystal growth theories described above are based on the assumption that crystal growth occurs in pure solution and the system is not affected by external factors. Crystal growth rate is affected by various parameters such as supersaturation, temperature of the system, impurities, solution pH, and stirrer speed.

The supersaturation is one of the most important parameters affecting rate of crystal growth. Temperature can change the relative rates of diffusion and surface integration steps for crystal growth. At higher temperatures the growth may be controlled by diffusion steps while at lower temperature growth it may be

controlled by integration step (Jones, 2002). The growth rate also increases when temperature increases (Garside et al., 1982, Maiwa et al., 2006) while the crystal size, shape and crystalline modification may all change with temperature (Ma et al., 2010).

A crucial factor influencing crystal growth is the presence of impurities in the solution. Some impurities can suppress growth entirely; some may enhance growth, while others may exert a highly selective effect, acting only on certain crystallographic faces and thus modified the crystal habit (Mullin, 2001).

The presence of impurities can influence crystal growth rate in a variety of ways;

a. Changing the properties of solution, the equilibrium saturation concentration, and the supersaturation.
b. Changing the characteristics of the adsorption layer at the crystal-solution interface,
c. It may be built into the crystals surface.

Impurities are often adsorbed on to crystal surfaces and retard the crystal growth. The mechanism of impurities being adsorbed onto the crystal surface is shown in Figure 2.14. As can be seen in Figure 2.14 there are three sites in which impurities are possibly adsorbed across the faces, at a kink, and at a step or ledge between steps.

When the seed crystals grow, the impurities are absorbed on the crystal surface. The impurities can block the growth sites. The blockage of the growth site depends on the amount of adsorption of the impurities on the crystal surface. According to Sung at al., (2002) the blockage of the growth site, caused by adsorption of impurities on the crystal surface, can inhibit surface integration. They found that increasing impurities can decrease the total surface integration coefficient because the adsorption of the impurities on the crystal surface increased. In contrast, the total mass transfer coefficient in the crystal growth was not seriously affected by the impurities because the impurities concentration in the solution was sufficiently diluted.

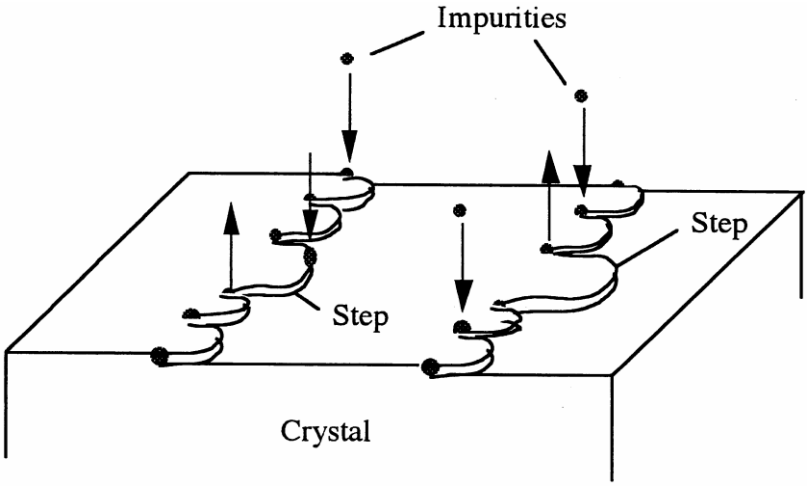

Figure 2.14 Sites for impurity adsorption on a growing crystal (Kubota et al., 1996)

In some cases, the solution pH influences the rate of crystal growth (Tai et al., 2006b). The crystal size, shape and crystalline modification may all change with solution pH (Ma et al., 2010). Effect of solution pH on crystal growth can change the relative rate of diffusion and surface integration steps (Tai et al., 2006a).

Generally, stirring has been adopted as an efficient method for crystallisation so as to maintain crystals in suspension, to assure an adequate rate of energy transfer, and to achieve uniformity of suspension properties throughout the crystallizer. Stirring the solution may help to attenuate the absorption layer so it can influence mass transfer between solution and crystal. Accordingly, the crystal growth rate increase with an increases in stirrer speed (Sung et al., 2002). However, increasing the stirrer speed introduce higher fluid velocity and more violent crystal-impeller collision.

2.6.3 Crystal size distribution analysis

The population balance serves as the basis for characterising the crystal size distribution (CSD) in any crystallisation system. For a batch crystallizer with no net inflow or outflow of crystal, the population balance can be written as (Randolph and Larson, 1988)

$$\frac{\partial(NF)}{\partial t} + NG\frac{\partial F}{\partial L} = 0 \qquad (2.57)$$

where N is the total number of crystals and F is the cumulative size distribution on a crystal number basis.

The presenting CSD is through the use of a crystal population density plots as depicted in Figure 2.15. This curve represents the dependence between the number of crystal per unit volume and crystal size. It is assumed that, in a suspension of growing crystals, at time t the number of crystals between size L_1 and L_2 can be found from the cumulative distribution as $N_1 - N_2$. After a certain time Δt, crystals with the original size L_1 have grown to size $L_1 + L_2$. The average growth rate of crystals will be

$$\boldsymbol{G(L,t)} \cong \frac{\boldsymbol{L_2 - L_1}}{\boldsymbol{(t+\Delta t)-t}} = \frac{\boldsymbol{\Delta L}}{\boldsymbol{\Delta t}} \qquad (2.58)$$

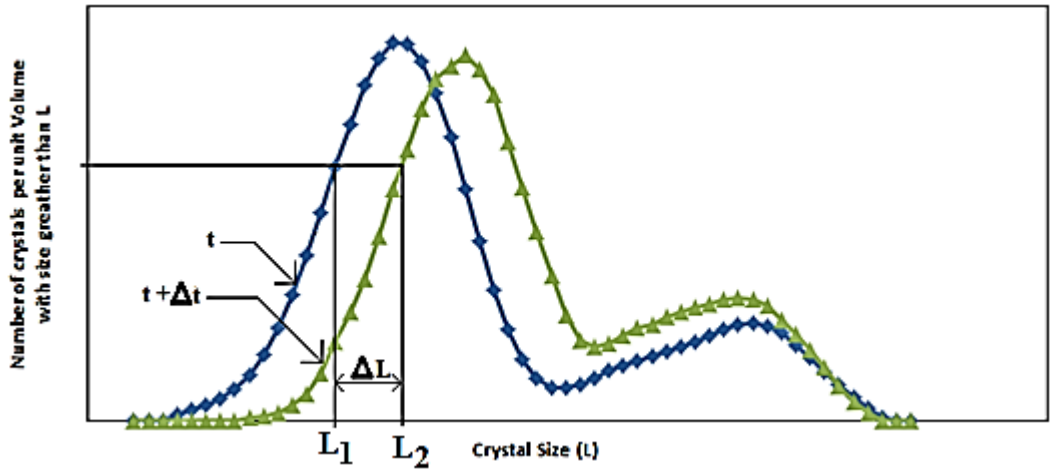

Figure 2.15 Determination of growth rate from cumulative size distribution.

2.7 Dissolution Study

Crystal dissolution plays a key role in many industrial applications and an understanding of the dissolution process allows for the optimization of design and processing conditions, as well as selection of a suitable solvent.

Dissolution is a process in which solids dissolve and enter into the solvent to produce a solution. Dissolution process is controlled by the affinity between the solid and solvent. The Nernst-Brunner stagnant film theory states that dissolution of a solid in a liquid can be described as the transfer of solute from the solid surface into the surrounding solvent (Figure 2.16). The dissolution process based

in Figure 2.16 is described as one where a solid particle is suspended in a liquid which is continuously exposed to the solid surface at a certain relative velocity.

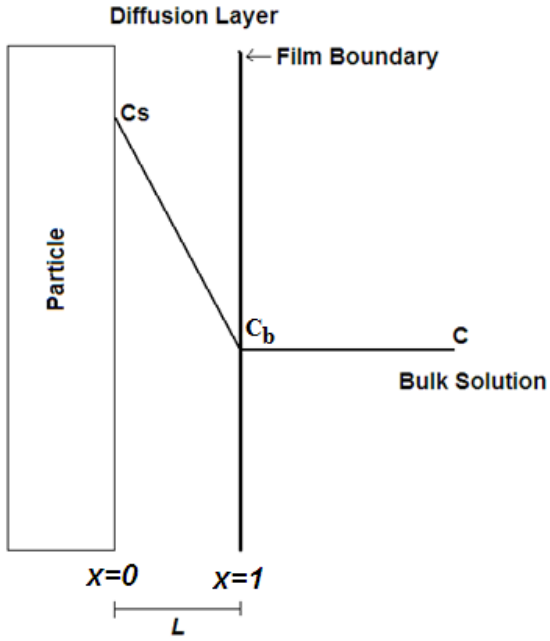

Figure 2.16 Dissolution of particle according to diffusion layer model by Nerst and Brunner (Banakar, 1992)

The dissolution process is assumed in steady state conditions and Fick's first law of diffusion can be applied.

$$\boldsymbol{J = -D\frac{\delta C}{\delta x}} \tag{2.59}$$

where J is the amount of substance passing perpendicularly through a unit surface area per unit time (mg.cm^{-2}.s^{-1}), D is the diffusion coefficient, and $\frac{\delta C}{\delta x}$ is the concentration gradient.

In Figure 2.16, the concentration gradient, $\frac{\delta C}{\delta x}$, is assumed linear, so $C = C_s$ at the surface ($x = 0$), and if $C = C_b$ is the bulk concentration at the interface between the bulk solution and the film ($x = 1$), then $\delta C/\delta x = (C_b - C_s)$. For a mass of substance dissolved in a given volume V of dissolution medium with a surface area A of dissolving solid particle. Eq. (2.56) can be written as

$$\boldsymbol{\frac{V}{A}\frac{dC}{dt} = \frac{-D(C_b - C_s)}{L} = \frac{D(C_s - C_b)}{L}} \tag{2.60}$$

$$\boldsymbol{\frac{dC}{dt} = \frac{-DA(C - C_S)}{V.L}} \tag{2.61}$$

D/L is dissolution rate of K_d, and Eq. (2.16) can be written

$$\frac{dC}{dt} = \frac{K_d A(C_S - C)}{V} \quad (2.62)$$

where K_d is the dissolution rate constant (m/s), A is surface area of suspended crystal (m^2), V is volume of liquid (m^3), C_S is saturation concentration or solubility in the dissolution medium (mol), C_b is mount dissolved or concentration of drug in solution (dissolution medium) at time t (mol).

If A/V is surface area of crystals per unit volume of solution, a, the Eq. (2.63) can be simplified,

$$\frac{dC}{dt} = K_d a(C_s - C_b) \quad (2.63)$$

2.7.1 Methods to increase the dissolution rate

2.7.1.1 Presence of mixing

The Nernst-Brunner stagnant film theory indicates that increasing the thickness of the diffusion layer decreases the dissolution rate. According to Kawashima (2006) the thickness of the diffusion layer is a function of the stirring rate. The various theories of dissolution states that the stirring condition can significantly affect diffusion-controlled dissolution, because the thickness of the diffusion layer is inversely proportional to stirrer speed (Banakar, 1992). According to Masuda et al., (2006), the dissolution rate is correlated with the stirring rate,

$$K = a(N)^b \quad (2.64)$$

where N is the stirring rate, K is the dissolution constant, and a and b are constant. For b = 1, the dissolution process is diffusion-controlled. The interfacial-reaction-controlled is independent of stirring rate when b = 0.

2.7.1.2 Interfacial surface area

Increasing effective surface area in contact with solvent effectively increases the dissolution rate. Eq. (2.63) may be modified according to the Nerst-Burnner diffusion model, where k in Eq. (2.63) become equivalent to the diffusion layer thickness, denoted by h, and divided by the diffusion coefficient of the solute D, and the equation may then be rewritten as:

$$\frac{dC}{dt} = \frac{DA}{h}(C_s - C) \quad (2.65)$$

For a constant surface area A and under condition ($C_s >> C$), Eq. (2.66) becomes:

$$\frac{dC}{dt} = \frac{DAC_s}{h} \quad (2.66)$$

or

$$\frac{dC/dt}{AC_s} = \frac{D}{h} \quad (2.67)$$

According to Eq. (2.68), the dissolution rate is proportional to both solubility and the surface area.

2.7.1.3 Temperature

Temperature influences the dissolution performance. Further crystal solubility is temperature dependent. So controlling temperature during the dissolution process is crucial. The effect of temperature variations of the dissolution system depends mainly on temperature-solubility curves of the crystal. Increasing temperature of a solvent increases the internal energy of both solvent and solute molecules. As a result, solute particles break loose and dissolve faster and thus generally higher temperatures result in higher dissolution rates, as reported magnesium oxide (MgO) (Fedoročková and Raschman, 2008), ulexite or sodium–calcium–borate hydrate ($Na_2O{\cdot}2CaO{\cdot}5B_2O_3{\cdot}16H_2O$) (Demirkiran, 2008), Probertite ($NaCaB_5O_9{\cdot}5H_2O$) (Mergen and Demirhan, 2009).

2.7.1.4 Solution pH

Dissolution rate of crystal can be influenced by solution pH. In most cases there is a change in pH of the dissolution medium associated with the addition or deletion of the constituents to the dissolution medium. Dissolution of solid in aqueous acidic solutions have been widely studied (Blesa et al., 1994, Demirkiran, 2008, Bhuiyan et al., 2009, Amram and Ganor, 2005). They all showed that decreasing pH in acidic solutions increases rate of dissolution. Faster disintegration and thus enhanced dissolution rates which was observed due to the higher acidity of the dissolution medium. Due to corrosive action of the acidic fumes, however, it is currently a general practice to use distilled water unless investigative studies show a specific need for an acidic solution in order to generate meaningful dissolution data. Such corrosive effect can be avoided by replacing hydrochloric acid with acidic buffers, such as sodium acid phosphate, to maintain low pH.

The effect of NaOH solution used in the dissolution of gibbsite ($Al(OH)_3$) showed that increasing the concentration of NaOH was not significantly increasing its dissolution rate (Pereira et al., 2009).

2.8 Struvite Study

2.8.1 Struvite Potential from Wastewater in Western Australia

Domestic wastewater can be classified in two categories namely greywater and blackwater (Babin, 2005). Greywater is wastewater from bathrooms, laundries, and kitchen sinks. Blackwater is the wastewater expelled through toilets, urinals or bidets that is characterized by a high level of human excrement and requires an intense treatment process before it is able to be reused. According to Water Corporation of Western Australia (2006), 150 to 200 liters of wastewater is discharged daily per person. According to Babin (2005) approximately 390 litres is produced per day per average household in Western Australia.

The three main sources of greywater are;

1. Bathroom greywater, makes up approximately 55% of the greywater produced by an average household. The dominant contaminants consist of soaps, shampoos, hair dyes, toothpaste, lint, body fats and cleaning products.
2. Laundry greywater, amount to 34% of household greywater. Contaminants consist of lint, oils, greases, chemicals, soaps, nutrients and other compounds.
3. Kitchen greywater, amount to 11% of household greywater originates. This wastewater is contaminated with food particles, cooking oils, grease, detergents and dishwashing powders.

Table 2.1 shows that the production of phosphorous and ammonia per day is about 3 grams per person and 9 grams per average household (assumed 3 persons). The population of Western Australia in 2009 was 2,224,300 people (Statistics, 2009). So, the amount of ammonia and phosphorous in 1 day is 6,600 tons, and 2,400 tons a year. This amount offers a potential in recovering struvite as a fertilizer. If the recovery of struvite is 95%, about 2,300 tons per year would be recovered.

On the other hand, the properties of domestic greywater lead to problems of scale formation in wastewater treatment plants where crystallisation occurs under natural conditions. Accumulation of struvite deposit in pipes and pumps increases

in maintenances, control and labour costs to remove struvite scale in wastewater treatment plants. The control of struvite deposition has been widely investigated, including the dilution of struvite concentration with effluent water (Borgerding, 1972), prevention action by chemical dosing of iron salts (Mamais et al., 1994), or addition of chemical inhibitors (Doyle et al., 2003, Snoeyink and Jenkins, 1980).

Struvite is chemically known as magnesium ammonium phosphate hexahydrate ($MgNH_4PO_4.6H_2O$). Struvite usually precipitates as stable white crystals in a 1:1:1 molar ratio according to the following reaction (Le Corre et al., 2005) where *n* can be 0, 1 or 2:

$$\mathbf{Mg^{2+} + NH_4^+ + H_nPO_4^{n-3} + 6H_2O \rightleftarrows MgNH_4PO_4.6H_2O + nH^+} \quad (2.68)$$

Its composition (i.e., nitrogen, phosphor, and magnesium ion in equal molar concentrations) makes it a potentially marketable product for the fertilizer industry, provided that its nucleation and the quality of crystals recovered can be controlled (Booker et al., 1999). Phosphorus recovery methods have been successfully applied in several bench and pilot scales such as in Japan (Ueno and Fujii, 2001), Netherland (Giesen, 1999), and Italy (Battistoni et al., 2005, Cecchi et al., 2003). Application of struvite crystals as fertilizer for agriculture showed that the Chinese cabbage growth rate increased as struvite dosage increased and the optimum dosage was 1.6 g struvite/kg soil (Ryu et al., 2012).

Table 2.1 Greywater composition compared with Raw Sewage (Babin, 2005)

Parameter	Unit	Greywater	Raw Sewage
Suspended Solids	mg/L	45 – 330	100 – 500
Turbidity	NTU	22 – >200	NA
BOD	mg/L	90 – 290	100 – 500
Nitrite	mg/L	<0.1 – 08	1 – 10
Ammonia	mg/L	<0.1 – 25.4	10 – 30
Total Phosphorous	mg/L	0.6 – 27.3	5 – 30
Sulphate	mg/L	7.9 – 110	25 – 100
pH		6.6 – 8.7	6.5 – 8.5
Conductivity	mS/cm	325 – 2240	300 – 800
Hardness (Ca & Mg)	mg/L	15 – 55	200 – 700
Sodium	mg/L	29 – 230	70 – 300

2.8.2 Struvite Characteristic

The chemical formula of struvite crystals is $MgNH_4PO_4.6H_2O$ with molecular weight of 245.43 g/mol and density of 1.711 g/cm^3 (Borgerding, 1972). The solubility of struvite in deionized water at 25^{O}C is 169.2 mg/l (Bhuiyan et al., 2007). Its solubility constant is $10^{-13.26}$ (Ohlinger et al., 1998). The struvite morphology is an orthorhombic structure with cell dimensions a_0 = 6.941 ± 0.002 Å, b_0 = 6.l37 ± 0.002 Å,c_0= ll.199 ± 0.002 Å (Abonna and Boistelle, 1979). Figure 2.17 describes a struvite structure consisting of regular PO_4^{3-} tetrahedra, distorted $Mg(H_2O)_6^{2+}$ octahedra, and NH_4^+ groups where they are held together by hydrogen bonding. The experiment conducted by Whitaker and Jeffery (1970) showed that the structure of struvite may be thought as a tri-dimensional framework of hydrogen bonding having an ionic character.

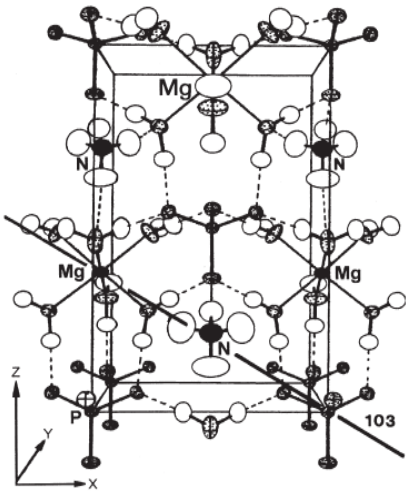

Figure 2.17 The struvite crystal structure (Whitaker and Jeffery, 1970)

2.8.3 Solubility of Struvite

Struvite production from wastewater containing phosphorous, ammonium and magnesium has gained substantial interest and progress in recent time. However, discrepancies continue to exist between reported values of some of the most important operating parameters for struvite crystallisation. The solubility of struvite can be investigated by studying its dissolution in water;

$$\mathbf{MgNH_4PO_4.6H_2O_{(S)} \rightarrow Mg^{2+} + NH_4^+ + PO_4^{3-} + 6H_2O} \quad (2.69)$$

One such parameter is the solubility product, K_{sp}. This parameter is important in the determination of supersaturation (S), the parameter that determines if struvite formation is possible or not. Solubility can be calculated from the total molar concentration of ions (Kc), or ion activity (Ksp) in the solution (Bouropoulos and Koutsoukos, 2000, Bhuiyan et al., 2007). Supersaturation is defined as the ratio of ion activity product (IAP) to the equilibrium solubility product of struvite (K_{sp}) Ksp and Kc values are given by the following general expressions:

$$\mathbf{K_{sp}} = \{\mathbf{Mg^{2+}}\}\{\mathbf{NH_4{}^+}\}\{\mathbf{PO_4{}^{3-}}\} = \boldsymbol{\gamma}_{\mathbf{Mg^{2+}}}[\mathbf{Mg^{2+}}]\,\boldsymbol{\gamma}_{\mathbf{NH_4^+}}[\mathbf{NH_4{}^+}]\,\boldsymbol{\gamma}_{\mathbf{PO_4^{3-}}}[\mathbf{PO_4{}^{3-}}] \quad (2.70)$$

$$\mathbf{K_c} = [\mathbf{Mg^{2+}}][\mathbf{NH_4{}^+}][\mathbf{PO_4{}^{3-}}] \quad (2.71)$$

$$-\mathbf{pK_{sp}} = \mathbf{logK_{sp}} \quad (2.72)$$

$$\boldsymbol{S} = \frac{\boldsymbol{IAP}}{\boldsymbol{K_{sp}}} \quad (2.73)$$

where γ is activity co-efficient of the ion.

Table 2.2 Reported Solubility Products for Struvite

Authors	Ksp	pKsp	Solution
Borgerding (1972)	9.41	3.89×10^{-10}	Wastewater
Abbona et al. (1982)	9.94	1.15×10^{-10}	Aqueous solution
Buchanan et al. (1994)	12.36	4.36×10^{-13}	Simulation
Webb and Ho (1992)	12.76	1.74×10^{-13}	Water
Burns and Finlayson (1982)	13.12	7.50×10^{-14}	Water
Aage et al. (1997)	12.93	1.17×10^{-13}	Aqueous solution
Taylor et al. (1963)	13.15	7.08×10^{-14}	Aqueous solution
Ohlinger et al. (1998)	13.27	5.37×10^{-14}	Synthetic supernatant
Bavic-Ivancic et al. (2002)	13.36	4.37×10^{-14}	Aqueous solution
Bhuiyan et al. (2007)	13.36	4.33×10^{-14}	Water

Solubility product, K_{sp}, is highly dependent upon solution pH. The solution pH influences the component concentrations. So, new equilibrium solubility is reached at each solution pH. If supersaturation is used as a control variable, it is essential to know the true value of K_{sp} for the pH range that the systems are expected to operate in. Although extensive studies on struvite solubility have been

reported in Table 2.2, there still exists significant variation between reported of *pKsp* values: $4.33 \times 10^{-14} - 1.15 \times 10^{-10}$ (K_{sp} from 9.41 to 13.36). This variation may be related to the large range of experimental methodologies. The standard method for the experimental determination of a K_{sp} value is dissolution of struvite using distilled water as solvent. In addition, the presence of common-ion, such as Cl^- ion, influences solubility product. The presence of common-ions in water is important in understanding ionic equilibrium, ion-solvent and ion-interaction in natural water. Accurate and reliable data on solubility of struite on common-ion system are necessary for many industrial processes where these systems are used as feed. Therefore, the study of the solubility of struvite in aqueous electrolyte solutions may help in the understanding of the solubility behaviour of struvite. The proposed studies are conducted under a range of solution pH, temperature, and Cl^- ions as impurities.

Solubility of struvite is influenced by several factors such as pH, temperature, degree of supersaturation, and the presence of other ions (Bouropoulos and Koutsoukos, 2000).

2.8.3.1 Effect of Temperature

Solubility usually increase with increasing temperature, though there are some materials whose solubilities constant or even decrease with increase of temperature. As can be seen in Figure 2.18, struvite solubility increases with temperature from 10 to 35^{O}C, but declines with increasing temperature above 35 ^{O}C. Bhuiyan et al., (2007) proposed that in the 10 – 35^{O}C, dissolution of struvite is endothermic whereas above 35^{O}C, the crystallisation become exothermic.

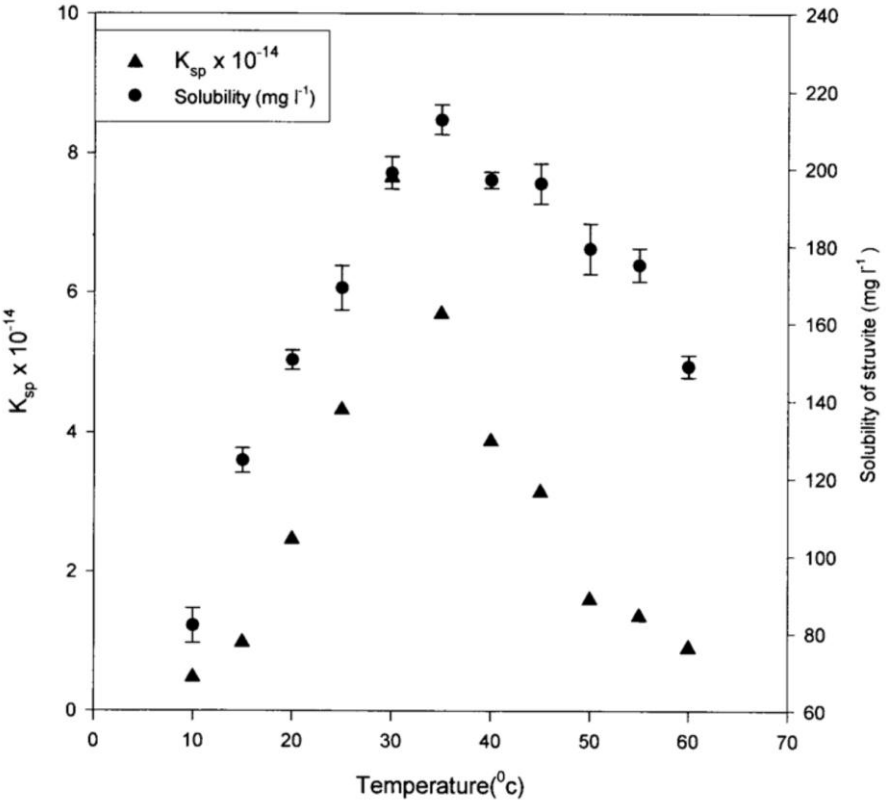

Figure 2.18 Various of solubility (mg/l) and K_{sp} of struvite with temperature (Bhuiyan et al., 2007)

2.8.3.2 Effect of solution pH

The solubility of struvite crystals is at a minimum at pH of about 10.5 (Figure 2.19). Figure 2.19 is a plot of several struvite solubility limit curves, at 25^{O}C, presented to illustrate the cumulative effects on the work of Stumm and Morgan (1995), including ionic strength (Snoeyink and Jenkins, 1980), magnesium phosphate complexes, and pK_{SO} 13.26 (Ohlinger et al., 1998).

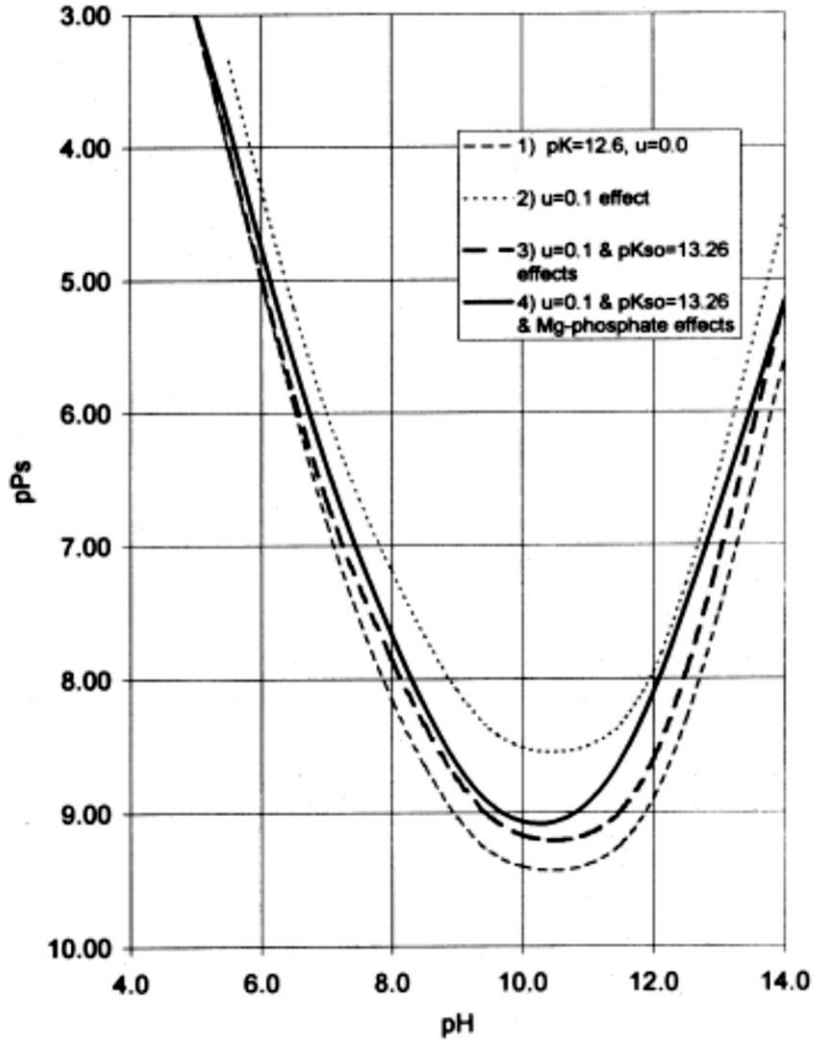

Figure 2.19 Struvite solution products versus pH, where *u* is ionic strength. (Ohlinger et al., 1998)

The conditional solubility product reached its minimum at pH = 10.7. In principle, a crystallisation is possible within the pH range 9 – 10 (Stumm and Morgan, 1995).

Solubility of struvite crystals depends on the ion activity product (*IAP*) of Mg^{2+}, NH_4^+, and PO_4^{3-}. The equilibrium *IAP* is 7.08×10^{-14} (Nelson et al., 2003). Struvite is formed in solution if the *IAP* from solid phase is greater than thermodynamic solubility product (K_{sp}). The *IAP* can be controlled by solution pH. The solution pH influences the activities of both NH_4^+ and PO_4^{3-} ions. Influence of solution pH on PO_4^{3-} ions has greater influence on the formation of struvite than NH_4^+ ions. Because concentration of NH_4^+ ions decreases

significantly from 99 to 64 % when the solution pH increases from 7 to 9, while PO_4^{3-}concentration increases 250 fold in the same range of pH change (Stumm and Morgan, 1995). The maximum ammonium ions is formed at pH < 9.4, and when pH > 9.4 ammonia will be formed (Weiner, 2008). The same results were also obtained by Zang, et al. (2009). Their experiments were done by using the coking wastewater resulting in maximum NH_4^+ removal at pH 9.5. In general, solubility of struvite crystals decreases with increasing solution pH.

2.8.3.3 Effect of impurities

Pure solutions are rarely encountered outside the analytical laboratory, and even then the impurity levels are usually well within detectable limits. Industrial solutions, on the other hand, are almost invariably impure, by any definition of them, and the impurities present can often have a considerable effect on the solubility characteristic of the main solute, such as ionic equilibrium, ion-solvent and ion-ion interaction.

Addition of NaCl in water increases the solubility of struvite crystals while its ionic strength decreases (Bhuiyan et al., 2007). Decreasing ionic strength is caused by a complex formation on bulk solution during dissolution of crystals. The experimental study conducted by Ronteltap et al., (2007) used urine, which has characteristic a high amounts of sodium, ammonium, carbonate and sulphate, to investigate its effect on solubility of struvite. The calculation of solubility showed that complex formation ($[MgCO_3]_{aq}$, $[MgHCO_3]^+$, $[MgPO_4]^-$, $[NH_4HPO_4]^-$, and $[NaHPO_4]^-$) has a substantial influence on the number of free ions that participate in struvite formation.

2.8.4 Nucleation of Struvite Crystals

Struvite nucleation occurs when the activities of solution containing Mg^{2+}, NH_4^+, and PO_4^{3-} ions exceed the respective solubility product. The majority of published works related on struvite nucleation were mostly conducted with reaction-controlled in aqueous solution at constant temperature and various initial solution pH (Bhuiyan et al., 2008, Bouropoulos and Koutsoukos, 2000). The supersaturated solution was made at constant temperature and pH (Kofina and

Koutsoukos, 2005, Bouropoulos and Koutsoukos, 2000) and nucleation studies resulted in two linear parts (homogeneous and heterogeneous nucleation). This beheviour may be impacted by stability of the solution because of solution pH, so the charge polarity of solution may be different (Degan and Kosec, 2000). However, fundamental nucleation theory states that both homogeneous and heterogeneous nucleation can occur.

The extent of struvite nucleation and characteristics of the precipitating solid depends on solution conditions such as, supersaturation, solution pH, temperature, and presence of foreign ions.

2.8.4.1 Effect of supersaturation

The driving force for the formation of struvite in aqueous supersaturated solution is difference between the chemical potentials,$\Delta\mu$, of the salt in the supersaturated solution μ_S and its corresponding value at equilibrium, μ_∞:

$$\Delta\boldsymbol{\mu} = \boldsymbol{\mu}_\infty - \boldsymbol{\mu}_S = \left[\boldsymbol{\mu}_\infty^0 + \mathbf{kT}.\ln\left(\mathbf{a}_{Mg^{2+}}.\mathbf{a}_{NH4^+}.\mathbf{a}_{PO_4^{3-}}\right)_\infty^{1/3}\right] - \left[\boldsymbol{\mu}_S^0 + \mathbf{kT}.\ln\left(\mathbf{a}_{Mg^{2+}}.\mathbf{a}_{NH4^+}.\mathbf{a}_{PO_4^{3-}}\right)_S^{1/3}\right] \quad (2.74)$$

Assuming that the chemical potentials of the standard states in the supersaturated solution and at equilibrium are equal, the difference in chemical potential is

$$\Delta\boldsymbol{\mu} = \mathbf{kT}\ln\frac{\left(\mathbf{a}_{Mg^{2+}}.\mathbf{a}_{NH4^+}.\mathbf{a}_{PO_4^{3-}}\right)_\infty^{1/3}}{\left(\mathbf{a}_{Mg^{2+}}.\mathbf{a}_{NH4^+}.\mathbf{a}_{PO_4^{3-}}\right)_S^{1/3}} = -\frac{\mathbf{kT}}{\mathbf{3}}\ln\mathbf{S} \quad (2.75)$$

where *k* is the Boltzmann's constant and *T* is the absolute temperature. The logarithmic term is supersaturation ratio *S* given by

$$\mathbf{S} = \frac{\mathbf{a}_{Mg^{2+}}.\mathbf{a}_{NH4^+}.\mathbf{a}_{PO_4^{3-}}}{\mathbf{K_{SO}}} \quad (2.76)$$

where K_{SO} is the thermodynamic solubility product of struvite.

$$\mathbf{SI} = \log \boldsymbol{S} \quad (2.77)$$

Saturation index (*SI*) is a measure of the deviation of the system from equilibrium and a measure of the driving force for the crystallisation. For *SI = 0*, the solution is saturated (equilibrium), for *SI > 0* the solution is supersaturated and

crystallisation may occur, while for $SI < 0$ the solution is undersaturated and dissolution may take place.

A number of computer models to calculate saturation index based on chemical equilibrium models have been developed and used by previous researchers, such as STRUVITE, MINTEQ+, MINTEQA2, and MINEQL+. Several researchers have also been used Phreeqc (Bouropoulos et al., 2004, Md. Ali and Schneider, 2005). PhreeqC is a computer program designed base on an ion-association aqueous model for simulating chemical reaction in polluted water (Parkhurst and Appelo, 1999). Moreover, PhreeqC provides well-established thermodynamic databases which can be used depending on user specification (Bhuiyan et al., 2007). The calculation of saturation index of struvite involves chemical equilibrium constant at $25^{O}C$, collected from other sources. Major equilibria involved in the computation of solution species are shown in Table 2.3.

The supersaturation is one of the most important factors to control struvite formation. If supersaturation is too high, primary homogeneous nucleation can occur in the solution.

2.8.4.2 Effect of solution pH

The supersaturation is a function of pH, as well as the concentrations of magnesium, ammonium, and phosphate. For struvite crystallisation, magnesium, ammonium and phosphate ion concentration are equally important, so the supersaturation takes account all three struvite constituent ion concentrations at a given pH.

Several authors have studied the effect of pH on struvite crystallisation. For instance, Booker et al. (1999) and Stratful et al. (2001) suggested an optimum pH range for the crystallisation of struvite is 8.5 – 9.5. They could precipitate up to 85 % of the theoretical yield. However at pH 7, no struvite was produced in any detectable quantities and at pH 7.5 only a minute amount of very small crystals were produced.

Table 2.3 Equilibria involved in the computation of the solution specification

Equilibrium	Log K	ΔH_r^o(kJ/mol)
$2H+ + HPO4^{2-} = H_3PO_4$	9.37	3.744
$H+ + PO_4^{3-} = HPO_4^{2-}$	12.37	-14.769
$H+ + HPO_4^{2-} = H_2PO_4^-$	7.2	-4.205
$Mg^{2+} + OH^- = MgOH^+$	2.6	
$H^+ + OH^- = H_2O$	14	-55.906
$H_2PO_4^- + Mg^{+2} = MgH_2PO_4^+$	0.45	14.225
$HPO_4^{-2} + Mg^{+2} = MgHPO_4$	2.87	13.807
$Mg^{+2} + PO4^{-3} = MgPO_4^-$	4.8	12.97
$H^+ + NH_3 = NH_3H^+$	9.24	-51.92
$Mg^{+2} + NH_3 = MgNH_3^{+2}$	0.24	19.037
$Mg^{+2} + 2NH_3 = Mg(NH_3)_2^{+2}$	0.2	0
$Mg^{+2} + 3NH_3 = Mg(NH_3)_3^{+2}$	-0.3	0
$Mg^{+2} + SO_4^{-2} = MgSO_4$	2.37	0
$CO3^{-2} + Mg^{+2} = MgCO_3$	2.98	11.351
$HCO_3^- + Mg^{+2} = MgHCO3^+$	1.07	3.305
$Cl^- + Mg^{+2} = MgCl^+$	-0.135	-0.586
$Mg^{+2} + NH_3H^+ + PO_4^{-3} = MgNH_4PO_4$	**	-23.62

(**) $-1157.45 - 0.784T - \frac{63.86}{T} + 556.83 \log T + \frac{19.54}{T^2}$(Bhuiyan et al., 2007)

2.8.4.3 Effect of Temperature

Temperature has a direct influence on the solubility of struvite and its thermodynamic properties (Wang et al., 2006). The experiment conducted by Bhuiyan (2009) clearly showed that the variation of solubility product increase with increasing temperature between 20 and 30 C, and reached its maximum value at 35^OC, thereafter it decreases. These results will directly impact on supersaturation where the relative supersaturation increases with increasing temperature until 35^OC and then decreases.

From classical nucleation theory, one of the variables that affects the nucleation rate is temperature (Eq. (2.79)) (Mullin, 2001).

$$\log t_{ind} \approx \left[\frac{\gamma^3}{T^3(\log S)^2}\right] \quad (2.78)$$

According to classical nucleation theory in Eq. (2.79) indicates that the decreasing induction time is not only caused by higher temperature but higher supersaturation and smaller interfacial energy of crystals.

2.8.4.4 Effect of Impurities

In the case of struvite crystallisation from wastewater sludge, foreign compound are numerous (amongst them potassium, chloride, calcium, carbonate) and could be adsorbed on to crystal surface and retard struvite formation.

Impurity effect on struvite crystallisation have been studied, such as the addition of calcium ions (Le Corre et al., 2005, Bouropoulos and Koutsoukos, 2000), carbonate ions (Le Corre et al., 2005), calprotection (Asakura et al., 1998), fluoride (Ryu et al., 2008), HCO_3^- (alkalinity) (Bhuiyan et al., 2008) and ethylenediaminetetraacetic acid (EDTA) (Doyle et al., 2003).

The effect of high impurities concentration clearly inhibited sturvite formation. According to Ryu et al (2005), with initial fluoride concentration below 592 mg/L, the NH4–N and PO4–P removal efficiencies increased by over 70% and 80%, respectively. However, initial fluoride concentration increased to over 600 mg/L, the NH4–N and PO4–P removal efficiencies decreased. In addition, the presence of impurities, such as calcium, can affect the shape, size and crystal purity (Mersmann, 2001). On the other hand, impurities can also be used to dissolve struvite crystals, as Doyle et al. (2003) showed that more struvite crystals can be dissolved 90% by EDTA.

A few studies have investigated the influence of impurities on nucleation of struvite crystals. The presence of impurities in the system can lengthen the induction time preceding the first occurrence of crystals (Bouropoulos and Koutsoukos, 2000, Kofina and Koutsoukos, 2005).

When impurity molecules adsorb onto the nucleus surface, interfacial tension (γ) and nucleation rate (J) can be affected. Therefore, an impurity in the solution can either promote nucleation through a decrease in γ as a result of adsorption on the nucleus or has no effect on J when there is no adsorption.

For those reasons, it becomes important to study the nucleation of struvite crystals in the absence and presence of impurities. The induction times were experimentally determined as function of initial pH by pH measurement. It is possible it has been possible to estimate the activation energy and to evaluate the interfacial tension between struvite crystals and the surrounding aqueous solution.

2.8.4.5 Measurement techniques on nucleation struvite

Various indicators have been used to detect the induction period which is a common measure of nucleation: light scintillations (Ohlinger et al., 1999), conductivity (Cheng and Li, 2010, Loewenthal et al., 1994), turbidity (Münch and Barr., 2001, Perera et al., 2009), pH monitoring (Suzuki et al., 2007, Rajesh et al., 2009), fourier transform infrared spectroscopy (Lindenberg and Mazzotti, 2009). Each method has a different sensitivity and indicated a different "end" for the induction period. The advantages of using pH monitoring for induction period measurements over more sophisticated methods are the low cost, availability, ease to use and more sensitive than visual detection of crystals.

Mixing speed can also influence nucleation. Ohlinger et al., (1999) showed that induction time is only marginally affected for agitation speeds speed from 360 to 1060 rpm. However, at lower stirrer speed ranged from 50 to 120 rpm, the induction time was more significant. In addition, Abonna and Boistelle (1985) showed that the induction time of struvite at a S = 2.5 was of 24 h without agitation.

Table 2.4 gives a hit of different induction time measurement for struvite.

Table 2.4 Induction times reported for struvite nucleation

	Crystallisation method	Induction time measurement method	Condition	Supersaturation S	Induction time	Agitation
Ohlinger et al., (1999)	Spontaneous crystallisation ($MgCl_2.7H_2O + NH_4H_2PO_4$)	Visual observation of light scintillations	pH 6.3–7.9; 22^OC	S = 1.6 S = 2.1 S = 3.1	33 min 1 min 0.33 min	570 rpm
Boistelle and Abonna (1985)	Spontaneous crystallisation ($MgSO_4.H_2O + NH_4H_2PO_4$)	pH measurement	Various initial pH solution; 25^OC	S = 1.4 S = 2.5 12 < S < 25	24 hr 24 hr 1 min	No agitation
Bouropoulos and Koutsoukos (2000)	Spontaneous crystallisation ($MgCl_2.7H_2O + NH_4H_2PO_4$ in 0.15 M NaCl)	pH Measurement	pH 8.25; 25^OC	S = 1.13 S = 2.27 S = 3.33	125 min 42 min 6 min	Magnetic stirrer
Kofina and Koutsoukos (2005)	Spontaneous crystallisation ($MgSO_4.7H_2O + NH4H_2PO4$)	pH measurement	pH 8.5; 25^OC	S = 2.1 S = 3.3 S = 4.3	24.7 min 11.8 min 4.2 min	Magnetic stirrer
Kabdasli et al., (2006)	Spontaneous crystallisation ($MgCl_2.6H_2O + NH_4H_2PO_4$)	Light scattering, pH measurement, turbidity, absorbance and particle size measurement	Various initial pH solution (8.5 – 9.0); 25^OC	S = 2.35 S = 3.21	14 min 3.5 min	Magnetic stirrer
Bhuiyan et al., (2008)	Spontaneous crystallisation ($(NH_4)_2HPO_4 + NH_4Cl + MgCl_2.6H_2O$)	pH measurement	$8.2 \leq pH \leq 8.51$; 25^OC	SI = 1.38 SI = 1.52 SI = 1.83	8.33 min 2.08 min 0.2 min	120 rpm
This study	Spontaneous crystallisation ($MgCl_2.7H_2O + NH_4H_2PO_4$ in excess Cl^- solution)	pH Measurement	pH 8 and 8.5; 20, 25 and 30^OC	1.2 < SI < 2	-	Magnetic stirrer

SI = Saturation index (See Eq. 2.13)

2.8.5 Growth of Struvite Crystals

Struvite crystallisation from wastewaters occurs when the concentration of Mg^{2+}, NH_4^{1+} and PO_4^{3-} exceed its solubility limit (Li and Zhao, 2003). Predicting and controlling struvute nucleation and growth from wastewater is fundamental for crystalliser design and is complex as it is controlled by a combination of thermodynamic and mass transfer properties along with various physico-chemical factors, such as solution pH, supersaturation, mixing, crystal sizes and the presence of foreign impurities.

Knowledge of the effect of solution pH, temperature, impurities, seed and hydrodynamic condition on the struvite crystallisation is very important for struvite formation. Despite the great interest of struvite formation mechanism, knowledge of struvite cyrstallisation and its kinetics is complex. Therefore, this study seeks to explore the effect of solution pH, impurities, crystal size and hydrodynamic condition on the struvite crystallisation especially on the kinetics of struvite crystal growth. Struvite crystallisation kinetics was studied under different condition to find out the kinetic rate constant.

2.8.5.1 Effect of Stirrer Speed

A large number of studies on struvite crystallisation is limited on the application oriented thermodynamics such as struvute solubility and much less on the kinetics (Matynia et al., 2006). The crystal growth kinetic is greatly influenced by hydrodynamic condition. In industrial practice, there is always a stirrer or other device in places that not only ensure homogeneity between crystals and solution but also accelerates the growth of crystals. There are few reported results a stirrer speed effect, the interrelationship between hydrodynamics and crystallisation is complex and poorly understood and, hence, a better understanding of the hydrodynamic influences on crystallisation processes is of significant industrial importance.

It is a well-known fact that the crystal growth kinetics is greatly influenced by hydrodynamic condition. Several authors have studied the crystal growth of struvite in different crystallizers such as stirred vessel (Matynia et al., 2006, Pastor et al., 2008, Wilsenach et al., 2007), stirrer with circulated liquid (Le Corre

et al., 2007), continuous draft tube (Koralewska et al., 2009), fluidized bed reactor (Bhuiyan et al., 2008), and aeration reactor (Suzuki et al., 2007).

A common crystallizer is a stirred batch reactor where an impeller is placed centrally in the vessel and to prevent swirling flow is added four baffles. Moreover, the baffles do not only serve to improve mass transfer, suspends crystals, but also produces a more uniform crystalline product and reduces batch time (Jones, 2002).

Uludag-Demirer and Othman (2009) showed that effect of stirring speed was not significant for struvite crystallisation . Stirrer speed can create segregation and attrition which influence the spontaneous nucleation rate, resulting in a change in crystals number, size, and thus final CSD (Triger et al., 2012). According to Jones (2002) the stirrer speed influences nucleation and growth of crystals. Nucleation of struvite investigated by Ohlinger et al. (1999) and Wang et al. (2006) showed that mixing could shorten induction period. Investigation conducted by Kim et al. (2009) showed that high mixing intensity (u) and mixing duration (t_d) at above 2×10^5 was effective for the removal of 80 % nitrogen and 70 % phosphorous. This indication shows that mixing not only accelerate nucleation but also effective in the removal of nitrogen and phosphorus.

The NH_4^+ removal efficiency was 44% and 38% at 400 and 160 rpm after 10 minutes reaction time, respectively (Zhang et al., 2012). There is no significant change with reaction time over 10 minutes and the optimum stirrer speed is around 160 rpm (Zhang et al., 2012). Some of authors studied struvite formation used stirrer speed range between 10 – 100 rpm (Rahaman et al., 2008, Capdevielle et al., 2013). Higher mixing intensity with uniform suspension favours crystal growth (Akrap et al., 2010). The lowest growth rate of 1.8 g/m^2.d occurred in the quiescent zone, but at high mixing speed, growth rate increases to be 22.4 g/m^2.d (Ohlinger et al., 1999). Higher mixing speed causes more attrition of crystal. In this case, it is caused by collisions amongst crystals and the wall of the crystallizer, baffle, impeller or other crystals (Akrap et al., 2010). Moreover, at low mixing speed, homogeneity of the slurry may not be achieved (Shimamura et al., 2003).

2.8.5.2 Effect of impurities

Any foreign substance other than the crystallizing compound is considered as an impurity. Thus, a solvent used for growth and any other compound deliberately added to the growth medium or inherently present in it is an impurity. Influence of impurities in growth media has been recognized in changing growth habits of crystal. Adsorption of impurities onto crystal faces changes the relative surface free energies of the faces and may block sites essential to the incorporation of new solute into the crystal lattice. These effects may results in changes in growth kinetics and hence inhabit modification of the crystalline phase.

Main wastewater contains many ionic species (e.g., Cl^-, K^+, etc.) that can influence the supersaturation of struvite by reacting with its component ions, Mg^{2+}, PO_4^{3-}, and NH_4^+. Moreover, the presence of impurities in solution can block or inhibit struvite growth. The presence of impurities can increase or decrease crystal size (Jones, 2002). The presence of impurities, such as calcium and carbonates ions (Le Corre et al., 2005), in solution affected the struvite growth rate, The study conducted by Kabdasli et al. (2006) showed that the effect of sodium, calcium, sulphate and carbonate-bicarbonates ions influenced induction time, struvite crystal morphology, and crystal sizes.

2.8.5.3 Effect of solution pH

Supersaturation and pH have been found to be the most influential parameters for struvite crystallisation (Mehta and Batstone, 2013). Struvite is highly soluble at acidic pH and highly insoluble in alkaline pH (Matynia et al., 2006, Münch and Barr., 2001). Increasing solution pH from 8 to 10 can achieve higher degree of P-removal through struvite crystallisation (Battistoni et al., 2001, Celen and Türker, 2001, Münch and Barr., 2001, Ohlinger et al., 1999, Stratful et al., 2001). According to Mavinic at al., (2003) 90% P-removal was achieved at pH of 8.3. Besides PO_4 removal, the NH_4 removal is also influenced by pH. Under fixed molar ratio of $Mg:NH_4:PO_4$, the NH_4 removal trend reflected that if pH values were maintained below 9.0, the removal efficiency increased with increase of pH, but decreased for pH values greater than 9.5 (Kumar and Pal, 2013).

In term of thermodynamic equilibrium, hydrogen ion are released in to solution during the struvite crystallisation. The crystallisation of struvite was inhibited due to low pH of solution (≤ 7) as ionic activity of HPO_4^{2-} decreases and favour greater NH_4^+ formation, whereas high pH values (≥ 11) strongly promotes NH_3 volatilization and result in other precipitates like $Mg_3(PO_4)_2$ and $Mg(OH)_2$ (Philippe et al., 2011, Kumar and Pal, 2013). When solution pH rises above 10.0 the following reactions take place easily (Maekawa et al., 1995).

$$\mathbf{3Mg^{2+} + 2PO_4^{3-} \longrightarrow Mg_3(PO_4)_2} \quad (2.79)$$

$$\mathbf{Mg^{2+} + 2H_2O \rightleftarrows Mg(OH)_2 \downarrow + H^+} \quad (2.80)$$

pH control is one of the main factors influencing the crystallizing process to remove nutrients such as nitrogen and phosphorus from solution to form struvite crystals (Perera et al., 2009, Münch and Barr., 2001). A small pH variation may reduce surface area available to the growth unit caused by changes significantly in the zeta potential of the particle leading to the eventual destabilization of suspension by aggregation (Bouropoulos and Koutsoukos, 2000).

Struvite formation will be favoured to precipitate if the ion activity product (IAP) of Mg^{2+}, NH_4^+, and PO_4^{3-} is greater than its solubility product (K_{SP}). The *IAP* is controlled by solution pH. The both of NH_4^+ and PO_4^{3-} ion activities are pH dependent. The pH effect on NH_4^+ activity has lower influence on the formation of struvite than does the pH effect on PO_4^{3-} activity (Stumm and Morgan, 1981). Nelson et al. (2003) studied the effect of pH on struvite crystallisation in anaerobic swine lagoon wastewater. They have reported that the rate constant based on fitting first order kinetic model of phosphorous concentration, and it is increased with increase in pH from 8.4 to 9.0. However, Nelson et al., (2003) study showed that the increasing rate of struvite crystallisation kinetic was affected by difference of supersaturation due to pH changing. Thus, for assessing the influence of pH on the kinetics of struvite crystallisation, this study was undertaken for the same supersaturation with varying solution pH.

2.8.5.4 Effect of temperature

Although temperature has a lower impact on sturvite crystallisation than other parameters, such as pH and supersaturation (Durrant et al., 1999), it influenced

solubility of struvite. Studies conducted by Aage et al., (1997) and Burns and Finlayson (1982) showed solubility product of struvite increased with increase in temperature. However, Bhuiyan et al., (2007) found that the solubility of struvite increased with temperature, until 35^{O}C, and then it decreases. The solubility product increased from 0.436×10^{-4} to 5.920×10^{-14} between 10^{O}C and 35^{O}C in the Bhuiyan et al., (2007) study. The solubility product is determined from the concentration of solution at equilibrium concentration. The solubility product is linked to the supersaturation in which crystals may occur. The temperature range between 20^{O}C and 35^{O}C is used by the author for this study.

Various temperatures are used for crystal growth study as it is possible to determine crystal growth mechanism. High temperature of crystallisation usually leads to diffusion-controlled growth, while low temperatures leads to surface integration controlled growth (Jones, 2002). Moreover, increase in temperature often increases the rate of crystal growth and it can affect crystal size shape and type.

2.8.5.5 Crystal Growth Kinetic of Struvite Crystal Using the Two-Step Growth Model

Struvite crystals can be formed by feeding magnesium ion solution to a crystallizer containing ammonium and phosphate ion solution. Then magnesium ions react with ammonium and phosphate ions to form struvite and to grow on struvite seeds suspended in the crystallizer.

Several combination factors that affect nucleation and crystal growth of struvite were reported, such as the phenomena of mass transfer between solid and liquid phases, thermodynamic of liquid-solid equilibrium (Mullin, 2001, Jones, 2002), kinetic of reaction (Ohlinger et al., 1999) and physico-chemical parameters, including pH (Bouropoulos and Koutsoukos, 2000, Nelson et al., 2003, Pastor et al., 2008), supersaturation (Doyle et al., 2002), mixing energy (Ohlinger et al., 1999), temperature (Bhuiyan et al., 2007), and the presence of foreign ions in the crystallisation solution (Le Corre et al., 2009).

Crystal growth rate data of struvite were not further analysed on the possible effect of physico-chemical parameters on two-step growth model. Bhuiyan et al.

(Bhuiyan et al., 2008) successfully investigated and applied the two step crystal growth model on struvite crystal growth to estimate mass-transfer and surface-reaction coefficients. The mass-transfer and surface-reaction coefficients were predicted at pH 8.07, mean particle size of 1.25 mm and superfacial velocity of 380 cm/m. According to Tai et al. (1999) the effect of mass-transfer and surface-reaction coefficient on two-step model crystal growth was influenced by crystal size and superficial velocity. In an agitated crystallizer, stirrer speed significantly affects the increase in mass transfer coefficient until the crystals become fully suspended in the solution, after which the rate of increase with further increases in stirrer speed is reduced considerably. Besides, the two-step model plays an important role to reveal the kinetic phenomenon of crystals formation in solution (Tai, 1997). Therefore, struvite crystal growth studies using two-step model will further investigated to see how the physico-chemical parameters of solution will impact on the mass-transfer and surface-reaction coefficients.

2.8.6 Dissolution of struvite crystals

Struvite dissolution reaction can be described using

$$\mathbf{MgNH_4PO_4.6H_2O \rightleftarrows Mg^{2+} + NH_4^+ + PO_4^{3-} + 6H_2O} \quad (2.81)$$

The dissolution kinetic of struvite in aqueous solution has important implications in industrial crystallisation process. Many studies on the dissolution of struvite crystals in various media have been found in literature. Bhuiyan et al., (2009) investigated the dissolution rate of struvite crystals in acid solution by kinetic model. In acid solution, the effect of pH showed that the dissolution rates for struvite were found to increase with decrease in pH due to proton promoted dissolution (Bhuiyan et al., 2009) The following species in the system involving Mg^{2+}, PO_4^{3-}, NH_4^+ aqueous solution can be formed when the pH is varied, such as H_3PO_4, $H_2PO_4^-$, HPO_4^{2-}, $MgOH^+$, $MgNH_4PO_4$, $MgPO_4^-$, $MgH_2PO_4^+$, and $MgHPO_4$ (Mijangos et al., 2004). The acid solution pH is widely used as solvent to dissolve crystals, however, it can have a negative impact such as its corrosive effect and making pH control more difficult (Hausmanns et al., 1996). The dissolution of struvite was investigated by Doyle et al., (2003) in aqueous ethylenediaminetetraacetic acid (EDTA) solution. Doyle et al., (2003) examined

the EDTA : magnesium ratio and found the greater the ratio the more rapid the dissolution of struvite over a 5 min period. Moreover, there are some concerns about its poor biodegradation in conventional wastewater treatment plants and natural environments (Sýkora et al., 2001). Roncal-Herrero and Oelkers (2011) have done a dissolution experiment of struvite crystals with pH ranged from 7.76 – 10.65. The pH range of experiment corresponded to the condition where struvite is most stable (Ohlinger et al., 1998). In experimental study at initial pH 7.8 showed that the concentration of Mg and PO_4 in the bulk solution against with time was consistent with their stoichiometric release from the struvite crystals. However, at pH 9.35, Mg ion was released from 3 to 8 times faster than PO_4 ions (Roncal-Herrero and Oelkers, 2011).

According to Appelo and Postma, (1999) the dissolution rate is influenced by the amount of crystals present, the change in their shape during dissolution and the composition of the solution. During dissolution of struvite crystals, the effect of amount of crystals present can influence rate of dissolution where increasing dissolution of struvite was inversely proportional to the amount of crystal present in solution (Bhuiyan et al., 2009).

According to Nerst-Burnner theory, the surface area of crystal is directly proportional to the dissolution rate. Since higher dissolution rate may be achieved through the increase in surface area, the surface area increases with decrease in crystal size (Banakar, 1992). The experimental study of different crystal size showed that the dissolution rate constant increased with decrease in crystal size (Shan et al., 2002, Mergen and Demirhan, 2009).

However, the dissolution mechanism cannot be predicted only by means of a kinetic model; the rate determining mechanism is also important. Diffusion-controlled mechanism is slightly dependent on temperature, while interfacial-reaction-controlled mechanism are strongly dependent on temperature (Demirkiran, 2009). Therefore, the value of the activation energy of a dissolution reaction may be used to predict the rate-controlling step. Bavic-Ivancic et al., (2002) have investigated dissolution mechanism of struvite by calculating activation energy at three different temperatures, and it can be concluded that dissolution rate mechanism is the process of desorption of the integrating ions.

Moreover, the dissolution can be illustrated as mass transfer of ions from crystal to solution, firstly, crystals are disintegrated at the crystals surface, and then the solute diffuses from the surface to the bulk solution. The thickness of diffusion layer is influenced by stirrer speed, so the dissolution rate mechanism is correlated with the stirring rate (Masuda et al., 2006). The change in activation energy as a function of stirring speed represents a change from a diffusion-controlled mechanism under lower stirring speed to a surface-controlled mechanism at high stirring speed (Metz and Ganor, 2001). Furthermore, the increase of rotary forces of impeller of agitator could enhance the dispersion and solubility (Qin et al., 2012).

2.9 Summary

- Crystallisation is widely utilized in the chemical and process industry. Crystallisation techniques are widely employed in the separation and purification of solid to produce a variety of materials of high purity at low cost. The crystallising solution is key variable influencing product of crystallisation because the rate of nucleation and growth is dependent on particular level of supersaturation. The supersaturation is achieved when concentration of solution is higher than its solubility of solute. The existing knowledge about nucleation is extensive and nucleation process occurs when a new crystal is produced in specific supersaturated solution known as the *metastable supersaturation*. There are two different mechanisms that produce nuclei such as primary and secondary nucleation. The next stage of the crystallisation process is for these nuclei to grow larger by the addition of solute molecules from the supersaturated solution.
- Solubility, being the key factor in the crystallisation process, is highly dependent on solution pH. Although there had been several studies on solubility of struvite, the standard method for the experimental determination of a K_{sp} value was dissolution of struvite using distilled water as solvent. As described in some literature, the solution pH influenced the changing component concentration. So, new equilibrium solubility is reached by each solution pH. If supersaturation is used as a variable control, it is essential to

know the true value of K_{sp} for the pH range that the systems are expected to operate in.

- Pure solutions are rarely encountered outside the analytical laboratory, and even then the impurity levels are usually well within detectable limits. The impurities present can often have a considerable effect on the solubility characteristic of the main solute, such as ionic equilibrium, ion-solvent and ion-ion interaction. Some literatures showed that the presence of impurities influence ionic strength of struvite crystals. The changing ionic strength is caused by a complex formation on bulk solution during dissolution of crystals. Accurate and reliable data on solubility of struvite on impurities system are necessary for many industrial processes where these systems are used as feed. Therefore, the study of the solubility of struvite in aqueous electrolyte solutions is vital before proper crystallisation studies can be performed.
- Predicting and controlling struvite nucleation and growth from wastewater is fundamental in crystalliser design. Information on nucleation of struvite is also limited in the literature. The majority of published works related on struvite nucleation were mostly conducted with reaction-controlled in aqueous solution at constant temperature and supersaturation. Supersaturation was calculated with various initial solution pH. However, the supersaturation calculated based on various solution pH may not be accurate. The different solution pH may cause change in charge polarity of solution. The present studies used calculation of supersaturation based on constant pH. The effect of pH, temperature, and impurities on the nucleation of struvite formed part of this study.
- The growth of struvite in various literature showed that solution pH is most important on growth of struvite. Nelson et al. (2003) studied the effect of pH on struvite crystallisation with first order kinetics based on phosphorous concentration. However, their study showed that increasing rate of struvite crystallisation kinetic was affected by difference of supersaturation due to pH changing. Thus, for assessing the influence of pH on the kinetics of struvite crystallisation, this study was undertaken for the same supersaturation at various solution pH. The effects of solution pH, temperature, impurities, seed

and hydrodynamic condition on struvite growth kinetic are part of the proposed study.

- Many studies on the dissolution of struvite crystals in various media have been found in literature. However, the dissolution process mechanism cannot be predicted only by means of a kinetic model; the rate determining mechanism is important. The dissolution kinetics of struvite crystals in deionized water was studied and the effect of stirrer speeds, temperature and crystal loading on dissolution was also studied.

CHAPTER 3
EXPERIMENTAL STUDIES OF STRUVITE SOLUBILITY, NUCLEATION, GROWTH, AND DISSOLUTION IN AQUEOUS SOLUTION

3.1 Introduction

In determining operating conditions for solubility, nucleation, growth and dissolution of struvite crystals to efficiently generate the required product crystals, it is necessary to consider complex interacting variables between solution, heat and population balances of the system with its strong dependence on fluid and particle dynamics (Mullin, 2001, Randolph and Larson, 1988, Jancic and Grootscholten, 1984). It is well known that the solution condition, such as temperature, solution pH, and salt effects may strongly influence the solubility of struvite. The development and design of solubility set-up and batch crystallisation with special specifications to study struvite solubility is presented in this chapter. The solubility unit was developed by Safaeefar (2007) using 5 small reactors. Next, the solubility unit was used to determine metastable zone width and nucleation of struvite crystals.

Batch crystallizer is commonly used to prepare a wide variety of crystalline products. Batch crystallizer is relatively simple and flexible, and requires a relatively low level of maintenance. Batch crystallizer which has been developed was used to study rate of crystallisation, crystal growth, and dissolution and to measure the effect of process conditions. Next preliminary preparation of experiments is presented, which includes the preparation of crystallising solution, and seed preparation.

3.2 Analytical Techniques

3.2.1 Gravimetric analysis

Gravimetric analysis is defined as a set of methods in analytical chemistry for the quantitative determination of substances based on the mass of a solid. The gravimetric analysis uses an analytical balance (Sartorius Model 1601 MP8).

In gravimetric methods for drying wet samples, the wet sample is heated in an oven at temperature of 25 – 35^{O}C for 24 hours and allowed to cool to room temperature in a desiccator. It is then weighed, and heated again for about 30 minutes. The sample is cooled and weighed a second time. The procedure is repeated until successive weighing resulted in no further weight losses. For struvite crystals the drying of these crystals must be below 40^{O}C. If the crystals are heated above 40^{O}C, NH_4^+ will volatilise (Bhuiyan et al., 2007).

3.2.2 Microscopy

The imaging of struvite crystallisation was taken based on microscopic methods. The advantages of microscopy are that individual particles may be observed while measuring or assessing their size, shape and composition. The images can be reviewed directly in a microscope, or scanning electron microscopy (SEM).

3.2.2.1 Scanning electron microscopy (SEM)

The SEM has a larger depth of field compared to optical microscopy that permits a large amount of the sample to be in focus at one time. The SEM also produces images of high resolution, which means that closely spaced features can be examined at high magnification. Figure 3.1 show a schematic representation of SEM. An electron gun projects a stream of monochromatic electron, which passes through apertures and lenses before it hits the sample. When the beam strikes the sample, secondary electrons are produced and are detected: this gives information on the topology of the sample. Before the beam moves to its next dwelling point the measurement count the number of interactions and displays a pixel on a CRT (cathode ray tube) whose intensity is determined by this number (the more reactions the brighter the pixel). This process is repeated until the grid scan is finished and then repeated, the entire pattern can be scanned 30 times per second.

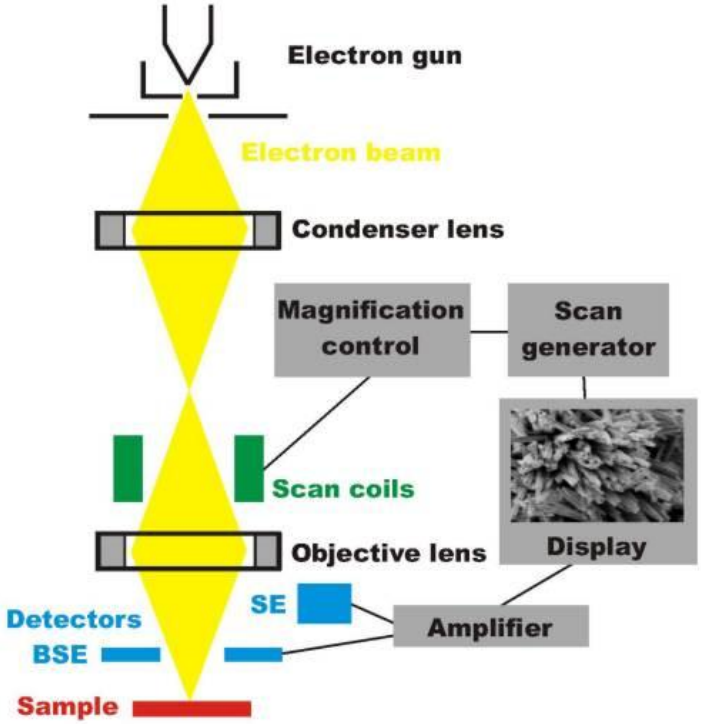

Figure 3.1 Schematic representation of a SEM (Hafner, 2013)

3.2.2.2 Optical microscopy

Optical microscopy uses for magnifying small objects. The first lens, called the objective, has a short focal length (a few mm), and creates an image of the object in the intermediate image plane. This image in turn can be looked at with another lens, the ocular or eye-piece, which can provide further magnification.

This microscopy method can be tedious and time-consuming. Microscopic observations were made using a Nikon eclipse ME600 metallurgical microscope (Figure 3.2), with automated video image capture (Nikon DXM1200F digital camera). Crystals were observed using reflected light. The images of the growing crystals were analysed using the Image Pro software. A calibration was first established by taking pictures of a graticule (x and y directions) using the 20, 50 and 150 times magnification lens on the optical microscope and the calibration information was applied to each of the images.

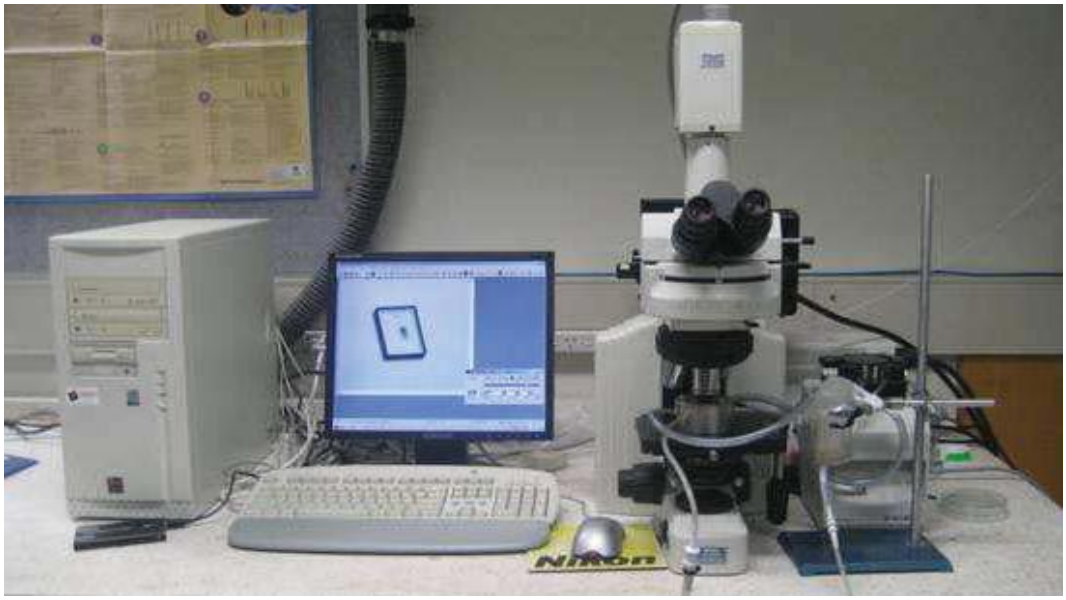

Figure 3.2 Optical microscope set up

3.2.3 Determination of crystal size distribution

Crystal size distributions (CSD) can be measured directly when samples of crystals can be sampled representatively from bulk crystals. One of the most popular analytical techniques for determination of crystal size distribution is laser light scattering method. Laser light scattering is a technique that can be used to determine the size distribution of any crystals. The advantages of this method are;

- Fast (individual measurements typically take only a few minutes)
- Wide range (0.5 to 1000 microns or more in one scan)
- Medium resolution
- Direct measurement (not related to fluid properties, etc.)

The only qualification of the technique is that each phase must be distinct optically from the other and the medium must be transparent to the laser wavelength. A Malvern Mastersizer with normal Fourier Optics was used for the determination of the crystal size distribution. A schematic diagram depicting the main features of the Malvern Mastersizer measuring system is given in Figure 3.3 which showed the relative position of the spray nozzle, detector plane, measurement electronic and the computer.

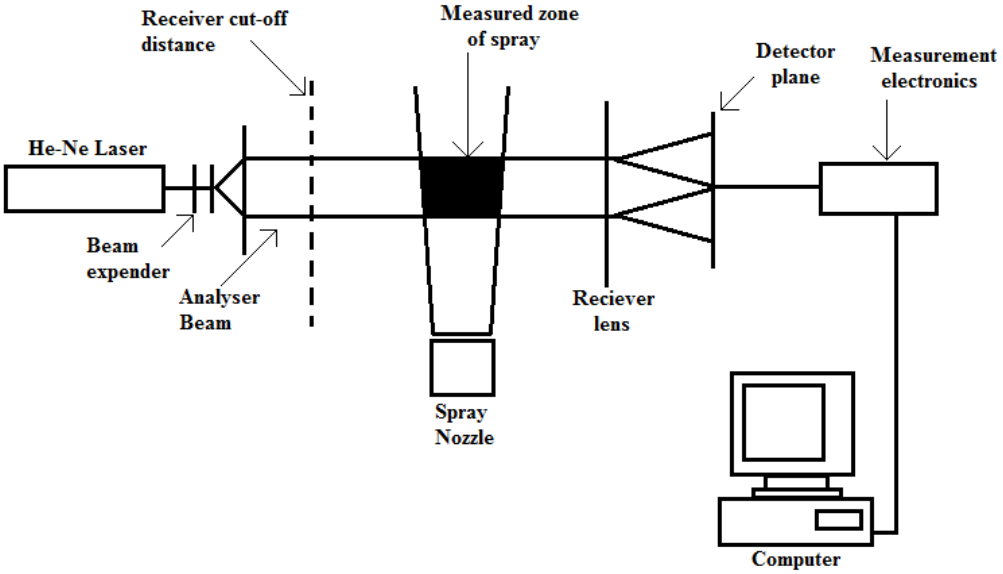

Figure 3.3 Schematic diagrams of the Malvern Mastersizer (Safaeefar, 2007)

The Mastersizer uses the Mastersizer's optical unit to capture the actual scattering pattern from a field of particles. Then, it can predict the size of particles from the pattern created.

The procedure for analysing CSD of struvite is as follows;

- Instrument preparation; the computer, optical unit and dispersion unit are connected and switched on. The flow cell is fitted and the pipes are connected to the dispersion unit according to the instructions. Setup size of measurement was in the range 0.02 – 10,000 μm and refractive index (RI) was 1.495.
- Add saturated solution into spray nozzle (Figure 3.3). Saturated solution was made by dissolution of struvite crystal for 24 hours.
    - Add the sample; the correct amount of sample added to the system was until obscuration of 10 – 30%. For example an obscuration of 30% means that 30% of the analyser beam (recorded during the background measurement step) has been lost to either scattering or absorption. The obscuration is simply the fraction of light "lost" from the analyser beam when the sample is introduced. Before the sample is added to the system it is usually best to pre-disperse the sample within a little of the dispersant to form a slurry.

- Measure the sample; the capture of the scattering pattern from sample results in raw data for the crystal size distribution of the sample.

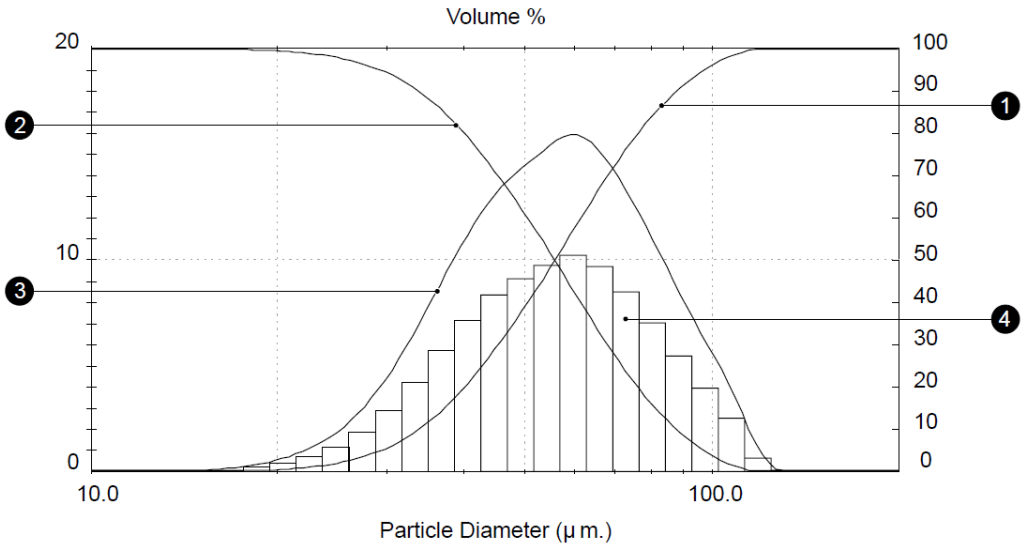

Figure 3.4 The Crystal Size Distribution Graph

Once the data has been analysed the information can be displayed in various ways. Usually the display will show a graph of the result and a table showing the same information in a tabular form. Figure 3.4 shows four of the more common graphical displays of the results.

The histogram (4) displays the result in the form of "in band" percentages. i.e. each bar in the graph represents a size band of particles (52 - 59 microns for example) and the height of the bar represents the percentage of the sample that is within that and. The histogram graph uses the left scale.

The "undersize" plot (1) displays the result in the form of "% of sample below a certain size of particle". For example by reading the values from Figure 3.4 may be able to determine that 10% of the sample is under 23 microns etc. (the exact value can be read from the table that will accompany the graph). The undersize plot is read from the right hand scale on the graph. The undersize plot is calculated from the initial size bands by fitting a curve to the analysis data so that values within a size band may be read.

The oversize plot (2) is similar to the undersize plot except that the result is in the form "% of sample above a certain size of particle". For example by reading the

values from Figure 3.4 may be able to determine that 90% of the sample is above 23 microns.

The correct amount of sample has to be passed through the laser beam to allow a good measurement to take place. Too little sample and there will not be enough scattered light to be detected. Too much sample and the light scattered from an individual particle will itself be scattered by other particles - this is known as multiple scattering.

The frequency curve (3) is calculated by differentiating the undersize curve. The frequency curve is particularly useful for displaying the results to show the "modes" or peaks in the graph. Several peaks in the graph indicate that there are distinct sizes of particles within the sample. This "at a glance" inspection of the results will be difficult if the result was shown as an undersized or oversize plot.

3.2.4 Methodology for analysis of Mg^{2+}, NH_4^+ and PO_4^{3-}

3.2.4.1 Mg Analysis with Atomic Absorption Spectrometry

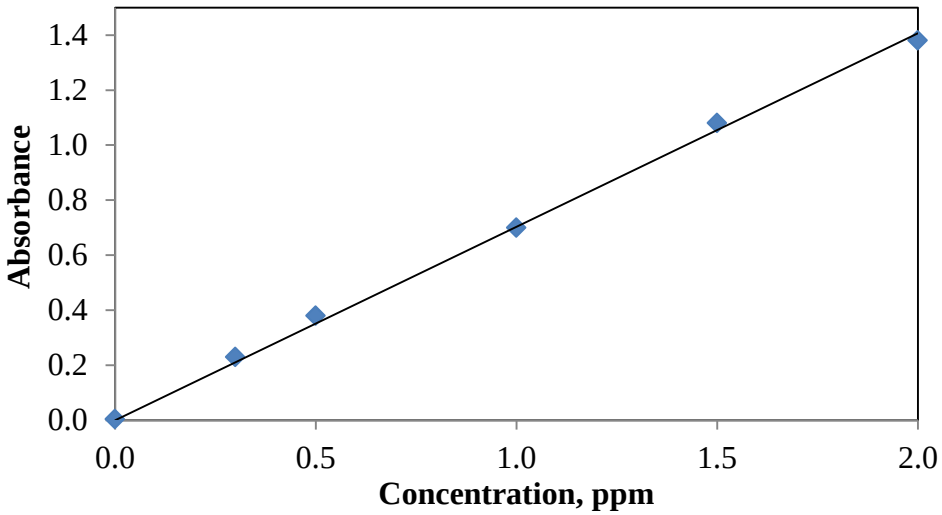

Figure 3.5 The standard calibration curve of the absorbance as a a function of Mg^{2+} concentration

Magnesium was measured by using an Atomic Absorption Spectrometry (AA 220FS model). The Atomic Absorption Spectrometry (AAS) was first calibrated by using samples of known Mg^{2+} concentration. A stock solution containing 100 mg/L of magnesium was first prepared. The optimum concentration range for the AAS to work for Mg^{2+} is 0.02 – 2 mg/L. A standard calibration curve was

prepared using 5 sample 0, 0.5, 1.0, 1.5 and 2 mg/L of Mg^{2+}. The absorbances were plotted as shown in Figure 3.5. This curve was used for the determination of Mg^{2+} ion concentration in the present study.

3.2.4.2 NH_4^+ Analysis with UV-Spectrometry

Ammonium was measured by phenate method using an UV-Spectrometry (V-670 model) (Warmadewanthi and Liu, 2009, Ohlinger et al., 1998). The UV-Spectrometry (UVS) was first calibrated by using samples of known NH_4^+ concentration at a wavelength of 630 nm. A stock solution containing 100 mg/L of ammonium was first prepared. The optimum concentration range for the UVS to work for NH_4 is 0.1 – 0.5 ppm. A standard calibration curve was prepared using 5 samples 0, 0.1, 0.2, 0.3, 0.4 and 0.5 ppm of NH_4. The absorbances were plotted as shown in Figure 3.6. This curve was used for the determination of NH_4^+ ion concentration for the present study.

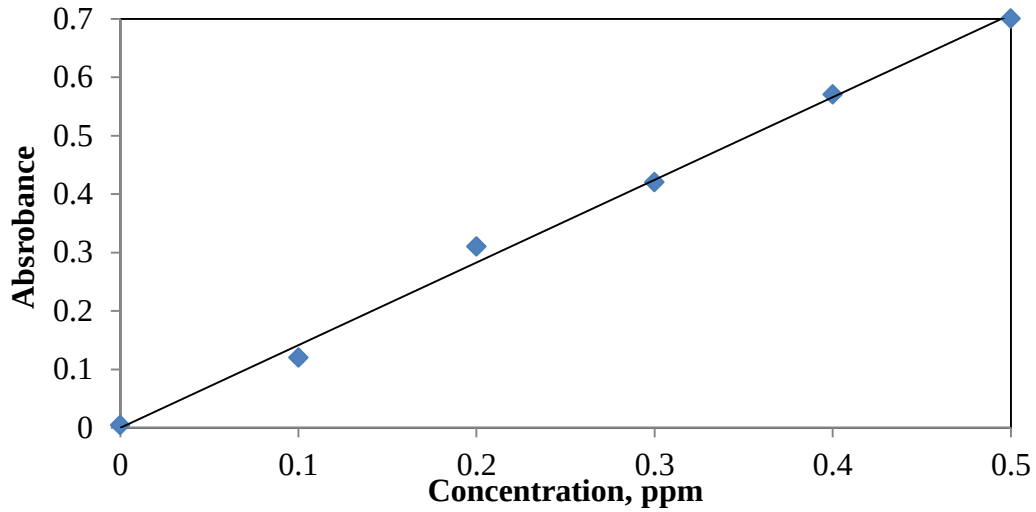

Figure 3.6 The standard calibration curve of the absorbance as a a function of NH_4^+ concentration

3.2.4.3 Phosphorous Analysis with UV-Spectrometry

Phosphorous was measured by phenate method using an UV-Spectrometry (V-670 model). The wave length was at 880 nm. The UV-Spectrometry (UVS) was first calibrated by using samples of known PO_4^{3-} concentration. A stock solution containing 100 mg/L of Phosphorous was first prepared. The optimum

concentration range for the UVS to work for PO_4 is 0.3 – 2.0 ppm. The absorbances were plotted as shown in Figure 3.7. This curve was used for the determination of PO_4^{3-} ion concentration for the present study.

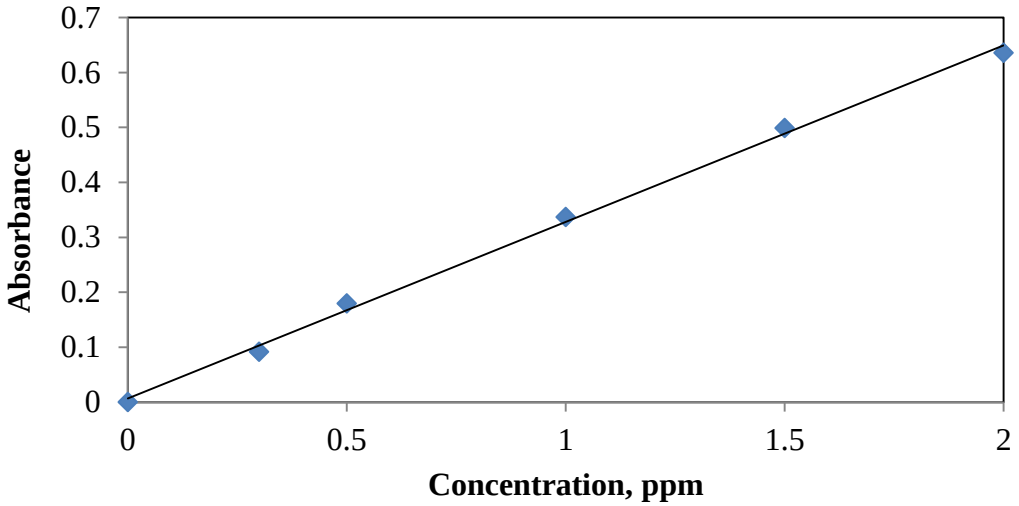

Figure 3.7 The standard calibration curve of the absorbance as a a function of PO_4^{3-}

3.3 Determination of Struvite Solubility

There are many techniques available for the measurement of the solubility of solid in liquid. However, no single method can be identified as being generally applicable to all possible types of systems. The choice of the most appropriate method has to be made in the light of the system properties, the availability of apparatus and analytical techniques, the skill and experience of the operator and the precision required and so on (Mullin, 2001). To avoid large errors, solubility must always be measured at a constant isothermal temperature with agitation employed. The agitation generally brings the liquid and solid phases into intimate contact and facilitates equilibrium. Equilibrium solubility is usually achieved after several hours, and in some cases days or even weeks. The long period of equilibrium is necessary because dissolution rates become very slow near saturation, and if shorter periods of time is used (one hour or less), the solubility will generally be underestimated (Mullin, 2001).

3.3.1 Experimental set-up

In this study, solubility measurements were conducted in a solubility unit that consists of five reactors and the process flow diagram of the set-up is the same as designed and used by Safaeefar (2007) (see Figure 3.8).

A magnetic stirrer was used to stir the solution in each of the reactors. Water bath was used to maintain isothermal conditions in the solubility unit. Two centrifugal pumps located at the input and outputs of the tank were used to circulate the water from the water bath to the solubility unit and from solubility unit to water bath. Valve was used to adjust input and output of water flow from the solubility unit and water bath. To avoid flooding and maintaining a stable water level, a bypass hose was fitted. The volume of glass solubility unit is 40 litres, which is capable of withstanding temperature up to 100^{O}C and is reinforced by silicon. The tank usually needs to hold water of about ~ 6 cm from tank bottom to avoid flooding when the electricity is turn off.

The holder of five small reactors (Erlenmeyer) is made out of stainless-steel equipped with a top retainer spring capable of firmly retaining glassware, which are held in place at the bottom of the tank by silicon.

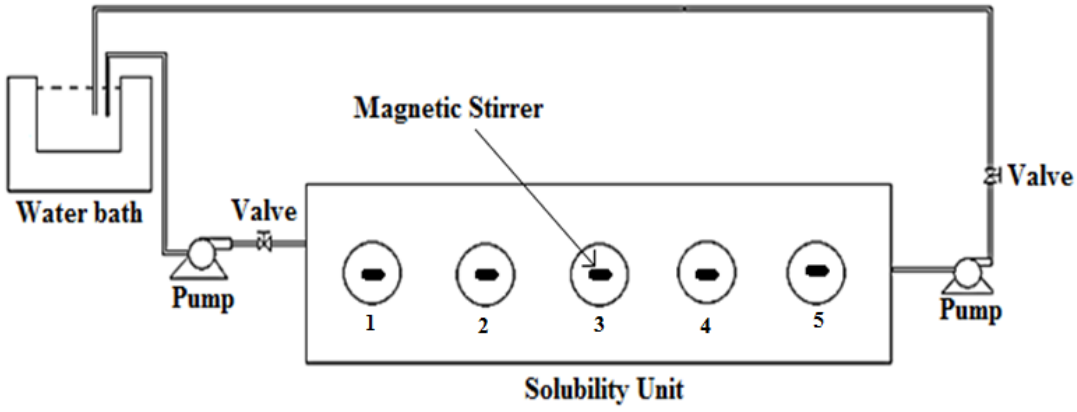

Figure 3.8 Solubility Experimental set up (Safaeefar, 2007)

3.3.2 Solubility experiment

The solubility of struvite at various initial solution pH and temperature were determined by equilibrating crystals and solution in the solubility unit. The initial solution pH investigated were at pH 3, 5, 7, 8, 9, and 11. Temperatures used were 20, 25, 30, 35, 40, 45, 50, 55, and 60^{O}C. An experimental solution of 100 ml

volume containing 0.45 g struvite, placed in a flask, was taken at various initial solution pH. Variation of initial solution pH was made by the addition of HCl and NaOH solution. pH measurements were made with a portable digital pH meter (WP-80 Model). After the temperature and solution pH reached the desired operating condition, the flasks, numbered 1, 2, 4 and 5 in solubility unit, were each sealed with a paraffin film to prevent evaporation of solvent. To identifying solution temperature in a flask within range of ± 0.1^{O}C, to a flask containing only water was placed in the middle of solubility unit (number 3), a thermometer was inserted to measure solution temperature (Figure 3.9). During the experiments, there were temperature differences between solution in flask and circulating water in solubility unit (Table 3.1).

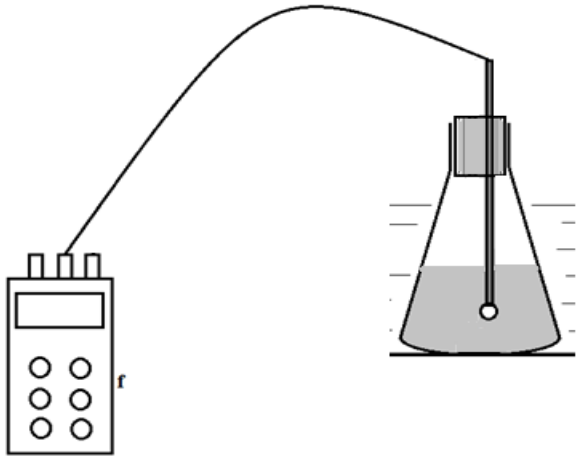

Figure 3.9 Temperature monitoring of the solutions

Table 3.1 The temperature difference between solution in flask and water in solubility unit

Temperature of experiment, ^{O}C	solution temperature in flask, ^{O}C	water temperature in solubility unit, ^{O}C
25	25 ± 0.1	25.9
30	30 ± 0.1	31.2
35	35 ± 0.1	35.7
40	40 ± 0.1	40.6
45	45 ± 0.1	45.5
50	50 ± 0.1	50.7
55	55 ± 0.1	55.8
60	60 ± 0.1	60.8

The solution were continuously stirred for 24 h to ensure saturation of the solution. Undissolved solid was allowed to settle without stirring, and after a further 2 hours samples of clear solution were checked for pH at equilibrium and the slurry filtered through a 0.22 µm membrane paper filter. The residue was dried overnight in an oven at 35^{O}C. The dried samples were weighed by using an analytical balance. The difference between the residue mass and the initial mass of struvite gave the solubility. The filtrate was then analysed for magnesium, ammonia, and phosphates. Analyses for ammonium and phosphate were made using UV-spectrometry as described in Section 3.2.4.2 and 3.2.4.3, respectively, Magnesium analysis was performed by atomic absorption spectrophotometry (see Section 3.2.4.1).

The impurities effect of chloride was studied by using NaCl, KCl, and $CaCl_2$. The aqueous chloride salts solutions with different concentrations were prepared by dissolving known amount of chloride salts in deionized water. The experimental procedure remained the same as above.

A small piece of the dried filter paper with magnesium ammonium phosphate precipitate on its surface was carefully cut and sputtered with coating carbon for field emission scanning electron microscopic analysis.

3.3.3 Solubility studies of struvite in the presence of chlorides

The effect of chloride salts on struvite solubility was studied using NaCl, KCl, and $CaCl_2$. The stock solutions were prepared by dissolving known amounts of NaCl, KCl, and $CaCl_2$ in deionized water. A range of solutions with different concentrations of chloride salts were made by diluting the stock solutions. A range of solutions was prepared between 0.3 – 1.5 M. The resulting chloride salt solutions were placed in the solubility unit by controlling temperature at 25^{O}C. The mixtures were continuously stirred for 24 h to ensure saturation of the solution. Undissolved solid was allowed to settle without stirring, and after a further 2 hours samples of clear solution were checked for pH at equilibrium and the slurry filtered through a 0.22 µm membrane paper filter. The residue was dried overnight in the oven at 35^{O}C. The dried samples were weighed by using an analytical balance. The difference between the residue and the initial mass of

struvite gave the solubility. The filtered samples were then analysed for magnesium, ammonia, and phosphates (see section 3.2.4.1, 3.2.4.2 and 3.2.4.3, respectively).

3.4 Determination of Metastable Zone Width

The experiments were conducted in Erlenmeyer flasks under constant temperature of $25^{O}C$ at different stirrer speeds. The experimental set-up can be seen in Figure 3.10. The synthetic solutions used in a series of batch experiments were 0.003, 0.004, 0.005 and 0.007 M (equimolar) of magnesium, ammonium and phosphate. The chemical of $MgCl_2.6H_2O$ was used as Mg^{2+} provider and $NH_4H_2PO_4$ was as NH_4^+ and PO_4^- provider. 100 ml volumes of solution in the absence of seeds were used for each of the experiments. Metastable zone width was determined with different stirrer speed of 50, 100, and 120 rpm. In each batch experiment, the solution pH was slowly adjusted using 0.01 M of NaOH solution. And then the pH drop and visually detectable crystallisation took place simultaneously. The time elapsed between pH adjustment and the first pH changes were defined as induction time. The rapid induction time was identified as metastable zone. pH measurements used portable digital pH meter (WP-80 Model).

3.5 Struvite Nucleation Studies

3.5.1 Synthetic liquor preparation

In this study, synthetic supernatant containing the constituent ions of struvite was used. The reagent salts used to prepare the synthetic liquor were analytical grade magnesium chloride ($MgCl_2$) and ammonium dihydrogen phosphate ($NH_4H_2PO_4$). Chloride salts, used as impurities, were sodium chloride (NaCl) and potassium chloride (KCl) and sodium hydroxide (NaOH) was used to adjust solution pH. $MgCl_2$ was obtained from Sigma and $NH_4H_2PO_4$ was obtained from Perth Scientific. All chemicals were of analytical grade and were used without further treatment. Double distilled water was used for all solution preparation. pH was measured by Orion pH meter.

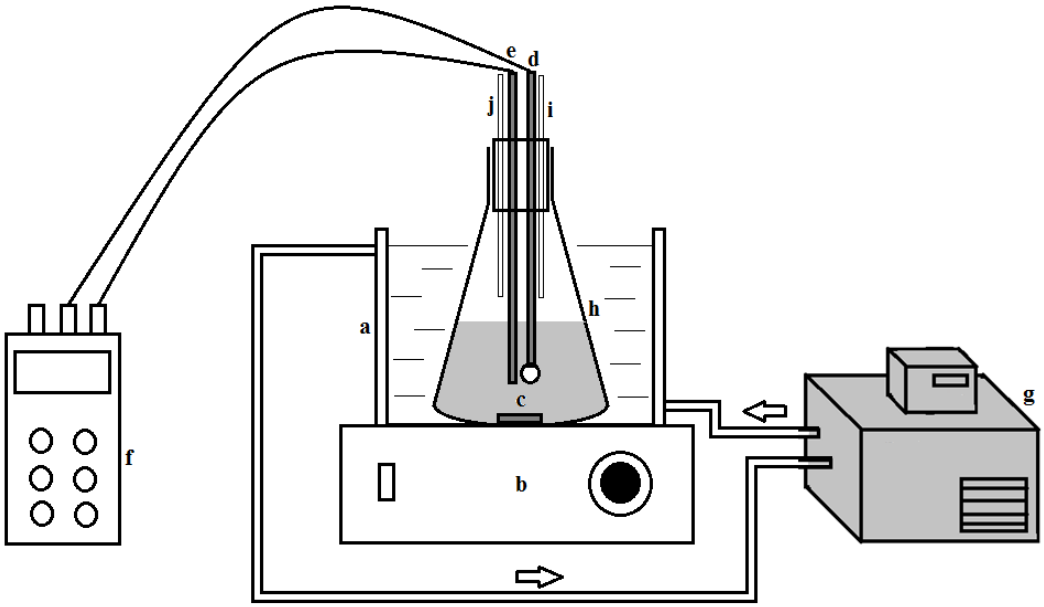

Figure 3.10 The experimental set-up; (a) water bath, (b) magnetic rotor, (c) magnetic stirrer, (d) pH electrode, (e) thermometer, (f) pH meter, (g) cryothermostat, (h) Erlenmeyer flask, (i) inlet for NaOH dosing, and (j) inlet for Magnesium dosing.

3.5.2 Batch experimental procedure

The experimental apparatus used in the study is shown in Figure 3.10. An Erlenmeyer flask of 250 ml was placed in the water bath containing circulating water. A stainless steel holder was used to keep the flask in place and a magnetic stirrer was used to stir the solution inside the flask. The water bath was maintained at a constant temperature by recirculating water through a pump which formed part of the cryothermostat. Water was heated at a given temperature in the cryothermostat.

In each experiment, the supersaturated solution was prepared by mixing equimolar quantities of Mg^{2+}, NH_4^+, and PO_4^{3-}. The desired quantity of $NH_4H_2PO_4$ solution were poured into an Erlenmeyer flask (working volume = 100 ml), and mixed by a magnetic stirrer. To avoid evaporation the Erlenmeyer flask was closed by using rubber stopper, and sealed with paraffin film. After the solution has achieved the desired temperature (within ± 0.01 C), a required quantity of $MgCl_2$ solution at the same temperature was added into the Erlenmeyer flask. 0.01 M solution of NaOH was slowly added by using a syringe to achieve the desired pH. The time that elapsed between pH adjustment, and the

first pH observed change is defined as the induction time. The experiment was stopped after the pH attained a new constant value. The experiments were conducted at initial pH of 8 and 8.5.

For studying impurities effect, the same procedure was used except that a desired concentration of chloride salts was added into the Erlenmeyer flask before the addition of $MgCl_2$. The solution condition was kept at pH 8. The concentration of chloride salts in the Erlenmeyer flask was varied between 8.06 – 16.38 mM after mixing of $MgCl_2$ and $NH_4H_2PO_4$, therefore the concentration of Cl^- ranged from 12.54 – 25.48 mMol. The excess Cl^- ion is defined as follows:

$$\boldsymbol{E} = \frac{[Cl^-]-[Cl^-_{eqm}]}{[Cl^-_{eqm}]} \quad (3.1)$$

Where Cl^- is the molar concentration of chlorine in solution and Cl^-_{eqm} is the chlorine introduced in solution through the equimolar feed as $MgCl_2$. The impurities effect studies have been carried out for a fixed value of excess chloride added as NaCl and KCl, namely E = 0.4.

The range of supersaturation was varied in between 1.02 and 1.45 for all experiments. Three temperature levels (20, 25 and 30^OC) were used for struvite nucleation study. The PhreeqC model was used for calculating the supersaturation of struvite in 0.00 – 16.38 mMol Cl^- ions solution at 20 – 30^OC. The calculated results are tabulated in Table 3.2 – 3.3.

The Phreeqc model calculation can be seen in Appendix B

Table 3.2 The supersaturation of struvite without the addition of NaCl, E = 0.

$MgCl_2$ (mM)	$NH_4H_2PO_4$ (mM)	SI	$MgCl_2$ (mM)	$NH_4H_2PO_4$ (mM)	SI
pH 8			pH 8.5		
T = 20^{O}C					
4.35	4.35	1.02	2.65	2.65	1.02
4.55	4.55	1.06	2.75	2.75	1.06
4.65	4.65	1.09	2.83	2.83	1.09
4.85	4.85	1.13	2.93	2.93	1.13
5.10	5.10	1.18	3.10	3.10	1.18
5.50	5.50	1.25	3.32	3.32	1.25
5.95	5.95	1.33	3.60	3.60	1.33
6.35	6.35	1.39	3.82	3.82	1.39
6.75	6.75	1.45	4.06	4.06	1.45
T = 25^{O}C					
5.10	5.10	1.02	3.10	3.10	1.02
5.30	5.30	1.06	3.23	3.23	1.06
5.50	5.50	1.09	3.32	3.32	1.09
5.70	5.70	1.13	3.45	3.45	1.13
6.00	6.00	1.18	3.63	3.63	1.18
6.50	6.50	1.25	3.90	3.90	1.25
7.00	7.00	1.33	4.24	4.24	1.33
7.50	7.50	1.39	4.50	4.50	1.39
8.00	8.00	1.45	4.80	4.80	1.45
T = 30^{O}C					
5.60	5.60	1.02	3.42	3.42	1.02
5.85	5.85	1.06	3.56	3.56	1.06
6.00	6.00	1.09	3.68	3.68	1.09
6.30	6.30	1.13	3.84	3.84	1.13
6.60	6.60	1.18	4.05	4.05	1.18
7.15	7.15	1.25	4.35	4.35	1.25
7.75	7.75	1.33	4.70	4.70	1.33
8.30	8.30	1.39	5.00	5.00	1.39
8.80	8.80	1.45	5.30	5.30	1.45

Table 3.3 The supersaturation of struvite with the addition of NaCl and KCl at pH 8, E = 0.4.

$MgCl_2$ (mM)	$NH_4H_2PO_4$ (mM)	NaCl or KCl (mM)	SI
T = 20^{O}C			
4.48	4.48	8.06	1.02
4.65	4.65	8.37	1.06
4.80	4.80	8.64	1.09
5.00	5.00	9.00	1.13
5.30	5.30	9.54	1.18
5.68	5.68	10.22	1.25
6.20	6.20	11.16	1.33
6.55	6.55	11.79	1.39
7.00	7.00	12.60	1.45
T = 25^{O}C			
5.25	5.25	9.45	1.02
5.50	5.50	9.90	1.06
5.65	5.65	10.17	1.09
5.90	5.90	10.62	1.13
6.20	6.20	11.16	1.18
6.70	6.70	12.06	1.25
7.25	7.25	13.05	1.33
7.75	7.75	13.95	1.39
8.25	8.25	14.85	1.45
T = 30^{O}C			
5.80	5.80	10.44	1.02
6.00	6.00	10.80	1.06
6.20	6.20	11.16	1.09
6.50	6.50	11.70	1.13
6.85	6.85	12.33	1.18
7.35	7.35	13.23	1.25
8.00	8.00	14.40	1.33
8.55	8.55	15.39	1.39
9.10	9.10	16.38	1.45

3.6 Crystal Growth Experimental Study in Batch Crystallisation.

The dimensions and arrangement of vessel, impellers, and baffles are factors that influence the amount of energy required for achieving a needed amount of agitation or quality of mixing.

3.6.1 Batch crystallisation apparatus

The schematic diagram of the batch experimental set-up is shown in Figure 3.11. The batch crystallizer was made of a cylindrical glass vessel (internal diameter ID

= 130 mm) covered with a double-jacket with a round bottom. The working capacity of the vessel was 1 litre.

In order to preclude the possibility of swirling and maximize the vertical movement of fluid in the crystallizer it was necessary to place four vertical baffles spaced at right angles to one another into the crystallizer wall.

The crystallizer was covered with a steel plate to minimize evaporation of solution. Temperature control within the crystallizer was achieved by pumping water from water bath enclosed in a cryothermostat with PID regulator for temperature control.

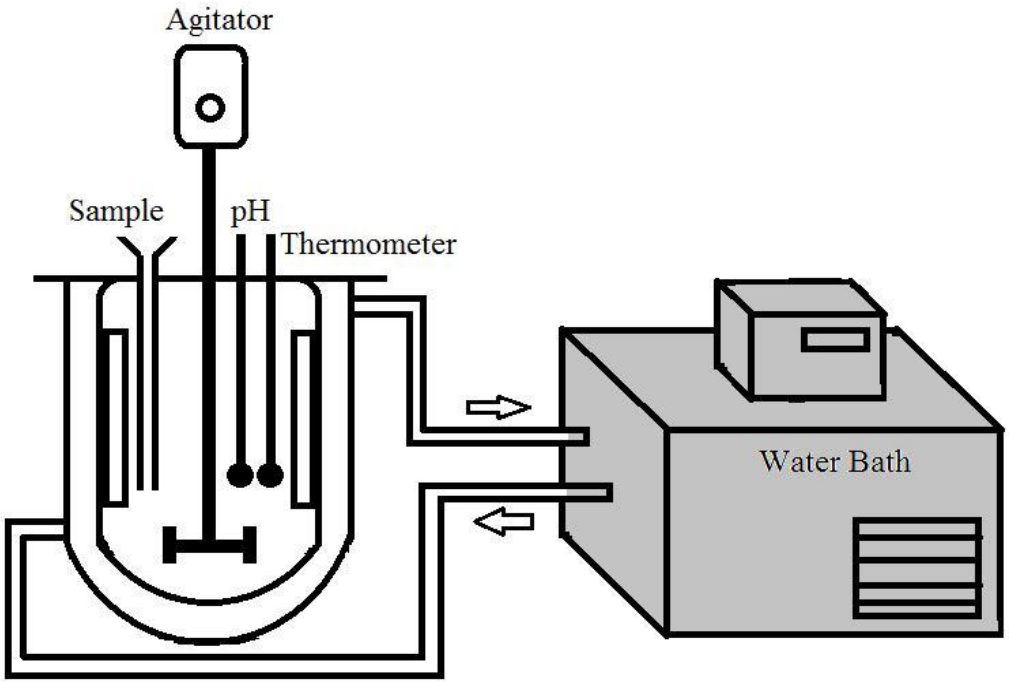

Figure 3.11 Batch crystallizer of struvite study

3.6.2 Baffle

In turbulent mixing, solid body rotation or central surface vortices may occur. Baffles were installed in the batch crystallizer to overcome this.

The use of baffles results in a circulation without aeration due to vortexing or severely unbalanced fluid forces on the impeller shaft. According to Couper et al., (2005) the optimum size of baffle width is one-twelfth the crystallizer diameter and a length extending from one half the impeller length. The size of baffle was 10 mm x 83 mm. To maximize and ensure particles suspended in all parts of

crystallizer the impeller was located at one-third the working liquid level from the crystallizer bottom and four baffles were placed on the wall of crystallizer with equal distance. Detailed dimensions are illustrated by Figure 3.12.

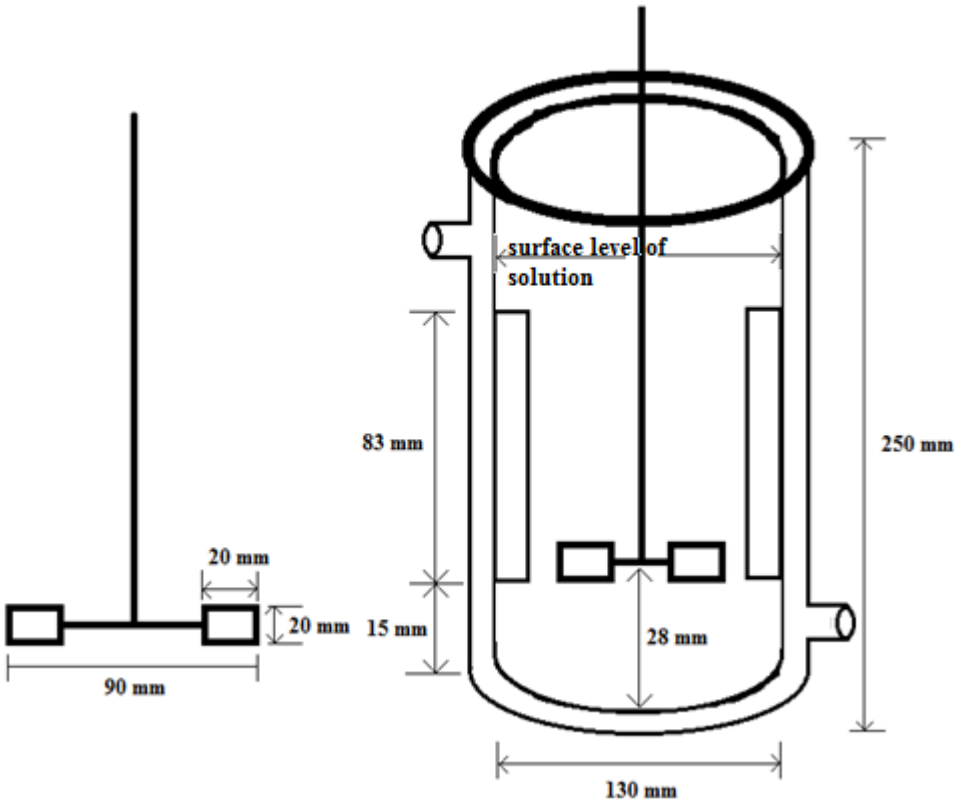

Figure 3.12 Crystallizer and impeller geometry

Baffles mounted at the crystallizer wall are to avoid dead zone where liquid is seldom exchanged and where impurities accumulate. Moreover, baffles are also needed to provide adequate mixing and suspension. Furthermore, baffles convert the tangential velocity imparted by impellers to axial flow which is needed both for crystal suspension and micromixing. Figure 3.13 shows typical flow patterns in baffled crystallizer with the baffle mounted at the wall.

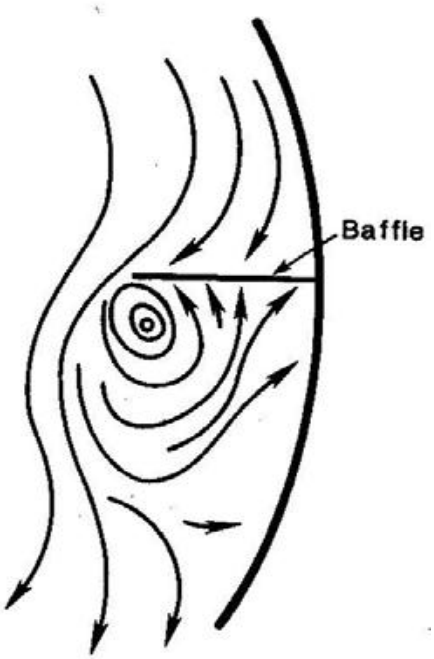

Figure 3.13 Baffle arrangement (Couper et al., 2005)

3.6.3 Impeller

Impeller is designed to circulate the liquid axially and to achieve primarily radial circulation. A rotating impeller in fluid results in flow and shear. The shear results from flow of one portion of the fluid pass another. For achievement of suspended solid in fluid, the impeller has to be considered flow pattern of fluid and friction from crystallizer surface, baffle and other internals. Because the performance of a particular shape of impeller usually cannot be predicted quantitatively, impellers are designed for two different types of turbulent flow (Couper et al., 2005). In this study, batch crystallizer was placed a 45^{O} pitched blade turbine constructed with four blades (Figure 3.14). Axial flow is produced by a 45^{O} pitched blade turbine. This type of impeller produces flow parallel to the impeller shaft and is usually used to blend liquids and to suspend solid in liquid, especially to sweep solids off the tank bottom when the discharge from the impeller is downward.

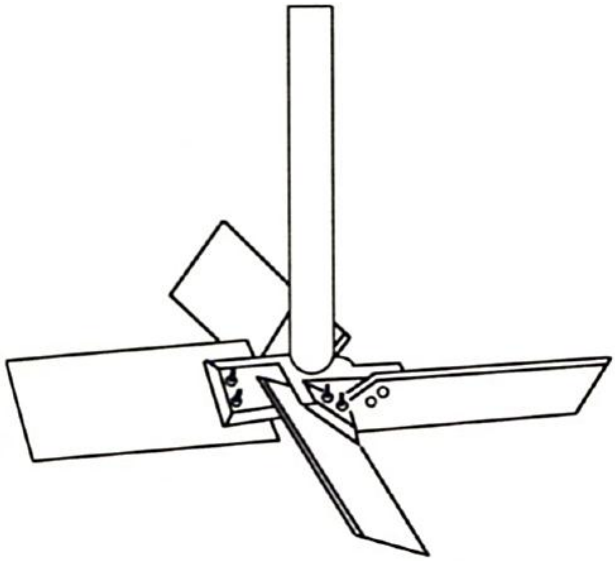

Figure 3.14 Representative 45^{O} pitched blade turbine constructed with four blades (Couper et al., 2005)

3.6.4 Batch crystallisation experiments

3.6.4.1 Solution preparation

The reagent salts used to prepare the synthetic liquor were analytical grade magnesium chloride ($MgCl_2$) to provide Mg^{2+} ions and ammonium dihydrogen phosphate ($NH_4H_2PO_4$) to provide NH_4^+ and PO_4^{3-} ions. Chloride salts, used as impurities, were sodium chloride (NaCl) and sodium hydroxide (NaOH) was used to adjust solution pH. Both solutions were stored separately and only mixed just prior to any experimental run. Extreme care was taken to keep the solution away from dust, insoluble matter, etc. In addition, all solutions were filtered before they were used for the experiments.

The concentrations of Mg^{2+}, NH_4^+, and PO_4^{3-} ions were prepared based on concentration in metastable zone. Calculation of saturation index (*SI*) of concentration in metastable zone can be seen in section 2.7.4.1.

3.6.4.2 Seed preparation

These seeds were prepared by immersing synthetic crystals of specific amount in a supersaturated solution and agitated gently in order to reduce agglomeration. Crystals that have been separated from agglomerate crystals were taken using a

plastic pipette to be placed and kept in a petri dish. The crystals were dried at room temperature in a desiccator. The dried crystals were transferred into a small weighed container. Next, the crystals were left in the container for 24 hours at room temperature. Then they were taken out, rinsed with two drops of deionized water, and dried immediately with filter paper. Their size distribution and morphology were determined by using a Malvern Master Sizer 2000 and microscope, respectively. The Fourier transform infrared spectroscopy (FTIR) was used to analyse potential changes in the inner structure of struvite crystals. These dried seed crystals were used for crystal growth experiments.

3.6.4.3 Experimental set-up

The experimental setup is shown schematically in Figure 3.11. All experiments were performed in the laboratory-scale jacketed stirred batch crystallizer with a working volume of 1 liter.

The study was conducted in the batch crystalliser with pH control at 25^{O}C. The operating conditions are listed in Table 3.4. One liter of supersaturated solution was introduced into the crystalliser. The crystallizer was covered with a steel plate to minimize evaporation of solution. After the supersaturated solution reached the desired temperature and pH, the supersaturated solution was allowed to settle at constant temperature and pH and no visible turbidity was observed for 20 minutes. Seed crystals of struvite were added into the crystallizer containing supersaturated solution maintained at 25^{O}C. The pH was maintained by addition of NaOH solution. Before operation the electrode was standardized with buffers of pH 4, 7 and 10, respectively. pH and temperature measurements were measured by using a portable digital pH meter (WP-80 Model). The experiment was conducted for 120 min with 1, 5, 10, 15, 20, 30, 40, 60, 80 and 120 min sampling times. Sample volumes of 2 ml were withdrawn from the crystalliser by a syringe and filtered with a 0.22 μm filter. After crystallisation for a definite time, the crystals were filtered from the residual slurry, and dried overnight in the oven at temperature 35^{O}C in order to measure crystal size distribution, weight, and FTIR analysis. The filtered were then analysed for magnesium, ammonia, and ortho-phosphates. Analyses for ammonium and ortho-phosphate were done in an UV-

spectrometry as described in Section 3.2.4.2 and 3.2.4.3, respectively. Magnesium analysis was performed by atomic absorption spectrophotometry (see Section 3.2.4.1). The crystal size distributions were measured by laser diffraction with a Malvern Master Sizer 2000 at the end of crystallisation (see Section 3.2.3).

Table 3.4 Operating condition of crystalliser experiments conducted in this work

Working temperature (^{O}C)	**25**
pH range	8 – 9
Supersaturation, *SI*	0.34 – 1.00
Stirrer speed, rpm	50 – 120
Seed size, μm	24.3 – 106
Impurities (NaCl), ppm	50 – 200

Investigation of stirrer effect was carried out at temperature 25^{O}C and pH 8 with stirrer speeds varying from 50 – 120 rpm. The stirrer speed was selected to ensure that seed crystals introduced would be well suspended in the crystallizer.

3.6.5 Effect of agitation speed on attrition

It was possible that struvite seed crystals might break into smaller crystals through collisions with the stirrer. For this reason, it was important to determine if prolonged agitation of the seed crystals in a saturated solution would result in seed attrition. Tests for the crystal attrition were conducted with stirrer speeds of 50, 100, 120 rpm in the batch crystallizer for 15 minutes. The saturated solution was prepared by dissolving struvite crystals for 24 hours. The analyses of attrition of crystals were measured before and after the agitation period, using a Melvern Master Sizer.

The resulting CSD for this test is depicted in Figure 3.15. The CSD for the seed sample agitated for 15 minute closely resembled, indicating that agitation did not cause attrition to occur.

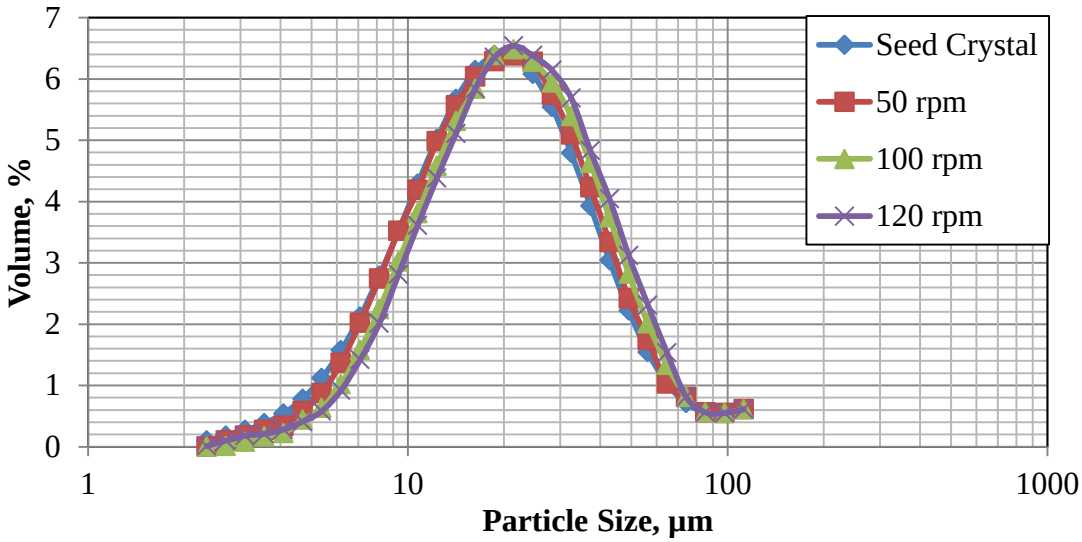

Figure 3.15 CSD of struvite seeds in saturated solution at different stirrer speeds.

3.7 Experimental Dissolution Study in Batch Crystallisation

The dissolution of struvite crystals was studied in the same crystallizer as shown in Figure 3.11. Struvite crystals (1000 mg) were added to 1000 ml of deionized water in the crystallizer at a given stirrer speed of between 120 and 400 rpm. At regular 5 minutes intervals, samples were withdrawn using a syringe, for 1 hour, and immediately filtered through a membrane filter (pore size 0.2 µm), and the concentration of filtrate was determined. For the temperature effect, the dissolution of struvite crystals was investigated using stirrer speed of 200 rpm at a given temperature between 20 and 35^{O}C. The effect of crystals size was carried out at 200 and 500 rpm and 25^{O}C. To see the dissolution pattern for a longer period of time, a similar set-up was also used to carry out the experiment for 50 hours.

Analyses for ammonium and phosphate were made using UV-spectrometry as described in Section 3.2.4.2 and 3.2.4.3, respectively, Magnesium analysis was performed by atomic absorption spectrometry (see Section 3.2.4.1). During the experimental runs, the system was continuously stirred at a constant rate. The temperature and pH of the system was measured using a WP-80 digital pH meter equipped with a thermometer probe. The size distribution of struvite crystals was determined during the dissolution by Malvern Mastersizer (see Section 3.2.3).

3.8 Summary

The development and design of the batch crystallisation systems used to investigate solubility, nucleation, growth and dissolution of struvite crystals is presented in this chapter.

- Solubility cell which has been designed with five small reactors was used to investigate struvite solubility. The method of solubility study is dissolution of struvite crystals agitated by a magnetic stirrer for 24 hours. Various solution pH, temperature and Cl^- ion were variables used for studying struvite solubility. Furthermore, solubility cell was also used to determine nucleation studies and, metastable zone width.
- Crystal growth was studied in a batch crystallizer equipped with an impeller and baffles. Seed crystals were uniformly suspended in the batch crystallizer. Effect of solution pH, seed loading, stirrer speed, temperature and presence impurities on crystal growth were investigated. Moreover, batch crystallizer was also used to measure kinetics of dissolution of struvite.
- Phosphate and ammonium concentration were determined with an UV-spectrometry, magnesium concentration was determined with an atomic absorption spectrophotometry. The size distribution of struvite crystals was determined by using a Malvern Mastersizer and crystals morphology through microscopy.

CHAPTER 4
EFFECT OF INITIAL SOLUTION pH, TEMPERATURE AND SALTS ON SOLUBILITY OF STRUVITE CRYSTALS

4.1 Introduction

Struvite is a white crystalline substance formed from magnesium, ammonium and phosphorous in equal molar concentrations ($MgNH_4PO_4.6H_2O$) according to the general reaction as shown below:

$$\mathbf{Mg^{2+} + NH_4^+ + PO_4^{3-} + 6H_2O \rightarrow MgNH_4PO_4.6H_2O} \quad (4.1)$$

The morphology of struvite is orthorhombic. The shapes of struvite are mostly in geometric form of spherical and cubic shapes. Struvite is known to form a hard scale in specific areas of wastewater treatment plants such as in sludge liquor pipes, centrifuges, belt presses, and heat exchangers (Doyle and Parsons, 2002). Besides causing process problems, struvite can also be used as a fertilizer.

The predominant parameters of controlling solubility of struvite crystals are temperature and pH. Elworthy et al.(1968) identified changes affected by temperature such as a change in the aqueous solubility properties of the crystal. The effect of temperature on the solubility of a substance is determined by the dissolution reaction characteristics of either exothermic or endothermic dissolution (Bhuiyan et al., 2007). Endothermic dissolution when energy is needed to dissolve the solid particles, while exothermic dissolution occurs when energy is given off by interaction of these particles with solvent (Bhuiyan et al., 2007). According to Bhuiyan et al. (2007), solubility of struvite increases with increasing temperature until it reaches the maximum solubility at $35^{O}C$ and then declined.

Several studies show that solubility of struvite is highly dependent on pH. Solubility decreases with increasing pH until about 9 after which it will increase (Doyle and Parsons, 2002). The apparent pH of minimum struvite solubility is documented in the range of 9 to 11 (Ohlinger et al., 1998, Nelson et al., 2003). In

principle, a crystallisation of struvite is possible in the pH range of 9-10 (Stumm and Morgan, 1981). In general, struvite solubility is a minimum at pH of about 9.

It was reported in the literature that the low solubilities in water of some solutes can be modified by the presence of co-solutes such as salts or by increasing the temperature. Two phenomena related to changes in the solubility can be observed: salting-in and salting-out effects (Singh et al., 2004, Soto et al., 2004). Experimental measurement of the solubility of struvite in NaCl solution has been studied by Bhuiyan et al (2007). The results revealed that the presence of NaCl solution changes the solubility of struvite and increases it. This phenomenon is known as salting-in effect.

This chapter is devoted to studying the impact of initial solution pH, temperature, and some chloride salts (NaCl, KCl, and $CaCl_2$) on solubility of struvite in water.

4.1.1 Solubility Product Calculation

The ionic strength is obtained from the Debye-Huckel theory to be

$$\mathbf{I} = \frac{\mathbf{1}}{\mathbf{2}}\sum_{\mathbf{i}} \mathbf{C_i z_i^2} \tag{4.2}$$

where C_i in mol/L represents the concentration of every ion, z_i is the ionic charge that is present in the solution.

The theory of interaction of ions in a solution incorporates both the electrostatic interaction between ions and the thermal motion of the ions. The basic theory is called the Debye-Hukel theory (Myerson, 2002). The Debye-Huckel theory can be calculated by using activity coefficients for single ions, so

$$\mathbf{\log \gamma_{\pm} = -0.5 z_i^2 I^2} \tag{4.3}$$

where z_i is the valance of ion *i*.

Solubility product (K_{sp}) was determined:.

$$\mathbf{K_{sp} = \gamma_{Mg^{2+}}[Mg^{2+}]\,\gamma_{NH_4^+}[NH_4{}^+]\,\gamma_{PO_4^{3-}}[PO_4{}^{3-}]} \tag{4.4}$$

$$\boldsymbol{pK_a = -logK_{sp}} \tag{4.5}$$

The calculation of solubility product was calculated by Excel program (see Figure A2.1 in Appendix A)

4.2 Materials and Methods

The solubility of struvite at various pH and temperature was determined by equilibrating crystals and solution in a solubility unit. The experimental set-up is described in Section 3.3.1. The unit consisted of five flasks; each of 200 ml capacity closed by a round glass stopper and the contents of each was kept stirred by a submersible magnetic stirrer. The flasks were sealed with a paraffin film to prevent evaporation of solvent. The flask was immersed in a thermostatic bath, capable of maintaining the temperature to within $\pm 0.1^{O}C$.

The solubility of struvite-water system was determined within the temperature range of 25 to $40^{o}C$ and initial solution pH between 3 and 11. The mass of crystals added to solution of 100 ml volume was 0.40 g struvite. The mixtures were continuously stirred for 24 h. The slurry was filtered through a 0.22 µm membrane paper filter. The residue was dried overnight in the oven at $35^{O}C$. The experimental solubility study in water system is described in Section 3.3.2. A small piece of the dried filter paper with magnesium ammonium phosphate precipitate on its surface was carefully cut and sputtered with carbon for field emission scanning electron microscopic analysis.

The effect of chloride salts in this study used NaCl, KCl, and $CaCl_2$. The aqueous chloride salt solutions with different concentration were prepared by dissolving known amounts of chloride salts in deionized water. The experimental procedure is presented in Section 3.3.3.

The filtered samples were then analysed for magnesium (see Section 3.2.4.1), ammonium (see Section 3.2.4.2), and phosphates (see Section 3.2.4.3). Analyses for phosphate and ammonia were made by using UV-spectrophotometer, Magnesium analysis was performed with an atomic absorption spectrophotometer. Thermal decomposition of struvite was analysed on a thermogravimetric analyser instrument (series Q500) under flowing nitrogen atmosphere and different heating rates. The conversion of the TGA curve to its derivative mode (DTA) was undertaken from the rate of mass loss curve as a function of temperature.

4.3 Results and Discussions

4.3.1 Effect of initial solution pH on struvite solubility

Struvite solubility study was carried out by dissolving the struvite crystals in water. Figure 4.1 shows the variation of pH at 25^{O}C for various initial pH values used. One of the factors that influence changes in pH during struvite dissolution process are the activity of phosphate ions (Nelson et al., 2003). When the initial solution pH was varied and the equilibrium pH is reached, the element Mg^{2+}, NH_4^+, and PO_4^{3-} can form ion complexes, such as NH_3, NH_4^+, H_3PO_4, $H_2PO_4^-$, HPO_4^{2-}, $MgOH^+$, $MgNH_4PO_4$, $MgPO_4^-$, $MgH_2PO_4^+$ and $MgHPO_4$ in the system (Bouropoulos and Koutsoukos, 2000, Ohlinger et al., 2000).

Experiments conducted at initial pH of 3 resulted in an equilibrium pH of 8.3. The equilibrium time was reached at approximately 20 minutes as clearly shown in Figure 4.1. At initial pH 3, activity of phosphate ions in solution follow the sequence H_3PO_4, $H_2PO_4^-$, HPO_4^{-2}, PO_4^{-3} resulting in increase of pH in the system (Mijangos et al., 2004).

When the initial solution pH was adjusted to 5 and 7, the temporal evaluation of pH shows that the equilibrium pH around 9.3 was reached in only 4 minutes (Figure. 4.1). At this point, $H_2PO_4^-$ and HPO_4^{2-} are the prevalent phosphate species in the solution phase. The equilibrium time is faster than for the solution at initial pH 3 due to the $H_2PO_4^-$ from decomposition of struvite crystal reacts with magnesium to form $Mg_3(PO_4)_2$, formation of $Mg_3(PO_4)_2$ reaches a maximum condition at pH 9 (Mijangos et al., 2004).

At initial solution pH of 9, the experiment showed that the pH is relatively stable. As can be seen in Figure 4.1, the pH increases slightly and gradually decreases to reach the equilibrium conditions at pH 9. At this condition the presence of phosphorous ion is predominantly HPO_4^{2-}.

Similarly, at initial solution pH of 11 only a slight decrease of pH was observed. Stability of the pH is influenced by the high content of HPO_4^{2-} in solution (Mijangos et al., 2004). According to Ali (2005), for solution condition at pH 11, NH_4^- has potential to transform NH_3.

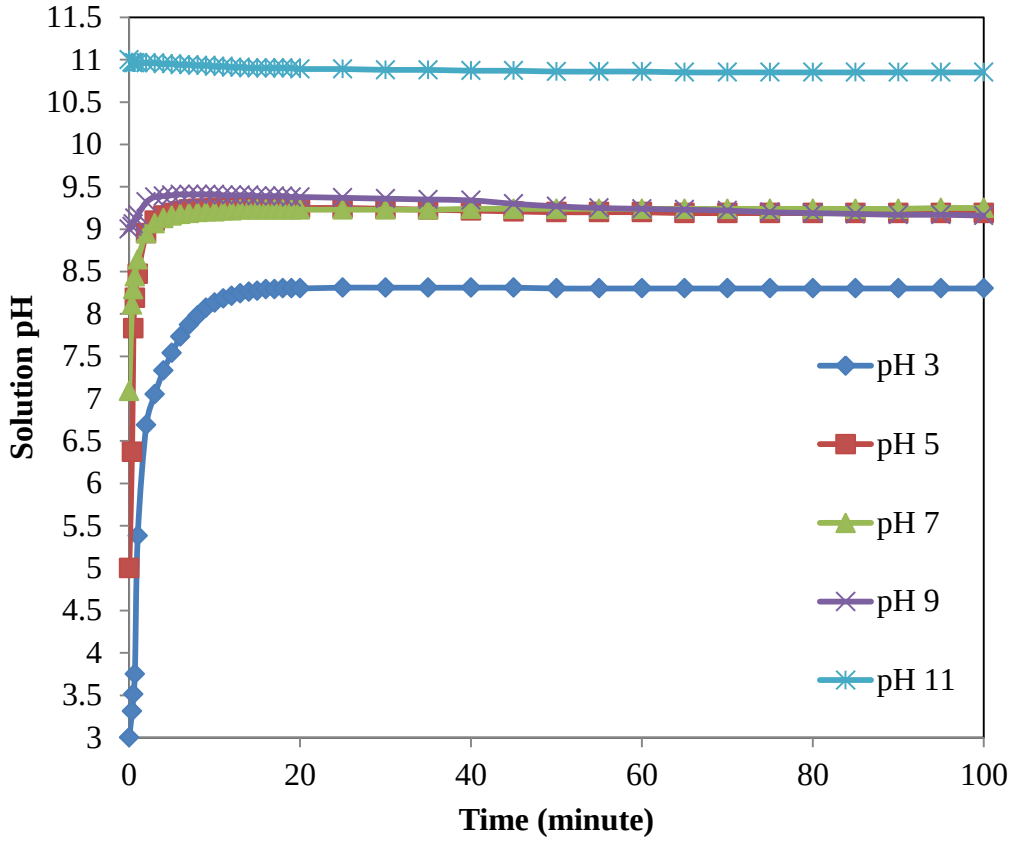

Figure 4.1 Variation of solution pH with time at 25^{O}C

The struvite solubility study in aqueous solution at different initial pH value is shown in Figure 4.2 which shows that solubility increased in acid solution going down from pH 7 to 3. This indicates that the acid solution, such as at pH 3, can decompose the struvite constituent ions into the solution. According to Mijangos et al., (2004), if acid was added into the solution, some of the PO_4^- ions become protonated and transformed into $H_2PO_4^-$, and HPO_4^{-2} base on the following equilibria reaction;

$$\mathbf{H^+ + PO_4^{3-} \rightleftarrows HPO_4^{2-}} \quad (4.6)$$

$$\mathbf{H^+ + HPO_4^{2-} \rightleftarrows H_2PO_4^-} \quad (4.7)$$

As a result, the concentration of PO_4^{3-} ion is reduced. In accordance with Le Chatelier's principle, the system will respond to this reduction by trying to produce more phosphate ion. So solid struvite would dissolve and the equilibrium will be shifted to the right based on struvite decomposition reaction. According to

Shukla et al., (2008) increasing the solubility at low pH values may be because H^+ ions provide localized acidification to dissolve the mineral and also because of the higher hydration of ions.

A similar behaviour was identified by solubility of struvite involving base solution where increase in initial solution pH from 8 to 11 increase in solubility of struvite crystal (Figure 4.2). The increasing solubility was caused by the following reaction

$$\mathbf{NH_4^- \rightleftarrows NH_3 + H^+} \quad (4.8)$$

$$\mathbf{NH_3 + Mg^{2+} \rightleftarrows MgNH_3^{2+}} \quad (4.9)$$

$$\mathbf{2NH_3 + Mg^{2+} \rightleftarrows (MgNH_3)_2^{2+}} \quad (4.10)$$

$$\mathbf{3NH_3 + Mg^{2+} \rightleftarrows (MgNH_3)_3^{2+}} \quad (4.11)$$

$$\mathbf{Mg^{2+} + OH^- \rightleftarrows Mg(OH)_2} \quad (4.12)$$

At initial solution pH of 11, the ammonium ion can be transformed to ammonia (NH_3) which can react with Mg to form $MgNH_3^{2+}$, $(MgNH_3)_2^{2+}$ and $(MgNH_3)_3^{2+}$. So the amount of Mg^{2+} and NH_4^- are reduced in the solution at pH 11. On the other hand, Mg^{2+} ions in bulk solution could react with OH^- ion to form Brucite ($Mg(OH)_2$)

It can be concluded that, if either enough acid or base is added, the phosphate and ammonium and magnesium ion concentration in the solution can be reduced so as to make the ion activity product smaller than the solubility product, K_{SP}, so that more struvite dissolves.

Figure 4.2 shows the variation of solubility in mg/L with different initial solution pH at temperature range 25 – 40^OC. The experimental data can be seen in Appendix A1. Figure 4.2 illustrates that the minimum solubility of struvite crystals occurred at range pH 7 – 9 for all temperatures. This result agrees with results published by several other authors (Buchanan et al., 1994, Ohlinger et al., 1998, Taylor et al., 1963, Loewenthal et al., 1994, Abbona et al., 1982, Nelson et al., 2003). A minimum solubility is reached at 174 mg/L of initial pH solution 7 – 9 at 25^OC. For all temperature studies shown in Figure 4.2 it can be concluded that the minimum solubility occurred at an initial pH of 8.5.

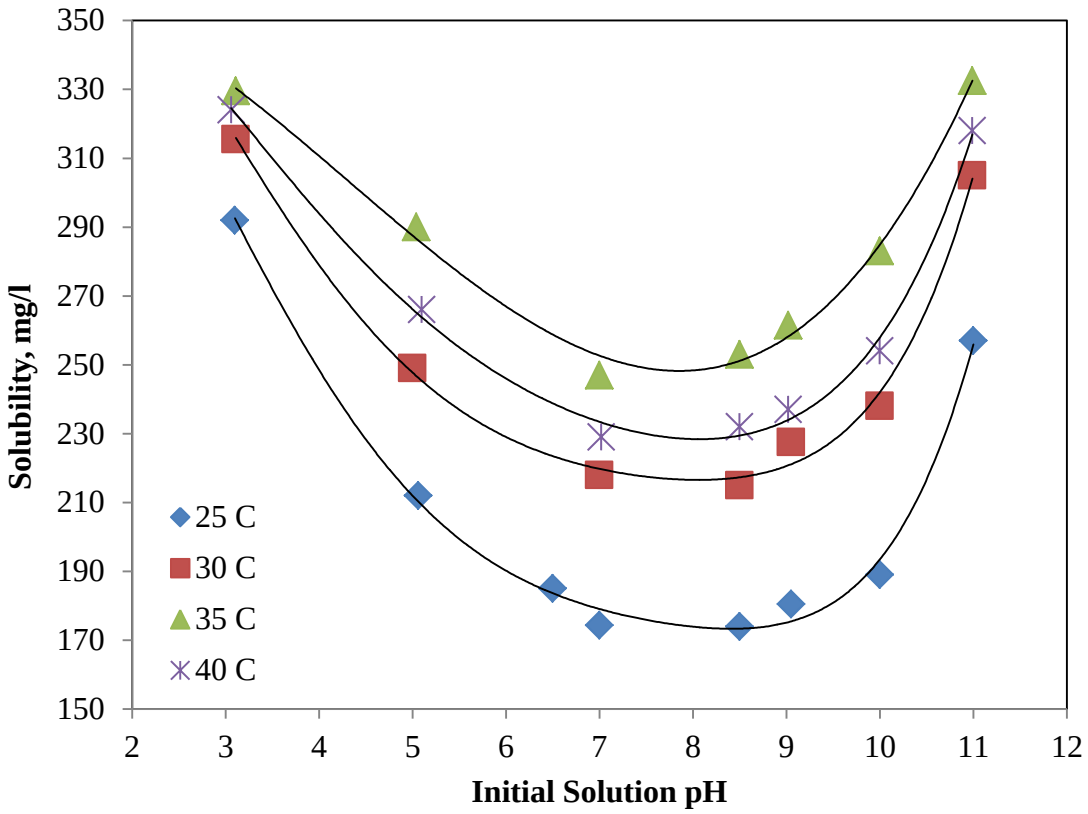

Figure 4.2 Solubility of Struvite for Various Initial Solution pH at Different Temperatures.

The variation of solubility of struvite in mg/L and K_{SP} values with different initial solution pH at 25^{O}C are shown in Figure 4.3. The minimum K_{SP} value was found to be around $2.89 \times 10^{-13} - 3.25 \times 10^{-13}$ (*pKa* value from 12.54 – 12.49) at pH 7 – 9 (in detail see Table A2.1 in Appendix A), while the solubility of struvite reaches a minimum value of 174 – 180 mg/L. The *pKa* value of this study compares very well with other studies (around 12.36 – 12.93) (Aage et al., 1997, Loewenthal et al., 1994, Webb and Ho, 1992, Snoeyink and Jenkins, 1980).

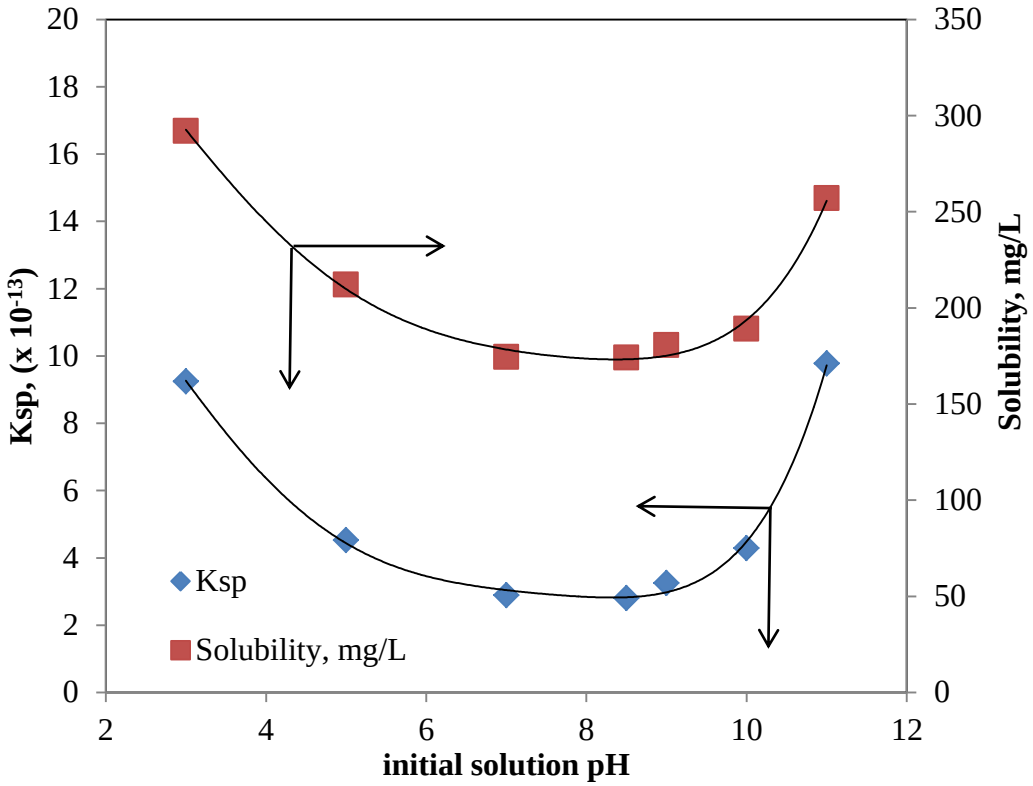

Figure 4.3 Variation of solubility (mg/L) and *Ksp* of struvite with initial solution pH at 25^{O}C

Figure 4.4 shows the concentration of NH_4^+, Mg^{2+} and PO_4^{3-} as a function of initial solution pH at 25^{O}C (In detail see Table A2.1, Appendix A). Figure 4.4 shows that the effect of initial pH used in the experiment is in the range 3-11. In acid condition or pH 3, struvite more easily dissolves than initial solution pH 9. So when initial pH of 3 used, ion formation of struvite will decompose and transfer to the solution. Decomposition of the formation struvite ions continue and become stable when the pH of the solution reached equilibrium at pH 8.5-9. Struvite is less soluble in the solution when the initial pH of 9 is used in the experiment. And the solution more easily reach saturation point. At initial solution pH 3, the concentration of PO_4^{3-} ion (12.9×10^{-5}mMol) in solution was higher than Mg^{2+} (10.1×10^{-5} mMol) and NH_4^+ (9.1×10^{-5} mMol) after 24 hours agitation in solubility unit. Molar ratio of NH_4^+: Mg^{2+}: PO_4^{3-} was 1:1.1:1.4. At initial solution pH 7, 8, and 9, the molar ratio of NH_4^+:Mg^{2+}:PO_4^{3-} was 1:1:1. Furthermore, the concentration of NH_4^+ ions was higher than others when initial

solution pH was increased between 10 and 11. It indicated that ammonium ion easily dissolved or decomposed from struvite crystals under basic solution conditions. Moreover, the concentration of Mg^{2+} ions was surprisingly lower than other ions at initial solution pH 10 and 11. In these latter cases, Mg^{2+} ions reacted with OH^- ion to formed $Mg(OH)_2$. Generally, constituent ions forming struvite crystals dissolved at 25^OC decreased with increase in initial solution pH and reached a minimum solubility at pH 7 – 9.

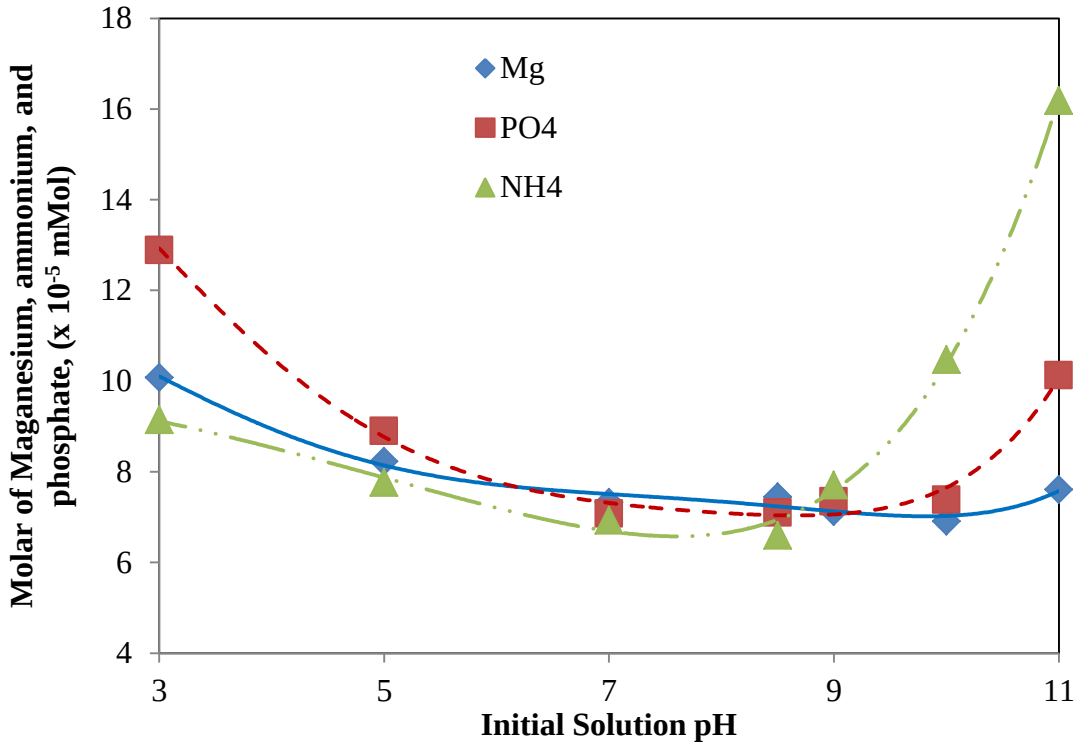

Figure 4.4 The effect of initial solution pH on soluble magnesium, ammonium and phosphate concentration at 25^OC.

4.3.2 Effect of temperature on struvite solubility

The temperature effect on the solubility of struvite crystals in water was studied in the temperature range 20 – 50^OC and initial pH 7. The results are given in Figure 4.5 Struvite solubility at 25^OC is 174 mg/L, compares very well with those reported by Bhuiyan et al., (2007) and Andrade and Schuiling (2001), 169 and 160 mg/L, respectively. The experimental results can be seen in Table A2.2 of Appendix A.

Figure 4.5 also shows the solubility increased with increasing temperature from 20^{O}C to 35^{O}C and then it decreases. The *Ksp* values of struvite crystal increased from 1.63×10^{-13} to $8.01 \times 10^{-13}$with increase in temperature. The *Ksp* value decreased from 8.01×10^{-13} to 2.82×10^{-13} with temperature range 35 – 50^{O}C.

The maximum solubility temperature of 35^{O}C found possibly indicated a phase transition with 8.01×10^{-13} of *Ksp* value. Temperature of solution exceeded 35^{O}C, it is possible that phase change of struvite to magnesium ammonium phosphate monohydrate ($MgNH_4PO_4.H_2O$) (Bridger et al., 1962).

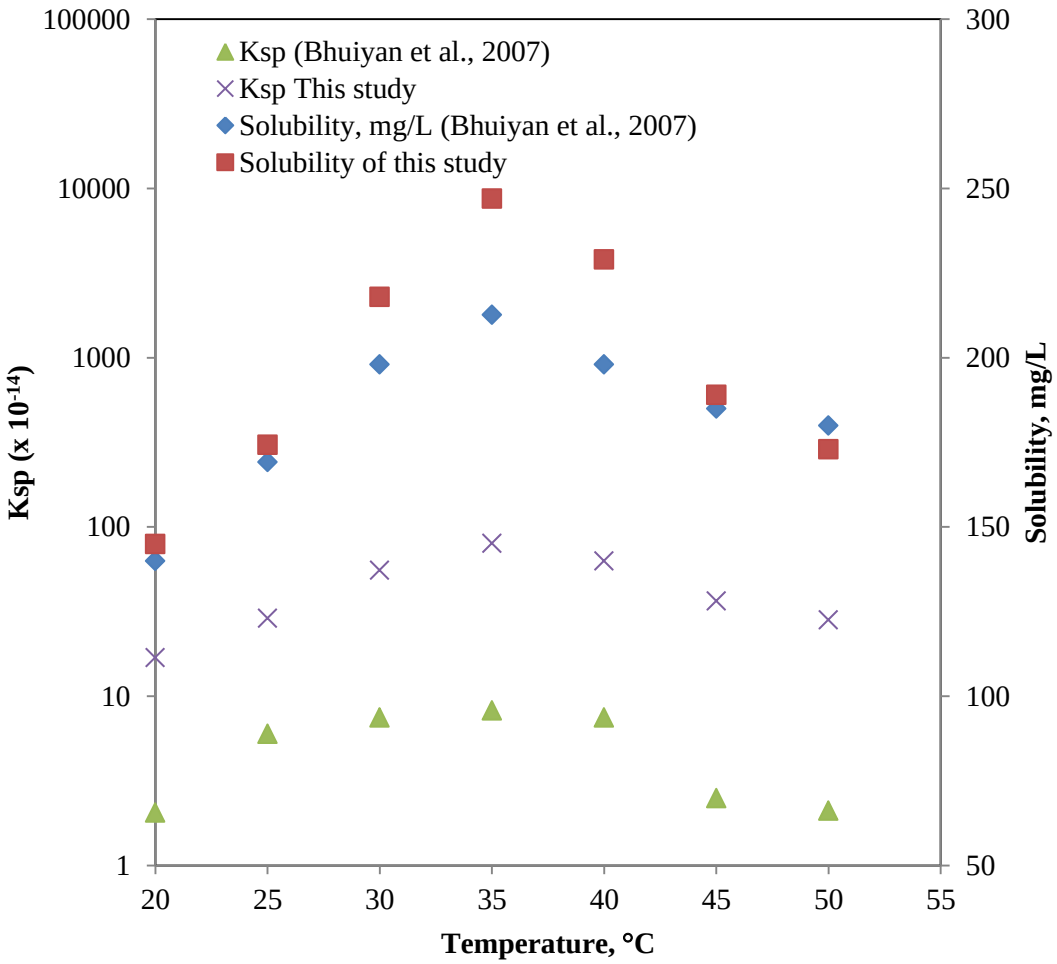

Figure 4.5 Solubility of Struvite of solution at different temperature at pH 7 (This work and Other Studies)

The phase change of struvite is followed by a change in structure, which is likely to affect the solubility of the compound (Bhuiyan et al., 2007). According to Bridger et al., (1962) struvite crystal in the hexahydrate or higher water presence makes it more soluble than monohydrate. Figure 4.5 shows that struvite solubility product was found to be higher at 40^{O}C (229 mg/L) than at 25^{O}C (174 mg/L). In these cases, struvite solubility was also found to be more soluble at 40^{O}C than at 25^{O}C.

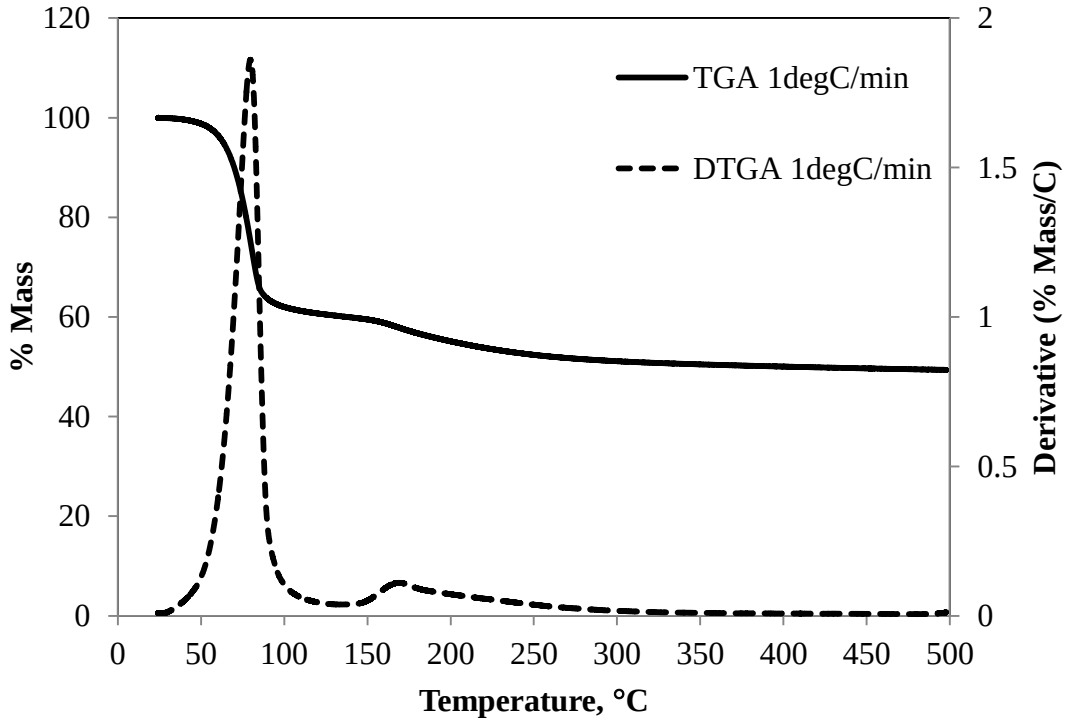

Figure 4.6 TGA and DTGA curve of Synthetic Struvite for Heating 1^{o}C min^{-1}

The thermogravimetric analysis (TGA) and derivative thermogravimetric analysis (DTGA) curve for synthetic struvite are shown in Figure 4.6. The TGA of struvite was under nitrogen gas and at different heating rate. These data indicate that mass loss begins at a temperature around 40^{o}C and is essentially complete when the temperature reached above 250^{o}C. At this point, 50.65 % of the original mass loss occurred. The mass losses correspond to the following decomposition reaction for struvite are as follows (Paulik and Paulik, 1975)

$$\mathbf{MgNH_4PO_4.6H_2O \rightarrow MgNH_4PO_4.H_2O + 5H_2O \uparrow} \quad (4.13)$$

$$\mathbf{MgNH_4PO_4.H_2O \rightarrow MgNH_4PO_4 + H_2O \uparrow} \quad (4.14)$$

$$\mathbf{MgNH_4PO_4 \rightarrow MgHPO_4 + NH_3 \uparrow} \quad (4.15)$$

According to reaction (Eq. 4.13), when struvite crystals were heated above 35^{O}C in water, crystallized water of struvite crystal was transfer to bulk solution. So, struvite crystals transform from hexahydrate to monohydrate.

Figure 4.7 shows the concentration of NH_4^+, Mg^{2+} and PO_4^{3-} as a function of temperature in deionized water. The experimental results can be seen in Table A2.2 of Appendix A. At temperature 20^{O}C the concentration of NH_4^+ ion in solution was lower than Mg^{2+} and PO_4^{3-} after 24 hours agitated in cell. Furthermore, the concentration of NH_4^+ ions was higher than others when temperature was increased above 25^{O}C. It is possible that $Mg_3(PO_4)_2$ may be formed in solution. Generally, constituent ions forming struvite crystals dissolved in deionized water increased with increase in temperature and reached a maximum solubility at 35^{O}C, and then the concentration ions of NH_4^+, Mg^{2+} and PO_4^{3-} decreased.

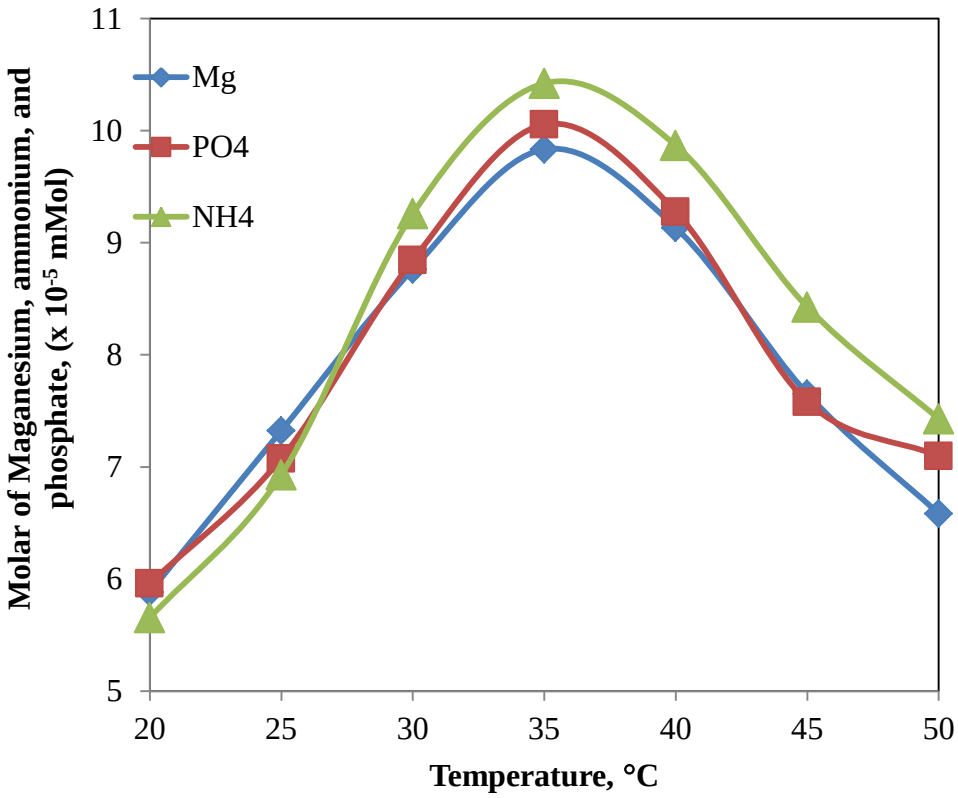

Figure 4.7 The effect of temperature on soluble magnesium, ammonium and phosphate concentration at deionized water

According to Bhuiyan et al., (2007) the effect of temperature on solubility of struvite was an indication of the quantity of heat released or absorbed. The heat released or absorbed depends on the energy needed to decompose the component ions of struvite crystals. The endothermic process describes a process for more energy required to decompose the component ions of struvite from crystals into the solvent. While energy released from the system is an exothermic energy.

The most general way to determine the effect of temperature on solubility is to calculate the value of solubility product at different temperatures (Myerson, 2002). An alternative approach is based on the estimated value of the enthalpy (ΔH_r^o) of the equilibrium over the studied temperature range. In fact, assuming that all saturated solutions have an ideal dilute behaviour, the influence of temperature on struvite solubility can be quantitatively described by the Van't Hoff equation as (Myerson, 2002):

$$-\ln \boldsymbol{Ksp} = \frac{\Delta \boldsymbol{Hr^0}}{\boldsymbol{R}}\left(\frac{\boldsymbol{1}}{\boldsymbol{T}}\right) + \boldsymbol{C} \qquad (4.16)$$

where R is ideal gas constant (8.314 J/mol.K).

The enthalpy of struvite solubility in deionized water can be determined by plotting $-ln\ K_{SP}$ as a function of $1/T$. The K_{sp} values can be seen in Table A2.2 of Appendix A2. The results are shown in Figure 4.8. The results are summarised in Table 4.1. The endothermic energy value of this study agrees favourably with Bhuiyan et. al., (2007) value and the text book values of 83.7 kJ/mol^{-1} (Faure, 1991).

Based on the K_{SP} value, the dissolution of struvite is accompanied by endothermic energy of 95.1 kJ/mol in range temperatures of 10 – 35^{O}C. In this condition, the solubility increases with increase in temperature and reaches the maximum solubility at 35^{O}C. After that, the dissolution of struvite releases an amount of heat (exothermic) of 76.5 kJ/mol; this results in a decrease in the solubility as the temperature increases.

Table 4.1 Standard molar enthalpies of struvite solubility calculated from Van't Hoff plots (ΔH^{O} in kJ/mol)

	ΔHr^{0}, kJ/mol (exothermic)	ΔHr^{0}, kJ/mol (endothermic)
This study	95.1	-76.5
Bhuiyan et al., (2007)	91.9	-76.9

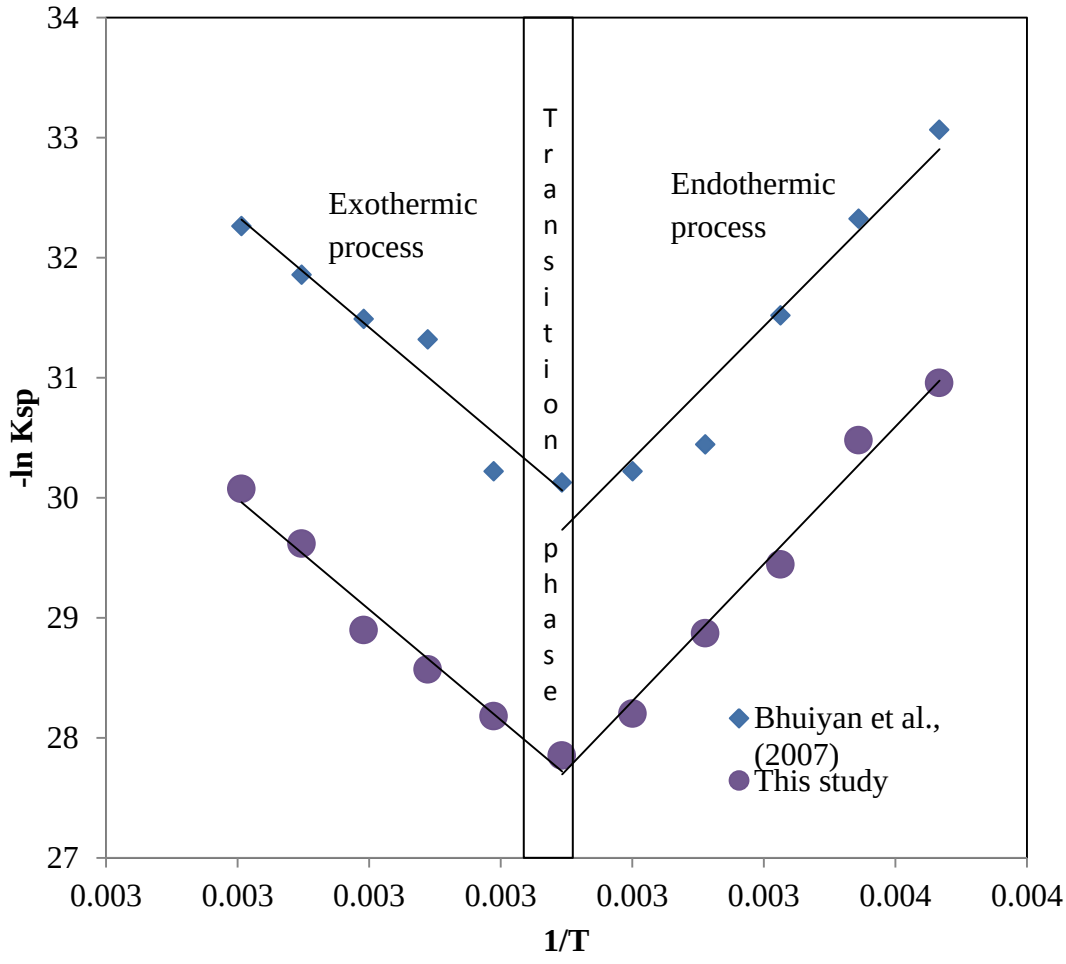

Figure 4.8 Struvite solubility in deionized water as a function of temperature

4.3.3 Effect of common-ion on solubility

Experimental results of struvite solubility in the common-ion of Cl^{-} derived from KCl, NaCl and $CaCl_2$ are illustrated in Figure 4.9. The effect of common-ion on struvite solubility was conducted at various concentrations of NaCl, KCl and

$CaCl_2$ within a range of 0.25 – 1.5 mM at 25^{O}C. Figure 4.9 shows that the presence of KCl, NaCl, and $CaCl_2$ has a significant effect on the solubility of struvite which may lead to increase with increasing Cl^- ion concentration in solution. Increasing solubility of struvite was caused by reacted Cl^- ion in solution with Mg^{2+} ions derived from dissolution of struvite which produce $MgCl^-$ ion. The reaction can be seen as listed in Eq. (4.17).

$$\mathbf{Mg^{2+} + Cl^{-} \rightleftarrows MgCl^{+}} \quad (4.17)$$

Excess Cl^- ion influenced the increase in solubility of an ionic precipitate when a soluble compound added to the solution in equilibrium with the precipitate combines with one of the ions of the precipitate. The Mg^{2+} ion continuously dissolves until ionic activity product (*IAP*) is equal to the solubility product of struvite (K_{SP}).

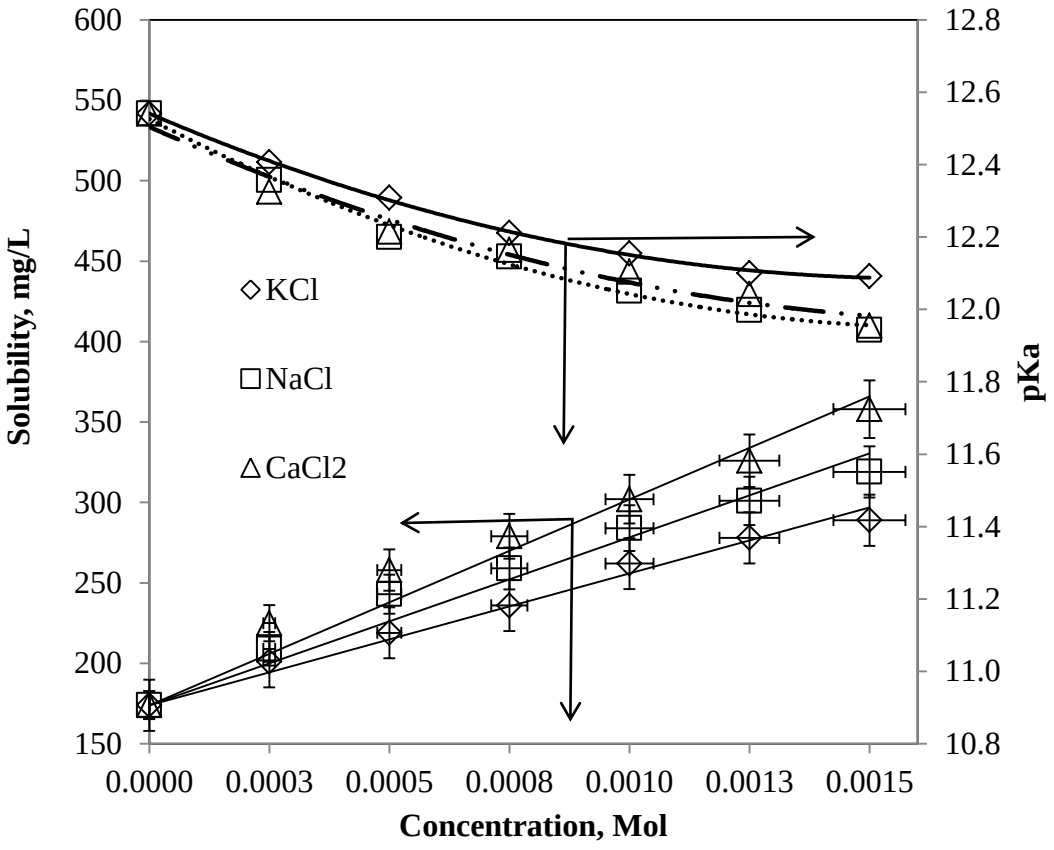

Figure 4.9 Solubility of Struvite in the presence of NaCl, KCl, and $CaCl_2$ at 25^{O}C.

As can be seen in Figure 4.9, the presence of NaCl, KCl and $CaCl_2$ has a salting-in effect on struvite over the whole range of salt concentration studied. Increasing

concentration of Cl^- ion added in the solution increased solubility of struvite. At any given molar concentration of salts, the solubility of struvite in $CaCl_2$ solution is the highest followed by NaCl and KCl, respectively. Solubility values are 302, 284, and 262 mg/L for $CaCl_2$, NaCl and KCl at 0.001 mMol of salt concentration, respectively. Core et al (2005) reported that the presence of Ca^{2+} ions may interact effectively with phosphate. Solubility of struvite in KCl solution increased from 174 to 289 mg/L (pKa = 12.54 – 12.09) at salt concentration 0 to 0.0015 mMol. The experimental results can be seen in Table A3.1, A3.2 and A3.3 of Appendix A.

The composition dependence of struvite solubility in aqueous KCl, NaCl, and $CaCl_2$ solution of various concentrations was correlated by means of a polynomial type equation:

$$\boldsymbol{F(Q) = A_0 + A_1(X) + A_2(X)^2} \quad (4.18)$$

Where Q represents solubility of struvite and X is the concentration (mol) of salts in the solution. The values of the parameters A_i (I = 0 to 2) were evaluated by the least-square methods. The parameters A_i are given in Table 4.2.

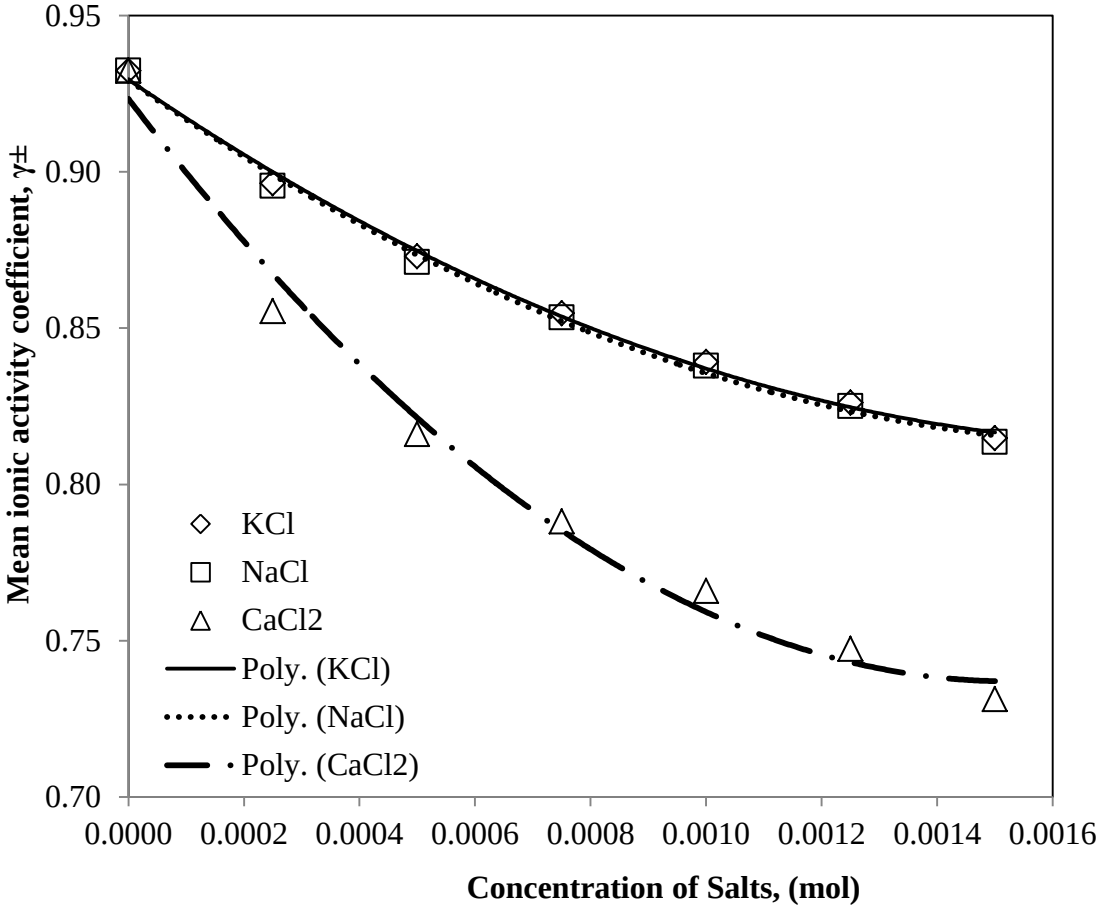

Figure 4.10 Mean ionic activity coefficient of struvite at different concentrations of salts at 25^{O}C

Estimated values of mean ionic activity coefficient ($\gamma\pm$) are calculated based on Eq. (4.3). Figure 4.10 shows that the γ± values decrease with increase in the salt concentration. The γ± value of NaCl present in solution is similar to KCl values while $CaCl_2$ values decreased more sharply.

Table 4.2 Parameters A_i of Eq. (14) for the system of struvite + salts at 25^{O}C

	A_0	A_1	A_2	R^2
Solubility product, *pKa*				
KCl	12.541	-567.54	176800	0.98
NaCl	12.526	-690.01	206612	0.98
$CaCl_2$	12.505	-594.13	164092	0.97
Mean ionic activity coefficient, γ±				
KCl	0.9296	-126.93	34426	0.99
NaCl	0.9294	-129.87	36043	0.98
$CaCl_2$	0.9234	-244.19	79961	0.98

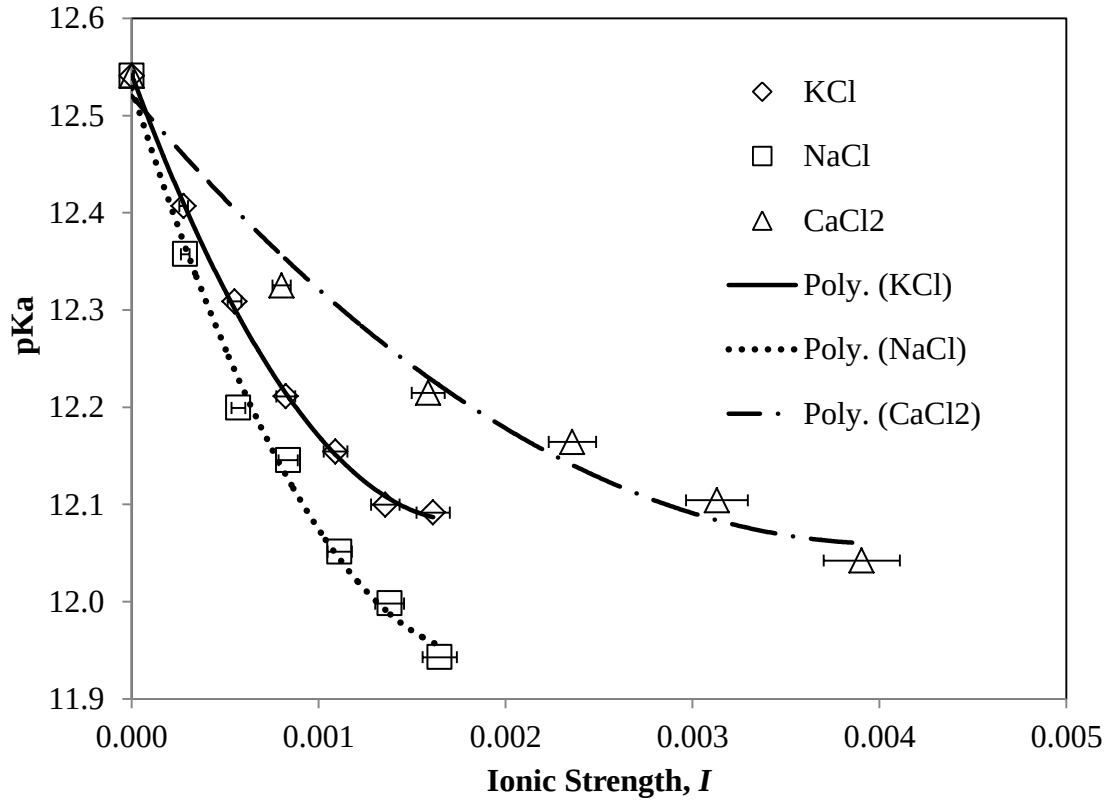

Figure 4.11 Solubility product of struvite at different ionic strength in aqueous salts solution at 25^{O}C

The *pKa* values presented in Figure 4.11 as a function of struvite ionic strength in aqueous salts solution decrease with an increase in the salt concentration. At any

given *pKa* value, the ionic strength of struvite solubility in $CaCl_2$ solution were higher than KCl and NaCl.

Given the ideal diluted behaviour of all the saturated solutions, the standard molar Gibbs free energy of transfer from pure water to aqueous solution of chloride salts, ΔG, can be expressed by:

$$\Delta \boldsymbol{G} = -\boldsymbol{RTln}\left(\frac{\boldsymbol{S_{salt}}}{\boldsymbol{S_{aq}}}\right) \quad (4.19)$$

where S_{aq} and S_{salt} are solubility of struvite in pure water and in aqueous chloride solution of a given concentration, respectively.

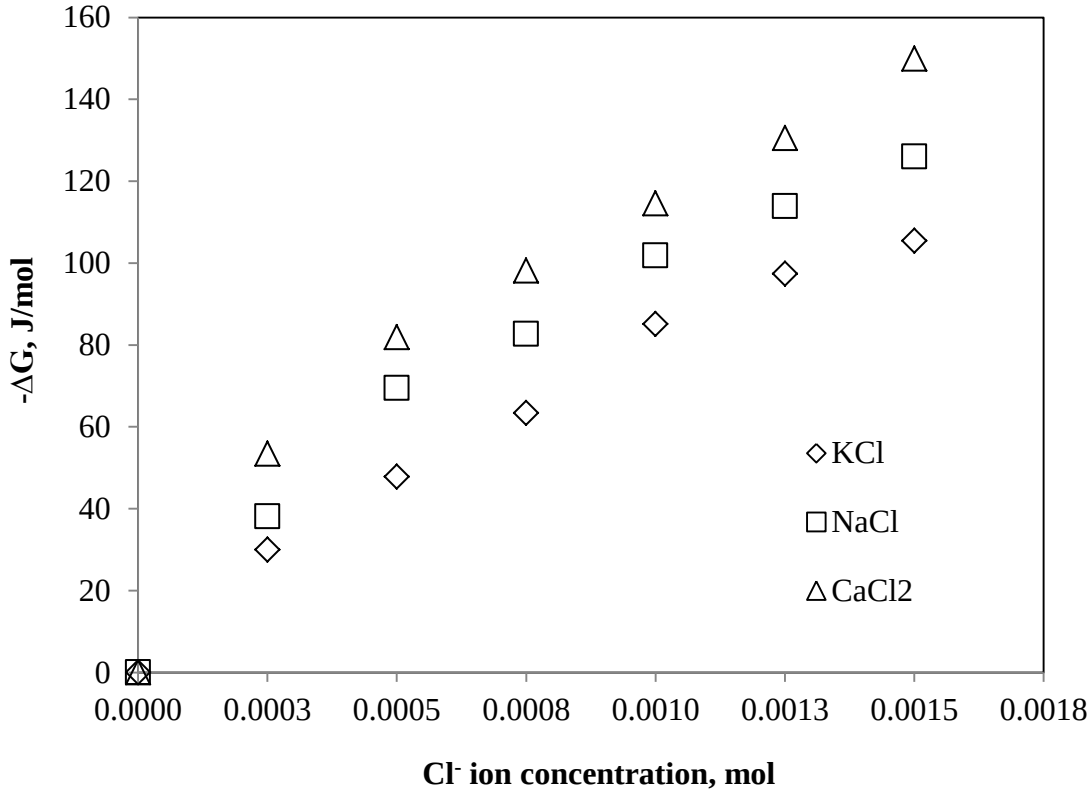

Figure 4.12 Standard molar Gibbs free energy of transfer of struvite from water to chloride solutions, as a function of salt molality, at 25^{O}C.

The standard molar Gibbs energy in chloride salts were calculated using Eq. (4.19). The ΔG of struvite at 25^{O}C as a function of chloride salts molality is represented in Figure 4.12. The general trend of all the struvite studies showed a ΔG increase with increasing chloride salts concentration. The general trend obtained for the salting-in effect showed a ΔG decrease in the following order: KCl > NaCl > $CaCl_2$.

These results confirm that the addition of $CaCl_2$ results in higher solubilities of struvite in water compared to that of KCl and NaCl. In general, the study observed increases in struvite solubility in the presence of metal chloride and consequently negative values of ΔG are obtained.

4.3.4 Effect of Initial Solution pH on Morphology of Struvite Crystal

Solid precipitates were characterized by scanning electron microscope (SEM) and XRD analysis. The struvite crystal before subjecting them to solubility studies is shown in Figure 4.13.

The difference between images in Figure 4.13(a) and 4.14 are influenced by the use of coating type. Carbon coating type was used in Figure 4.13 (a) while gold coating type was used in Figure 4.14. The gold coating can produce a clear image compared with carbon coating. XRD data indicated single–phase struvite (orthorhombic) space group with the experimental lattice parameters of a = 11.215, b = 6.954, c = 6.141. In Figure 4.13(b), the patterns confirmed that orthorhombic struvite was dominant crystal phase.

The formation of struvite crystals can be formed in the pH range of 7-11. In this range pH, a few crystals can possibly form as trimagnesium phosphate [$Mg_3(PO_4)_2.6H_2O$], magnesium hydrogen phosphate [$MgHPO_4.3H_2O$], and bobierrite [$Mg_3(PO_4)_2.8H_2O$] (Musvoto et al., 2000). These three kinds of the crystals formed are influenced by solution pH and concentration of magnesium and phosphate.

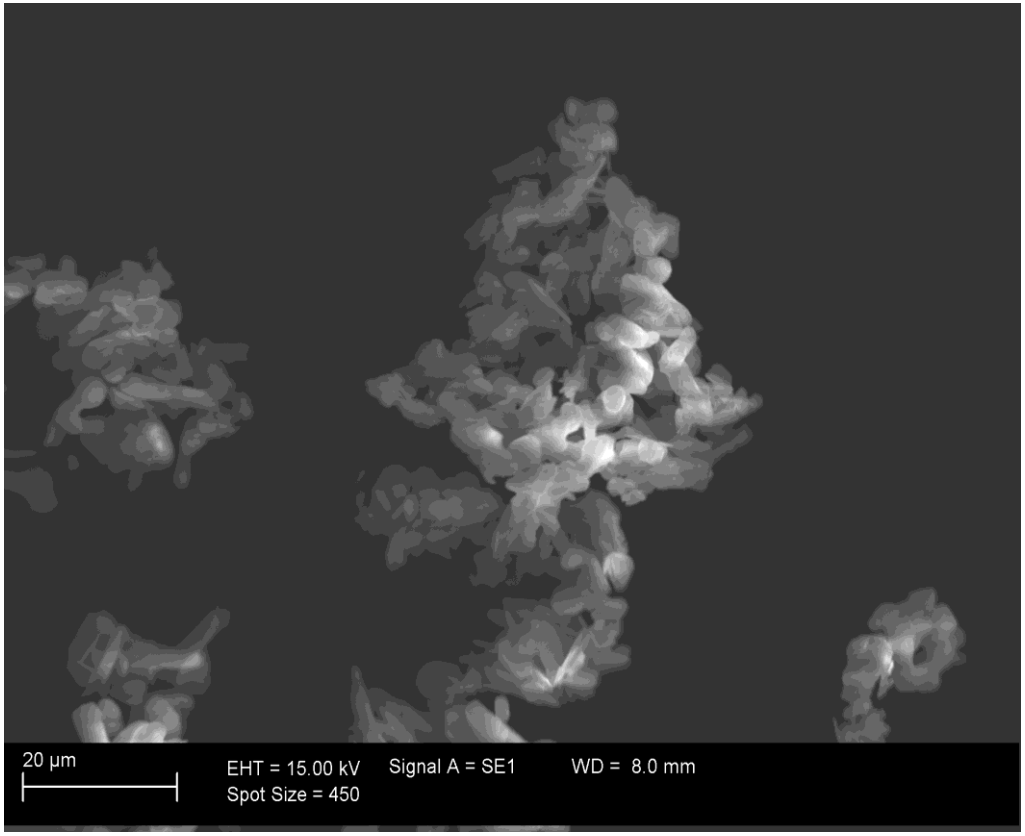

(a)

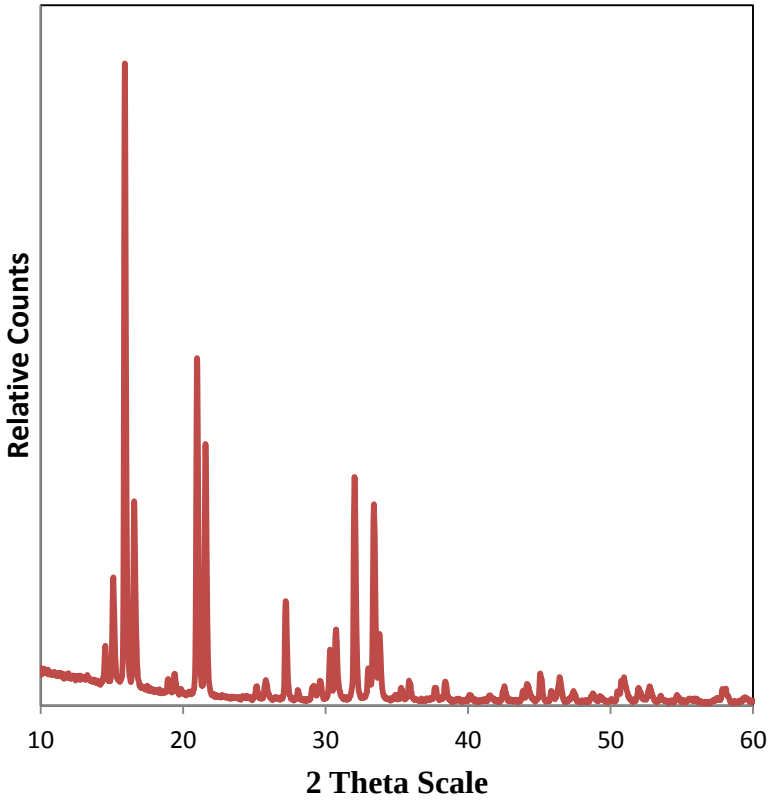

(b)

Figure 4.13 SEM Image and XRD trace of Struvite Before Solubility Study

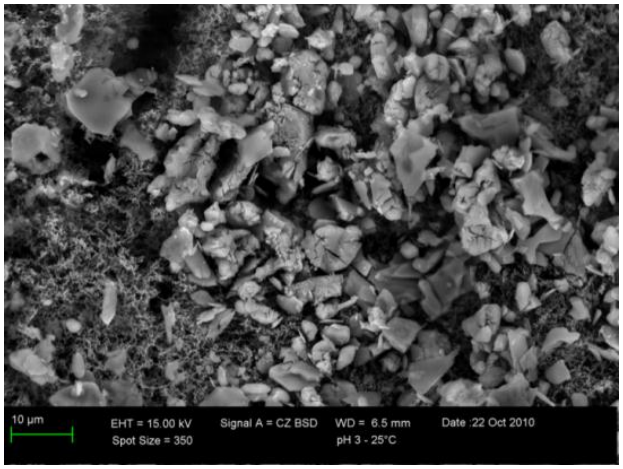

(a)

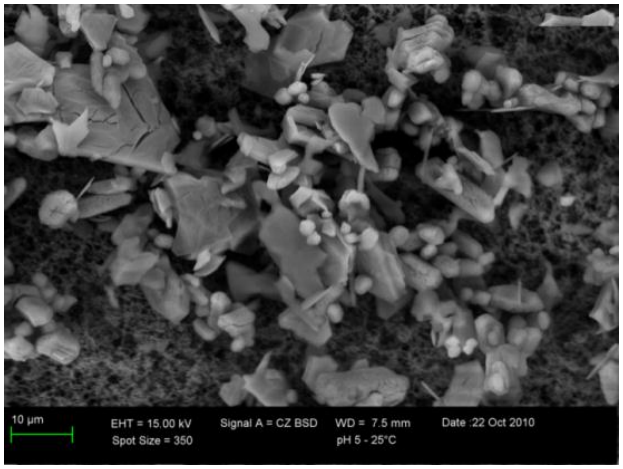

(b)

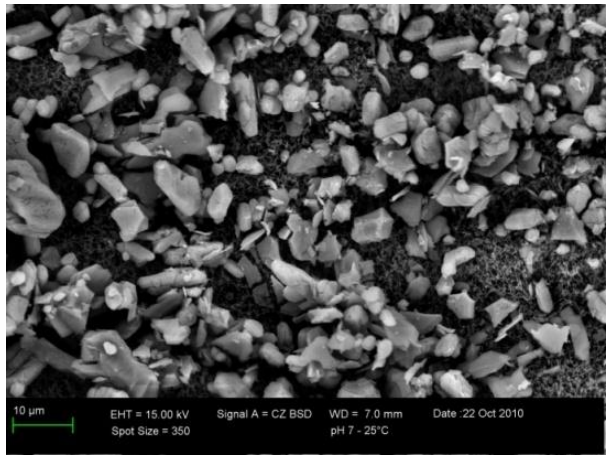

(c)

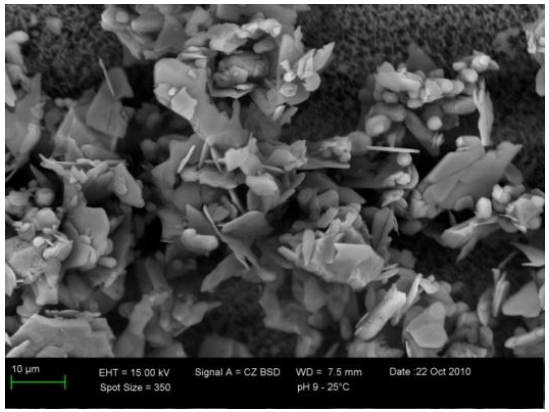

(d)

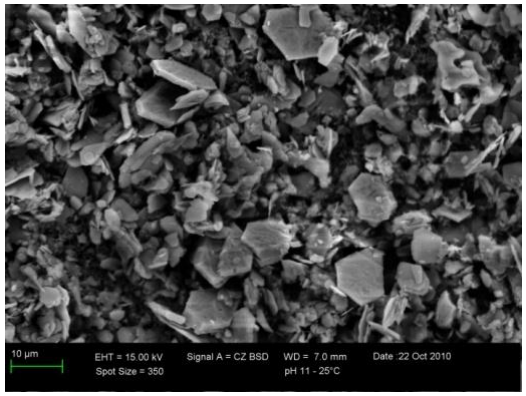

(e)

Figure 4.14 Typical SEM morphologies for the struvite crystals at different pH values at 25^0C (a, 3; b, 5; c, 7; d, 9 and e, 11)

In this study, the morphology was investigated at different solution pH. When struvite crystals dissolved in solution, struvite crystals decompose to produce three component ions, namely Mg^{2+}, $PO4^{3-}$, and NH_4^+. This decomposition was followed by a process of change in crystal morphology. At initial pH 3, the equilibrium pH was 8.4 after allowing 24 hours for the dissolution process. The SEM images are shown in Figure 4.14(a) where the crystals were formed after the dissolution process at 25^OC and initial pH 3. The solids remained at pH 3 were amorphous when observed by SEM. The amorphous condition may be influenced by phosphate ions. In acid conditions, phosphate species ($H_2PO_4^-$) decomposed from struvite was approximately 95% of phosphate (Mijangos et al., 2004), so that the crystals were amorphous.

At initial pH 5, the equilibrium conditions were reached at pH 9.2. Crystals produced on initial pH 5 in Figure 4.14(b) were platelets and spherical due to phosphate species of $H_2PO_4^-$ was less than the initial pH 5. Figure 4.14(c) was rhombohedral for initial pH of 7. According to Mijangos et al (2004), total $H_2PO_4^-$ and HPO_4^{2-} is 10 % of total concentration of phosphate. The crystals at pH 5 looked more crystalline. Figure 4.14(d) was platelets and spherical for initial pH 9. Owing to the decomposition of the species phosphate (HPO_4^{2-}) from struvite was only approximately 5 % of total concentration of phosphate. Figure 4.14(e) shows hexagonal platelets and smaller crystals. The morphology of crystals not only was affected by species of phosphate but also base condition. Hexagonal crystals produced at pH 11 is possibly influenced by the reaction of Mg^{2+} and OH^- to form brucite ($Mg(OH)_2$).

The characteristic precipitate produced by various initial solution pH is shown in Figure 4.15. There were strong peaks of struvite in precipitates formed at different initial solution pH. Figure 4.15(a)(b) shows that the magnesium peak was higher than phosphorous peak. It can be indicated that phosphorous more dissolves than magnesium. According to EDS analysis at Figure 4.15(c)(d), the phosphorus atomic concentration is equal to magnesium concentration. Furthermore, the magnesium peak was higher than phosphorous peak when initial solution pH 11 was used to dissolves struvite for 24 hour (Figure 4.15(e)). The highest magnesium pH due to OH^- ion reacted with Mg^{2+} to form $Mg(OH)_2$.

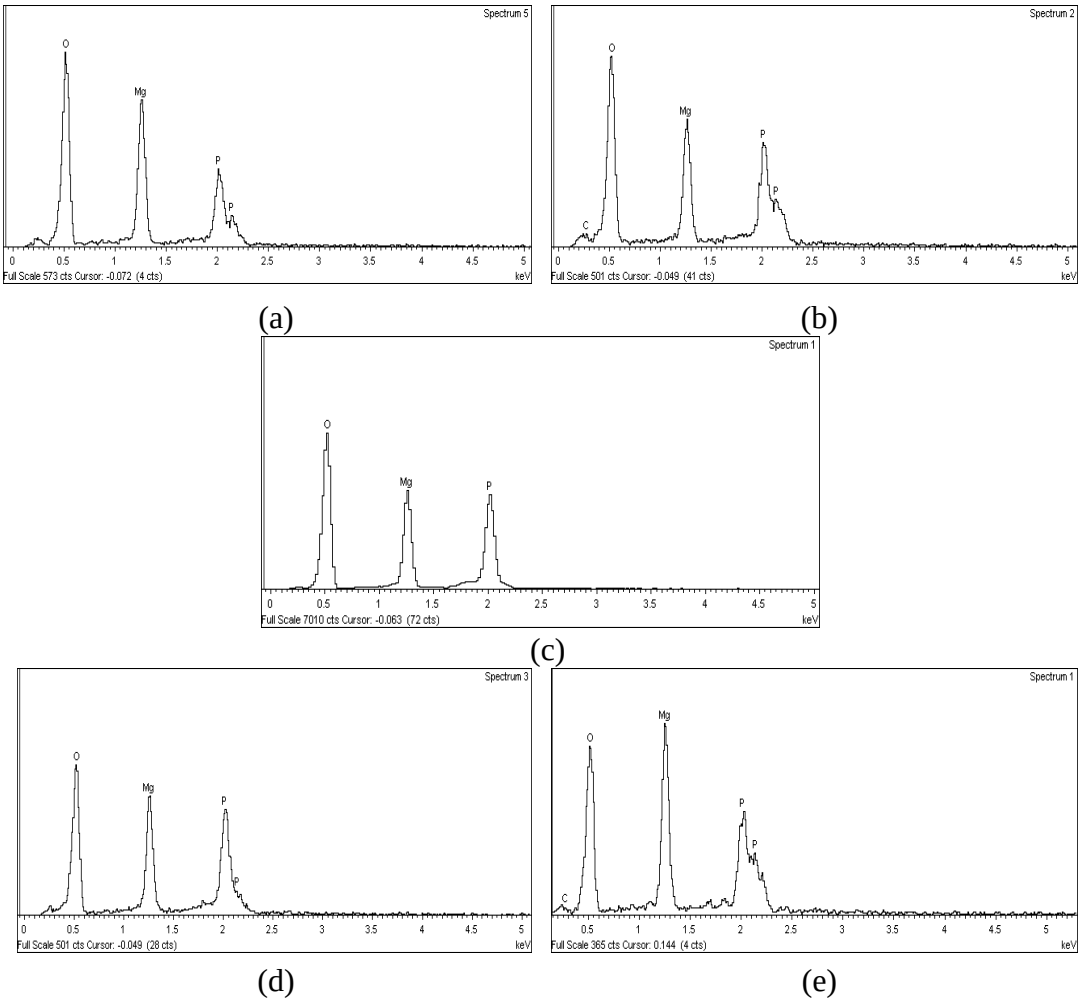

Figure 4.15 EDS data for dissolution of struvite crystals with different initial pH solution; (a) pH 3; (b) pH 5; (c) pH 7; (d) pH 9; (e) pH 11

4.4 Summary

The solubility of struvite was studied at different initial solution pH, temperature and the presence of different chloride salts. Based on the experimental data, the following conclusions can be made:

- The solubility of struvite at different initial solution pH increases with decrease in pH from 7 to 3. In the alkaline region, solubility increases with higher initial solution pH from 9 – 11.
- A similar behaviour was observed with temperature where the solubility was a maximum at 35^{O}C. It is possible that a phase transition occurs at 35^{O}C indicating that at lower than 35^{O}C, struvite exists as one crystallisation form but transforms to another form above 35^{O}C.

- Based on the K_{SP} value, the dissolution of struvite is accompanied by endothermic energy of 95.1 kJ/mol in temperatures range of 10 – 35^{O}C. After that, the dissolution of struvite releases an amount of heat (exothermic) of 76.5 kJ/mol; this results in a decrease in the solubility as the temperature increases.
- The study observed increases in struvite solubility in the presence of chloride (Cl^-) ions. Interestingly, in $CaCl_2$ solution the solubility of struvite was the highest compared to KCl and NaCl. The chloride salts effect can be correlated to a ΔG decreasing order, i.e., KCl > NaCl > $CaCl_2$.
- Morphology of product crystals was affected by phosphorous ions at various solution pH. The acidic solution decomposes more of phosphorus ions resulting in amorphous crystals at initial pH of 3.

CHAPTER 5
IMPACT OF VARIOUS PHYSICO-CHEMICAL PARAMETERS ON SPONTANEOUS NUCLEATION OF STRUVITE ($MgNH_4PO_4.6H_2O$) IN WATER: KINETICS AND NUCLEATION MECHANISM

5.1 Introduction

Struvite ($MgNH_4PO_4.6H_2O$) usually precipitates as stable white crystals in a 1:1:1 molar ratio of Mg^{2+}, NH_4^+ and PO_4^{-3} according to the following reaction (Le Corre et al., 2005) where *n* can be 0, 1 or 2:

$$\mathbf{Mg^{2+} + NH_4^+ + H_nPO_4^{n-3} + 6H_2O \rightleftarrows MgNH_4PO_4.6H_2O + nH^+} \quad (5.1)$$

Magnesium, ammonium, and phosphate ions are released as the result of solids degradation in an anaerobic digestion of wastewater treatment plant. Under certain physico-chemical conditions, these dissolved wastewater constituents can combine to form struvite according to Eq. (5.1) which causes scale deposition on pipe walls, pump and equipment surfaces of anaerobic digestion and post-digestion processes. The blockage of pipes leads to an increase of pumping cost and also reducing plant capacity (Doyle and Parsons, 2002). It is not only pipes that are affected by struvite deposits, centrifuges, pumps, heat exchanger and aerators are also prone to fouling by struvite. Primarily as a problem to eliminate or inhibit struvite formation (Doyle and Parsons, 2002), struvite also offers itself as a fertilizer which encourage wastewater treatment companies to study its possible recovery (Le Corre et al., 2007). For those two reasons, it has become important to study the principles of struvite nucleation and to assess the various controlling physico-chemical parameters on struvite crystallisation. Predicting struvite crystallisation potential is critical to designers and operators for anticipating potential struvite formation problems. Struvite crystallisation can be separated into two basic stages: nucleation and growth. Nucleation occurs when ions combine to form crystal embryos that can act as the foundation for growth into detectable crystals (Ohlinger et al., 1999). Crystal growth continues until

equilibrium is reached (Doyle and Parsons, 2002). Predicting and controlling of these two stages is complex as they are controlled by a combination of factors including thermodynamics of liquid-solid equilibrium, phenomena of mass transfer between solid and liquid phases and kinetics of reaction. There are also various physico-chemical parameters such as solution pH, supersaturation (i.e. combined concentrations of Mg^{2+}, NH_4^+, and PO_4^{3-} exceeding the struvite solubility limit), temperature, interfacial energy, agitation energy and presence of other interfering ions (Uludag-Demirer et al., 2005, Ohlinger et al., 1998, Le Corre et al., 2005, Bhuiyan et al., 2008, Chien et al., 1999) which strongly influence the mechanism of crystal nucleation of struvite. Increases in temperature or supersaturation, or a decrease in the interfacial energy are expected to produce an increased nucleation rate (Mullin, 2001, Judge et al., 1999).

Homogeneous nucleation occurs spontaneously, whereas heterogeneous nucleation takes place due to presence of impurity particles and secondary nucleation occurs in the presence of seed crystals. The time taken for nucleation to occur where duration from the achievement of supersaturation to the appearance of crystal nuclei (often termed the induction time) has been reported to dictate the formation of a precipitate and hence scaling formation (Doyle and Parsons, 2002). Söhnel and Garside (1992) presented the development of a fundamental model to describe crystal nucleation and growth during the induction period, which, they reported, accurately predicts the observed behaviour of many moderately and sparingly soluble crystal precipitates. Various indicators have been used for the determination of crystallisation induction period: observation of light scintillations (Ohlinger et al., 1999, Galbraith and Schneider, 2009), conductivity measurement (Kabdasli et al., 2006), pH monitoring (Kofina and Koutsoukos, 2005, Bhuiyan et al., 2008) and absorbance measurements (Kabdasli et al., 2006). Each and every method has their own advantages and limitations. However, little is known about its tendency to nucleate and precipitate. Bouropoulos and Koutsoukos (2000) and Ohlinger et al., (1999) reported that struvite nucleation is proportional to the supersaturation. The pH, agitation energy, supersaturation and the presence of foreign ions are the important factors affecting induction time (Bhuiyan et al., 2008). The reduction of induction time with an increase in solution pH and

temperature was also reported by Bhuiyan et al. (2008). Temperature has a direct influence on the solubility of struvite and thermodynamics properties (Ronteltap et al., 2010) and hence nucleation rate. The pH range within which struvite can precipitate was identified as 7-11 (Matynia et al., 2006). The influence of pH and supersaturation on the crystallisation rate and crystal characteristics of struvite has been demonstrated by several investigators (Le Corre et al., 2005, Bhuiyan et al., 2008, Doyle and Parsons, 2002) but as yet little interest has been given to the influence of foreign ions on struvite nucleation and crystallisation. Theoretically, impurities in solution can affect the nucleation and growth rate of crystals due to blocking of active growth sites inhibiting the increase of crystal size (Le Corre et al., 2005). In the case of struvite crystallisation from wastewater sludge, foreign compounds such as potassium, chloride, calcium carbonate, zinc are numerous. There are few reported results on the effects of impurities such as chloride ion (Bouropoulos and Koutsoukos, 2000, Le Corre et al., 2005), carbonate ions (Le Corre et al., 2005), fluoride ion (Ryu et al., 2008), and ethylenediaminetetraacetic acid (EDTA) (Doyle et al., 2003) on struvite crystallisation from synthetic supersaturated solution. Impurity molecules adsorbed onto the nucleus surface can result in change of interfacial energy and nucleation rate. To further examine the nucleation behaviour, this study was undertaken to estimate nucleation rate parameters of struvite formation in a stirred batch crystalliser while examining the influence of pH, temperature, supersaturation, and salt (NaCl and KCl) impurities on nucleation. From the experimental results, the activation and interfacial energies during struvite formation could be determined so that a better understanding of the phenomenon can be obtained.

5.2 Experimental Nucleation Studies

Struvite nucleation studies were done in 250 ml Erlenmeyer flask agitated by magnetic stirrer and conditions described in Section 3.5.2. Two series of experiments were carried out. Firstly, nucleation of struvite was studied without Cl^- ion addition as impurities. Secondly, nucleation struvite crystal study was conducted with Cl^- ion addition. NaCl and KCl was used to Cl^- ion addition. These experiments permitted comparison to be made between two methods when

using the same levels of supersaturation with regard to different pH and temperature.

Supersaturation was created by mixing equimolar quantities of Mg^{2+}, NH_4^+, and PO_4^{3-} ions based on PhreeqC model. The preparation of Mg^{2+}, NH_4^+, and PO_4^{3-} ions solution can be seen in Section 3.5.1. The PhreeqC calculation results can be seen in Table 3.2 and Table 3.3 of section 3.5.2. Supersaturated solutions were agitated at 120 rpm for all the experiments.

5.2.1 Theory on calculation of the saturation index.

Saturation index (SI), see Eq. (5.6), of solution values were calculated by the PhreeqC model. The supersaturation ratio *S* is given by

$$\mathbf{S} = \frac{\mathbf{a_{Mg^{2+}}.a_{NH4^+}.a_{PO_4^{3-}}}}{\mathbf{K_{sp}}} \tag{5.2}$$

where a is the activities of the species.

According to Bhuiyan et al (2009), the thermodynamic solubility product of struvite on equilibrium with pure and solid phase struvite is;

$$\mathbf{K_{sp}} = \{\mathbf{Mg^{2+}}\}\{\mathbf{NH_4^+}\}\{\mathbf{PO_4^{3-}}\} \tag{5.3}$$

$$\mathbf{K_{sp}} = \boldsymbol{\gamma}_{\mathbf{Mg^{2+}}}[\mathbf{Mg^{2+}}].\boldsymbol{\gamma}_{\mathbf{NH_4^+}}[\mathbf{NH_4^+}].\ \boldsymbol{\gamma}_{\mathbf{PO_4^{3-}}}[\mathbf{PO_4^{3-}}] \tag{5.4}$$

$$\mathbf{K_c} = [\mathbf{Mg^{2+}}][\mathbf{NH_4^+}][\mathbf{PO_4^{3-}}] \tag{5.5}$$

where $\{Mg^{2+}\}$, $\{NH_4^+\}$ and $\{PO_4^{3-}\}$ are ion activity of magnesium, ammonium and phosphate, respectively, $[Mg^{2+}]$, $[NH_4^+]$ and $[PO_4^{3-}]$ are concentration of the ion magnesium, ammonium and phosphate, respectively, and $\gamma_{Mg^{2+}}$, $\gamma_{NH_4^+}$ and $\gamma_{PO_4^{3-}}$ are activity coefficient of the ion magnesium, ammonium and phosphate, respectively, K_{sp} is solubility product in terms of ion activity, K_c is solubility product in terms of concentration.

The SI value for struvite is used as an indication of supersaturation. If the SI is negative, the system is undersaturated with respect to struvite. If the SI is positive, the solution is supersaturated (Appelo and Postma, 1999). The SI values were calculated for all the experiments using the PheerqC model.

$$\mathbf{SI} = \mathbf{log\,S} = \mathbf{log}\frac{\frac{[\mathbf{Mg^{2+}}][\mathbf{NH_4^+}][\mathbf{PO_4^{3-}}]}{\mathbf{K_{sp}}}}{\boldsymbol{\gamma}_{\mathbf{Mg^{2+}}}.\boldsymbol{\gamma}_{\mathbf{NH_4^+}}.\boldsymbol{\gamma}_{\mathbf{PO_4^{3-}}}} \tag{5.6}$$

Effect of temperature on solubility product can be calculated as below (Bhuiyan et al., 2007):

$$\log K_{sp} = -1157.45 - 0.784T - \frac{63.86}{T} + 556.83 \log T + \frac{19.54}{T^2} \qquad (5.7)$$

The equilibria and the corresponding stability constants used for supersaturation calculation are summarized from Martell et al., (Martell et al., 1998) and Bhuiyan et al., (Bhuiyan et al., 2007) (see Table 2.3 in Section 2.8.4.2). Supersaturations were calculated by PhreeqC model (see Appendix B1).

5.3 Results and Discussions

5.3.1 Effect of pH on spontaneous nucleation of struvite crystals

pH is one of the important driving forces controlling the formation of struvite (Doyle and Parsons, 2002). The initial experiments undertaken used pH as an indicator of struvite nucleation. As the struvite precipitates, it triggers a release of proton ions in solution and hence a change in pH occurs during the nucleation process. The drop in pH is characteristic of the onset of nucleation at which the first time crystals of struvite occurs and is linked to the rate of struvite nucleation.

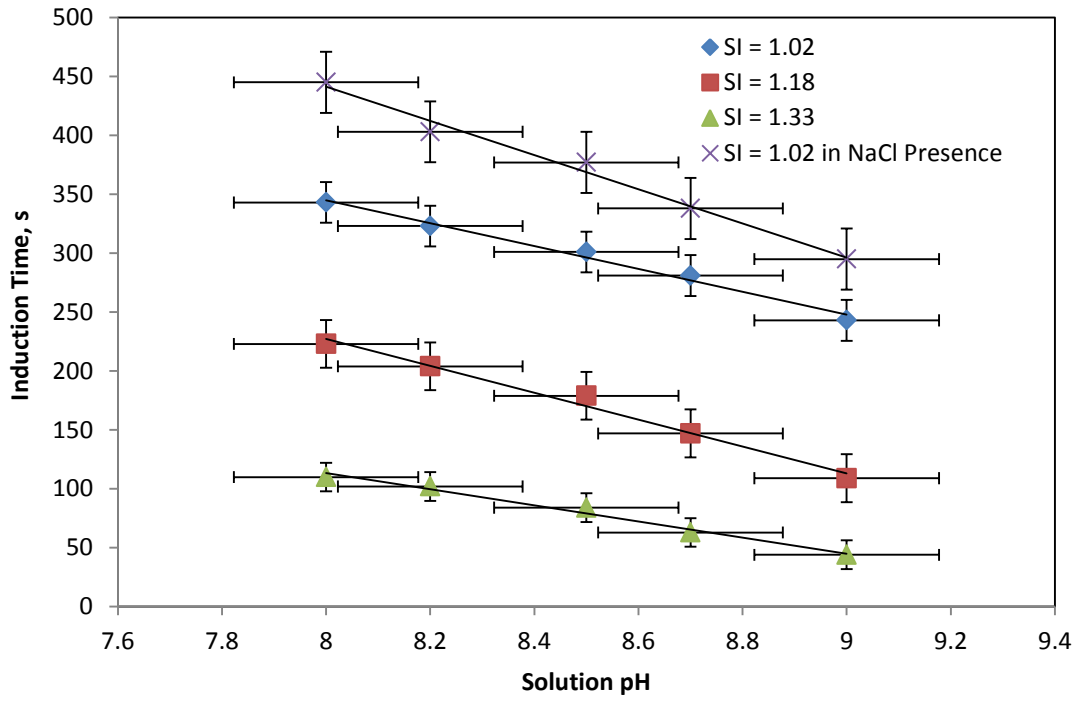

Figure 5.1 Variation of induction time with initial pH and *SI* at 25^{O}C

The effect of the initial solution pH on induction time was investigated at the same initial supersaturation with a molar ratio of Mg, NH_4 and PO_4 ion concentration in solution of 1:1:1. Figure 5.1 shows the variation of induction time with initial solution pH for various selected initial supersaturations. It was found that induction time decreased with increase in solution pH (Figure 5.1).

Figure 5.1 also shows the effect of excess Cl^- in the form of NaCl addition. For any given solution pH, the presence of NaCl resulted in higher induction time (Figure 5.1). The presence of Cl^- ions may affect equilibrium solubility, solution structure, and complex formation (Mullin, 2001) and hence interference on nucleation. Similar observation was reported by Söhnel and Mullin (1988) and it was found that an increase in the crystal-solution interfacial energy is due to the presence of foreign ions.

5.3.2 Effect of supersaturation on spontaneous nucleation of struvite crystals

To study the effect of supersaturation, experiments were conducted with changes of supersaturation index (SI = 1.02 to 1.33) at a constant temperature of 25 ^{0}C. Figure 5.1 also shows the effect of supersaturation and initial solution pH on induction time. It was found that induction time decreased with increase in supersaturation at any particular initial solution pH. The rapid induction time for higher supersaturation is due to a higher driving force for mass transfer from liquid to crystal phase.

5.3.3 Effect of temperature on kinetics of struvite nucleation

The induction time is strongly affected by both the temperature and supersaturation of the solution. Batch experiments were investigated for temperatures of 20, 25, and 30^{O}C. Table 5.1 represents the variation of induction times obtained at various levels of initial supersaturation and temperatures at pH 8. It was found that increase in supersaturation substantially decreases the induction period for all temperatures. For a given supersaturation, the induction time decreased with increase in temperature. According to the classical nucleation theory, the decrease in induction time at higher solution temperature is caused not

only by the effect of temperature but also by the lower interfacial energy of crystals (Mullin, 2001, Tai and Chien, 2002).

Table 5.1 Induction time on spontaneous nucleation of struvite crystals with various temperature and *SI* at pH 8

Temperature	Induction time, s		
	SI = 1.02	SI = 1.18	SI = 1.33
20	432	261	139
25	343	223	110
30	271	173	96

For the effect of temperature on any rate processes, such as nucleation, Arrhenius equation is commonly used. The activation energy of nucleation, E_{act}, can be calculated by the following Arrhenius equation;

$$\frac{\mathbf{d \ln k_N}}{\mathbf{dT}} = \frac{\mathbf{-E_{act}}}{\mathbf{RT^2}} \quad (5.8)$$

where k_N is empirical constant.

By the integration of Eq. (5.8),

$$\mathbf{k_N = k_0 . exp\left(\frac{-E_{act}}{RT}\right)} \quad (5.9)$$

This empirical equation has been simplified by Cheng and Li (2010), so:

$$\mathbf{t_{ind} = \tau . exp\left(\frac{-E_{act}}{RT}\right)} \quad (5.10)$$

$$\mathbf{\log \frac{1}{t_{ind}} = \log \tau - \frac{E_{act}}{2.303\ R\ T}} \quad (5.11)$$

Where t_{ind} is the induction time, τ is a constant, E_{act} is the activation energy (J mol^{-1}) for the process, and R is the gas constant (8.314 J/K.mol). Activation energy represents the minimum energy that is required for a chemical reaction to take place. Figure 5.2(a) and 5.2(b) is a plot of *log* $(1/t_{ind})$ versus *1000/T* for three different initial levels of supersaturation. From the slope of these straight lines, the average values of E_{act} of 30.1 kJ.mol^{-1} and 24.9 kJ.mol^{-1} were obtained at pH 8 and 8.5, respectively. The finding E_{act} shows that energy required ions of struvite formation to react to produce a crystal at solution pH 8 were higher than pH 8.5. It can be indicated that struvite nucleation occurred on pH 8.5 was faster than pH 8. Similar range of values of activation energy for nesquehonite ($MgCO_3 \cdot 3H_2O$) and

ammoniumsilicate was also reported by Cheng and Li (2010) and Zang et al (2003), respectively.

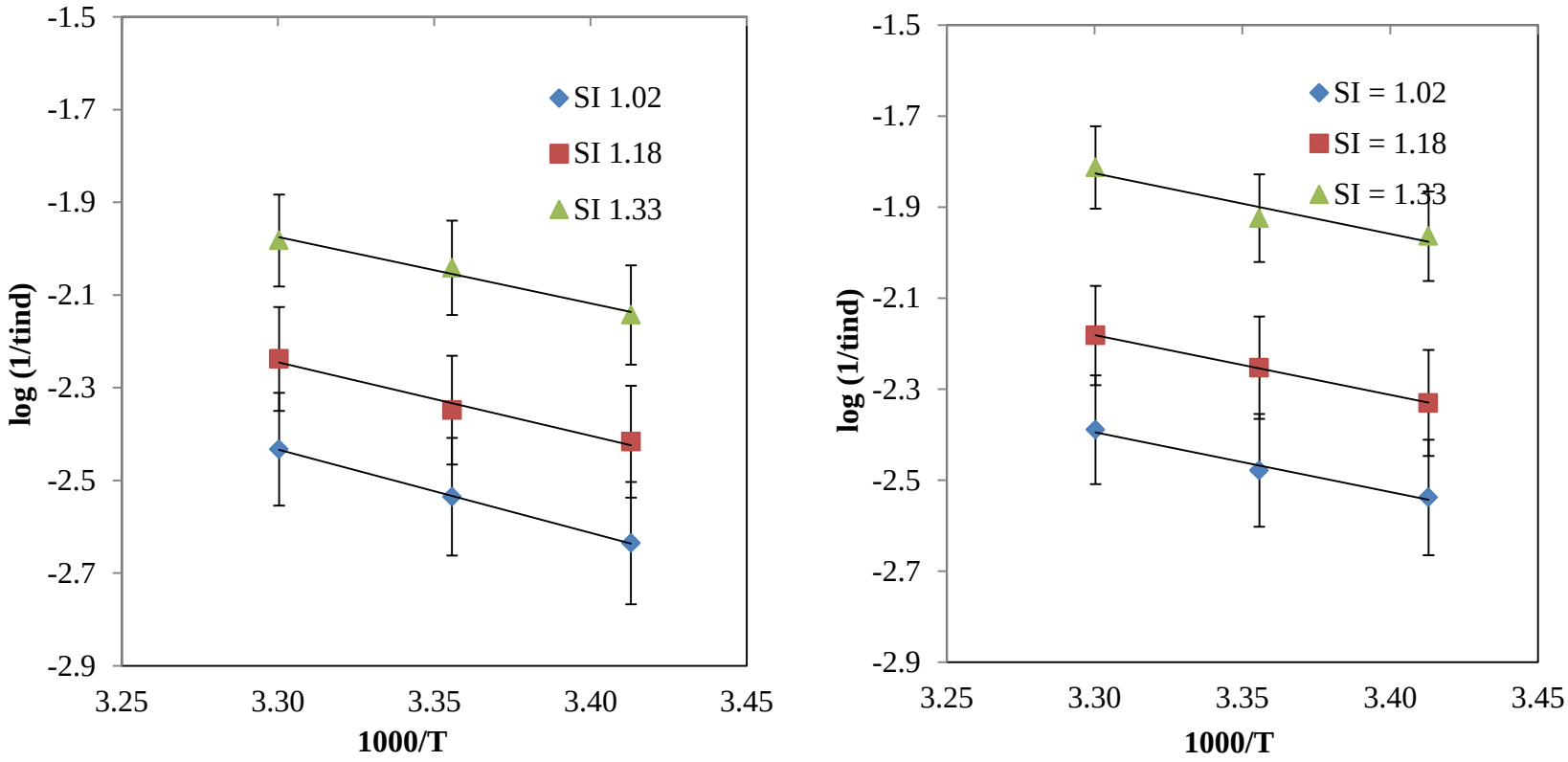

Figure 5.2 Dependence of induction time on temperature; (a) pH = 8; (b) pH = 8.5

An equation developed by Nielsen (1964), Nyvlt (1971) and Sohnel and Garside (1992) for calculation of homogeneous nucleation rate is:

$$\boldsymbol{J = k_N . S^n} \quad (5.12)$$

where k_N is the nucleation rate constant and n is the kinetic order of nucleation.

A simplifying assumption was used that the induction time may be considered to be inversely proportional to the rate of nucleation. So induction period (t_{ind}) may be used to determine the nucleation rate (J) (Chien et al., 1999).

$$\mathbf{J = \frac{1}{t_{ind}}} \quad (5.13)$$

Combining Eq. (5.12) and (5.13) results in Eq. (5.14)

$$\mathbf{t_{ind} = (1/k_N) . S^{-n}} \quad (5.14)$$

$$\mathbf{\frac{1}{k_N} = K} \quad (5.15)$$

where K is empirical constant

The semi empirical correlation of induction time on supersaturation (Eq. 5.14) can be simplified into Eq. (5.16) below and the data plotted in Figure 5.3.

$$\mathbf{\log t_{ind} = \log K - n \log S} \quad (5.16)$$

where K and n are empirical constants obtained via straight line fitting to experimental data in Figure 5.3. And $\log S$ is equal to SI (See Eq. 5.6)

The dependence of the induction time on supersaturation is shown in Figure 5.3(a) and 5.3(b) for pH 8 and 8.5, respectively. The fitting parameters from Figure 5.3(a) and 5.3(b) are presented in Table 5.2.

The various calculated nucleation kinetic parameters are tabulated in Table 5.2. It can be seen that the empirical constants, K, are higher at lower temperatures. The order nucleation kinetic of struvite decreased with increase in temperature. When compared with the nucleation kinetic parameters between pH 8 and pH 8.5 on without Cl^- addition in Table 5.2, the effect of solution pH can decrease empirical constant K values. On the other hand, nucleation order n was not affected by increasing solution pH.

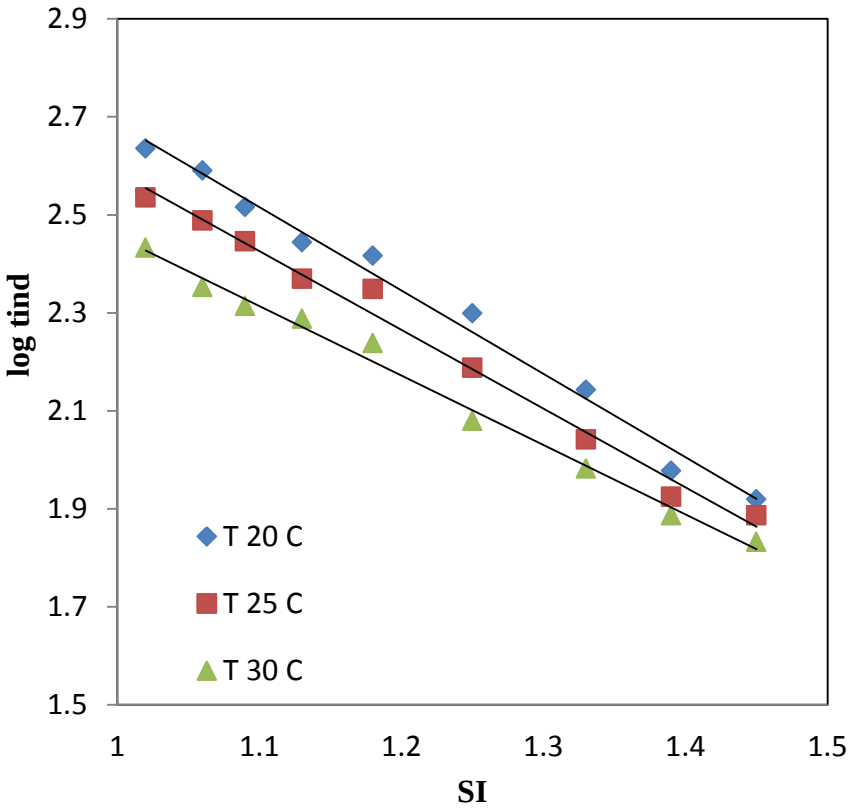

(a)

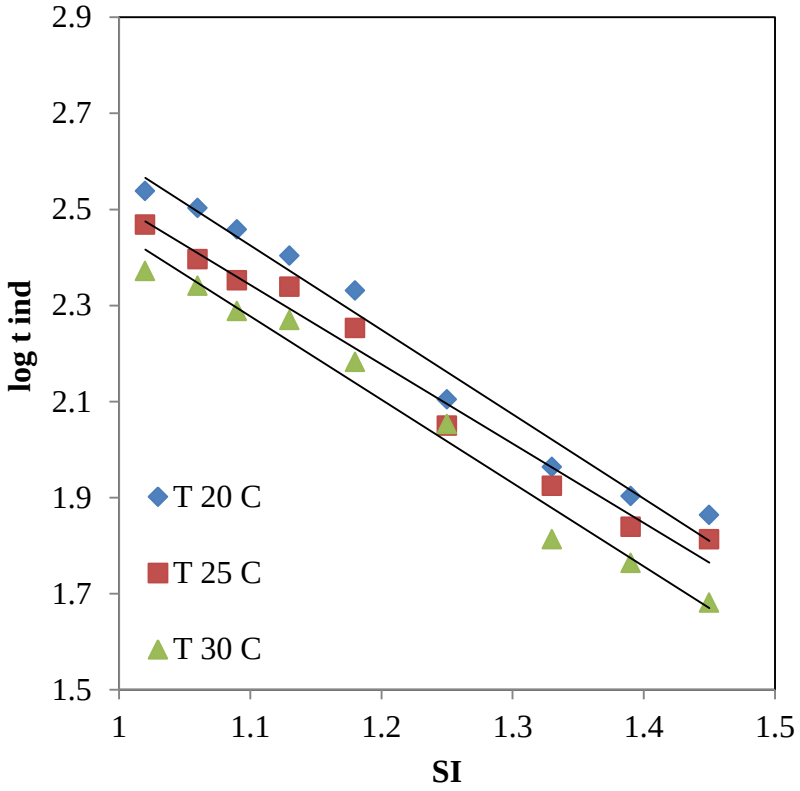

(b)

Figure 5.3 Induction time as a function of initial supersaturation and at different temperatures; (a) pH 8, (b) pH 8.5.

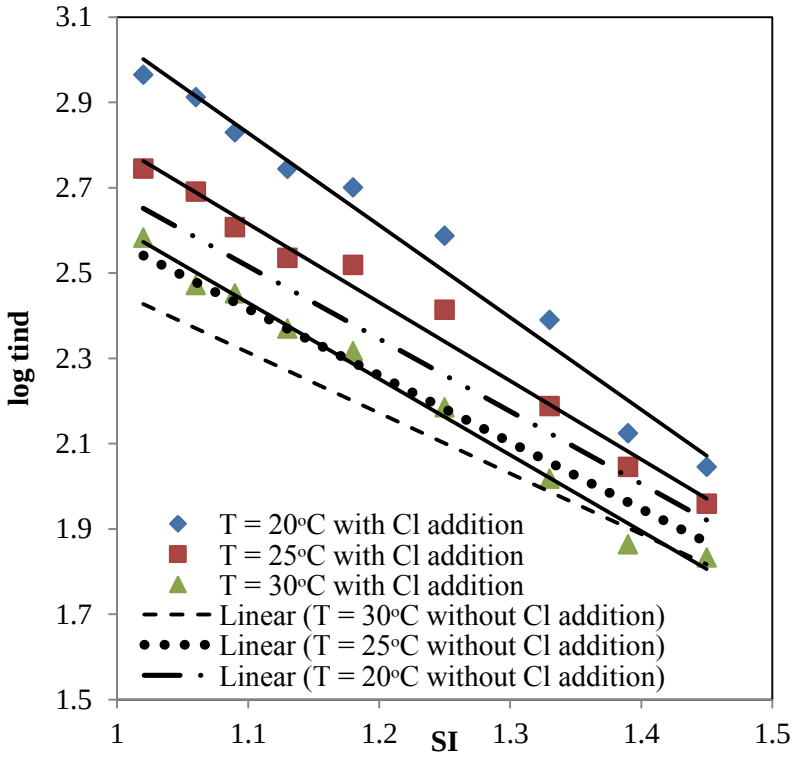

(a)

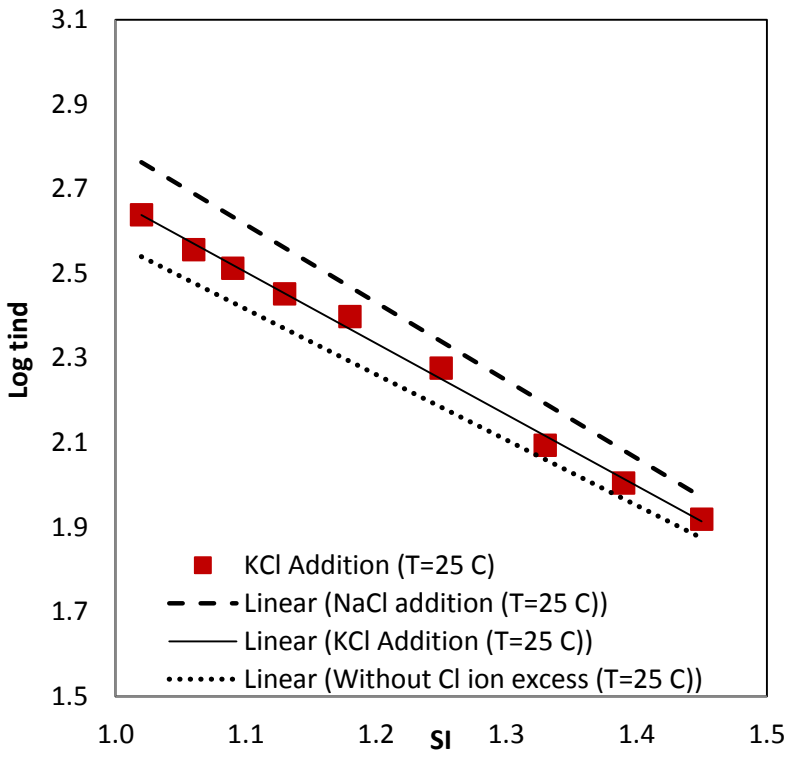

(b)

Figure 5.4 Induction time as a function of initial supersaturation and at different temperatures; (a) pH 8 with and without NaCl addition and (b) pH 8 with and without NaCl and KCl addition at only 25^{O}C.

Table 5.2 The various kinetic parameters on struvite nucleation

T (C)	K	n	R^2
pH 8.0 without Cl^- ion addition			
20	24320	1.7	0.96
25	15600	1.6	0.98
30	7450	1.4	0.97
pH 8.5 without Cl^- ion addition			
20	22800	1.7	0.96
25	14500	1.6	0.97
30	7420	1.3	0.97
pH 8 with NaCl addition			
20	189850	2.2	0.98
25	43740	1.8	0.97
30	20240	1.7	0.97
pH 8 with KCl addition			
20	61720	1.9	0.98
25	21880	1.7	0.97
30	16200	1.6	0.98

5.3.4 Inhibition of spontaneous nucleation of struvite due to presence of excess chloride ions

In this study, the excess Cl^- ions were obtained in a batch experiment at pH 8 by adding sodium chloride (NaCl) or potassium chloride (KCl). The experimental data of induction time obtained at different supersaturations with and without the addition of excess Cl^- ions at pH 8 are shown in the *log* t_{ind} - *SI* plots of Figure 5.3(a)(b) and 5.4(a)(b) for $E = 0$ and 0.4, respectively. The results showed that the induction time continuously decreased with increasing supersaturation. The effect of excess CI^- ions in a solution showed that induction time increased in the presence excess Cl^- ions. Figure 5.4(b) shows that the effect of excess Cl^- ions on the induction time is more significant at lower supersaturations. In general, the effect of excess Cl^- ions in a solution may affect the induction time considerably

(Mullin, 2001). This may be due to adsorption or chemisorption of foreign ions on nuclei or heteronuclei, by changing the equilibrium solubility or by the solution structure, by chemical reaction or by complex formation in the solution (Mullin, 2001).

The various calculated nucleation kinetic parameters (*K* and *n*) are tabulated in Table 5.2. It can be seen that the empirical constants, *K*, are larger at lower temperatures. When compared with the data at pH 8 without presence of excess Cl^- in Table 5.2, the effect of excess Cl^- can significantly increase empirical constant *K* values and nucleation order *n*.

For comparison purpose, two forms of excess Cl^- ions, in the form of either NaCl or KCl were used. Figure 5.4(b) shows the effect of KCl and NaCl on the induction time. It can be seen that, for fixed value of supersaturation, the presence of excess chloride ions in solution has a strong retarding effect on induction time, Na^+ ions having a more significant inhibition than K^+. This is because of different ionic charges. Figure 5.5 gives the effect of Na^+ and K^+ on the induction time for $SI = 1.02$. It can be seen that the presence of Na^+ and K^+ ions in solution affects the behaviour of the induction time, increasing with NaCl and KCl concentration up to a maximum at about *E* of 0.1 to 0.3, and reduces thereafter at higher *E* values. A comparison between Na^+ and K^+ ion for the same range of excess Cl^- ions shows that the influence of Na^+ in increasing the induction time is stronger than that of K^+ over all concentration ranges.

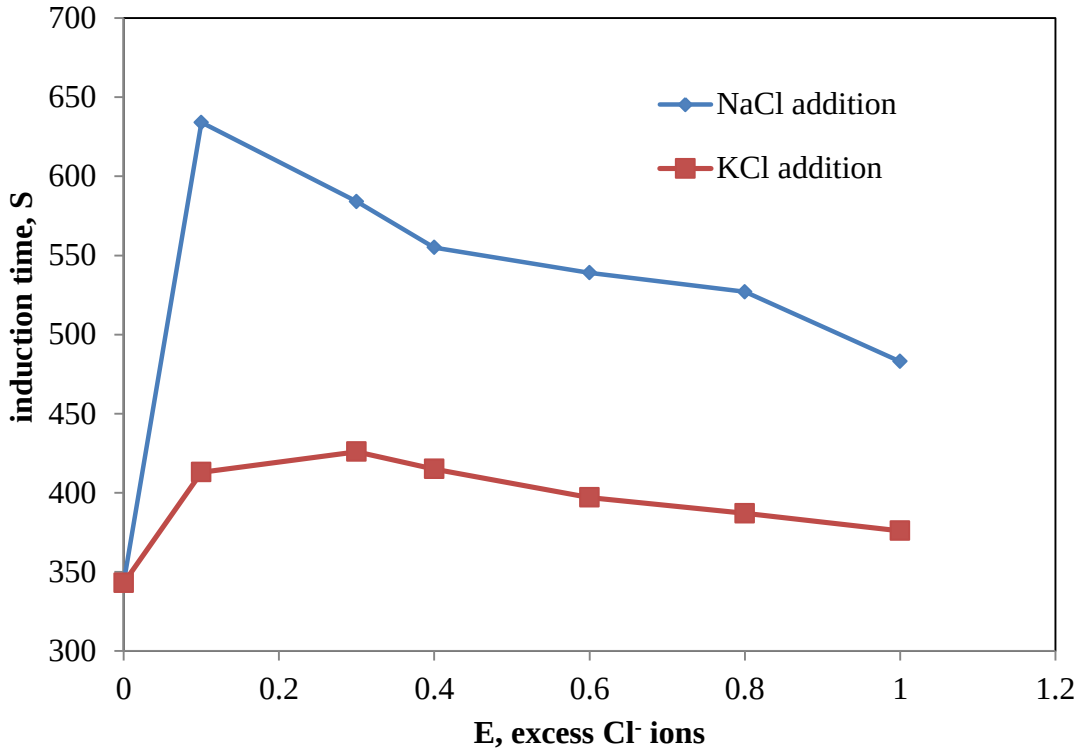

Figure 5.5 Effect of Na^+ and K^+ on the induction time for SI = 1.02 at 25^OC and pH 8.

Furthermore, the plotting of Eq. (5.11) for three different levels of supersaturation is shown in Figure 5.6 for the effect of the presence of excess chloride. The same linear relationship was compared with those shown in Fig. 5.3(a), and reproduced in Figure 5.6. The slope of the straight line is higher when excess chloride is present, suggesting that with excess chloride ions of either NaCl or KCl, there is more inhibition for nucleation than in the case of equimolarty (Pokrovsky, 1998) where no NaCl or KCl was added. From the slope of these straight lines, the average activation energies are 64.5 and 51.7 $kJ.mol^{-1}$ for NaCl and KCl addition, respectively. These values are much higher than the case with no NaCl and KCl added (30.1 $kJ.mol^{-1}$). This shows that foreign ions increase the activation energy for struvite nucleation, showing that primary nucleation of struvite can be inhibited by the presence of excess chloride ions such as NaCl and KCl. The activation energy in the presence of NaCl was higher than in the presence of KCl.

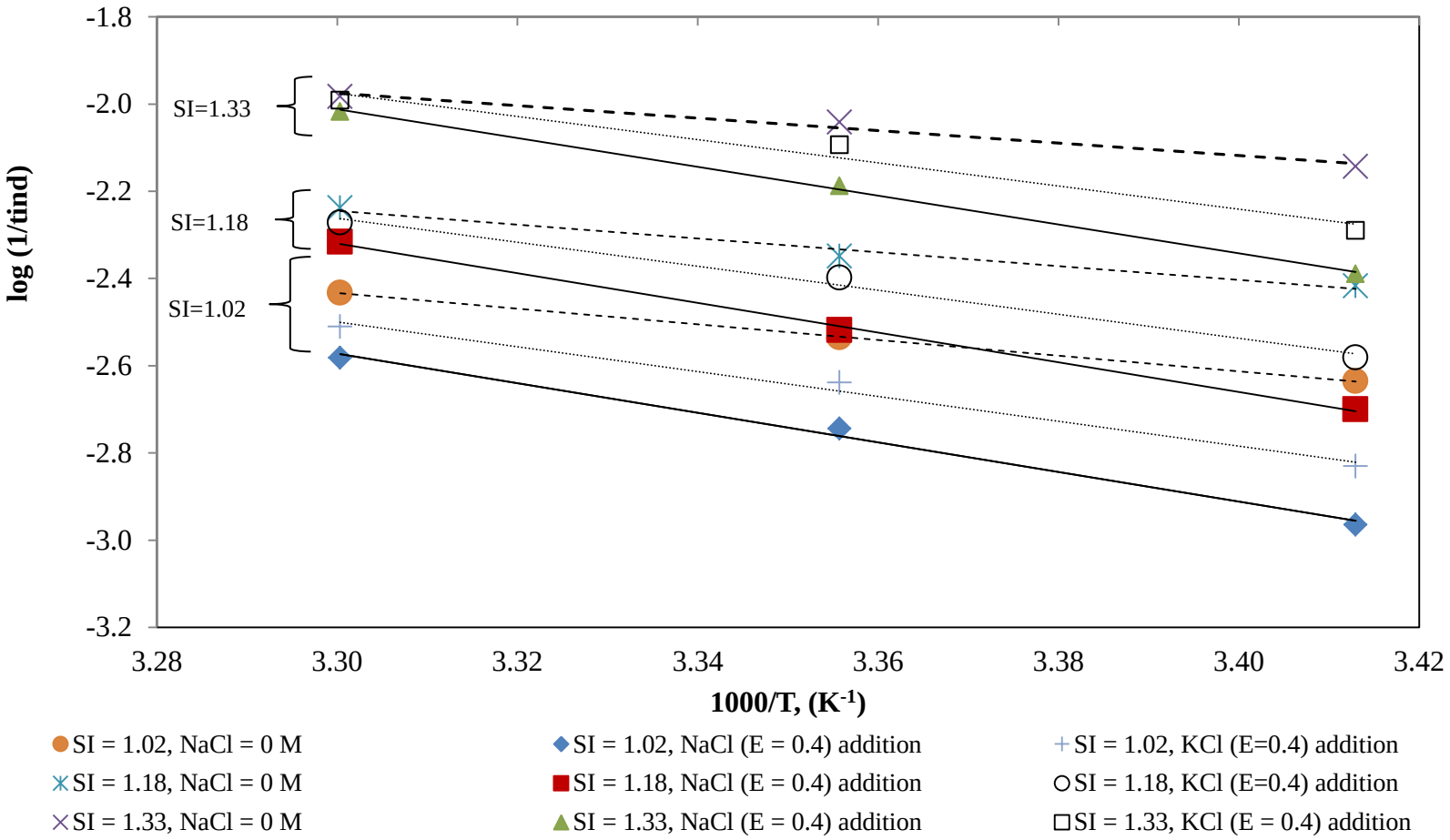

Figure 5.6 Dependence of the induction time on the inverse of temperature at pH 8 and with and without the presence of NaCl and KCl.

5.3.5 Mechanism of nucleation and thermodynamic parameters.

The nucleation rate based on classical homogeneous nucleation theory can be expressed as

$$J = A \exp\left[-\frac{\beta.\gamma_S^3.V_m^2.N_A}{(RT)^3.(\ln S)^2}\right] \quad (5.17)$$

where J is nucleation rate (cm^{-3} s^{-1}), A is the frequency constant, β the geometric factor (for cube is 32), N_A the Avogadro number, R the gas constant, V_m the molar volume, S activity-based supersaturation ratio, T the absolute temperature, γ_s the interfacial energy

The induction time can be related to the supersaturation by

$$\log t_{ind} = A + \frac{B}{(\log S)^2} \quad (5.18)$$

where A and B are constants according to the nucleation classical theory

$$B = \frac{\beta.\gamma_S^3.V_m^2.N_A}{(2.303RT)^3} \quad (5.19)$$

where υ_m is the molecular volume of struvite (= molar volume/(Avogadro's number x density x number of ions in formula unit) = $7.99 \times 10^{-23} cm^3/mol$), β is a shape factor (=32 for cubes), so

$$B = \frac{\beta.\gamma_S^3.v_m^2}{(2.303RT)^3} \quad (5.20)$$

The interfacial energy γ_S is

$$\gamma_S = 2.3RT\left(\frac{B}{\beta.v_m^2}\right)^{1/3} \quad (5.21)$$

The validity of Eq. (5.18) is based on the assumption that nucleation time is much longer than the growth time ($t_n >> t_g$) (Söhnel and Mullin, 1988). Then the induction period can be used to represent the time needed for critical nuclei formation. To verify whether this was the case for struvite, *log* t_{ind} was plotted versus (log S)$^{-2}$ as shown in Figure 5.7. It can be seen that the measured induction time for struvite crystallisation is followed by a linear relationship given by Eq. (5.18). Figure 5.7 illustrates two characteristics of nucleation. Region II for low supersaturation is characteristic of heterogeneous nucleation mechanism; Region I for high supersaturations indicates homogeneous nucleation mechanism dominates.

The data resulted in two distinct linear parts showing the dependence of nucleation on different nucleation mechanisms. Homogeneous nucleation region has higher slope and occurred at higher supersaturations and the region of lower slope occurred at lower supersaturations due to heterogeneous nucleation (Söhnel and Garside, 1992). The value of the slope of B_{hom} is higher than B_{het} as given in Table 5.3. The nucleation is largely homogeneous at high supersaturation, while heterogeneous nucleation prevails at relative supersaturation up to 1.5 for all temperature and pH ranges studied. Figure 5.7 showed mechanism of nucleation at three levels of temperatures on solution pH 8 and 8.5 and Figure 5.8 showed mechanism of nucleation at three levels of temperatures on solution pH 8 for different excess of Cl^- ion. From the experimental data shows that the transition point between homogeneous and heterogeneous nucleation changed at supersaturation 1.6 when chloride ions was added. It was indicated that change of slope (B_{hom} or B_{het}) necessarily resulted the change of nucleation mechanism. From the experimental value Table 5.3 shows addition chloride ions increased B_{hom} or $B_{het.}$ This transition from homogeneous to heterogeneous nucleation is affected by the presence of excess chloride ions. Their calculated corresponding values are listed in Table 5.3.

The value of B_{hom} is consistently higher than B_{het} for all experimental data. Calculated results of interfacial energy for two nucleation mechanisms ($\gamma_{s,hom}$ and $\gamma_{s,het}$) in Table 5.3 indicate that interfacial energies decrease with higher solution pH and for higher temperatures. For any given solution pH, interfacial energy of crystals increases with decrease in temperature. This is consistent that interfacial energy impacts on induction time. The effect of excess chloride shows that interfacial energy increases with its presence at all temperatures. The inhibition effect of added NaCl and KCl may be due to complex ion formation or due to foreign ion adsorbed onto nuclei surface.

A comparison of the interfacial energy derived from this study compares very well with results of Bouropoulus and Koutsoukos (2000) but much larger than reported results of Bhuiyan et al., (2008), Kofina and Koutsoukos (2005) and Ohlinger et al., (1999).

Table 5.3 Interfacial energy on struvite nucleation

T (C)	Calculated from Eq. (5.18)		Calculated from Eq. (5.21)	
	B_{het}	B_{hom}	γhet (mJ m^{-2})	γhom (mJ m^{-2})
pH 8.0 without Cl^- ion addition				
20	0.98	2.14	15.67	20.37
25	0.83	1.97	15.08	20.13
30	0.77	1.66	14.97	19.33
pH 8.5 without Cl^- ion addition				
20	0.86	1.92	15.05	19.62
25	0.82	1.83	15.04	19.65
30	0.76	1.71	14.89	19.54
pH 8 with NaCl addition				
20	1.26	2.86	18.74	22.42
25	1.01	2.43	16.14	21.60
30	1.07	2.11	16.71	20.95
pH 8 with KCl addition				
20	1.12	2.38	16.41	21.09
25	0.98	2.02	15.96	20.31
30	0.90	1.90	15.77	20.23

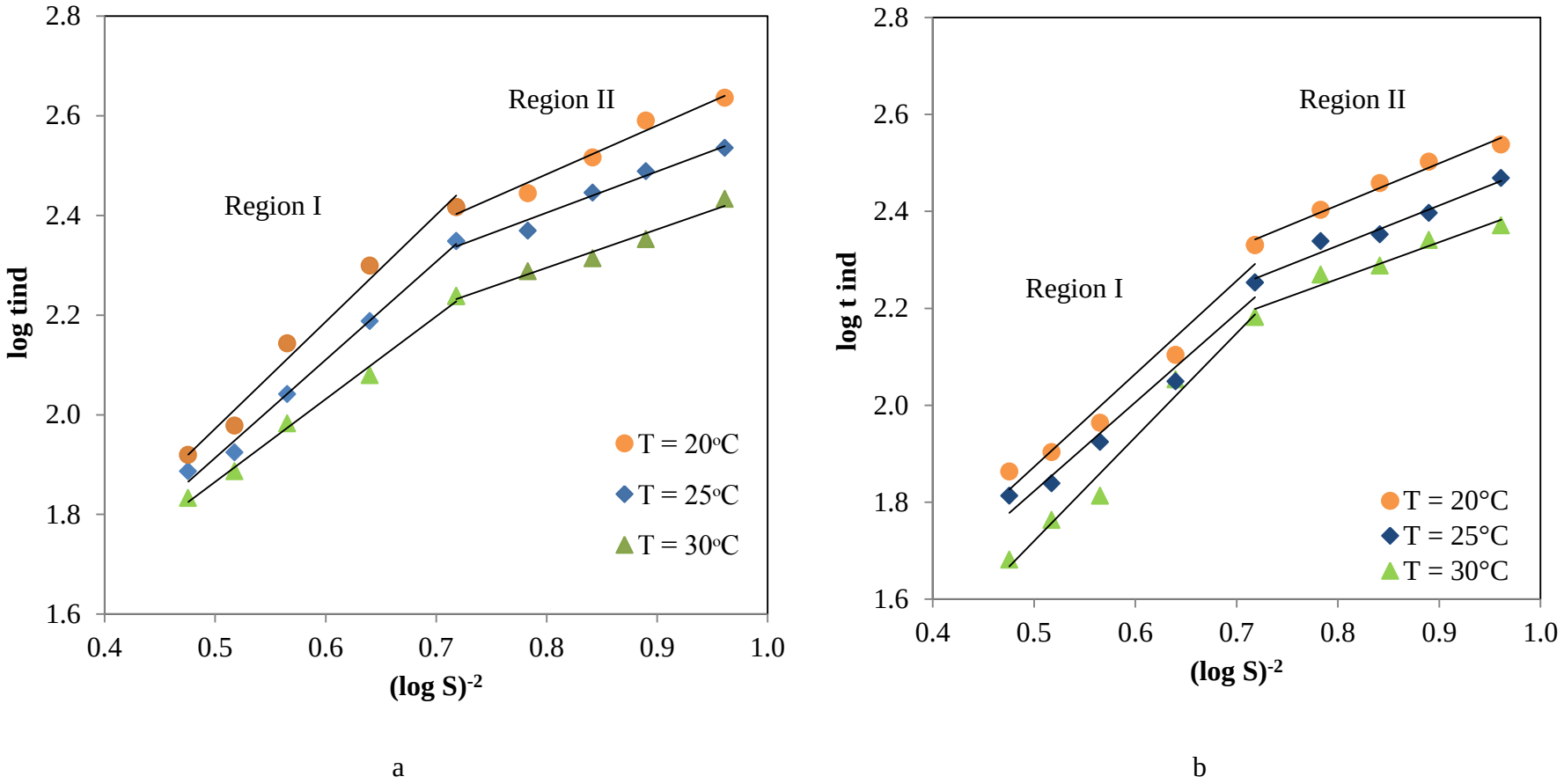

Figure 5.7 Induction period as a function of supersaturation at three levels of temperature at different solution pH; (a). pH 8 and (b). pH 8.5 without excess Cl^- ions

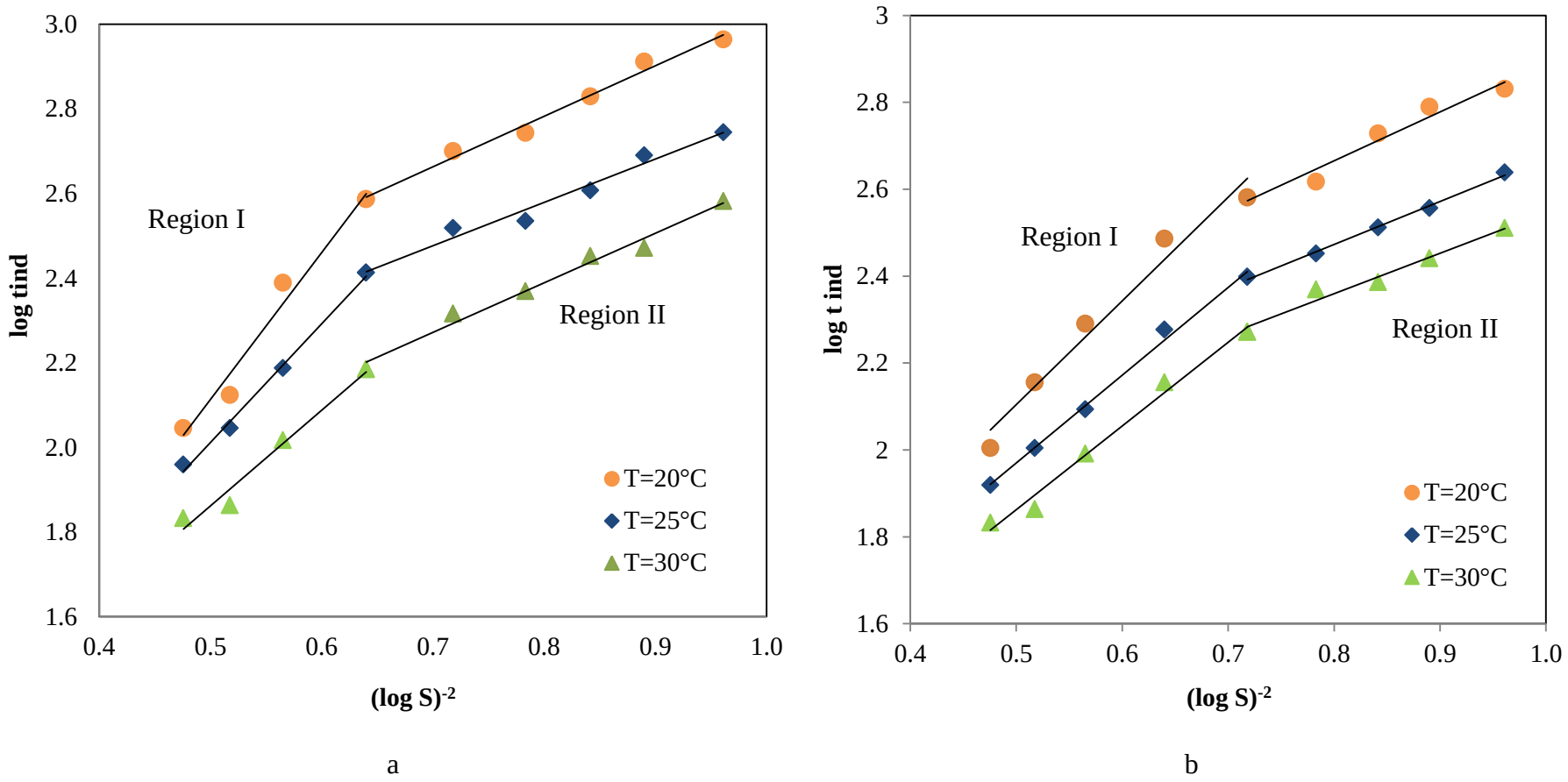

Figure 5.8 Induction period as a function of supersaturation at three levels of temperature at different excess Cl^- ion; (a). NaCl and (b) KCl

5.3.6 Crystal morphology at different solution pH with and without NaCl and KCl addition.

The micro-pictures of crystals, shown in Figure 5.9, obtained in the experiments were investigated by using an optical microscope. The crystal morphologies for pH 8 and 8.5 without excess Cl^- ion showed similar needle-like crystal shapes and dimensions (see Figure 5.9(a) and 5.9(b), respectively). The crystals in the presence of NaCl and KCl (Figure 5.9(c) and 5.9(d)) were similarly needle-like shape. Thus, the morphology in all the different cases, different pH and the presence or absence of excess Cl^- ions remain similar for all.

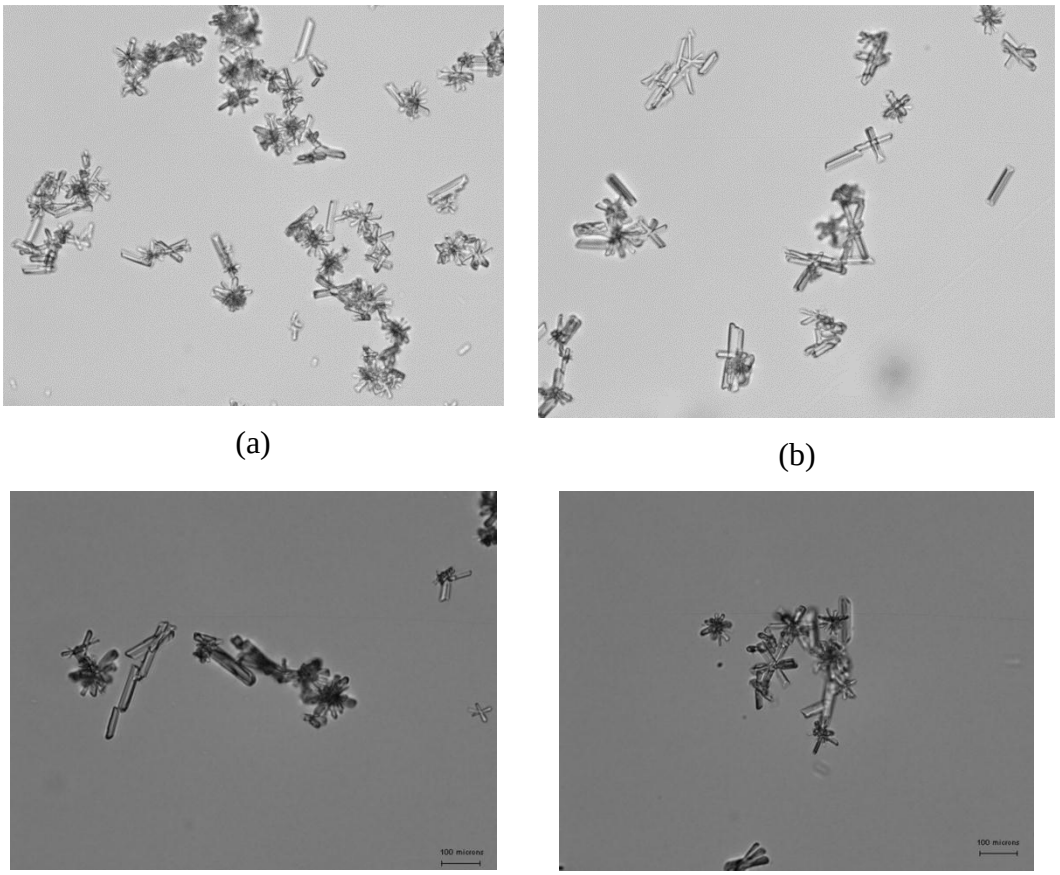

(a) (b)

(c) (d)

Figure 5.9 Morphology of struvite crystals obtained in experiments based on the same magnification; (a) pH 8 without Cl^- addition, (b) pH 8.5 without Cl^- addition, (c) pH 8 with NaCl addition, (d) pH 8 with KCl addition

5.4 Summary

The impact of various physico-chemical parameters, such as solution pH, supersaturation, temperature and presence of foreign ion, on spontaneous nucleation of struvite crystals are reported here.

- The results show that the induction time decreased with an increasing pH, temperature, and supersaturation. The presence of excess chloride in the form of NaCl and KCl has an inhibitory effect on the nucleation of struvite.
- The classical nucleation theory is applicable to explain the effect of various physico-chemical parameters on struvite nucleation. The activation energy for struvite nucleation was calculated as 30.1 $kJ.mol^{-1}$ and 24.9 $kJ.mol^{-1}$ at pH 8 and 8.5, respectively. The lower activation energy at pH 8.5 accounts for the shorter induction time obtained at pH 8.5.
- The classical nucleation theory is applicable to explain the effect of various physico-chemical on struvite nucleation. The activation energy for struvite nucleation was calculated as 30.1 $kJ.mol^{-1}$ and 24.9 $kJ.mol^{-1}$ at pH 8 and 8.5, respectively. The lower activation energy at pH 8.5 accounts for the shorter induction time obtained at pH 8.5. The activation energies in the presence of NaCl and KCl were higher (64.5 and 51.7 kJ/mol, respectively) at pH 8. The higher activation energy with NaCl and KCl addition can account for their inhibitory effect.
- The interfacial energy between struvite crystals and supersaturated solution decreased with increase in pH but increased in the presence of either NaCl or KCl.
- The morphology at different pH and the presence or absence of excess Cl^- ions is similar, being needle-like in structure.

CHAPTER 6
THE INFLUENCE OF VARIOUS PHYSICO-CHEMICAL PROCESS PARAMETERS ON STRUVITE CRYSTALLISATION IN WATER: CRYSTAL GROWTH KINETICS

6.1 Introduction

Magnesium, ammonium and phosphate are released during anaerobic digestion of wastewater sludge and also during dewatering operation (Nelson et al., 2003). Under certain conditions, these dissolved wastewater constituents can combine to form struvite, an orthorhombic crystalline minerals as per the following chemical reaction

$$\mathbf{Mg^{2+} + NH_4^+ + PO_4^{3-} + 6H_2O \rightarrow MgNH_4PO_4.6H_2O} \quad (6.1)$$

Accumulation of struvite on pipe walls and equipment surface associated with anaerobic digestion system and post digestion processes is well known problem that plagues the wastewater treatment (WWTP) industry (Matynia et al., 2006, Bhuiyan et al., 2008, Ohlinger et al., 1999, Le Corre et al., 2007, Le Corre et al., 2005). Remediation is often impractical and not cost effective.

In general, struvite formation can be divided into stages: nucleation and growth, both of which have been discussed in detail in Section 2.8.4 and Section 2.8.5, respectively. Crystal formation primarily occurs by nucleation from combination of constituent ions called embryos and nuclei growth in sequence, i.e. enlargement of crystal until equilibrium (Jones, 2002, Myerson, 2002, Söhnel and Garside, 1992, Mersmann, 2001). Predicting and controlling struvite nucleation and growth from wastewater is fundamental in crystalliser design. Predicting struvite formation potential is not only critical to struvite problem. However, predicting or controlling these stages is complex as it is controlled by a combination of thermodynamic and mass transfer properties along with various physico-chemical factors, such as solution pH, supersaturation, mixing, crystal sizes and the presence of foreign impurities. The crystals growth rate depends on

supersaturation, solution pH, impurities and hydrodynamic condition in the crystallizer.

Knowledge of the effect of solution pH, temperature, impurities, seed and hydrodynamic condition on struvite crystallisation is very important for control of struvite formation. Despite of the great interest of struvite formation mechanism, knowledge of struvite crystallisation and kinetics measurements are scarce in the literature. Therefore, this study attempted to explore the effect of solution pH, temperature, impurities, crystal size and hydrodynamic condition on the struvite crystallisation especially on the kinetics of struvite crystal growth. Struvite crystallisation kinetics was studied under different condition to find out the kinetic rate constant.

6.2 Materials and Methods

6.2.1 Chemicals

Struvite crystallisation was carried out by using the following chemicals: magnesium chloride hexahydrate ($MgCl_2.6H_2O$), and dihydrogen ammonium phosphate ($NH_4H_2PO_4$). Stock solution of $MgCl_2$, as Mg^{2+} provider, is made by dissolving crystals of $MgCl_2{\cdot}6H_2O$ in distilled water. The stock solution of $NH_4H_2PO_4$, as NH_4^+ and $H_2PO_4^-$ provider, prepared in the same manner. Both solutions were stored separately and only mixed just prior to any experimental run. Extreme care was taken to keep the solution from dust, insoluble matter, etc. In addition, all solutions were filtered before they were used for the experiments. The solution was adjusted at pH 8, 8.5 and 9 using 0.1 M sodium hydroxide (NaOH) solution.

Supersaturated solutions used in this experiment were prepared based on concentrations within the metastable zone width. The metastable zone width experiment was conducted in Erlenmeyer flask under constant temperature of 25^OC at different stirrer speed. The experimental set-up can be seen in Figure 3.10 (Section 3.5.2). The synthetic solutions used in a series of batch experiments were 0.003, 0.004, 0.005 and 0.007 M (equimolar) of magnesium, ammonium and phosphate. The detailed determination of metastable zone width is in Section 3.4.

6.2.2 Seed preparation

Seeds were prepared by dissolving synthetic crystals of specific amount in a supersaturated solution and agitated gently in order to prevent the agglomerate. Crystals that have been separated from agglomerate crystals was taken using a plastic pipette and kept into a petri disk. Crystals were then dried to reduce the water content at room temperature. The dried crystals were transferred into a small container and the crystals were rinsed with two drop of deionized water, and dried immediately with the filter paper. Seed crystal size was determined by Malvern Master Sizer 2000 and morphology was measured by scanning electron microscope. The Fourier transform infrared spectroscopy (FTIR) was used to analyse potential changes in the inner structure of struvite crystals. These dried seed crystals were used to crystal growth experiments. The seed preparation is described in detail on Section 3.6.4.2.

6.2.3 Experimental set-up and procedure

The experimental setup is shown schematically in Figure 6.1. All experiments were performed in the laboratory-scale jacketed stirred batch crystallizer with a working volume of 1 liter. The crystallizer consisted of a cylindrical glass vessel with a round bottom and 130 mm internal diameter. The vessel was fitted with four vertical equidistant baffles (15 mm x 83 mm) which were placed along the wall of the crystallizer (details in Section 3.6.2). The solution was stirred by an impeller (number of blades 4; blade length 20 mm; blade width 20 mm). The impeller was located at one-third the working liquid level from the crystallizer bottom (details in Section 3.6.3). The crystallizer was covered with a steel plate to minimize evaporation of solution. Temperature control within the crystallizer was achieved by pumping water from a water bath enclosed in a cryothermostat with PID regulator for temperature control through the water jacket. The operating conditions are listed in Table 6.1. The detailed experimental growth procedure is described in Section 3.6.4.3.

After crystallisation for a definite time, the crystals were filtered from the residual solution, and dried overnight in the oven at temperature $35^{O}C$ in order to measure crystal size distribution, weight, and FTIR analysis. The filtrates were then

analysed for magnesium, ammonium, and orto-phosphates. Analyses for ammonium and ortho-phosphate were analysed by UV-spectrophotometer (see Section 3.2.4.2 and 3.2.4.3, respectively). Magnesium analysis was performed by atomic absorption spectrophotometry (see Section 3.2.4.1). The crystal size distributions were measured by laser diffraction with a Malvern Master Sizer 2000 at the end of crystallisation (see Section 3.2.3).

For the effect of stirrer speed, it was essential to ensure that no serious breakage of crystals occurred during the crystallization process. Test for crystal attrition in the seed feed tank were conducted at agitator speeds of 50, 100, 120 rpm for 15 minutes. The experimental study is detailed in Section 3.6.5 and it showed that there was no significant attrition caused by the agitator.

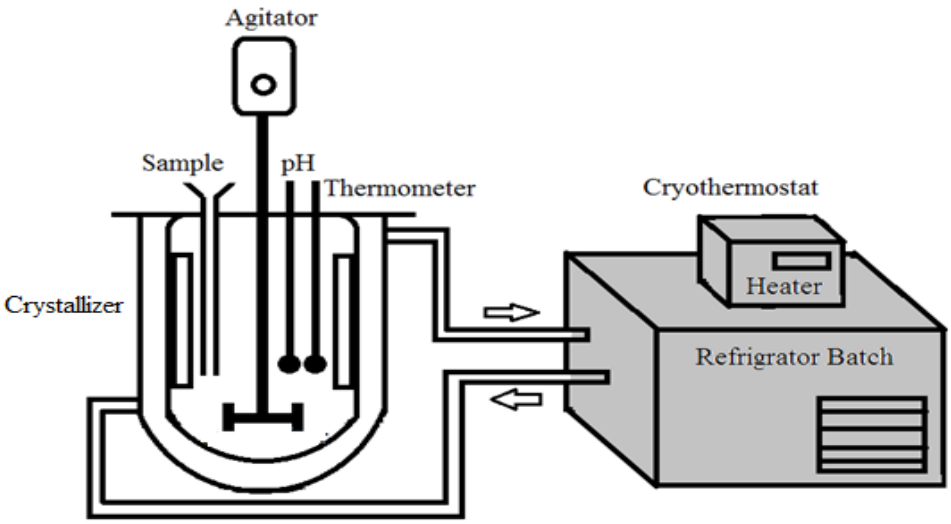

Figure 6.1 Laboratory Batch Crystalliser

Table 6.1 Operating conditions of crystalliser experiments used in this study

Working temperature (^{O}C)	25 – 30
pH range	8 – 9
Supersaturation, *SI*	0.34 – 1.00
Stirrer speed, rpm	50 – 120
Seed size, μm	24.3 – 106
Impurities (NaCl), ppm	50 – 200

6.2.4 Crystal Growth Calculations

Crystal growth calculations were done through the use of crystal size distribution plots as shown in Figure 6.2. This curve represents the dependence between the number of crystals per unit volume and crystal size. It is assumed that, in a suspension of growing crystals (seed crystals) at time *t* the number of crystals at size L_1 is indicated on y-axis of Figure 6.2. After a certain time, the seed crystal grew to size L_2. The average growth rate of crystals will be

$$\mathbf{G(L,t)} \cong \frac{\mathbf{L_2 - L_1}}{\mathbf{(t+\Delta t) - t}} = \frac{\mathbf{\Delta L}}{\mathbf{\Delta t}} \qquad (6.2)$$

Calculation of crystal growth from Figure 6.2 was done by using three to four points along the size distribution curves.

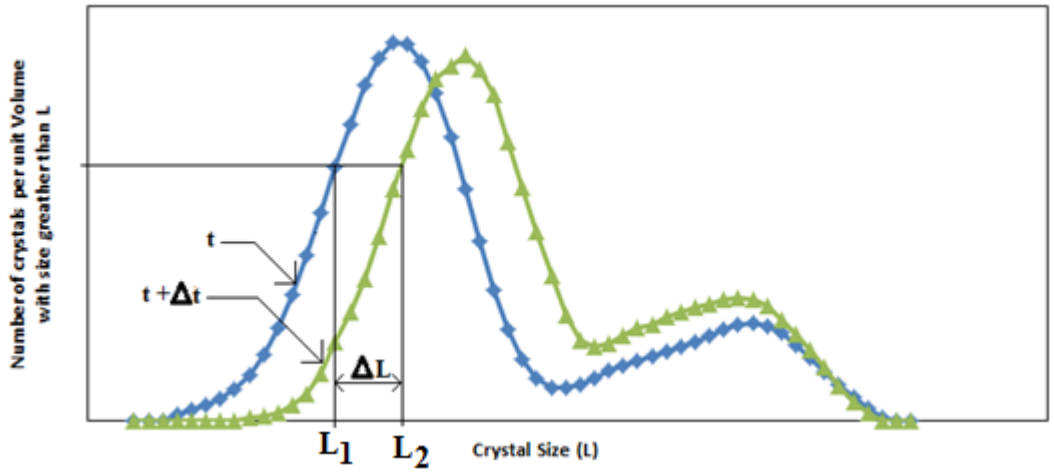

Figure 6.2 Determination of growth rate from cumulative size distribution

6.2.5 Supersaturation calculation

The supersaturation was calculated using the specification PhreeqC program (Parkhurst and Appelo, 1999). The saturation index (*SI*) value for struvite is used as an indication of supersaturation. If the SI is negative, the system is undersaturated with respect to struvite. If the SI is positive, the solution is supersaturated. The SI values were calculated for all the experiments using the PheerqC model. The SI values calculated based on PhreeqC model can be seen in Appendix B.

$$\mathbf{SI} = \mathbf{log\,S} = \mathbf{log}\frac{[\mathbf{Mg^{2+}}][\mathbf{NH_4^+}][\mathbf{PO_4^{3-}}]}{\frac{\mathbf{K_{sp}}}{\gamma_{\mathbf{Mg^{2+}}}\cdot\gamma_{\mathbf{NH_4^+}}\cdot\gamma_{\mathbf{PO_4^{3-}}}}} \quad (6.3)$$

From Eq. (6.3) the relative supersaturation is given by

$$\mathbf{S} = \frac{[\mathbf{Mg^{2+}}][\mathbf{NH_4^+}][\mathbf{PO_4^{3-}}]}{\frac{\mathbf{K_{sp}}}{\gamma_{\mathbf{Mg^{2+}}}\cdot\gamma_{\mathbf{NH_4^+}}\cdot\gamma_{\mathbf{PO_4^{3-}}}}} \quad (6.4)$$

According to Bhuiyan et al (2009), the thermodynamic solubility product of struvite on equilibrium with pure and solid phase struvite is;

$$\mathbf{K_{sp}} = \boldsymbol{\gamma}_{\mathbf{Mg^{2+}}}[\mathbf{Mg^{2+}}].\boldsymbol{\gamma}_{\mathbf{NH_4^+}}[\mathbf{NH_4^+}].\ \boldsymbol{\gamma}_{\mathbf{PO_4^{3-}}}\left[\mathbf{PO_4^{3-}}\right] \quad (6.5)$$

where K_{sp} is solubility product in terms of ion activity and $\gamma_i$is activity coefficient of the ion *i*.

The supersaturation concentration of Mg^{2+}, NH_4^+ and PO_4^{3-} was determined based PhreeqC model (see Appendix B)

6.2.6 Kinetic Study and Theory

The rate of kinetic was determined by fitting our experimental data with first and second-order kinetic models. The general equation can be written simply as follows;

$$-\mathbf{dC/dt} = \mathbf{k(C - C_S)^n} \quad (6.6)$$

where *k* is rate constant, *n* is order of reaction, *C* is the reactant concentration at time *t*, C_S is the reactant concentration at equilibrium and $-dC/dt$ is the rate of phosphate disappearance of a reactant.

The first-order kinetic model was applied to the experimental kinetic as per method by Nelson et al., (2003), Quintana et al., (2005) and Rahaman et al., (2008). The linearized form of first-order kinetic model Eq. (6.6) can be written as.

$$\mathbf{ln(C_t - C_S) = -k_1 t + ln(C_i - C_S)} \quad (6.7)$$

where C_t is the reactant concentration at time *t*, C_i is initial concentration, *t* is reaction time and k_1 is first-order constant.

$$\mathbf{ln}\left(\frac{\boldsymbol{C_t}}{\boldsymbol{C_S}} - \mathbf{1}\right) = -\boldsymbol{k_1 t} + \mathbf{ln}\left(\frac{\boldsymbol{C_i}}{\boldsymbol{C_S}} - \mathbf{1}\right) \quad (6.8)$$

where $C_t/C_S = S_t$ and $C_i/C_S = S_i$

$$\mathbf{ln(S_t - 1) = -k_1 t + ln(S_i - 1)} \quad (6.9)$$

where S_t is supersaturation at time t and S_i is supersaturation at time t=0. A plot of $\ln(S_t - 1)$ against time should give a straight line with slope -k_1.

Similarly, the linearized form of a second-order kinetic model can be written as

$$\mathbf{1/(C_t - C_s) = 1/(C_i - C_s) + k_2 t} \quad (6.10)$$

$$\mathbf{1/(S_t - 1) = 1/(S_i - 1) + k_2 t} \quad (6.11)$$

where k_2 is second-order constant. A plot of $1/(S_t - 1)$ against time should give a straight line with slope –k_2.

6.2.7 Diffusion-Reaction Theory of Struvite Crystal Growth Mechanism: Effect of Various Process Parameters

There are also two major steps in series which are involved in the growth of a crystal (Dutta, 2007);

(i) Convective transport of the solute from the bulk of the supersaturated solution to the surface of a crystal and

(ii) Surface integration or accumulation of the solute molecules in the growing layers of a crystal

The crystal growth rate can be calculated based on the resistance offered by the above two steps. Second step followed first order kinetics and depends on the degree of supersaturation ($C - C_S$) at the crystal surface. Basically, crystals growth mechanism can be the combination of diffusion and reaction processes and hence called diffusion-reaction theory of crystal growth (Dutta, 2007, McCabe et al., 2005). The rate of increase in the mass of a single crystal can be written as;

$$\mathbf{\frac{dm_c}{dt} = K_L A_c (C - C_S)} \quad (6.12)$$

where K_L is the overall mass transfer coefficient for the growth process which combines the above two resistance, m_c is mass of a single crystal, A_c is area of a single crystal, C is bulk solute concentration and C_s is saturation concentration of the solute at the given temperature.

Alternatively, growth rate can also be expressed as the rate of change of the "characteristic size" of a crystal. The characteristic size (L) is related to the mass (m_c), area (A_c) and volume (V_c) of a crystal through a "shape factor" as follows,

$$\mathbf{m_c = \rho_c \phi_c L^3;\ A_c = \phi_a L^2} \text{ and } \mathbf{V_c = \phi_v L^3} \quad (6.13)$$

where ρ_c is crystal density (for struvite 1.7 g/cm^3) (Mijangos et al., 2004, Doyle and Parsons, 2002), ϕ_v is volume shape factor (for cube 6) and ϕ_a is area shape factor (for cube 1)

Hence the crystal growth rate can also be expressed as

$$\mathbf{G = \frac{dL}{dt} = (K_L \phi_a / 3\rho_c \phi_v)(C - C_S) = K_G (C - C_S)/C_S = K_G S} \quad (6.14)$$

where *G* is a measure of the crystal growth rate and

$$\mathbf{K_G = K_L \phi_a C_S / 3\rho_c \phi_v} \quad (6.15)$$

Eq. (6.15) depends on the various system parameters such as supersaturation, solution pH, temperature and impurities NaCl addition. If the process is integration or accumulation of solute molecule on the surface of seed crystal, the above second step follows nonlinearity and hence the crystal growth can also be written as power law equation (Myerson, 2002)

$$\mathbf{G = k_G S^g} \quad (6.16)$$

or

$$\mathbf{\log G = \log K_G + g \log S} \quad (6.17)$$

where K_G is growth constant, g is order of the crystal growth rate and S is supersaturation.

The above mechanistic power law growth rate equation was fitted with our batch struvite crystalliser experimental data. The overall mass transfer coefficient (K_L) can be obtained from the value of K_G at various physico-chemical process parameters. The slope of plot between *log G* versus *log S* gives the value of crystal growth order (g) parameter and intercept give K_G value at different physico-chemical parameters.

6.3 Results and Discussion

6.3.1 Metastable zone

The solubility data, measured over the initial concentration of Mg, PO_4 and NH_4 range between 0.001 and 0.006, are plotted in Figure 6.3. The solubility curve was calculated by PhreeqC model. Supersaturation curves at 50, 100 and 120 rpm was predicted when primary nucleation occurred rapidly. As shown in Figure 6.3, the

solubility of struvite depends strongly on solution pH. At lower solution pH, the solubility of struvite was higher.

The variations of metastable zone width with initial concentration for all the stirrer speeds examined are also presented in Figure 6.3. It can be seen that at higher speeds, 120 rpm, primary nucleation of struvite occurred more readily. The experimental results confirm the well-known effects of stirrer speed on metastable zone width . It is evident that higher agitation speeds can cause more turbulence of the system which narrows the metastable zone width.

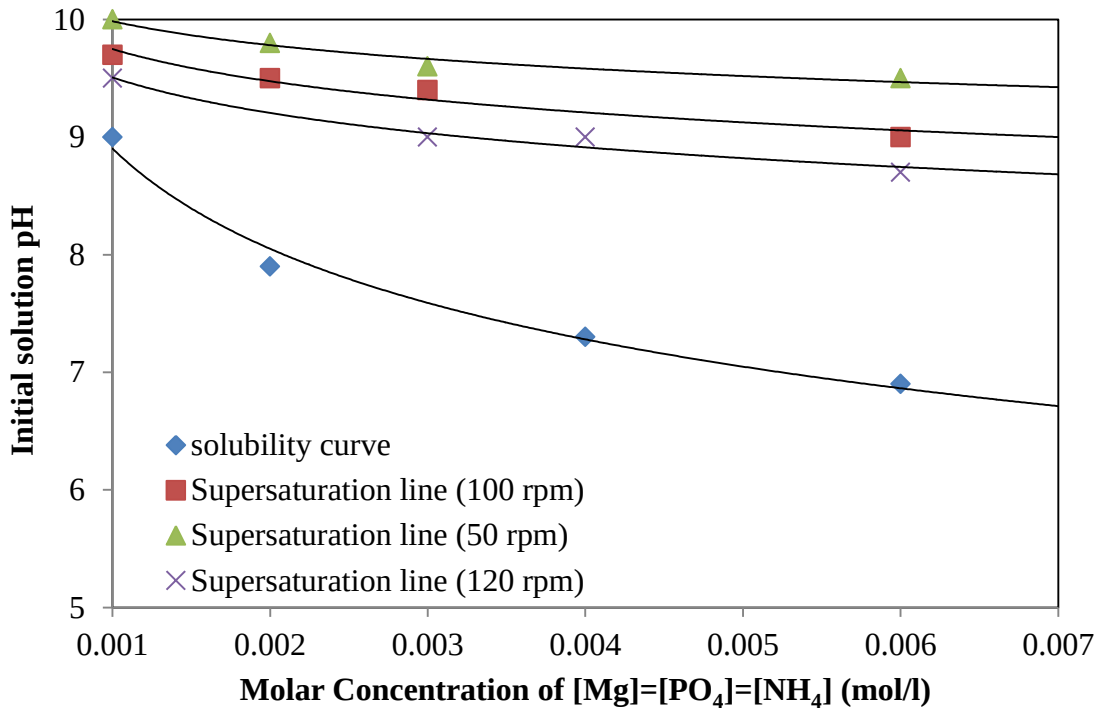

Figure 6.3 Metastable zone width measured as an initial concentration of Mg, PO_4 and NH_4 at different stirrer speeds and $25^{O}C$.

6.3.2 Effect of seed loading and size on crystal growth

The effect of seed loading on the decay of supersaturation in solution is shown in Figure 6.4. The experimental results can be seen in Table C1.1 of Appendix C. It can be seen from the plot that the increasing seed loading increased rate of struvite formation. Increasing mass of seeds provides more surface area of crystals available for crystal growth, more solute molecules may attach onto these surfaces, enhancing the growth rate and thus weakening the nucleation rate

accordingly. However, in the case of lower seed loading, the contribution of newly generated secondary nuclei to the decay of supersaturation becomes significant (Frawley et al., 2012, Huang et al., 2010).

Results of decay of supersaturation measurement versus supersaturation for struvite of different size of seed crystals are presented in Figure 6.5. The experimental results can be seen in Table C2.1 of Appendix C. As can be seen in Figure 6.5 the growth rate increases with decrease in seed size. Increasing crystal growth rate growth was caused by increase in total area available for growth in which the smaller seed crystals providing a larger surface area compared to larger seed crystals of the same mass (Frawley et al., 2012).

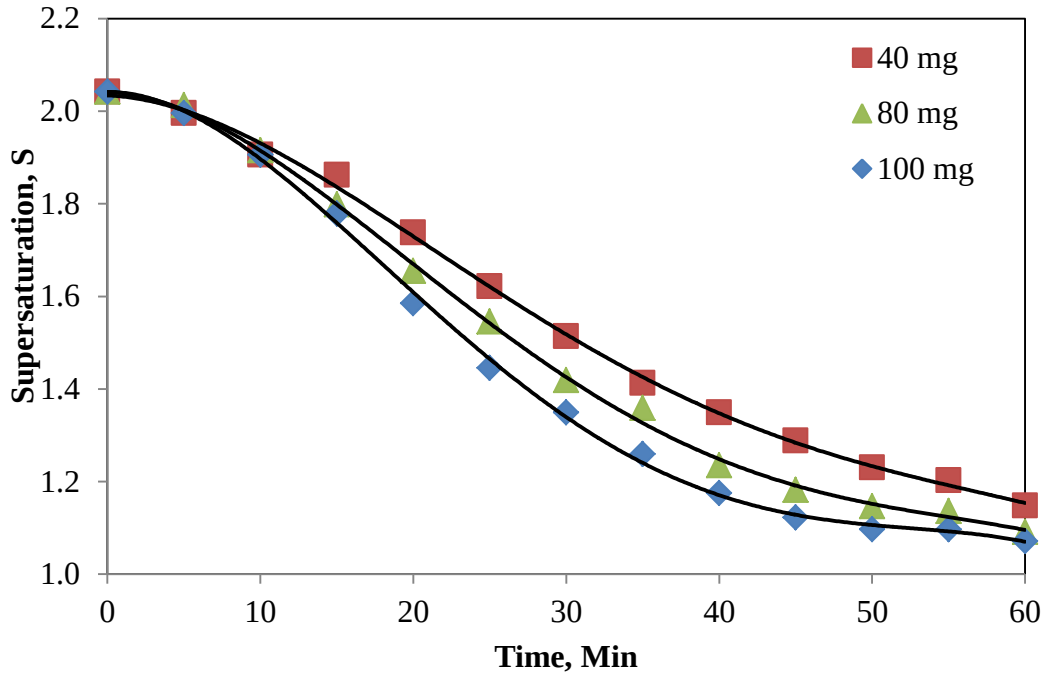

Figure 6.4 Effect of seed size on the decay of supersaturation. pH 8, temperature 25^{O}C, seed size 24.3 μm and agitator speed 120 rpm.

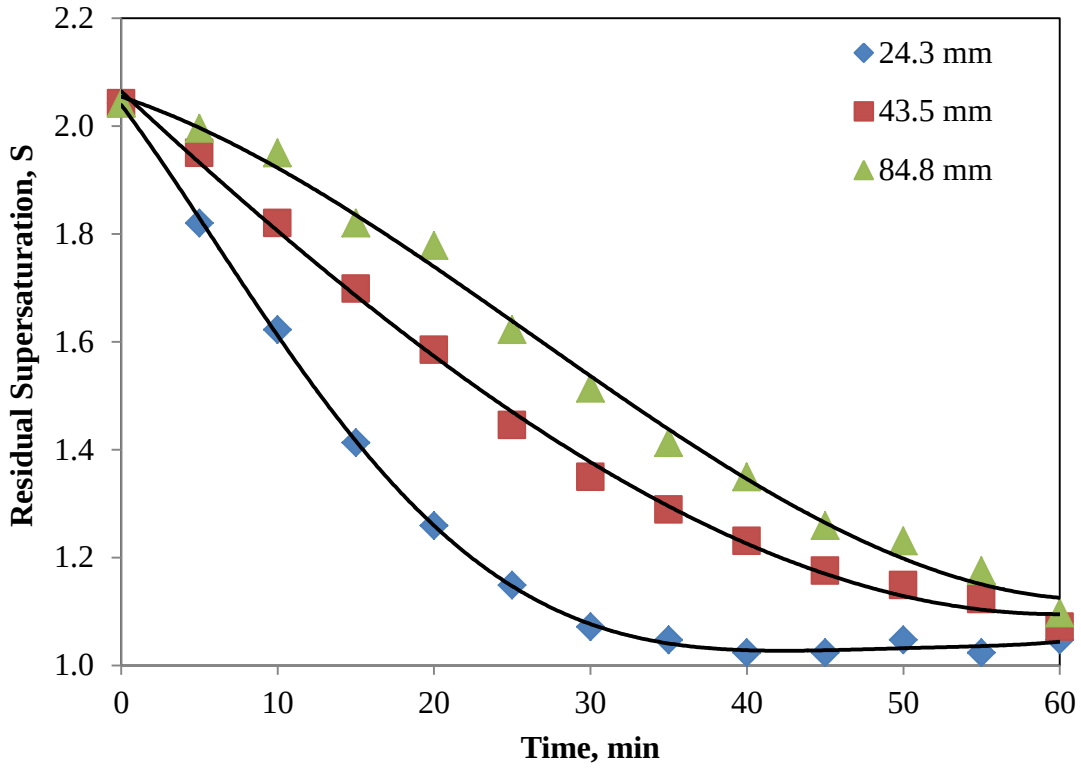

Figure 6.5 Effect of average seed size on the decay of supersaturation for a solution temperature, pH and seed loading of 25^{O}C, 8 and 100 mg, respectively.

6.3.3 Effect of solution pH and supersaturation on struvite crystal growth kinetic

Solution pH control is one of the important factors for removal of nutrients such as nitrogen and phosphorus from solution by struvite crystallisation (Perera et al., 2009, Münch and Barr., 2001). Controlling solution pH during struvite crystallisation not only could increase struvite formation (Perera et al., 2009) but also could accelerate growth rate (Omar and Ulrich, 2003). A small changing of solution pH may reduce available surface area to the growth unit. It was caused by changes significantly in the zeta potential of the particle leading to the eventual destabilization of suspension by aggregation (Bouropoulos and Koutsoukos, 2000).

To investigate the effect of supersaturation on the formation of struvite, the disappearance of ortho-phosphate ions were monitored during the experimental run. As shown in Figure 6.6, the percentage removal of PO_4 increased with

increase in supersaturation at a constant solution pH of 8 and it is more significant at higher supersaturation.

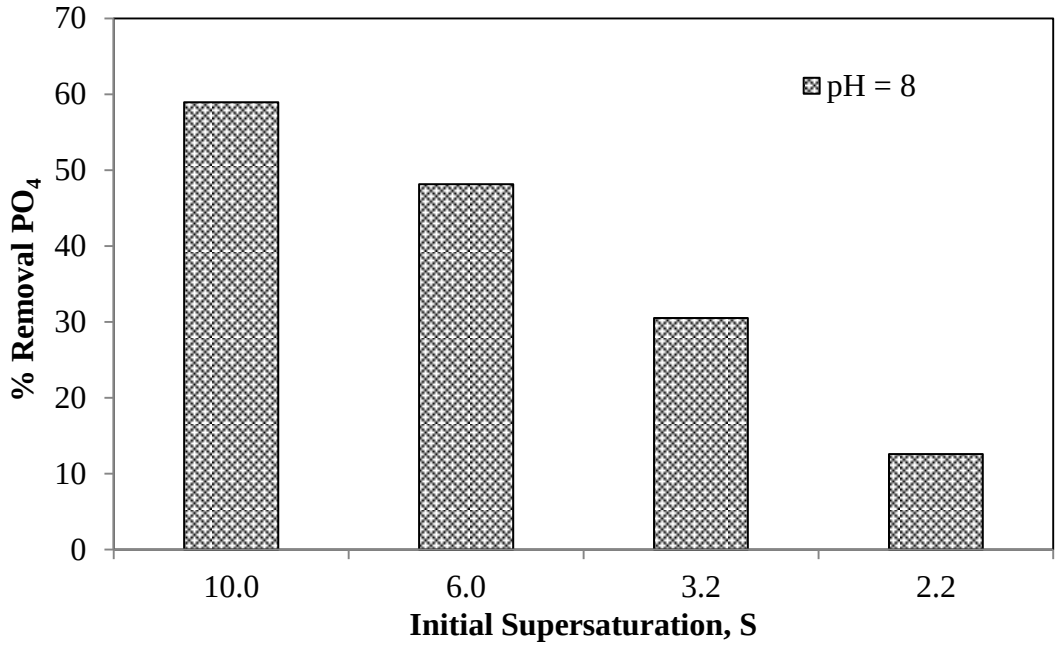

Figure 6.6 Effect of supersaturation on the removal of PO_4 under constant solution pH 8, agitator speed 120 rpm and temperature $25^{O}C$ for 2 hours process

Figure 6.6 shows different results obtained for the percentage PO_4 removal at constant pH experiments. The percentage PO_4 removal was always higher for constant pH (at pH 8) experiments and more significant at higher supersaturations. The change of solution pH was an indicator of struvite nucleation (see Chapter 5). As struvite precipitates, it triggers a release of proton ions in solution and hence a change in pH occurs during the nucleation process. The drop in pH is characteristic of the speed at which the first crystals of struvite occurs and is linked to the rate of struvite formation. Figure 6.7 shows the change in solution pH with time for range of supersaturation 2.2 – 10. It was found that the increase in supersaturation leads to an increase in the change of solution pH and a reduction in induction time (Figure 6.7).

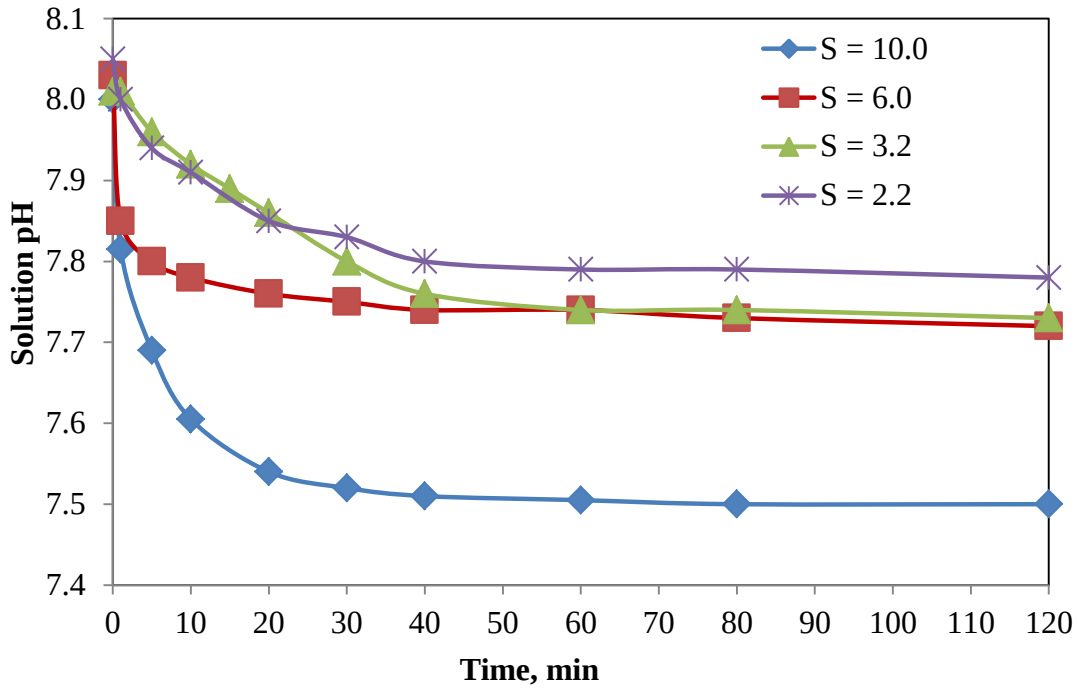

Figure 6.7 Change of solution pH with time at various supersaturation

From this experiment, the PO_4 concentration of 2 mMol/L (189.9 mg/L) was chosen for conducting experiments on the effect of solution pH on PO_4 removal by struvite crystallisation (Figure 6.8). The decay of supersaturation of PO_4 concentration in bulk solution reached steady state at 30, 40, and 60 min after the addition of seed crystal at a pH of 8.0, 8.5 and 9.0 respectively. For solution pH 8, 12.6% of PO_4 was removed from the solution. Percentage removal of PO_4 increased significantly with higher solution pH. Increasing solution pH from 8 to 9 increased PO_4 removal to 58.9 %. It can be seen that operating the crystallizer at pH 9.0 becomes imperative for higher PO_4 removal (Adnan et al., 2004). On the other hand, the low pH may be an option to prevent scale formation of struvite crystals in wastewater treatment.

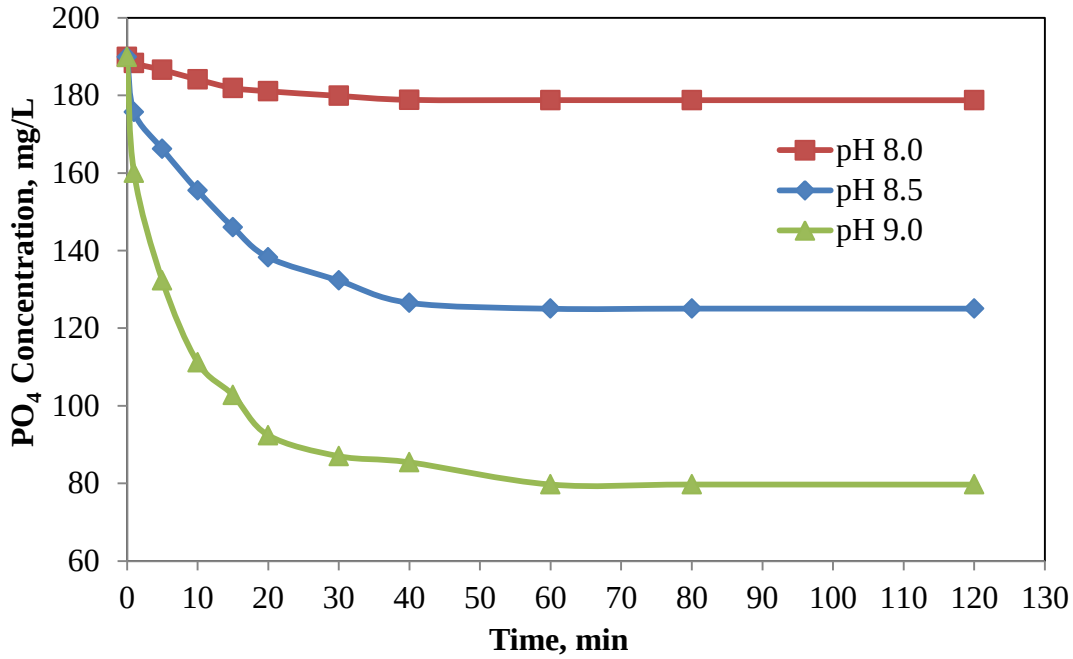

Figure 6.8 Effect of solution pH on PO_4 removal

Figure 6.9 shows that the higher PO_4 removal efficiency occurred at higher solution pH with faster rate. The kinetic experimental data were plotted as *ln* $(C_t - C_S)$ versus *time (t)* generates straight line with different slopes which are shown in Figure 6.9(a), 6.9(b) and 6.9(c), respectively. Further, the values of linear regression coefficients (R^2) indicate the applicability of first-order kinetic model to the experimental observation. The estimated rate constants were 3.7, 5.1 and 6.9 hr^{-1} for solution pH of 8.0, 8.5 and 9.0, respectively. The results indicate that increasing solution pH increases the rate of struvite crystallisation. However, the increasing rate of crystallisation was indicated by increasing supersaturation due to change in solution pH. Based on calculation by using PhreeqC model, the changing initial solution pH increased supersaturation from 1.23 to 10.23.

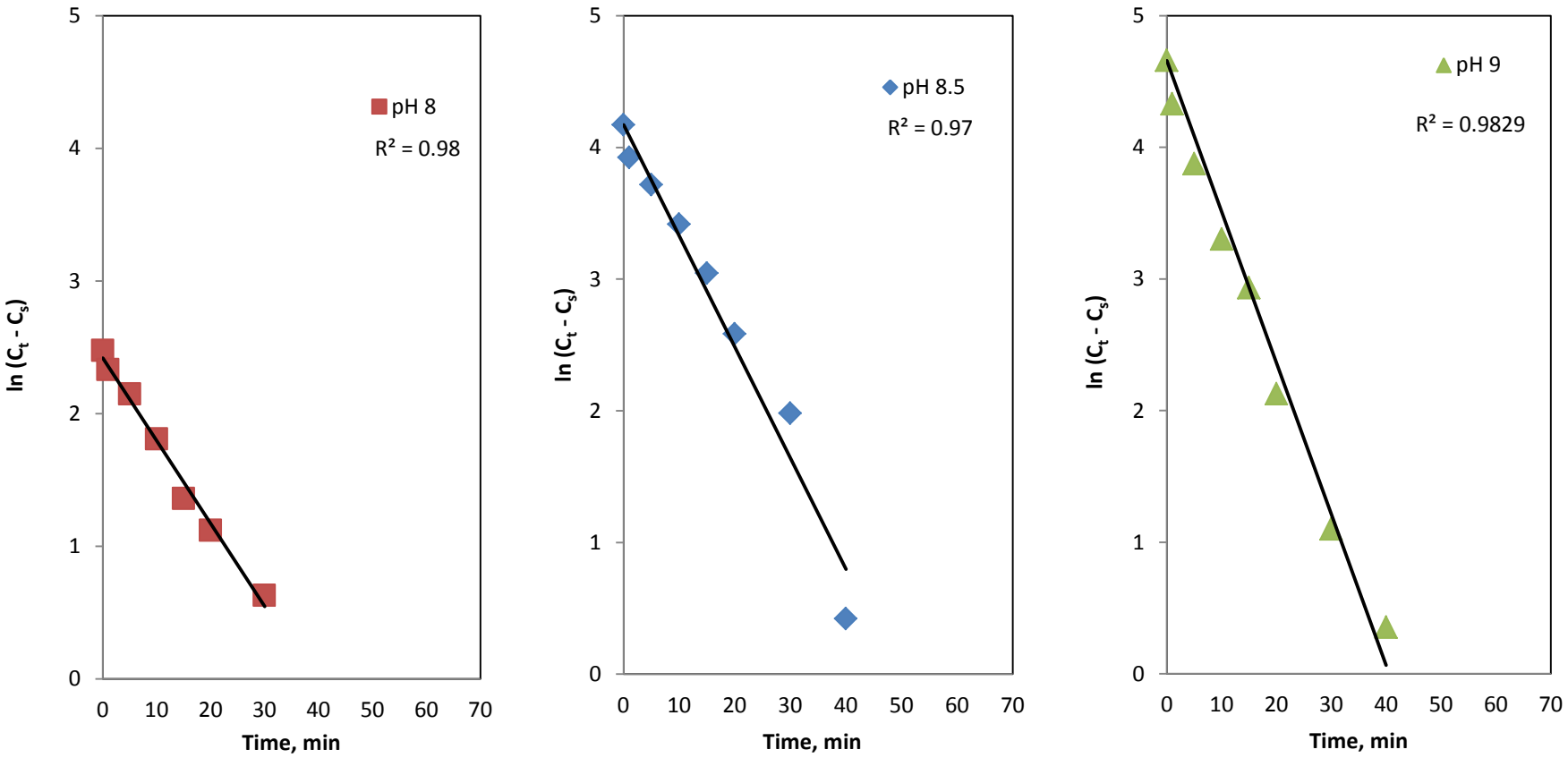

a b c

Figure 6.9 Plot of *ln (C – C_e)* versus time for pH 8.0, 8.5, and 9.0 at 25^{O}C and 120 rpm

Further investigation, in the present study, predicted rate of struvite crystallisation at the same supersaturation. This investigation was to identify the rate of struvite crystallisation at different solution pH. The supersaturation was chosen at *S* of 2.04 which is close to solubility of struvite crystals. Thus, rate of struvite crystallisation is slow and easily identified as secondary nucleation. Based on PhreeqC model calculation, the concentration of Mg, PO_4 and NH_4 conducted in batch crystalliser was 1.03 mMol/L, 1.54 mMol/L and 2.5 mMol/L for a solution pH 9.0, 8.5 and 8.0, respectively. The supersaturation was monitored during the experimental run by monitoring concentration of Mg, PO_4 and NH_4 over the period of time. The PhreeqC model was used to calculate decreasing supersaturation. The experimental results can be seen in Table C2.1 of Appendix C and the results are presented in Figure 6.10.

The effect of solution pH on the decay of supersaturation in solution is shown in Figure 6.10. It can be seen from the plots that with increasing solution pH, the supersaturation decreases faster. The marked dependence of growth rate on pH values is probably due to the change of surface charge on crystal surface (Tai et al., 2006b, Stubičar et al., 1993). Similar observations were reported by Rahaman et al., (2008) for different system.

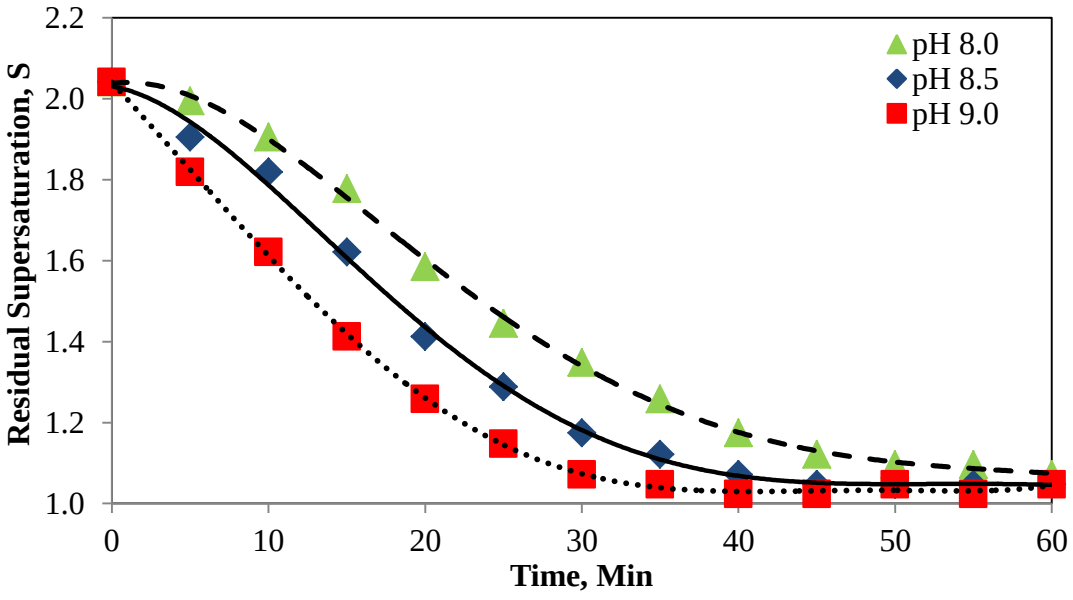

Figure 6.10 Effect of pH on the decay of supersaturation curve for supersaturation, temperature and stirrer speed of 2.04, 25^{O}C and 120 rpm, respectively.

Subsequently the experimental data were fitted with both first-order (Eq. (6.9)) and second-order kinetics (Eq. (6.11)) and these are shown in Figure 6.11(a) and 11(b), respectively. The higher value of linear regression coefficient (R^2) showed that the decay of relative supersaturation followed first order kinetics which also confirms the high dependence of growth observed at higher stirrer speeds. The fitted rate constants (k_1) for first-order kinetic model were 3.0, 4.3 and 5.8 hr^{-1} for a solution pH of 8.0, 8.5 and 9.0, respectively. Similar trend was observed by Nelson et al. (2003). The obtained first order rate constant from this study was 5.8 hr^{-1} at a solution pH of 9.0 which comparatively lower value with 12.3 hr^{-1} reported by Nelson et al., (2003). This lower value in rate constant is advantageous for crystalliser design. The lower rate constant reported in the present study is most likely a result of different supersaturation in the measurement.

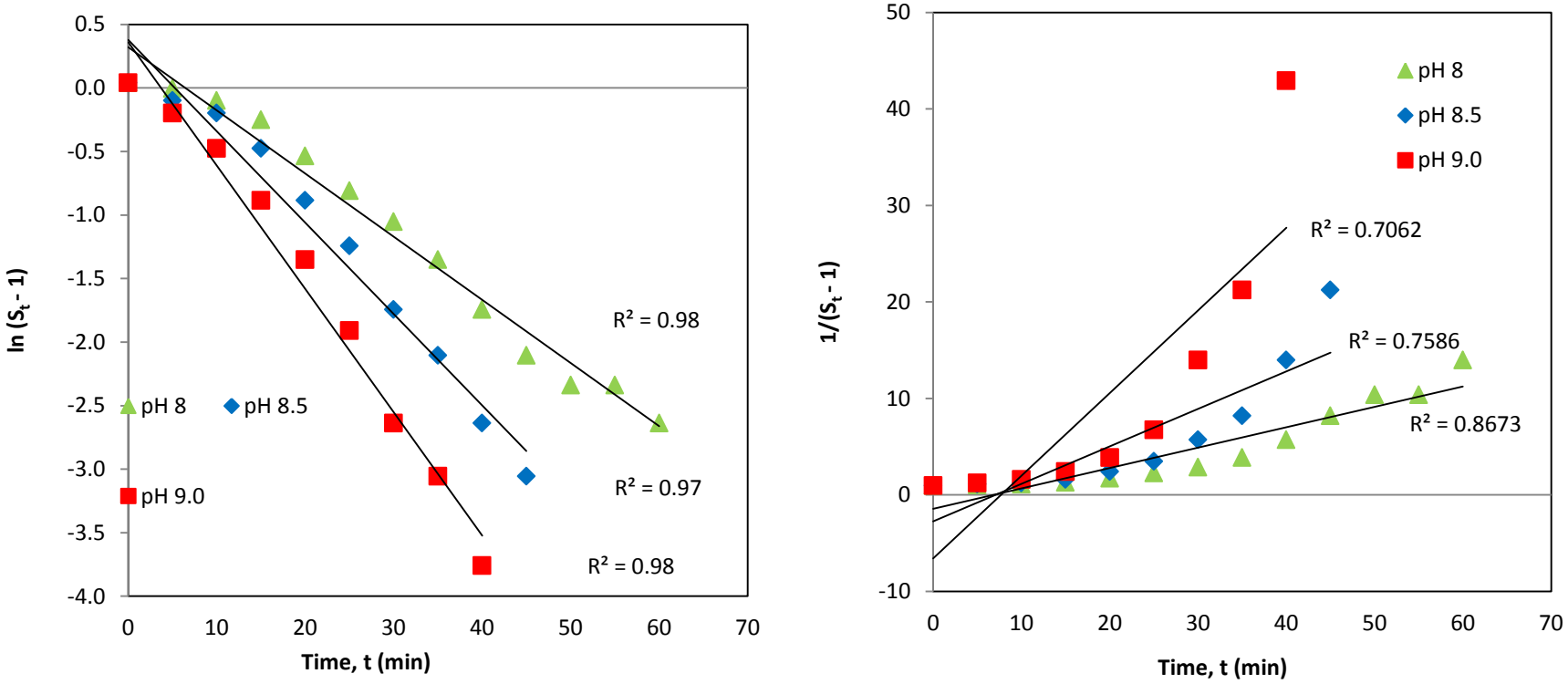

(a) (b)

Figure 6.11 Comparison of the kinetic equation between (a) first-order kinetic and (b) second order kinetic (b) at supersaturation = 2.04 25^{O}C and 120 rpm

The struvite growth rate at various supersaturation, S, from 2.04 to 10.00, were measured for three different solution pH, i.e., 8.0, 8.5 and 9.0 conducted in batch crystallizer at 120 rpm and 25^{O}C. The seed crystals suspended in the solution was 100 mg with an average size of 43.5 µm. During the experimental run, the solution was maintained at constant pH by addition of NaOH. The experimental results can be seen in Table C2.2 of Appendix C. Based on power law expression (Eq. 6.17), results of crystal growth measurement versus supersaturation for struvite are presented in Figure 6.12. It can be observed that the growth rate increases with increase in supersaturation for all solution pH range. This is because of increasing concentration driving forces. Furthermore, at given supersaturation, increasing solution pH increased growth of struvite crystals. For supersaturations from 2.04 to 10.00, the growth of struvite crystals increased with increase in solution pH. The growth rate constants were estimated from model fitting Eq. (6.17) (Figure 6.12) and the fitted kinetic parameters are presented in Table 6.2.

Table 6.2 Fitted growth mechanistic model fitted parameters for different solution pH

Solution pH	Mean saturation concentration (C_S), mMol/L	Growth Parameters (Eq. 6.17)			Overall Mass Transfer Coefficient (Eq. 6.15)
		g	$K_G \times 10^{-9}$, m/s	R^2	$K_L \times 10^{-5}$, m/s
8.0	1.9	1.1	1.1	0.96	0.2
8.5	1.2	1.2	2.3	0.95	0.7
9.0	0.8	1.3	3.3	0.97	1.4

High linear regression coefficient (R^2) indicates the applicability of power law struvite kinetics model. According to Nielsen and Toft (1984) the growth mechanism from surface integration (n = 2) to controlled diffusion (n = 1) was observed as the supersaturation of the solution increased, which was explained due to the increase of the mass transfer rate (K_L). In the present study, the growth kinetic order indicated that the crystallisation induced by struvite seed crystals indicated the process is controlled by the diffusion step for all solution pH. The rate constants were found to be a function of solution pH (Table 6.2). The rate

constant (K_G) value increases with increasing solution pH. The value of K_G under various process condition (Table 6.2) is very much comparative to the value reposted by many other investigation for different struvite formation system (Mehta and Batstone, 2013, Matynia et al., 2006, Koralewska et al., 2007, Hutnik et al., 2013). The increase in the rate of crystal growth was attributable by increase in rate of desupersaturation. The increased decay of supersaturation rate would give more mass transfer (K_L) in which crystal growth could take place. Further, Table 6.2 also shows the overall mass transfer coefficient (K_L) which is calculated by Eq. (6.15) increased with increase in solution pH.

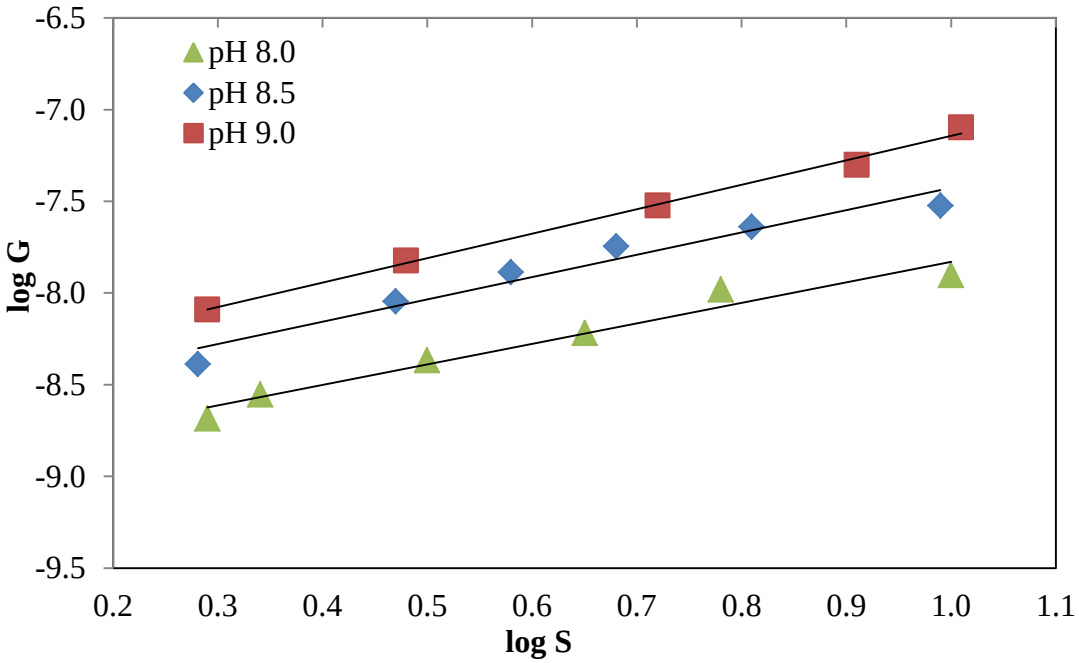

Figure 6.12 Crystal growth rate of struvite as a function of supersaturation for three levels of constant pH at 25^{O}C and 120 rpm

6.3.4 Effect of stirrer speed

The range of stirrer speeds selected to ensure homogeneous suspension and no significant breakage of the crystals were 50, 100, and 120 rpm. Seed sizes were suspended in a saturated solution at the various stirrer speeds for 15 min before analysing the resultant crystals for their size distribution (Figure 6.13). Figure 6.13 clearly shows that crystal size distribution for seed crystals and stirrer speed

were not significantly changed. Thus the selected stirrer speeds were in the range 50 to 120 rpm.

In this study, the solution supersaturation was calculated by adjusting the concentration of Mg, PO_4 and NH_4 at constant pH. The solutions of Mg:NH_4:PO_4 were made in a theoretical equimolar ratio of 1:1:1 To investigate the effect of stirrer speed on the formation of struvite, the supersaturation was monitored during the experimental run by measuring concentrations of Mg, PO_4 and NH_4.

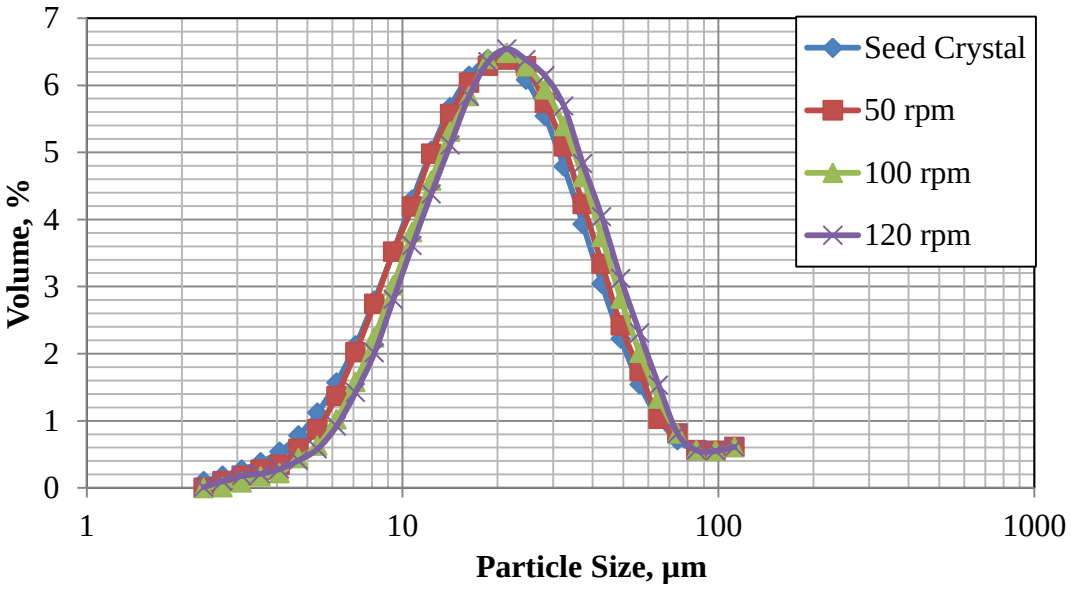

Figure 6.13 Crystal size distribution conducted with saturated solution at different stirrer speeds for 15 minutes

According to plotting Table C3.1 of Appendix C, the decay of supersaturation during crystallisation is shown in Figure 6.14. The decay of supersaturation curves for different stirrer speeds show that decay of supersaturation is a strong function of the stirrer speed. It can be observed that the induction period is significantly affected by stirrer speed. The decay of supersaturation curves show that the induction time of secondary nucleation at low stirrer speed of 50 rpm was 10 min but dropped to about 1 min for 100 and 120 rpm. This shorter induction time indicated higher rates of secondary nucleation at higher stirrer speeds. Higher speeds caused higher fluid and seed velocities, increasing the frequency of crystal-crystal, crystal-impeller, and crystal-crystallizer surface collisions, thereby causing higher rates of secondary nucleation as reported by Frawley et al., (2012).

After the induction time, crystal growth continued until equilibrium is reached. The equilibrium time of struvite crystallisation was determined when the supersaturation did not change anymore with time. For the three stirrer speeds studied, 50, 100, and 120 rpm, the equilibrium time was 60, 45, and 40 minutes, respectively, from the point of seed introduction into the crystallizer. Figure 6.14 also showed that more growth occurred at higher stirrer speeds as the slope of the supersaturation curve was steeper for higher stirrer speeds.

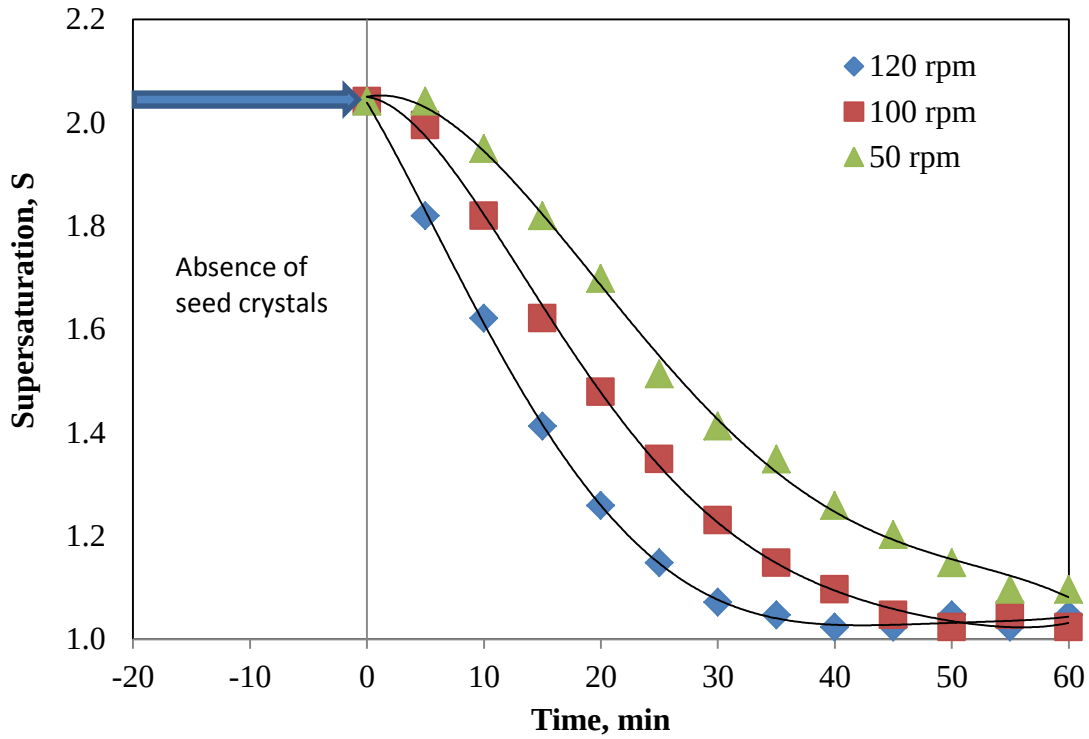

Figure 6.14 Decay of supersaturation curves of struvite crystallisation at supersaturation 2.04 for different values of stirrer speeds at pH 9 and temperature 25^{O}C.

The experimental data were fitted with both first-order (Eq. 6.5) and second-order kinetics (Eq. 6.7) and these are shown in Fig. 6.15(a) and 6.15(b), respectively. The value of linear regression coefficient (R^2) resulting from Figure 6.15(a) showed that the decay of supersaturation followed first order kinetic model. It confirmed that the high dependence of growth observed at higher stirrer speeds.

The experimental results agreed with the first-order kinetic model prediction. Similar trend in the variation of the rate constant was observed by Nelson et al., (2003) and Quintana et al., (2005) The rate constants resulting from different

stirrer speeds at supersaturation 2.04 are 2.6, 3.7 and 5.8 h^{-1} for 50, 100, and 120 rpm, respectively. A significant increase in value of k is caused by higher turbulence level in the system resulted by agitation (Uludag-Demirer et al., 2005). In addition, the higher agitation resulted in a thinner boundary layer as growth is mass transfer controlling.

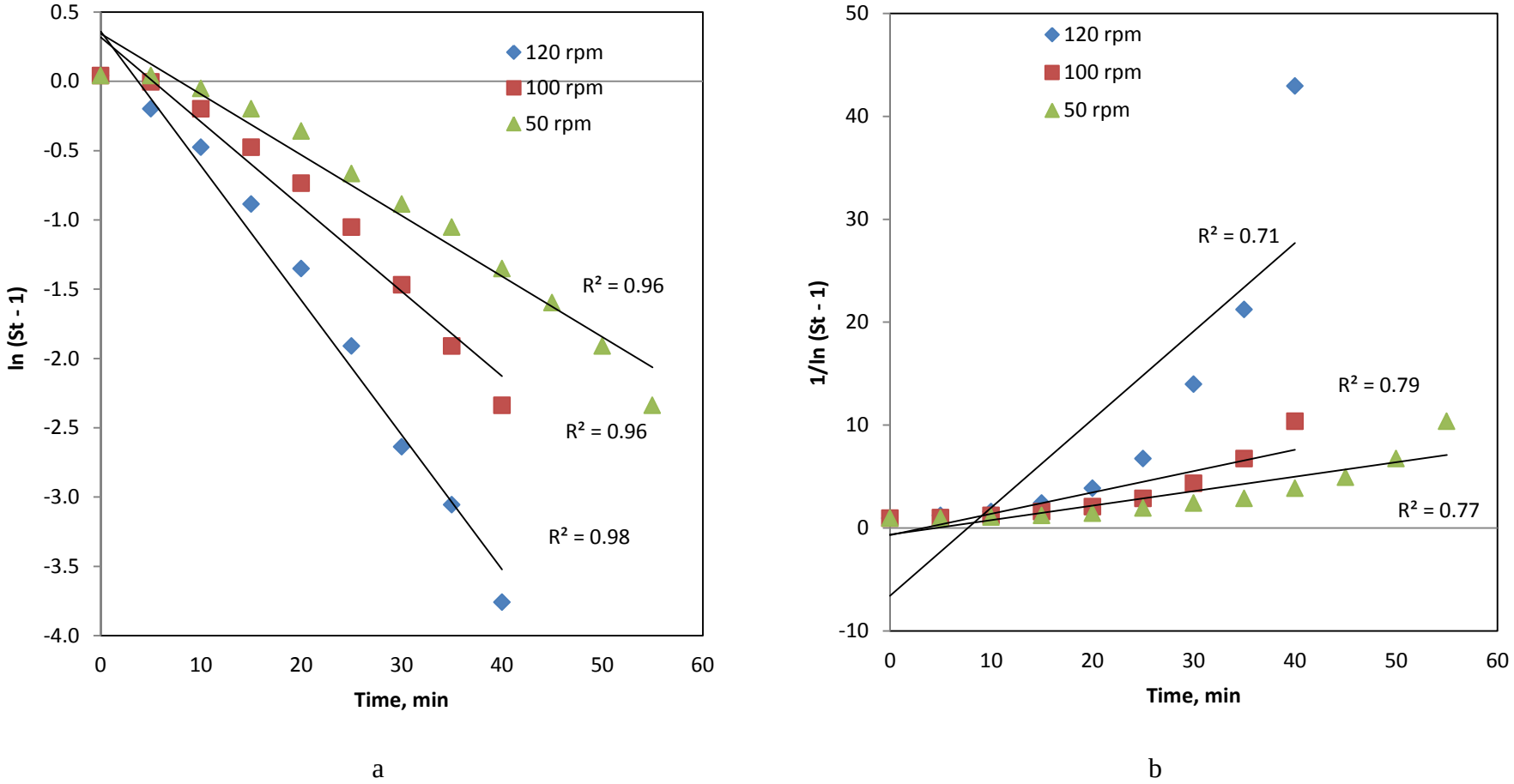

a b

Figure 6.15 Comparison of the kinetic equation between (a) first-order kinetic and (b) second order kinetic at supersaturation 2.04, pH 9, 25^{O}C, 100 mg of seed loading and 43.5 µm seed size

Experiments were also conducted for different stirrer speed, namely, 50, 100, and 120 rpm, at solution pH 9 in the crystallizer loaded with an appropriate amount of 100 mg of 43.5 µm struvite seeds. The plotting from Table C3.2 of Appendix C are shown in Figure 6.16. The crystal growth rates increased with increase in supersaturation for all stirrer speeds. For a given supersaturation, the crystal growth rates increase with increase in stirrer speed. At higher supersaturations, the crystal growth rates significantly increased with increase in stirrer speed. However, an increasing stirrer speed is not always advantageous in an operation, since increasing stirrer speed can cause crystal breakage and consume more energy. In this case, it is caused by collisions amongst crystals, collision of crystal with wall of the crystallizer, baffle and impeller surface. On the other hand, at lower stirrer speed, during the experiment runs, not much crystals mass was visible in suspension zone. In suspension zone, having higher supersaturation, is favourable for the faster growth of the small crystals. When the small crystals grow to larger crystals, the larger crystals have higher settling velocities and need larger stirrer speed to stay in solution. As a result, the relative speed, resulted by stirrer, between the crystals and the solution will increase with increasing crystal size and leads to a faster mass transfer step in the case of larger crystals, i.e. faster growth (Bhuiyan et al., 2008).

The fitted growth model parameters are shown in Table 6.3 which indicates that the crystal growth rate increased with increase stirrer speeds. The growth rate at different stirrer speed was predicted by using power law expression of Eq. (6.17). The growth rate order changes between 1.2 and 1.3 with increased stirrer speed in struvite system (Table 6.3). These values indicate that crystal growth of struvite is controlled either by a combination of controlled diffusion step I and surface integration at step II. Moreover, the constant value of K_G and K_L increased with higher stirrer speed (Table 6.3). It is evident that growth rate of struvite crystal increased with stirrer speed. In this case, it is caused by collisions amongst crystals, collision of crystal with wall of the crystallizer, baffle and impeller surface. On the other hand, at lower stirrer speed, during the experiment runs, not much crystals mass was visible in suspension zone. Higher supersaturation is favourable for the faster growth of the small crystals. When the small crystals

grow to large crystals, the large crystals have higher settling velocities and need larger stirrer speed to be stay in solution. As a result, the relative speed, resulted by stirrer, between the crystals and the solution will increase with increasing crystal size and leads to a faster mass transfer step in the case of larger crystals, i.e. faster growth rate (Bhuiyan et al., 2008).

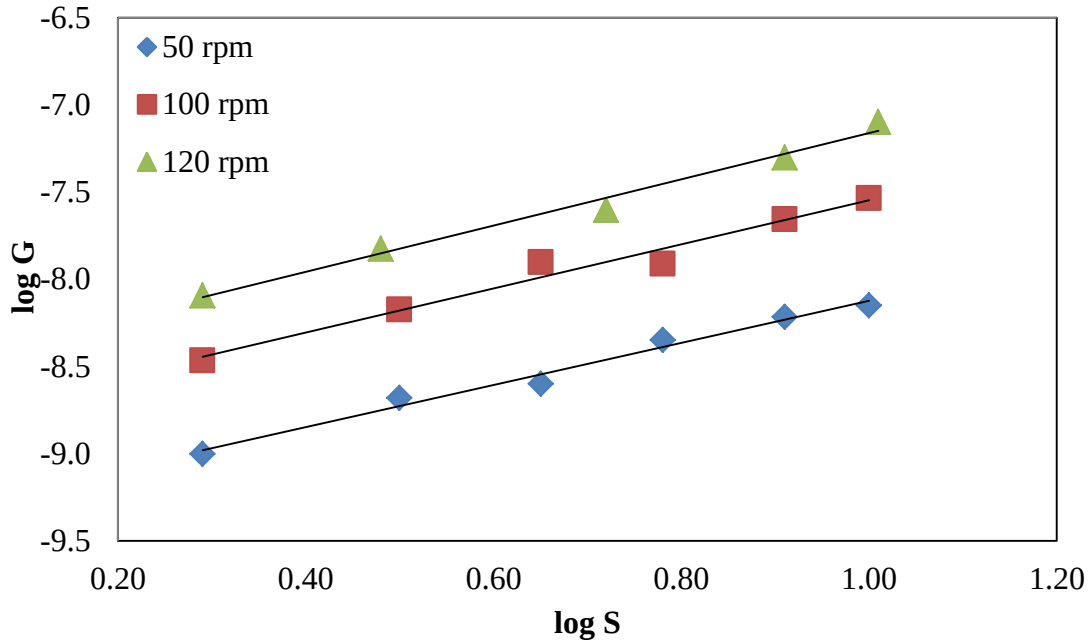

Figure 6.16 Crystal growth rate of struvite as a function of supersaturation for three levels of stirrer speeds at 25^{O}C and pH 9

Table 6.3 Fitted growth mechanistic model fitted parameters for different stirrer speed

Stirrer Speed, (RPM)	Mean saturation concentration (C_S), mMol/L	Growth Parameters (Eq. 6.17)			Overall Mass Transfer Coefficient (Eq. 6.15)
		g	$K_G \times 10^{-9}$, m/s	R^2	$K_L \times 10^{-5}$, m/s
50	0.8	1.21	0.5	0.98	0.2
100	0.8	1.36	1.6	0.97	0.7
120	0.8	1.36	3.3	0.98	1.4

In order to investigate the effect of the stirrer speed on overall crystal growth rate, samples were withdrawn and analysed by a Malvern Analyser at different time

intervals during the crystallisation. The time evaluation of the crystal size distribution obtained are shown in Figure 6.17.

Figure 6.17 indicates that the seed crystals (0 minute) in the batch crystallisation grew to larger crystals, as indicated by the CSD moving towards the larger sizes with time. However, the overall crystal growth rates are different for different agitator speeds. At lower agitator speed (Figure 6.17.A), crystal growth rate decreased when compared with higher stirrer speeds (Figure 6.17.A.B). During the experimental run, it was observed that at lower agitator speeds the crystals were more located at the bottom half of the crystallizer. In this case, the complete suspension was not achieved, so the seed crystals were not suspended in an environment of higher supersaturation resulting in lower growth rate.

The CSD move towards coarser fraction as impeller speed increased. It indicates that at higher stirrer speeds the hydrodynamic conditions are more suitable for crystal growth. In this case, the agitation condition provided the state of complete suspension of crystals particle and the maximum surface area of the crystals is exposed to the solution for mass transfer. Therefore, at higher speed it could cause crystal breakage, which is by collision between crystals and wall of the crystallizer, impeller or other crystals.

A

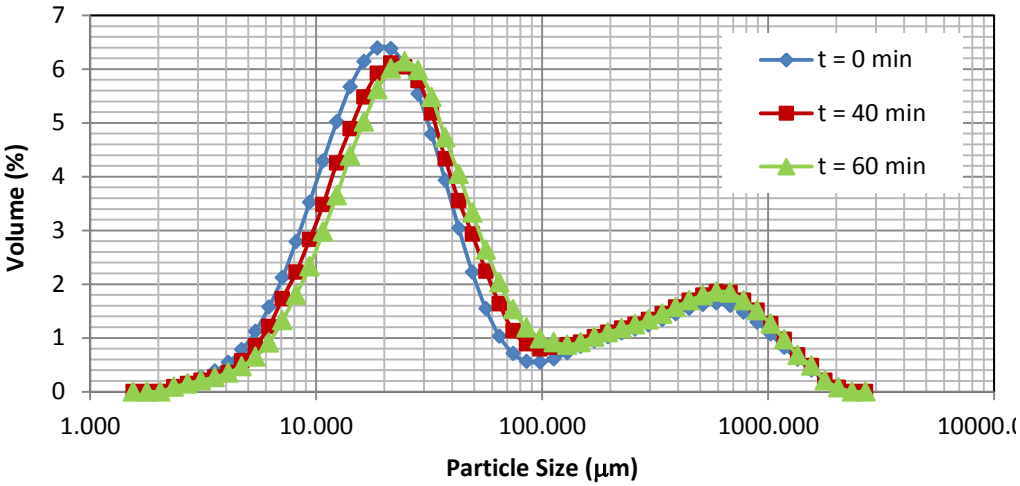

B

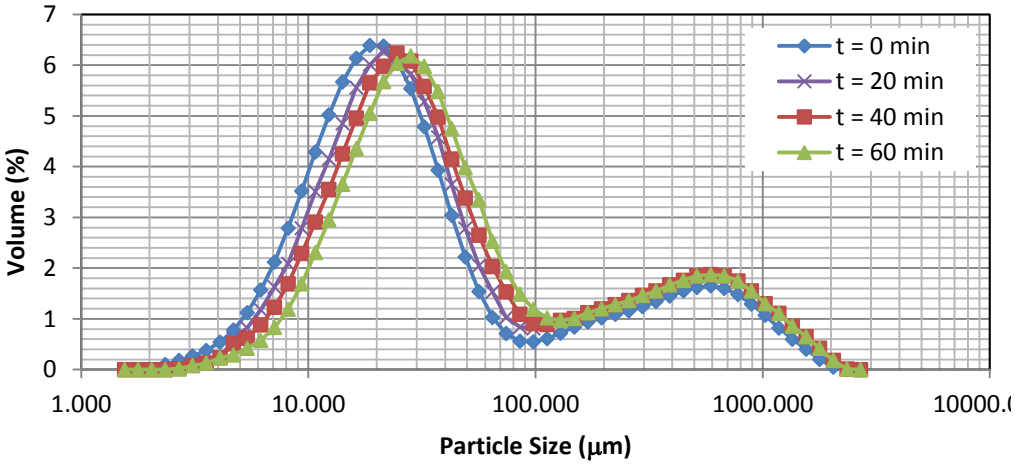

C

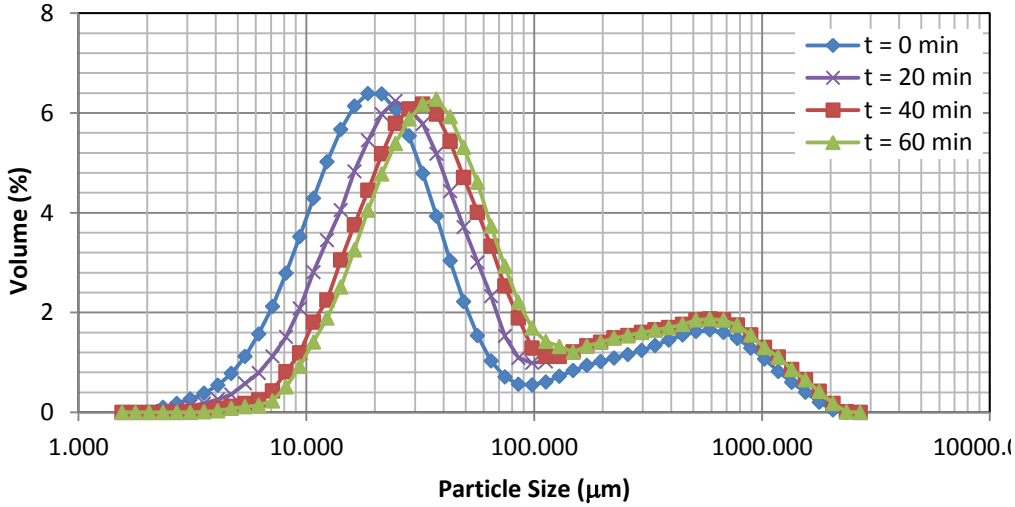

Figure 6.17 Crystal size distribution of struvite crystals at different growth times for various stirrer speeds: (A) 50 rpm; (B) 100 rpm; and (C) 120 rpm

6.3.5 Effect of temperature on struvite crystal growth kinetics

The effect of solution temperature on the decay of supersaturation of struvite was investigated in this study at 20, 25 and 30^{O}C. The struvite growth rates were measured in the supersaturation range under the influence of three levels of temperatures of 20, 25 and 30^{O}C with operating condition fixed as follows: pH 9, 120 rpm and 43.5 µm of seed size. Figure 6.18 show that increasing temperature from 20^{O}C to 30^{O}C greatly enhances the growth rate of struvite from solution. This study showed contradictory results to the results from the experiment conducted by Moussa et al., (2011) where the decreasing growth rate of struvite was caused by different supersaturation used in temperatures range. So the decreasing growth rate was practically caused by difference in supersaturation. In present study the same supersaturation was used. The increasing growth rate may be caused by increasing activity of ions. At higher temperatures, the cluster adsorbed onto the crystal surface were more active in causing a higher surface-integration rate (Chang and Tai, 2010).

The data results of Table C4.1 of Appendix C which are plotted by Eq. (6.17) were in Figure 6.19. The plotting results which are presented in Table 6.4 shows that the growth rate constant (K_G) increased with increase in temperature. Based on the cluster transformation mechanism, activation of constituent ion in higher temperature may provide more available clusters for growth and it is possible that the transformation became more significant at higher temperature (Chang and Tai, 2010). Thus, it can be indicated that the K_L values increased with increase in temperature (Table 6.4).

Table 6.4 Fitted growth mechanistic model fitted parameters for struvite crystal at different temperature

Temperature (^{O}C)	Mean saturation concentration (C_S), mMol/L	Growth Parameters (Eq. 6.17)			Overall Mass Transfer Coefficient (Eq. 6.15)
		g	$K_G \times 10^{-9}$, m/s	R^2	$K_L \times 10^{-5}$, m/s
20	0.7	1.05	2.5	0.98	1.2
25	0.8	1.36	3.3	0.97	1.4
30	0.9	1.47	5.2	0.98	2.0

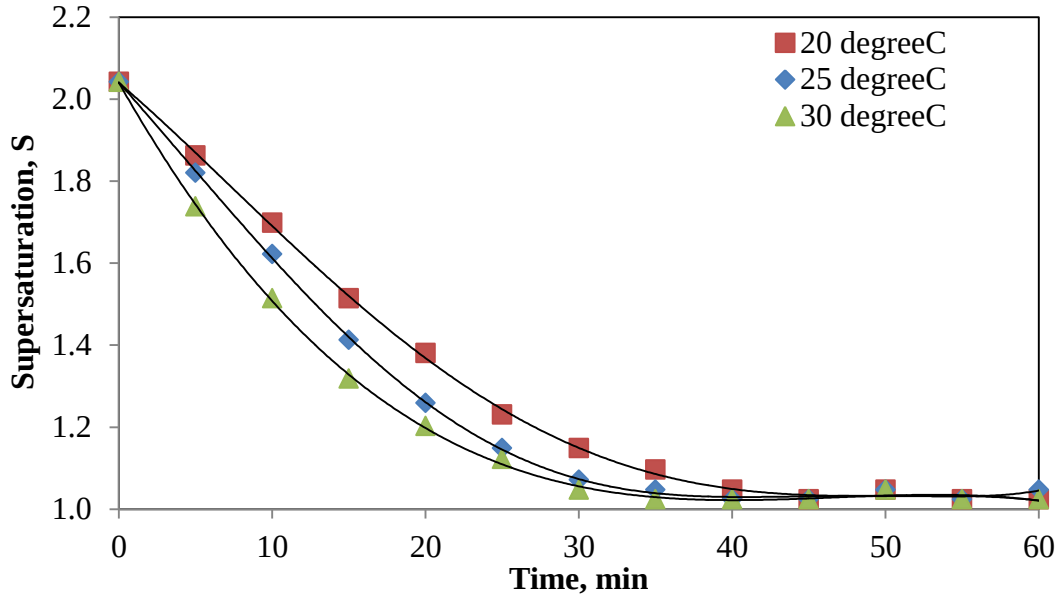

Figure 6.18 Decay of supersaturation curves of struvite crystallisation at initial supersaturation 2.04 for different temperature at pH 9 and 120 rpm.

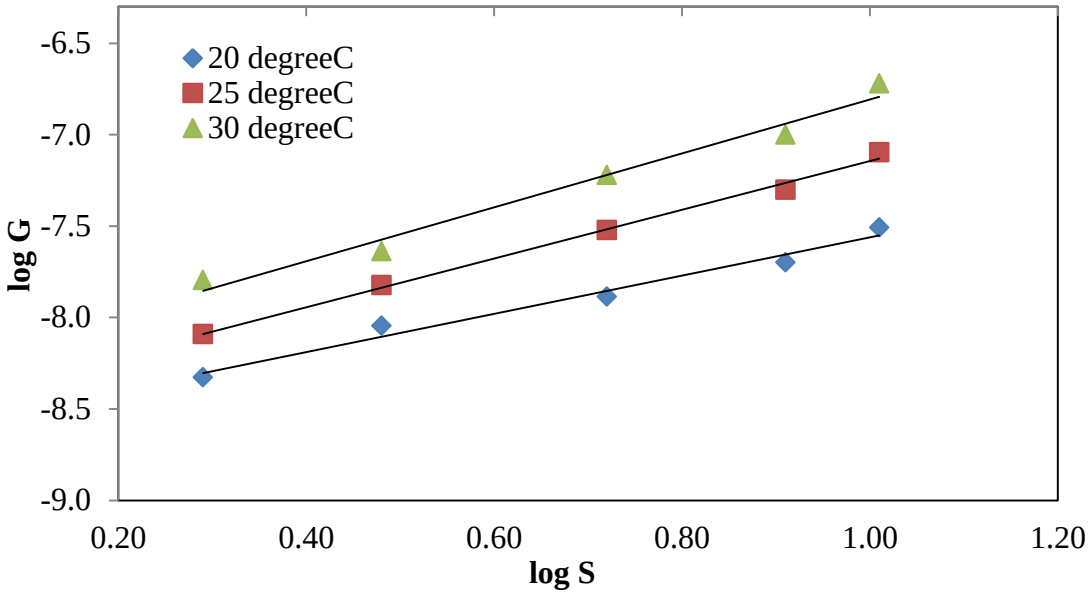

Figure 6.19 Crystal growth rate of struvite as a function of supersaturation for three levels of temperature

In order to estimate the activation energy of the growth of struvite, the activation energy of crystals growth, E_{act}, was calculated by the following Arrhenius equation;

$$\boldsymbol{K_G = K_0 . \exp\left(\frac{-E_{act}}{RT}\right)} \quad (6.18)$$

This empirical equation has been simplified:

$$\boldsymbol{\log K_G = \log K_0 - \frac{E_{act}}{2.303\ R\ T}} \quad (6.19)$$

where K_0 is a constant, E_{act} is the activation energy (J mol^{-1}) for the process, and R is the gas constant (8.314 J/K.mol). Activation energy represents the minimum energy that is required for a growth struvite crystal to take place. Figure 6.20 is a plot of *log* K_G versus *1000/T* for growth of struvite crystal obtained in temperature ranged examined, and the value of activation energy of growth of struvite crystals E_{act} of 55.42 kJ.mol^{-1} were obtained by fitting the data the Arrhenius relation at pH 9.

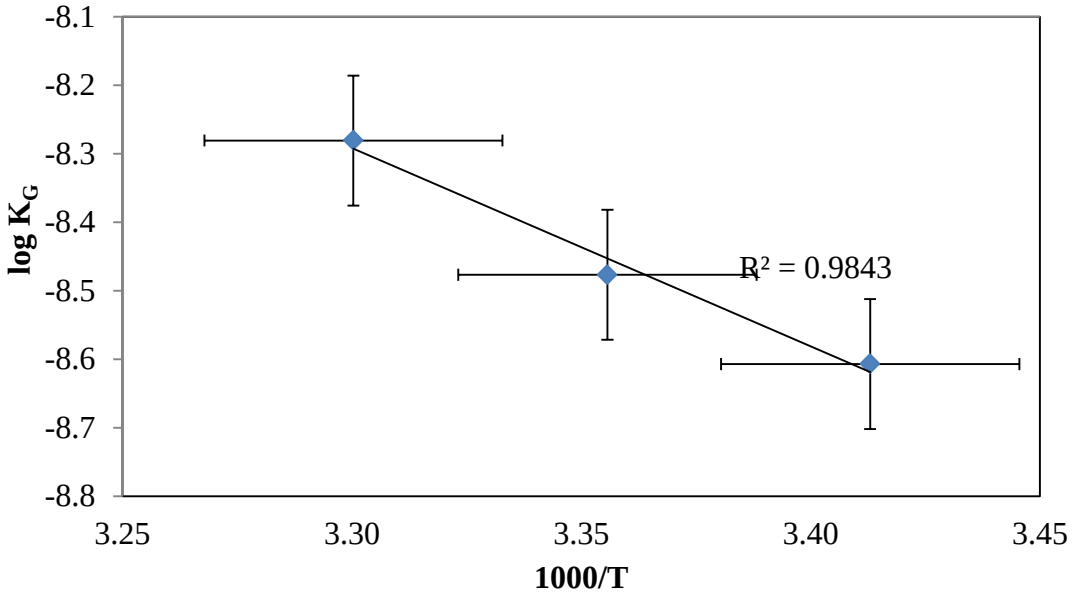

Figure 6.20 A plot of Arrhenius Eq. (6.19) for struvite crystal

6.3.6 Effect of Impurities NaCl Salts Addition on Crystals Growth Kinetics

The presence of impurities or foreign ions in a system may enhance or suppress the growth. In this present study, NaCl was used as impurity in struvite system. Experiments were conducted for various NaCl concentrations of 0, 50, 100, 200 and 600 ppm in aqueous solution of struvite. The experimental results can be seen in Table C4.2 of Appendix C. The linearized struvite kinetics plots based on power law expression of Eq. (6.17) were plotted with observation and are presented in Figure 6.21. However, fitting parameters are presented in Table 6.5. It was found (Table 6.5) that NaCl addition in a system can have a significant effect on the growth of struvite crystal. The growth rate (K_G) increased with increase in range NaCl 50 – 600 ppm. In this situation, the NaCl addition may not only change the properties of solution but also alter the characteristic of the adsorption layer at the crystal-solution interface (Mullin, 2001). According to Tai et al. (2006b), the increased presence of NaCl in the system decreased the double-layer thickness between solution and crystal, so the adsorption of growth unit on the crystals surface was easier under such a smaller double layer thickness. However, at 600 ppm NaCl obtained in the experimental study showed decreasing

growth rate (K_G). Decreasing growth rate was caused by adsorbed NaCl on the crystal surface. So the crystal growth rate may inhibit.

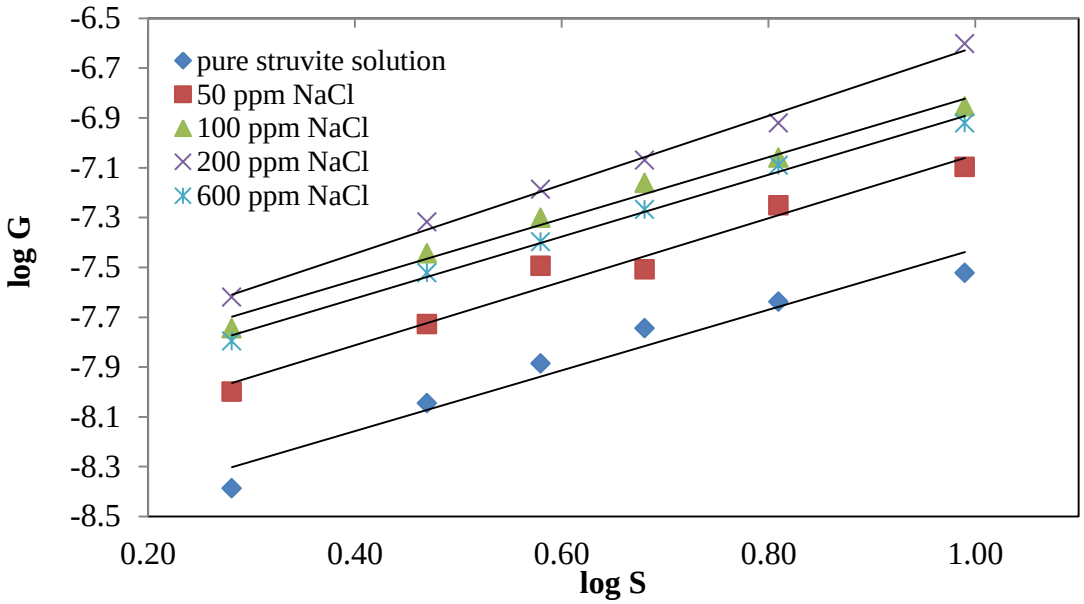

Figure 6.21 Crystal growth rate of struvite as a function of supersaturation for three levels of NaCl concentration at 25^{O}C, pH 8.5 and 120 rpm.

From Table 6.5 the growth rate order (g) was between 1.2 and 1.4. Moreover, for the NaCl concentration-dependent growth rate of struvite shown in Figure 6.22. Thus from Figure 6.22, the crystal growth process of struvite is diffusion controlled for NaCl addition below 100 ppm. As NaCl addition increases form 50 – 200 ppm, the mass transfer becomes significant (K_L). After the NaCl addition exceeds around 300 ppm, the growth rate decrease.

Table 6.5 Fitted growth mechanistic model fitted parameters for struvite crystal at different concentration NaCl

NaCl addition (ppm)	Mean saturation concentration (C_S), mMol/L	Growth Parameters (Eq. 6.17)			Overall Mass Transfer Coefficient (Eq. 6.15)
		g	$K_G \times 10^{-9}$, m/s	R^2	$K_L \times 10^{-5}$, m/s
0	0.8	1.22	3.3	0.97	1.4
50	0.8	1.27	4.8	0.96	2.1
100	0.8	1.33	9.0	0.98	3.9
200	0.8	1.38	10.0	0.97	4.3
600	0.8	1.24	7.6	0.97	2.2

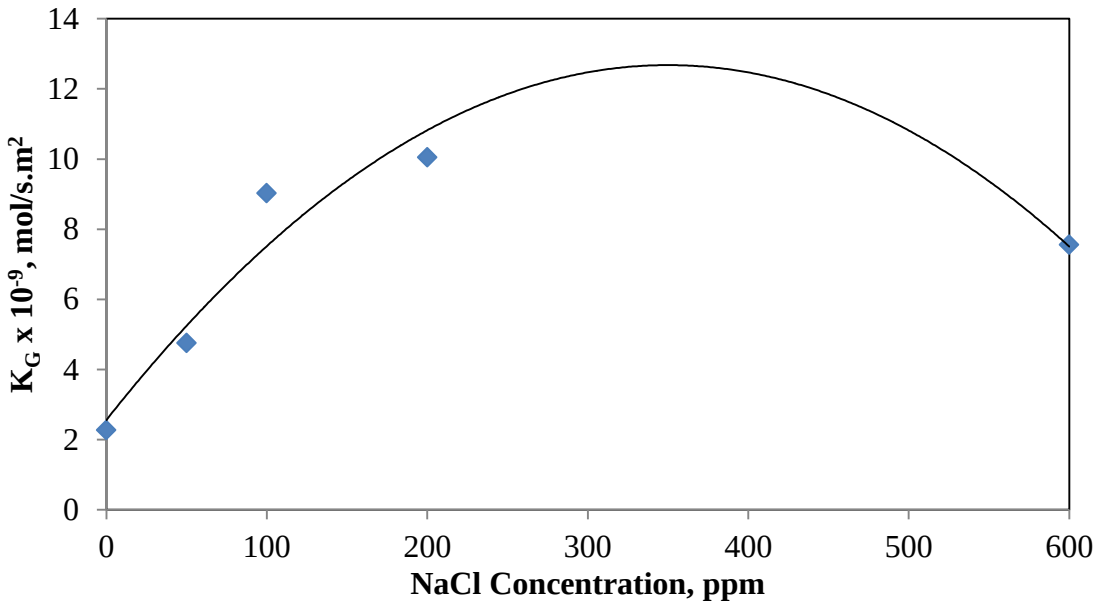

Figure 6.22 Plots of growth rate constant versus NaCl concentration addition for struvite crystals.

6.3.7 Struvite crystal product characteristics

Scanning electron microscope with EDS analysis at seed and struvite product crystals at a solution pH of 8.0, 8.5 and 9.0 and temperature 25^{O}C are shown in Figure 6.23(a) and Figure 6.23(b)(c),(d), respectively. The product crystals have a similar shape (Figure 6.23(b),(c) and (d)) to the seed crystals (Figure 6.23(a)) indicating there was no phase transformation during growth. Further struvite

crystals have a distinctive orthorhombic structure and also cube needle like structure shown in Figure 6.23(a) and 6.23(b),(c) and (d).

According to EDS analysis, the phosphorus atomic concentration is equal to magnesium concentration. Figure 6.23(a) shows that the seed struvite crystals formed as no trace of other compounds have been found. The product struvite crystals from EDS analysis matches with seed struvite crystals. It also showed a composition at P, Mg and O. Struvite product when crystallisation was occurred at pH 9 shows that phosphorus peak was higher than magnesium peak. The formation of this precipitate at the surface of crystals would thus explain the multitude of background peak observed on FTIR pattern while struvite peak are identified.

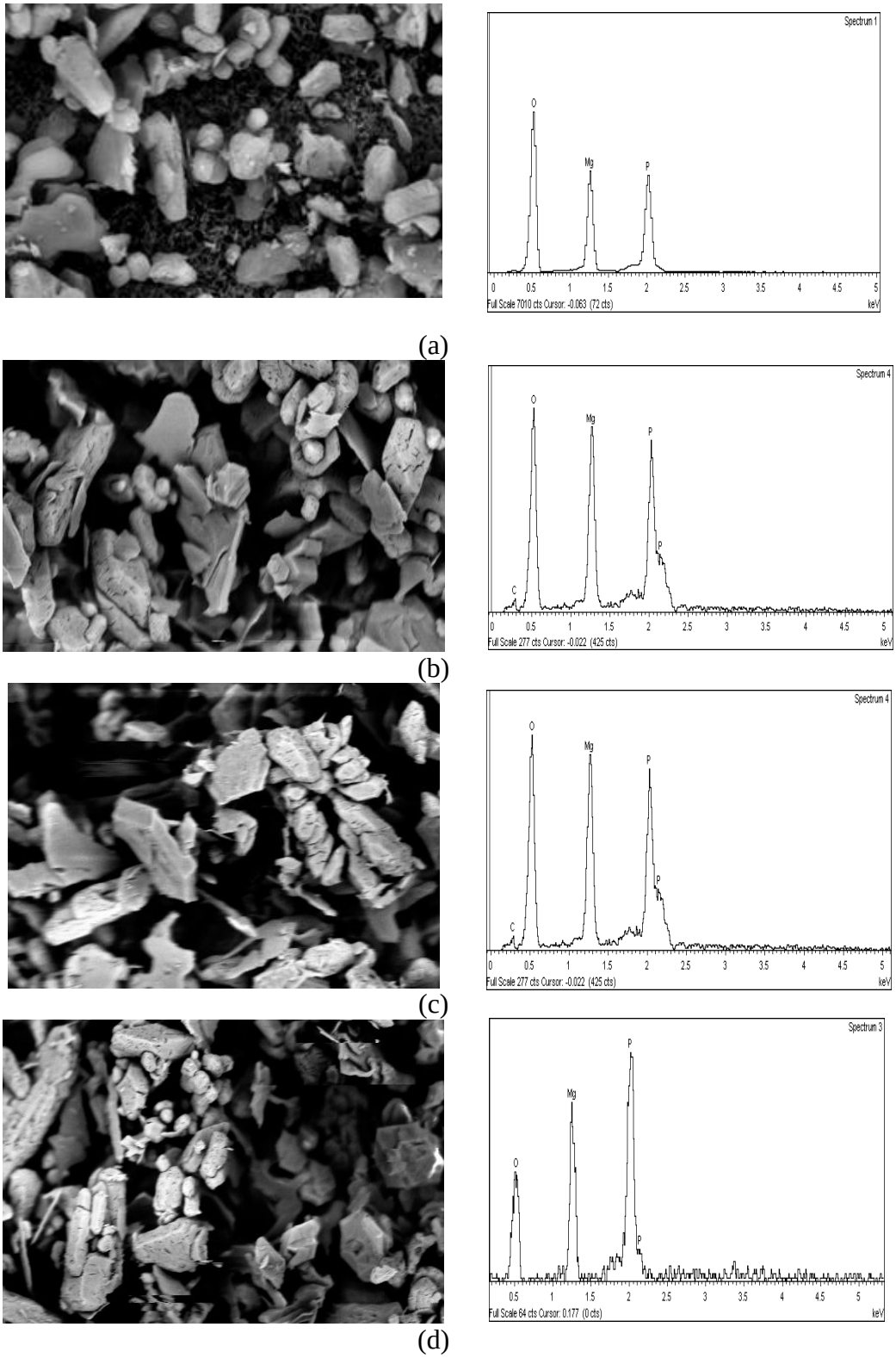

Figure 6.23 Scanning Electron Microscopy of struvite; (a) Seed crystals; (b) product crystal at pH 8; (c) product crystal at pH 8.5 (d) product crystal at pH 9, at 25^{O}C and 120 rpm

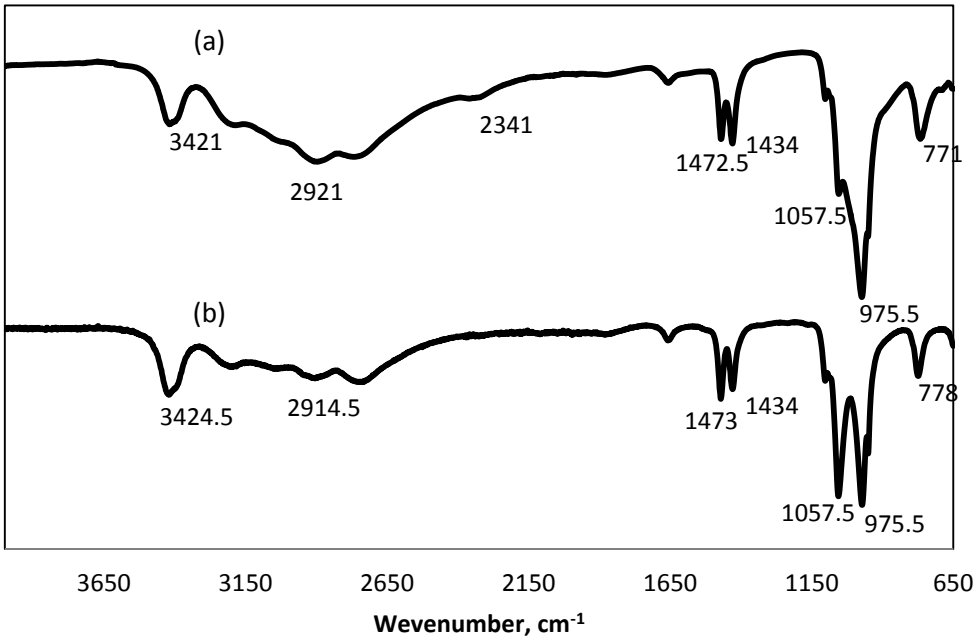

Figure 6.24 FTIR spectra of struvite crystals. (a) seed crystals; (b) product crystal at pH 9, 120 rpm and 25^{O}C

The Fourier transform infrared spectroscopy (FTIR) was used to analyse potential changes in the inner structure of struvite crystals. Figure 6.24 shows the FT-IR spectrum of struvite seed and product struvite crystal. The absorptions occurring at 3421, 3424.5 cm^{-1} are due to O-H and N-H stretching vibration. This also suggests the presence of water of hydration. The absorption occurring at around 2921 and 2914.5 cm^{-1} is due to NH_4^+ ion (Chauhan et al., 2008). The weak bands appeared at 2341 cm^{-1} in the spectrum can be assigned due to H–O–H stretching vibrations of cluster of water molecules of crystallization. The absorption occurring around 1472.5 and 1434 cm^{-1} have been attributed to N-H bending vibration (Banks et al., 1975). The absorptions taking place at around 1057.5 and 975.5 cm^{-1} are due to ionic phosphate (Suguna et al., 2012). A medium absorption band at around 771 and 778 cm^{-1} indicates the wagging modes of vibration of the coordinated water and the Metal–Oxygen bond in the complex.

According to FTIR spectra patterns, as shown in Figure 6.24(a) and 6.24(b), it was confirmed that no substantial crystalline change was found between seed crystals and crystal product. However, the minor differences in the relative

intensities of their peaks might be attributed to differences in the degree of crystallinity of the samples.

The images of the final crystals of struvite at various stirrer speeds produced by optical microscope are shown in Figure 6.25. There is clear evidence that stirrer speed has a significant influence on the final product size of struvite crystals. At 50 rpm (Fig. 6.25(A)), the image crystals appear to be smaller, and gradually increase in size with higher stirrer speed (Fig. 6.25(B)(C)).

A

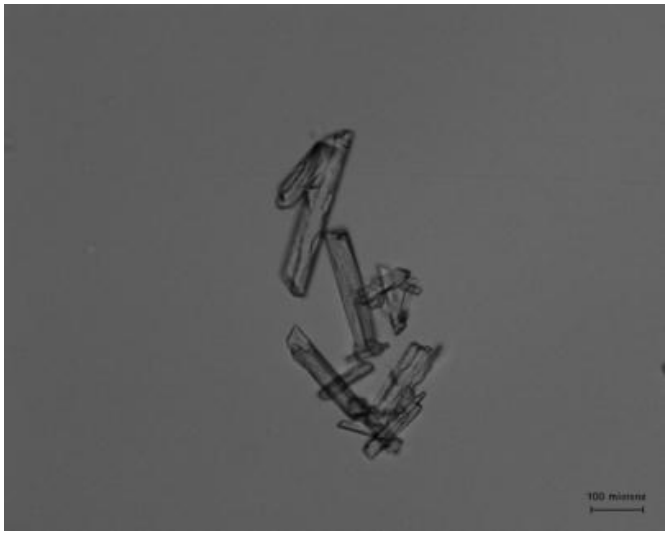

B

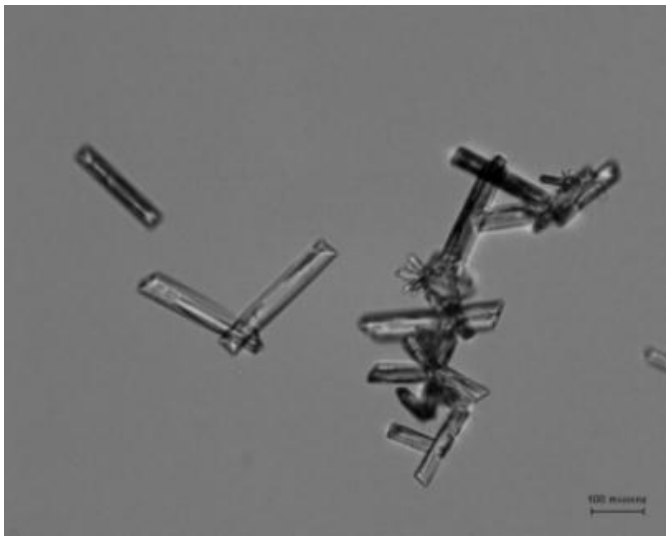

C

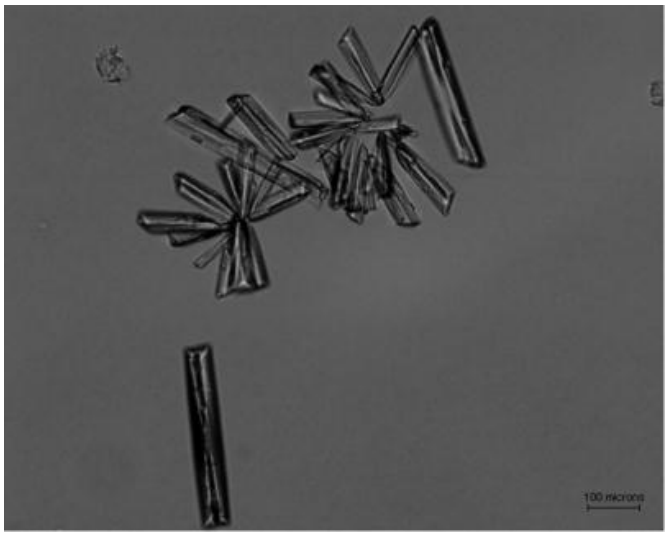

Figure 6.25 The images of struvite crystals obtained at various stirrer speeds; (A) 50 rpm, (B) 100 rpm, (C) 120 rpm

The measured CSD for the seeds and the final distribution using Malvern Mastersizer are shown in Figure 6.26. The results are shown in volume %, as obtained from the instrument and on a logarithmic size scale, to better distinguish the particular features of the size distributions. Figure 6.26 clearly shows that during the crystallization the crystals become larger with increase in relative supersaturation (*S*). Increasing final product size distribution was due to increase in driving force of solution.

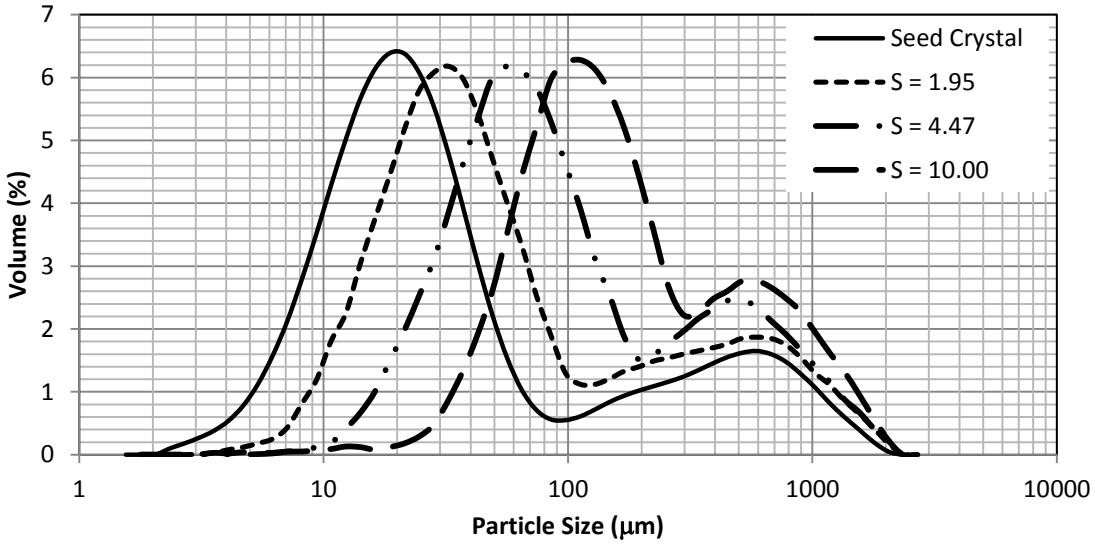

Figure 6.26 Effect of supersaturation on final product size distribution of struvite crystal at 25^{O}C, solution pH of 8.5 and 120 rpm with seed loading 100 mg and mean size 24.3 μm

The size distributions of final crystal products obtained at different impeller speeds are presented in Figure 6.27. The curves of successive cumulative distribution presented, clearly show that during the crystallization the crystals become larger with increase stirrer speed. As can be seen on Figure 6.27, it can be indicates that at 120 rpm the hydrodynamic condition are more suitable for crystal growth than 50 rpm and 100 rpm. In this case, the agitation condition of 120 rpm provided the state of complete suspension of sturvite crystals and the maximum surface area of the crystals is exposed to the solutions for mass transfer. On the other hand, 120 rpm, it was not occurred crystal breakage which is caused by collision between crystals and walls of the crystallizer, impeller or other crystal. However, at 50 and 100 rpm, secondary nucleation was occurred. The

photographs of the final crystals of struvite obtained at various agitation speeds made by optical microscope are given in Figure 6.25.

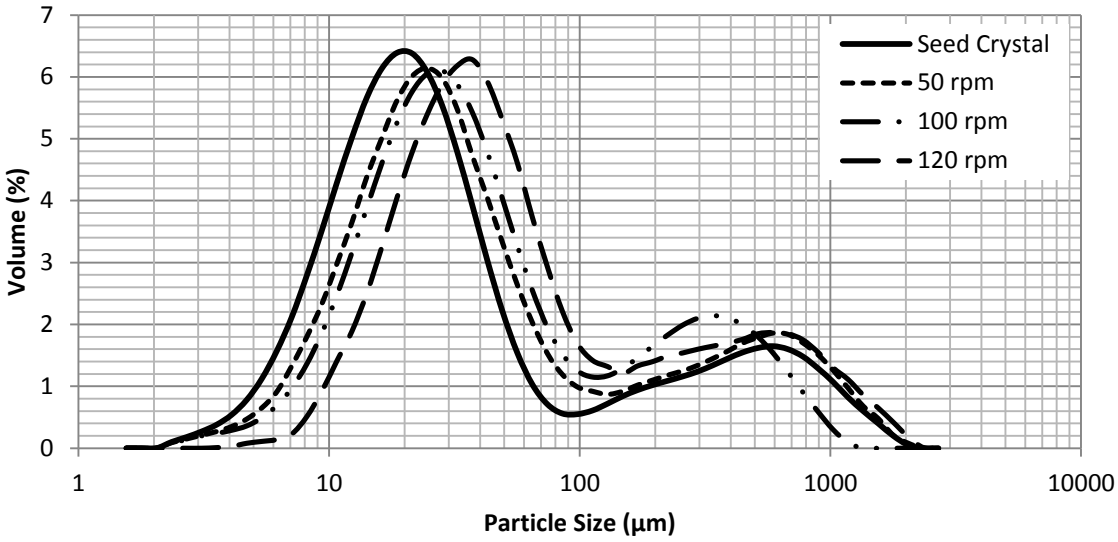

Figure 6.27 Effect of stirrer speed on final product size distribution of struvite crystal at 25^{O}C, solution pH of 8.5 and relative supersaturation 2.04 with seed loading 100 mg and mean size 24.3 µm

XRD data indicated single–phase struvite (orthorhombic) space group with the experimental lattice parameters of a = 11.215, b = 6.954, c = 6.141. In Figure 6.28, the patterns confirmed that orthorhombic struvite was dominant crystal phase and no difference in the XRD pattern observed for seed crystals and product crystal. Similar observation was reported by many investigators (Mehta and Batstone, 2013, Bouropoulos and Koutsoukos, 2000, Bhuiyan et al., 2008).

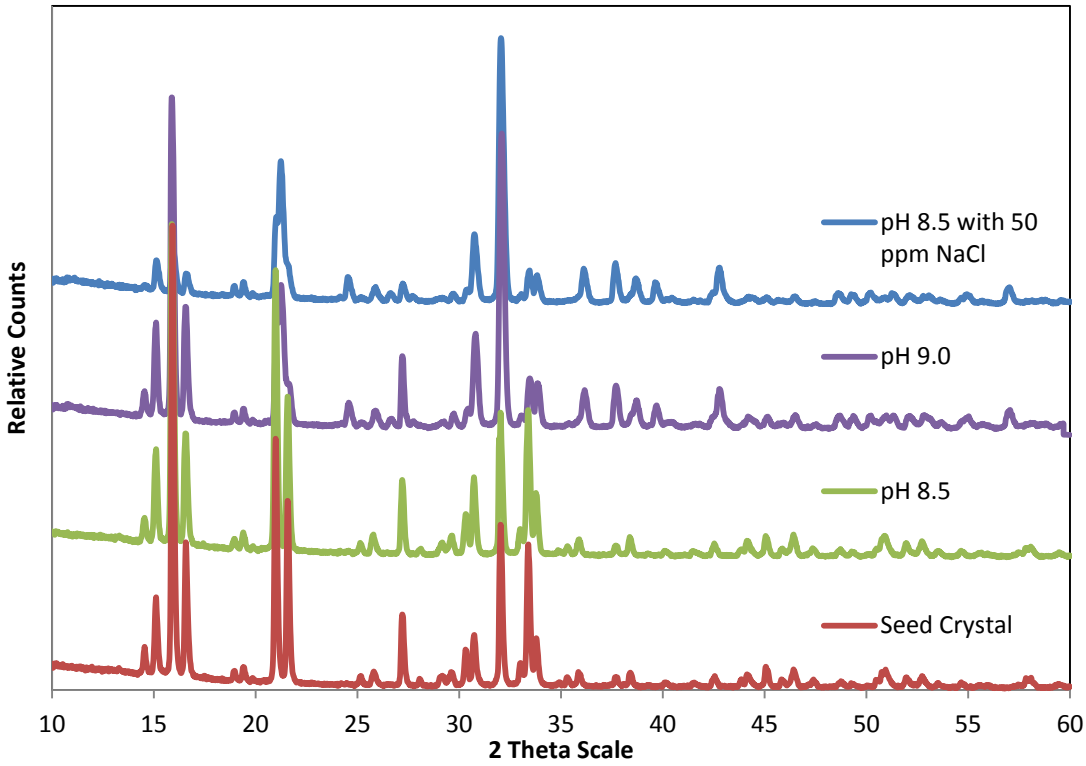

Figure 6.28 XRD trace for seed crystals and struvite product at different pH

6.4 Summary

- The impacts of physico-chemical process parameters such as seed loading, temperature, solution pH, stirrer speed, and impurities on struvite crystal growth mechanism have been successfully investigated.
- The kinetic rate of decay of supersaturation was identified by using supersaturation 2.04 which is close to solubility curve. Seed loading may increase rate of struvite precipitation.
- The pseudo-first order and pseudo-second order kinetic models were employed to analyse the rate of decay of supersaturation data of solution pH, temperature and stirrer speed and much useful kinetic information are revealed.
- The experimental results agreed with the first-order kinetic model prediction. The obtained rate constant, *k*, can be used to explain the struvite precipitation behaviour. In the batch stirrer crystalliser, struvite precipitation was strongly dependent of solution pH, temperature and stirrer speed.

- A classical diffusion-reaction mass transfer crystal growth mechanism is applicable under various physico-chemical parameters. Several process variables were investigated such as solution pH (8 – 9), temperature (20 – $30^{O}C$) stirrer speeds (50 – 120 rpm) and presence of impurities (50 – 200 ppm NaCl). The various growth kinetic parameters and overall mass transfer coefficients under various process conditions have been determined. However, the NaCl addition exceeds 100 ppm, the growth rate of struvite was constant.

CHAPTER 7
EFFECT OF VARIOUS PROCESS PARAMETERS ON THE DISSOLUTION KINETICS OF STRUVITE CRYSTALS IN WATER

7.1 Introduction

Struvite ($MgNH_4PO_4.6H_2O$) is a crystal that is often found in wastewater treatment plant. Struvite crystals are often found in wastewater treatment plant and the deposit increases operating cost of industrial equipment, such as pump, aerator, centrifuge, and other equipment in the wastewater treatment plant. On the other hand, struvite has economic value that can be used as fertilizer.

Dissolution of struvite has been studied from different point of view and its chemical and physical properties have been clearly described (Bavic-Ivancic et al., 2002). Struvite dissolution reaction can be described using

$$\mathbf{MgNH_4PO_4.6H_2O} \rightleftarrows \mathbf{Mg^{2+} + NH_4^+ + PO_4^{3-} + 6H_2O} \quad (7.1)$$

Many studies on the dissolution of struvite crystals in various media have been found in literature. As described in Section 2.8.6.

In this study, the dissolution kinetics of struvite crystals in deionized water (pH 7) was studied. An analytical equation describing the relationship between the solute concentration and the dissolution time was determined. Effect of stirrer speeds, temperature and crystal size was also studied. Activation energies, from either diffusion-controlled or interfacial-reaction-controlled were accounted for by using dissolution rate equations.

7.2 Mass transfer theory on dissolution kinetic of struvite seed crystals

Dissolution process is controlled by the affinity between the solid and solvent. The Nernst-Brunner stagnant film theory noticed that dissolution of a solid in a liquid can be described as the transfer of solute from the solid surface into the surrounding solvent (Banakar, 1992). The dissolution kinetics is described in Section 2.7. The kinetics of dissolution can be predicted by using Eq. (7.2) and Eq. (7.3)

$$\frac{dC}{dt} = K_L a(C_s - C_b) \quad (7.2)$$

where K_L is mass transfer coefficient for crystal dissolution (m/s) and a is surface area of crystal (m^2/m^3). If $K_L.a$ is volumetric mass transfer coefficient, it is equal to K, so Eq. (7.2) can be written as below

$$dC_b/dt = K(C_s - C_b) \quad (7.3)$$

$$dC_b/(C_S - C_b) = Kdt \quad (7.4)$$

which on integration yield

$$\ln(C_S - C_b) = \ln C_S - K.t \quad (7.5)$$

Where K is appearant dissolution rate constant (s^{-1})

The above mechanistic power law dissolution rate equation was fitted with our batch struvite crystalliser experimental data. The slope of plot between *log* $(C_S - C_b)$ versus t gives the value of K value at different physico-chemical parameters. The value of K_L can be predicted from K value.

7.3 Experimental

Struvite crystals were first prepared by crystallisation from aqueous supersaturated solution using a jacketed glass batch crystallizer with a working volume of 1000 ml at 25^OC and pH 9. The reagent salts used to prepare the supersaturated solution were analytical grade magnesium chloride ($MgCl_2$) and ammonium dihydrogen phosphate ($NH_4H_2PO_4$). Sodium hydroxide (NaOH) was used to adjust solution pH. $MgCl_2$ was obtained from Sigma and $NH_4H_2PO_4$ was obtained from Perth Scientific Australia. All chemicals were used without further treatment. Double distilled water was used for all solution preparation. pH was measured by an Orion pH meter. After the solutions were mixed in the crystallizer, seed crystals were introduced to produce larger crystals that were used for dissolution studies. The crystals were dried at room temperature for 24 hours. The crystals sizes were measured by laser diffraction with a Malvern Master Sizer 2000 at the end of crystallisation. These crystals were used with an

average size *L* for dissolution studies. The Fourier transform infrared spectroscopy (FTIR) was used to analyse potential changes in the inner structure of struvite crystals.

The dissolution of struvite crystals was studied in the same crystallizer used to crystal growth study. The experimental study is described in Section 3.8. Analyses for ammonium and phosphate were made using UV-spectrophotometer (see Section 3.2.4.2 and Section 3.2.4.3, respectively). Magnesium analysis was performed by atomic absorption spectrophotometry (see Section 3.2.4.1).

7.4 Results and Discussion

7.4.1 Dissolution of struvite crystals in deionized water

The dissolution rate of struvite seed crystals was investigated as a function of time by changing the concentration of ions of struvite in deionized water at a solution pH of 7 which is shown in Figure 7.1. The dissolution rate was evaluated by measuring three different ion concentrations Mg^{2+}, $PO_4^{3-}$and NH_4^+ in bulk solution with different time interval. The total concentration of struvite in solution was evaluated by calculating the average of these three ion concentrations (see Table D1.1 in Appendix C). It can be seen in Figure 7.1(a) and 7.1(b) that the dissolved struvite concentration systematically increased with time. Figure 7.1(a) shows that the ion concentrations did not reach equilibrium after only 1 hour (= 60 min). Figure 7.1(b) shows that equilibrium was reached after 24 hours. The equilibrium indicated that dissolution of struvite reached a solubility limit about 24 hours. The dashed line indicates the solubility limit. Figure 7.1(a) and 7.1(b) also shows that the concentration of three component of struvite ions in bulk solution are in a molar ratio $Mg:NH_4:PO_4$ of 1:1:1.

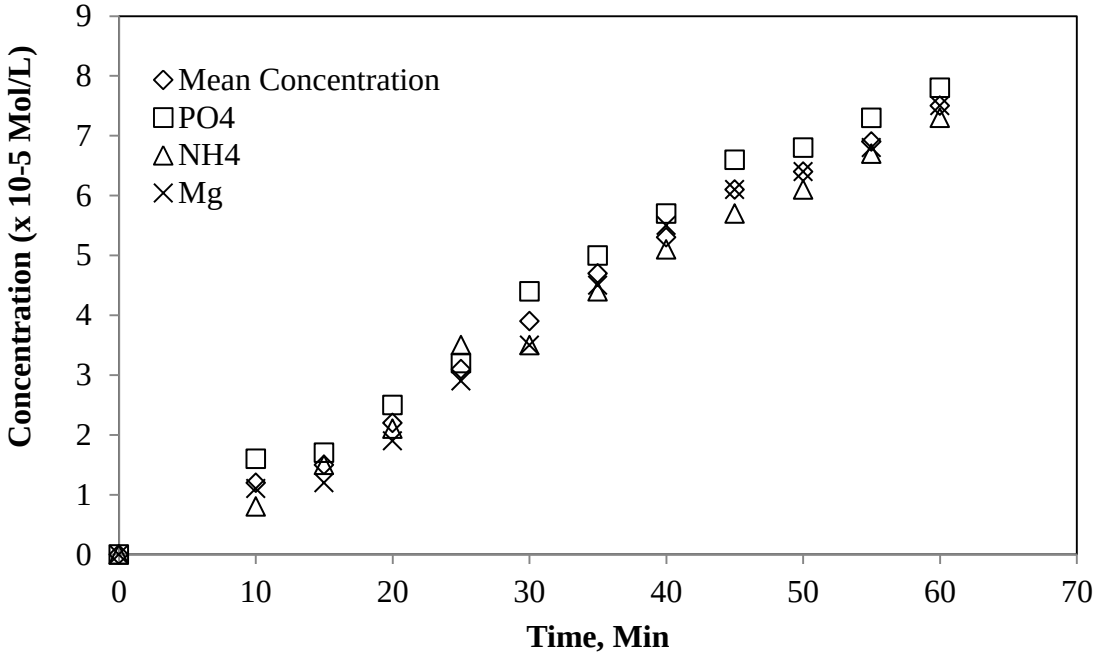

a

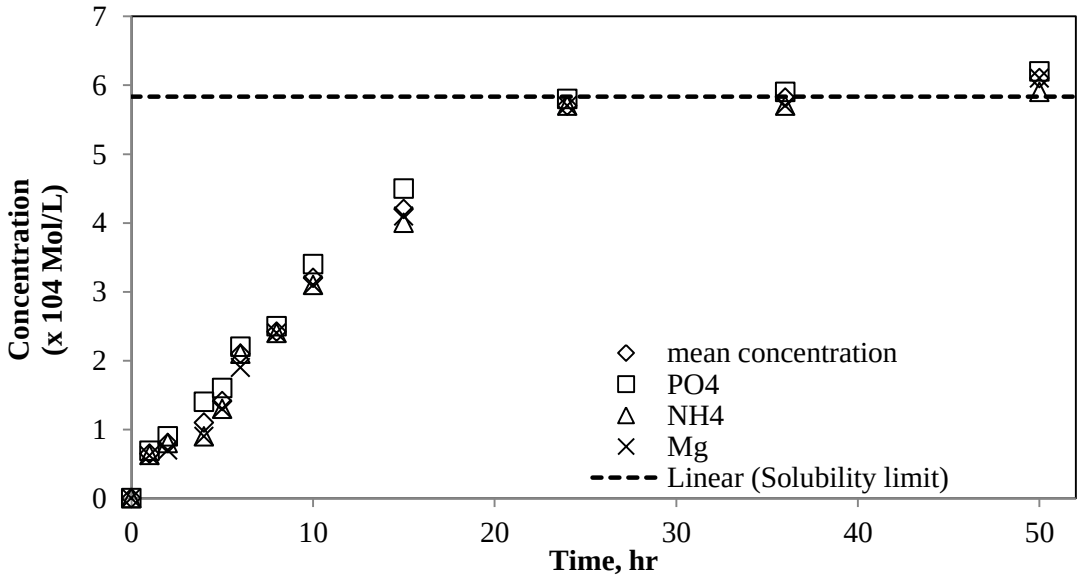

b

Figure 7.1 Ion concentration in deionized water during dissolution of struvite crystals at 25^{O}C, 120 rpm, loading mass of 1000 mg and crystal size of 24.3 μm (a) 60 min, (b) 50 h

7.4.2 Effect of Stirrer Speeds

The dissolution of struvite were carried out at stirring speeds of 120, 200, 300, 400, 500 and 800 rpm using deionized water for 60 minutes of dissolution time. The experiments were all conducted at 25^{O}C with average seed crystals size of 24.3 µm. The plotting data of Table D1.1 and D.22 in Appendix D are described in Figure 7.3. It can be observed from Figure 7.3 that increasing stirrer speeds consistently increases dissolution of constituent ions of struvite crystals up to 400 rpm. Figure 7.2 drawn for the mean of total concentration of Mg, PO_4 and NH_4, shows that dissolution rate increased with increasing stirrer speed up to 400 rpm, but the dissolution rate was relatively stable when the stirrer speed was in excess of 400 rpm. This is because of convective mass transfer and decrease in boundry layer thickness (L).

Figure 7.3 shows the dissolution rate mechanistic plot of Eq. (7.5) at different stirrer speed. The values of overall mass transfer coefficient (k_L) for crystal dissolution of struvite determined are presented in Table 7.1. Accordingly, the overall mass transfer coefficient increased from 1.6×10^{-5} to 5.4×10^{-5}m/s with increase in stirrer speeds from 120 to 400 rpm. The dissolution rate reached a stable point around 5.7×10^{-5} m/s when stirrer speed was up to 400 rpm. The obtained value of K_L from 1.6×10^{-5} to 6.0×10^{-5} m/s are in the standard range of values of liquid phase mass transfer coefficient in the range of 10^{-5} m/s (Dutta, 2007). The rapid increase in K_L values presented in Figure 7.3 for lower stirrer speed up to 400 rpm can be explained by mass transfer strongly influencing the dissolution. At higher than 400 rpm, the boundary layer became thinner and dissolution rate is controlled by surface integration.

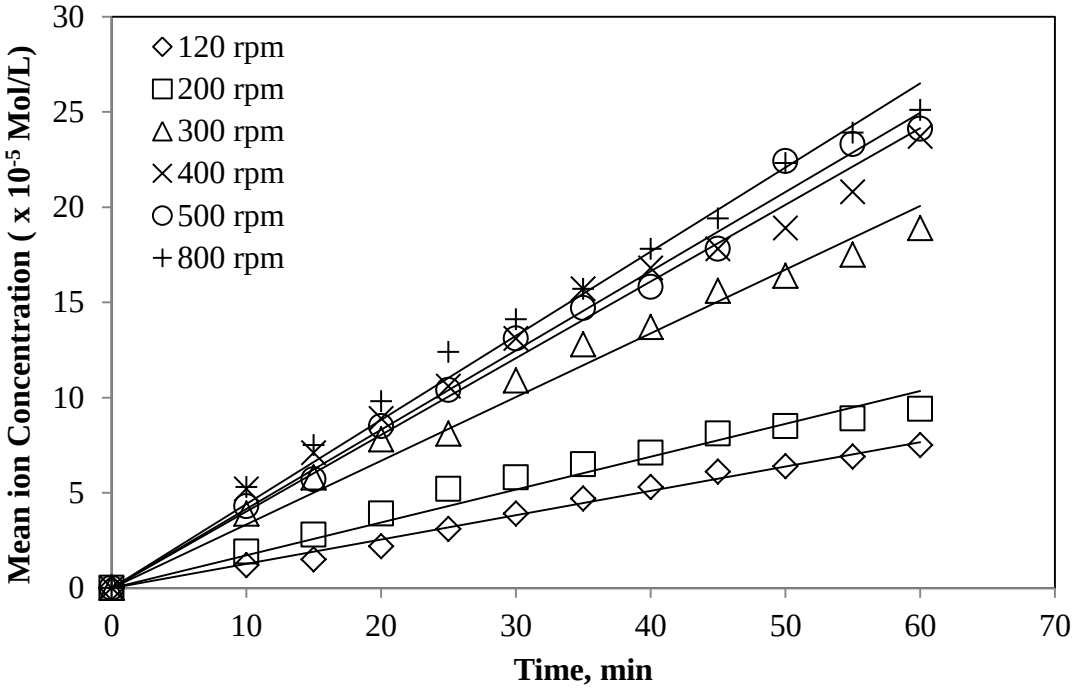

Figure 7.2 Concentration in deionized water during dissolution of different stirrer speeds at 25^{O}C, 1000 mg, and 24.3 μm

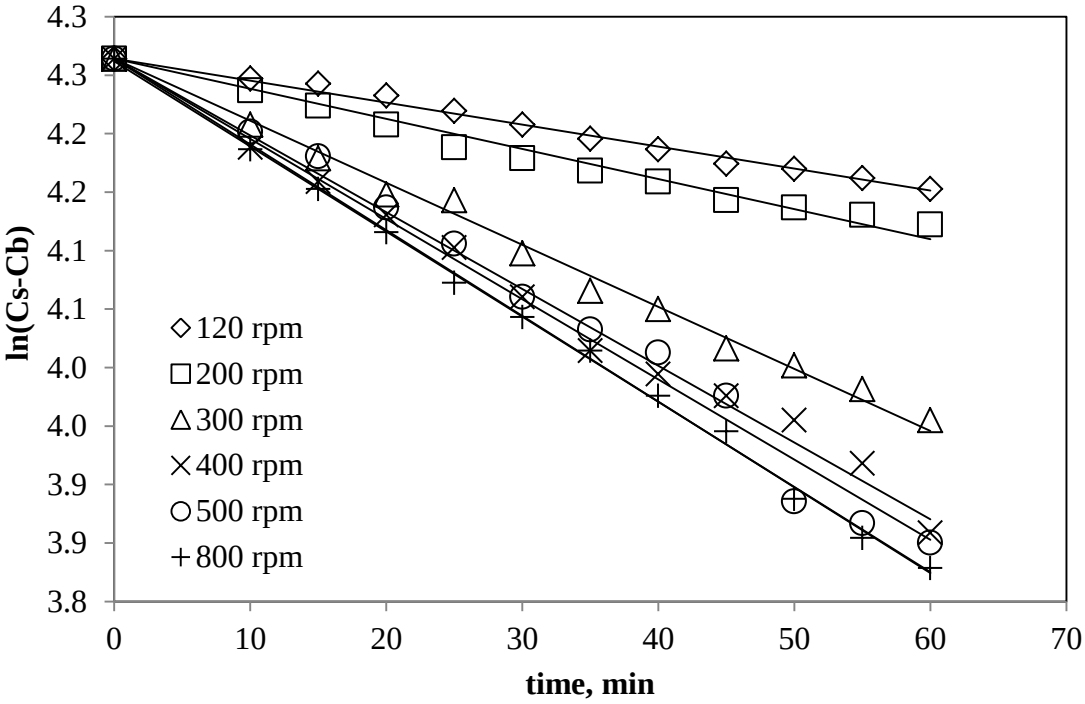

Figure 7.3 Agreement of experimental data with Eq. (7.5) model for different stirrer speed

Table 7.1 The overall mass transfer coefficient (K_L) for crystal dissolution of struvite on different stirrer speed at 25^{O}C

Stirrer Speed	$\boldsymbol{K_L \times 10^{-5}}$ (m/s)	R^2
120	1.6	0.99
200	2.4	0.99
300	4.4	0.98
400	5.4	0.98
500	5.6	0.97
600	5.8	0.99
800	6.0	0.98

The various theories of dissolution state that the stirring condition can significantly affect diffusion-controlled dissolution, because the thickness of the diffusion layer is inversely proportional to stirrer speed (Banakar, 1992). According to Masuda et al., (2006), the dissolution rate can be correlated with the stirring rate,

$$\boldsymbol{K_L = a(N)^b} \quad (7.6)$$

where N is the stirring rate, K_L is the dissolution rate constant, and a and b are constant. For b = 1, the dissolution process is diffusion-controlled. The interfacial-reaction-controlled is independent of stirring rate when b = 0. The plotting experimental data between K_L and N can clearly be seen from Figure 7.4. It can be seen in Figure 7.4 that the b value was 1.1 and 0.1 for range stirrer speeds of 120 – 400 rpm and over 400 rpm, respectively. It can be concluded that diffusion-controlled mechanism occurred at stirrer speeds of 120 - 400 rpm and changed to a surface integration-controlled mechanism at over 400 rpm.

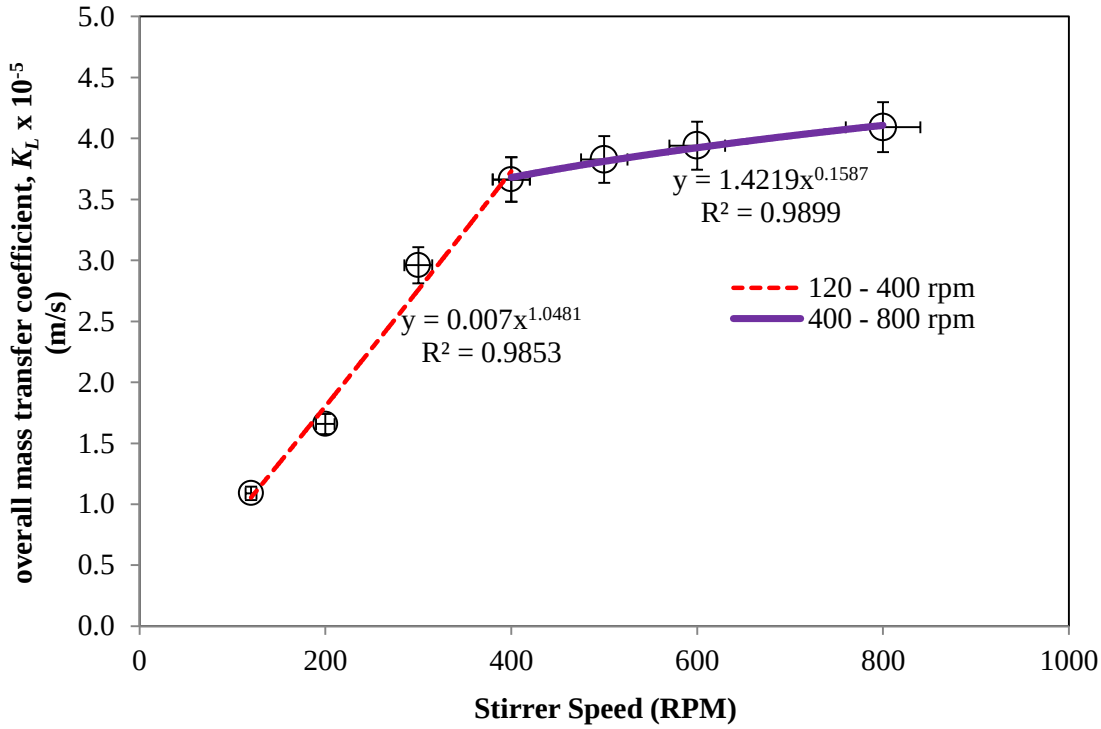

Figure 7.4 The relationship between the K_L value and stirrer speed with 5 % error bar

7.4.3 Temperature Effect

The dissolution rate of struvite in deionized water at different temperatures from 20 – 35^{O}C was investigated as a function of time at 200 and 500 rpm. The seed of struvite crystals added in crystallizer was 1000 mg with average crystals size of 24.3 µm. The plotting data of Table D1.3 in Appendix D are shown in Figure 7.5. The dissolution of struvite crystals at various temperatures showed that rate of dissolution increased as the temperature increased from 20^{O}C to 35^{O}C at 200 rpm (Figure 7.5). Increased temperature of solvent provides energy to the crystal to break the bonds holding the molecules in the solid. So, the dissolution rate increases with an increase in the temperature. Furthermore, the increasing dissolution rate causes more solvent molecules to interact with the solute molecules.

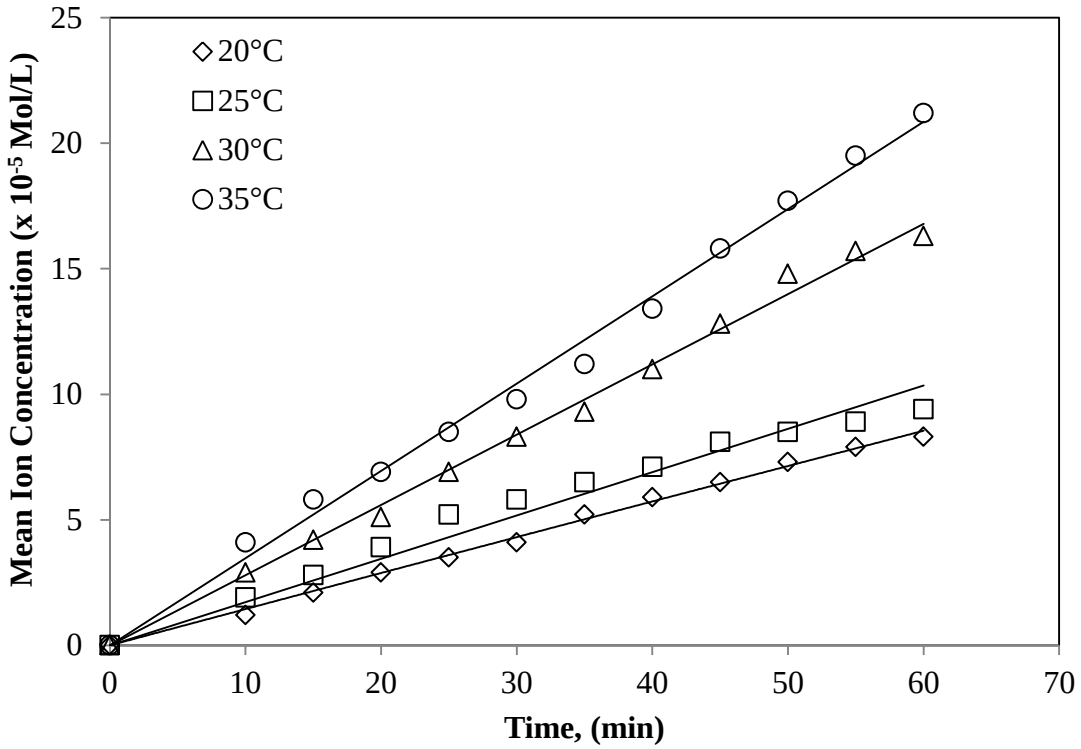

Figure 7.5 The dissolution of struvite at different temperatures at 200 rpm, loading mass of 1000 mg and crystal size of 24.3 μm.

Figure 7.6 shows the dissolution rate mechanistic plot of Eq. (7.5) at different temperature at 200 rpm. The fitted dissolution mechanistic various temperatures are presented in Table 7.2.

Table 7.2 The overall mass transfer coefficient (k_L) for crystal dissolution of struvite on various temperatures

Stirrer speed, RPM	Temperature, ^{O}C	$\boldsymbol{K_L \times 10^{-5}}$ (m/s)	R^2
200	20	2.3	0.98
	25	2.4	0.99
	30	2.9	0.98
	35	3.2	0.98
500	20	3.4	0.98
	25	5.6	0.98
	30	7.1	0.98
	35	9.6	0.97

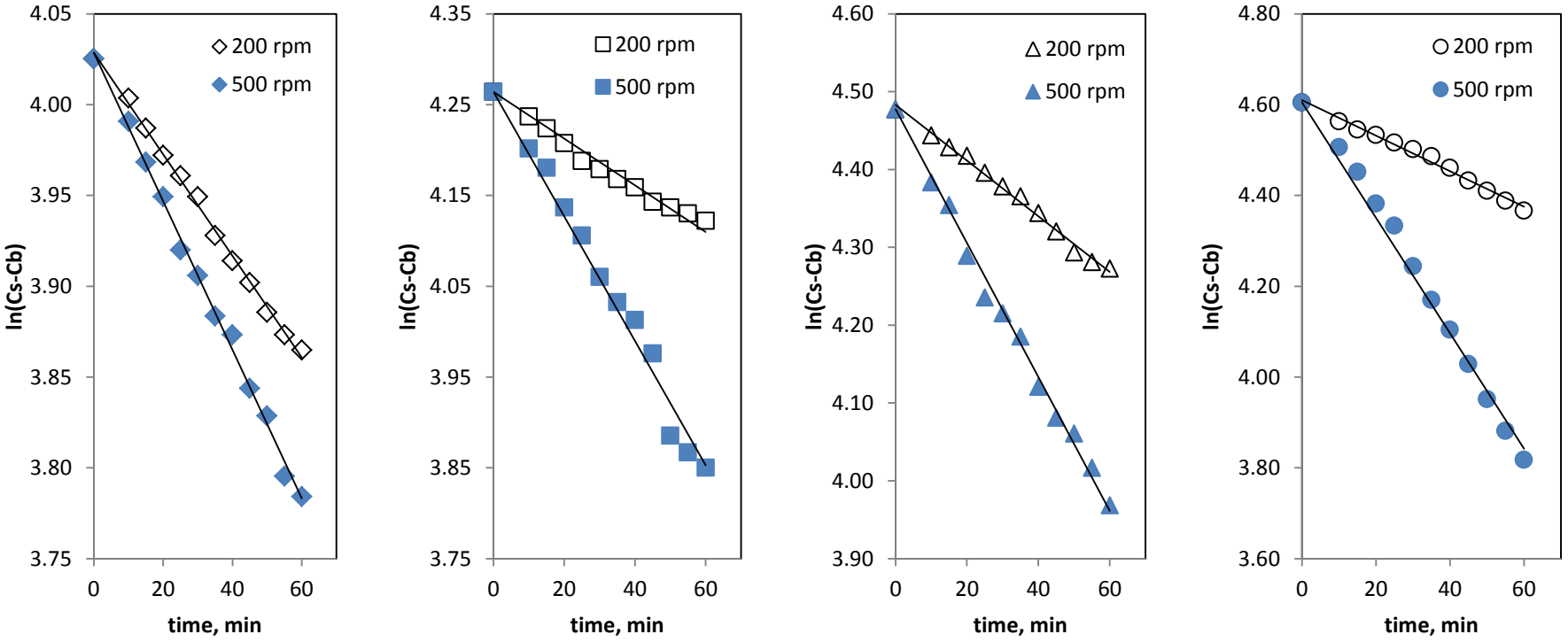

Figure 7.6 Agreement of experimental data with Eq. (7.5) model for different temperature at 200 rpm. a. 20^{O}C; b. 25^{O}C; c. 30^{O}C; d. 35^{O}C

The activation energy of dissolution process was determined from the Arrhenius equation:

$$\boldsymbol{K_L = k_0 \exp(-E/RT)} \quad (7.7)$$

$$\boldsymbol{\log K_L = \log k_0 - \frac{E}{2.3RT}} \quad (7.8)$$

where K_L is overall mass transfer coefficient, k_0 is a pre-exponential factor, E is activation energy, R is gas constant (8.314 J/K.mol) and T is temperature (K). A plot of the logarithm of dissolution rate at various temperatures against the reciprocal of the absolute temperature is shown in Figure 7.7. It can be seen that the dissolution rate, *k,* increased with increasing temperature at both stirrer speeds of 200 rpm and 500 rpm.

Typical values of activation energy indicate the dissolution mechanism. An activation energy value of between 10 and 25 kJ/mol indicates the dissolution to controlled by diffusion (Bavic-Ivancic et al., 2002, Demirkiran, 2009), while surface integration-controlled has activation energies value of above 40 kJ/mol (Bavic-Ivancic et al., 2002, Demirkiran, 2008, Demirkiran, 2009). According to Eq. 7.8, the slope of curve between *log k* versus *1000/T* should give a straight line whose slope equals to *–E/2.303R*. Figure 7.7 shows the Arrhenius plots for dissolution of struvite at two stirrer speeds in deionized water. The activation energies derived from these curves were found as 17.92 kJ/mol and 54.56 kJ/mol for the stirrer speed of 200 and 500 rpm, respectively. Babic-Ivancic et al., (2002) studied dissolution of struvite in water using high stirrer speeds found an activation energy of 44.8 and 37.6 kJ/mol for rod-like and dendrites crystals, respectively. These high values of present study (500 rpm) may be due to difference types of seed crystals. The value of the activation energy in the present study indicates that the mechanism of struvite dissolution is controlled by diffusion at 200 rpm. At 500 rpm, the mechanism was controlled by surface integration.

Figure 7.8 is a theoretical plot based on Eq. (7.8) describing the effect of temperature on dissolution rate of a surface integration-controlled mechanism with activation energy 54.56 kJ/mol and a diffusion-controlled mechanism with activation energy of 17.92 kJ/mol. The extrapolation data calculated by using both

activation energies were set arbitrarily so the crossing temperature would be around 11^{O}C. Temperature of 11^{O}C is a temperature transition when surface integration-controlled mechanism intercept with diffusion-controlled involved an increase in activation energy from 17.92 kJ/mol to 54.56 kJ/mol.

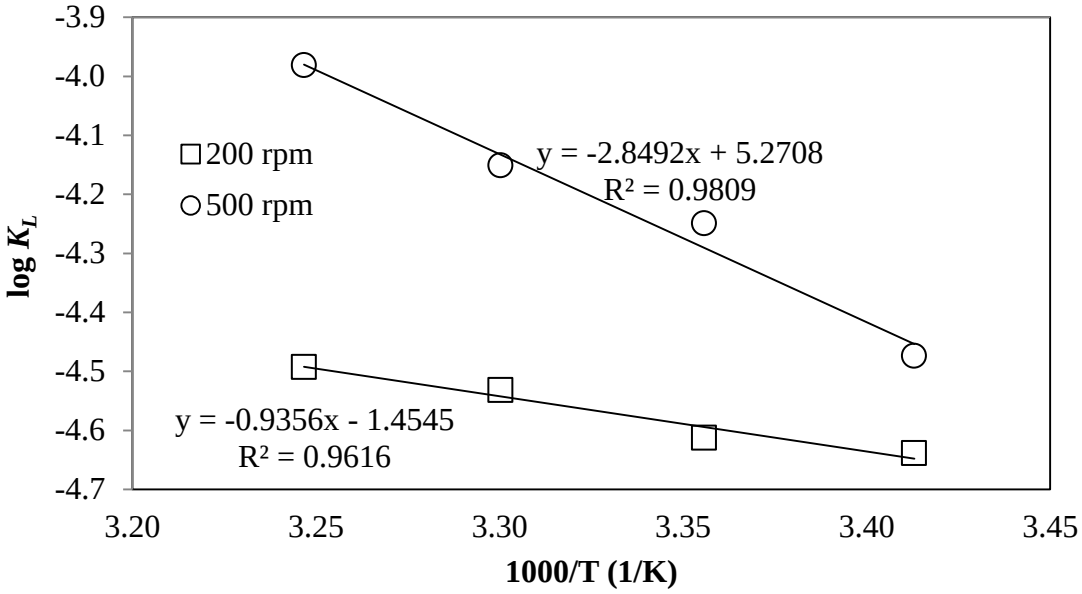

Figure 7.7 Arrhenius plot of struvite dissolution as a function of the reciprocal of the absolute temperature for 200 and 500 rpm and loading mass of 1000 mg and crystal size of 24.3 μm.

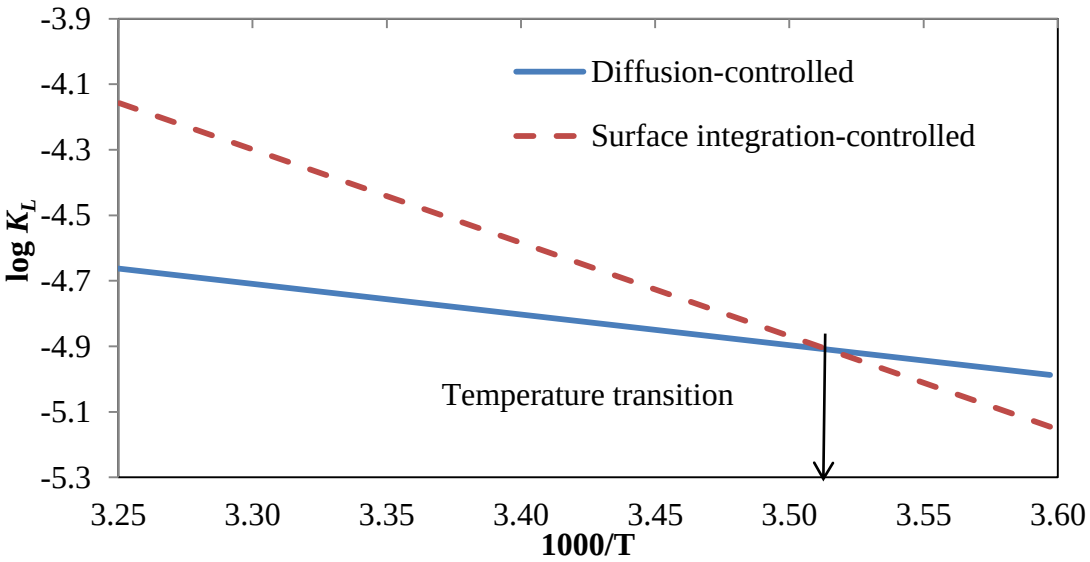

Figure 7.8 Arrhenius plots of two mechanisms

7.4.4 Effect of crystal sizes

Different crystal sizes were produced by seed crystals in different supersaturated solutions. By adjusting the concentrations of Mg^{2+}, PO_4^{3-} and NH_4^+ ion, seed struvite crystals grew to produce struvite crystals of different sizes were obtained. The crystal size distribution profiles of each crystal suspension are shown in Figure 7.9. The morphology of struvite crystal produced in different concentration of Mg^{2+}, PO_4^{3-} and NH_4^+ ion with low stirrer speed are shown in Figure 7.10. From the optical images, it was found that the crystals were the same shape, being needle-like in structure. The Fourier transform infrared spectroscopy (FTIR) was used to analyse potential changes in the inner structure of struvite crystals. According to FTIR spectra patterns, as shown in Figure 7.11 it was confirmed that no substantial crystalline change was found in the different crystal sizes. However, the minor differences in the relative intensities of their peaks might be attributed to differences in the degree of crystallinity of the samples. From these analyses of struvite crystals at different sizes, these crystals can be used for further study on effect of crystal size on dissolution of struvite. The absorptions occurring at 3426 and 3430 cm^{-1} are due to O-H and N-H stretching vibration. This also suggests the presence of water of hydration. The absorption occurring at around 2921.6 cm^{-1} is due to NH_4^+ ion (Chauhan et al., 2008). The weak bands appeared at 2341 cm^{-1} in the spectrum can be assigned due to H–O–H stretching vibrations of cluster of water molecules of crystallization. The absorption occurring around 1472.5 and 1434 cm^{-1} have been attributed to N-H bending vibration (Banks et al., 1975). The absorptions taking place at around 1055.5 and 975.5 cm^{-1} are due to ionic phosphate (Suguna et al., 2012). A medium absorption band at around 773 and 780 cm^{-1} indicates the wagging modes of vibration of the coordinated water and the metal–oxygen bond in the complex.

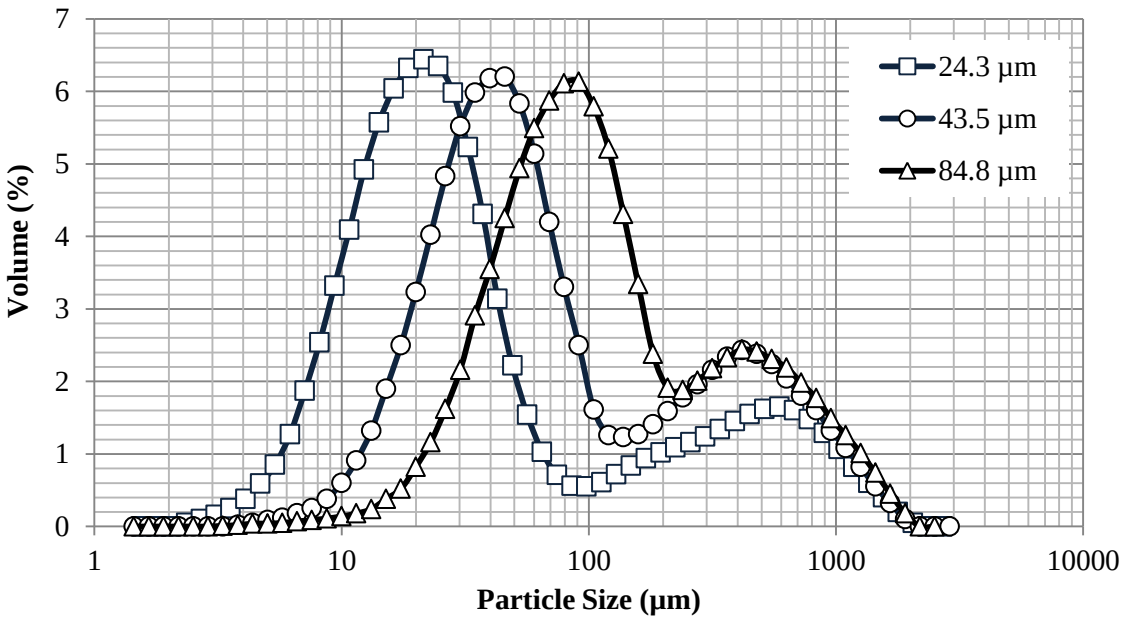

Figure 7.9 Crystals size distribution profile of struvite crystals used in the experiments

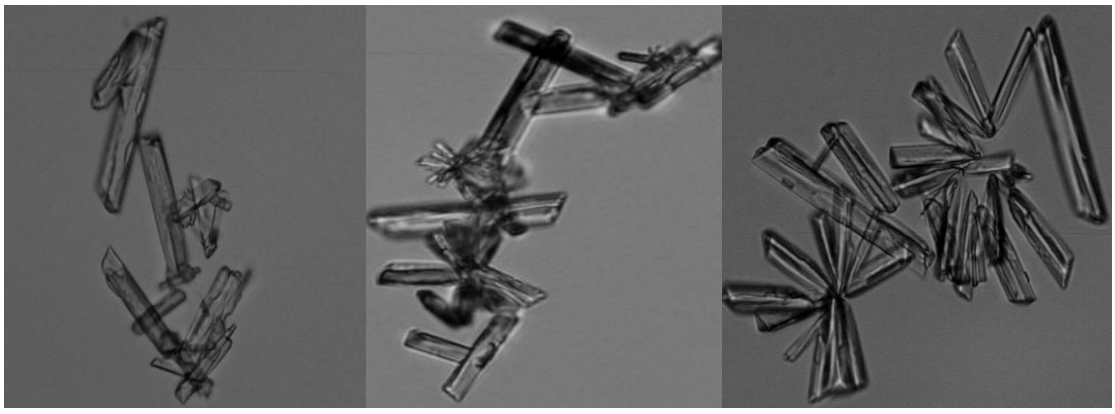

Figure 7.10 Optical images of struvite crystal: (a) 24.3µm, (b) 43.5 µm and (c) 84.8 µm

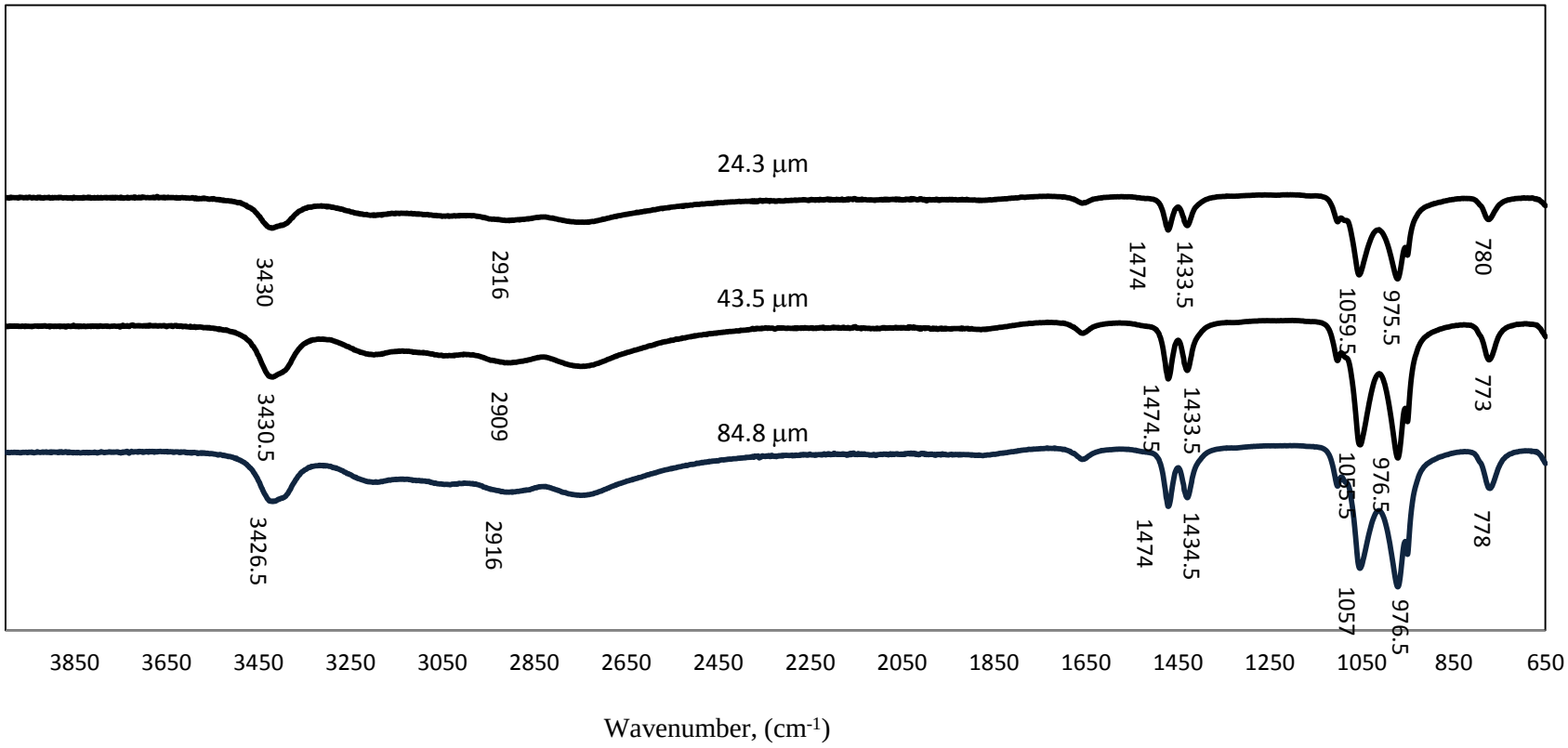

Figure 7.11 FTIR spectra of struvite crystals grown to different sizes

The effect of crystal size on dissolution rate was studied using average size fractions: 24.3, 43.5 and 84.8 μm. The temperature and stirring speed were kept constant at 25^{O}C and 200 rpm, respectively. The plotting data of Table D1.4 in Appendix D are presented in Figure 7.12. It can be seen that the dissolution of struvite improved at lower crystal sizes. Struvite concentration of 9.9×10^{-5} mMol/L resulted for crystal size of 24.3 μm dissolved in 1 hour. In the case of the largest crystal fraction of 84.8 μm, struvite concentration of only 7.1×10^{-5} mMol/L was attained an hour. This enhance dissolution rate for smaller crystals can be attributed to the tremendous increase in surface area of struvite crystals available for dissolution and the reduced diffusion layer thickness because smaller crystals have higher relative velocities while suspended in the crystallizer (Hintz and Johnson, 1989).

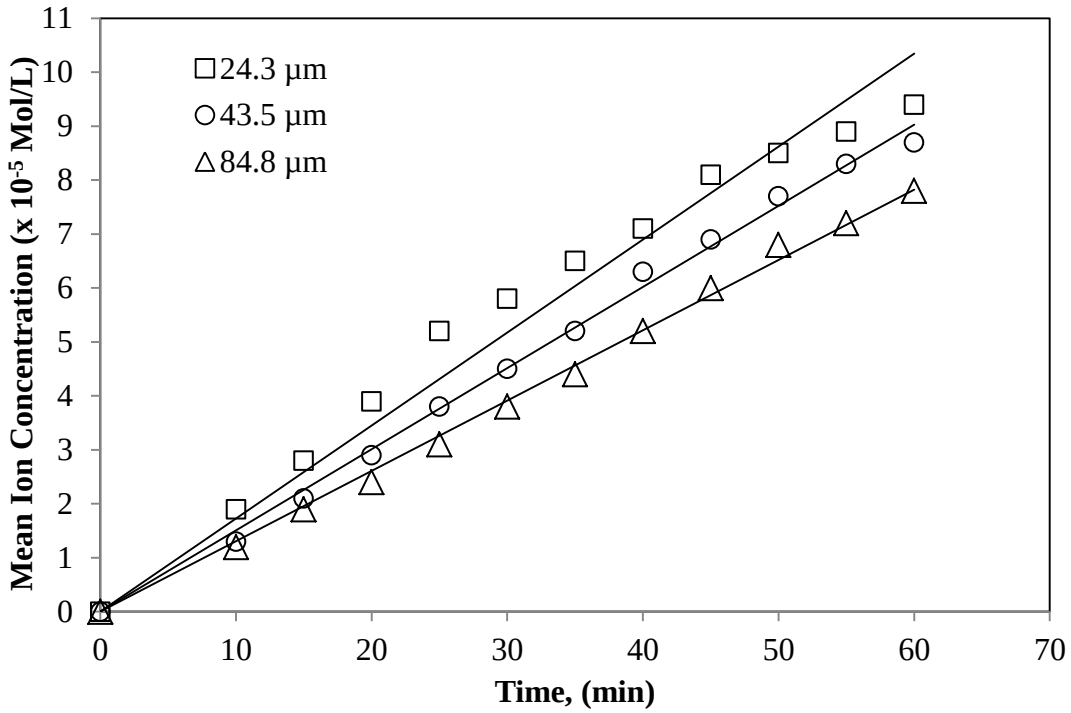

Figure 7.12 Effect of initial crystal size on dissolution of struvite crystals in deionized water at 25^{O}C, 200 rpm and 1000 mg mass loading.

In Figure 7.13, the solid curves show the calculated values obtained by fitting with Eq. (7.5), which trace well the experimental values. The fitting results can be seen in Table 7.3. In Table 7.3 values of volumetric mass transfer coefficient ($K_L a$) obtained by curve fitting Figure 7.13 are given as follows; 3.0×10^{-3},

2.3×10^{-3} and 2.0×10^{-3} for initial size of 24.3, 43.5, and 84.8 µm, respectively. The values of $K_L a$ decreased with an increase in crystal size, indicating that smaller crystals dissolve more rapidly than large crystals. However, the K_L values are almost the same within a margin of error of 2 %. This result indicates that the rate of dissolution of struvite from the crystal surface does not depend on the size of crystals, at least for those crystals with L in the range from 24 to 85 µm. Similarly results have been reported by Shan et al., (2002). The experimental study conducted by Bhuiyan et al., (2009) on crystal size of 0.5 – 2.0 mm and pH 6.05 the dissolution constant, 0.05×10^{-10} m/s. The highest value of K_L (2×10^{-7} m/s) due to different size of seed crystal and pH solution. Moreover, seed crystal size of present study was higher than Bhuiyan et al., (2009) study. Moreover, the K_L value of present study are in the standard range of K_L value of liquid phase reported by Dutta (2007)

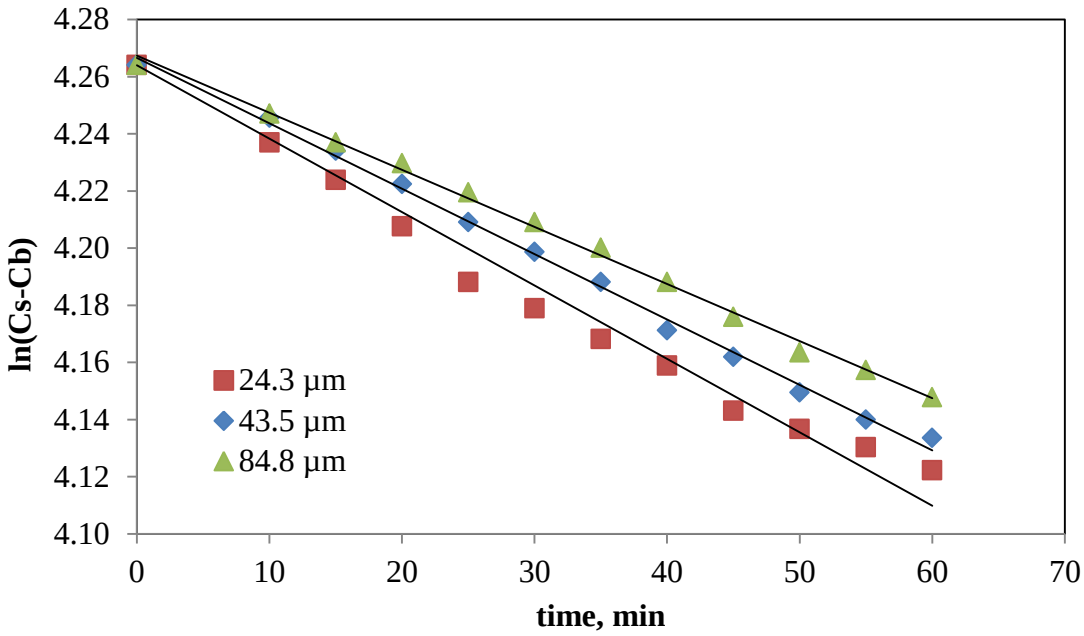

Figure 7.13 Agreement of experimental data with Eq. (7.5) model for different seed crystal size at 200 rpm and 25^{O}C

Table 7.3 The mass transfer parameters determined from dissolution of struvite crystals

Size, L	$K_L a \times 10^{-3}$	Specific Surface Area, m^2/g	$K_L \times 10^{-5}$,(m/s)
24.3	3.0	2.03	2.4
43.5	2.3	1.66	2.3
84.8	2.0	1.40	2.4

7.5 Summary

In this study, the dissolution rate of struvite seed crystals in deionized water was investigated under various process parameters.

- The effect of stirrer speeds, temperature and crystal size on the dissolution rate were examined and evaluated. When struvite crystals of a given size were dissolved under different stirrer speeds, the dissolution rate increased with an increase in the stirrer speed, but reached a maximum with a stirrer speed of 400 rpm.
- The stirrer speed of 400 rpm is the transition point at which the dissolution mechanism changes from diffusion control to surface integration controlling.
- The effect of temperature showed that dissolution rate increased with increase in temperature.
- The change in activation energies as a function of stirrer speeds showed that the activation energy increased with increase in stirrer speed. Temperature transition, 11^{O}C is a temperature transition when diffusion-controlled mechanism at 200 rpm intersects to chemical-reaction-controlled at 500 rpm involved an increase in activation energy from 17.92 kJ/mol to 54.56 kJ/mol.
- The smaller the crystals, the faster the dissolution rate. This was mainly due to higher surface area available for dissolution with smaller crystal sizes used. The overall dissolution mass transfer coefficient under different physico-chemical process parameters are obtained and are applicable for struvite crystallization design.

CHAPTER 8
CONCLUSIONS AND RECOMMENDATIONS

8.1 Introduction

The solids degradation in an anaerobic digestion of wastewater treatment plant releases magnesium, ammonium, and phosphate ions. Under certain conditions, these dissolved wastewater constituents can combine to form struvite. Accumulation of struvite on pipe walls and equipment surface associated with anaerobic digestion system and post digestion processes is a well-known problem that plagues the wastewater treatment (WWTP) industry. Primarily, as a problem to eliminate or inhibit struvite formation, struvite also offers itself as a fertilizer which encourages wastewater treatment companies to study its possible recovery. For those two reasons, it has become important to study the principles of solubility, nucleation, growth and dissolution of struvite crystals under various physico-chemical parameters.

8.2 Overall Conclusion

8.2.1 Solubility Studies (Chapter 4)

Solubility products of struvite (*Ksp*) were determined by using activity coefficient model calculated based on the Debye-Huckel theory. The *Ksp* values decreased with increase in initial solution pH from 3 to 9 with minimum *Ksp* value 1.91×10^{-13} at initial pH 9 and temperature 25^{O}C. *Ksp* values increased for pH > 9. The effect of temperature on *Ksp* value in deionized water (pH 7) showed that the solubility increased with increasing temperature from 20^{O}C to 35^{O}C (*Ksp* values 1.69×10^{-13} to 7.99×10^{-13}, respectively) and then it decreases from 7.99×10^{-13} to 2.83×10^{-13} with temperature range 35 – 50^{O}C. Based on the K_{SP} value, the endothermic energy was 95.1 kJ/mol in range temperatures of 10 – 35^{O}C and exothermic energy was 76.5 kJ/mol in range temperature 35 – 50^{O}C.

The effect of common-ion on struvite solubility was conducted at various concentrations of NaCl, KCl and $CaCl_2$ within a range of 0.25 – 1.5 mM at 25^{O}C. The solubility of struvite in $CaCl_2$ solution is the highest followed by NaCl and

KCl, respectively. The Gibbs free energy obtained for the salting-in effect showed a ΔG decrease in the following order: KCl > NaCl > $CaCl_2$.

8.2.2 Spontaneous nucleation studies (Chapter 5)

Spontaneous nucleation was identified based on changing solution pH between initial solution pH and the first observed pH change. The effect of the initial solution pH showed that induction time decreased with increase in initial solution pH from 8 to 9. The rate of nucleation increased with increase in supersaturation, it is due to a higher driving force for mass transfer from liquid to crystal phase.

The effect of temperature showed that the spontaneous nucleation rate increased with increase in temperature. The increasing nucleation rate was due to decreasing interfacial energy of crystals. The various calculated nucleation kinetic parameters resulted in decreasing nucleation constant, *K*, and order, *n* with increase in temperature. Activation energy calculated from experimental data was 30.1 $kJ.mol^{-1}$ and 24.9 $kJ.mol^{-1}$ at pH 8 and 8.5, respectively.

Mechanism of nucleation and thermodynamic parameters was predicted based on classical nucleation theory. The data resulted in two distinct linear parts showing the dependence of nucleation on different nucleation mechanisms such as region I (homogeneous nucleation mechanism) for high supersaturations and region II (heterogeneous nucleation mechanism) for low supersaturation.

Effect of Cl^- ion in a solution by adding sodium chloride (NaCl) or potassium chloride (KCl) may affect the induction time. The presence of excess chloride ions in solution has a strong retarding effect on induction time, Na^+ ions having a more significant inhibition than K^+. The average activation energies are 64.5 and 51.7 $kJ.mol^{-1}$ for NaCl and KCl addition, respectively.

The crystal morphologies for pH 8 and 8.5 without excess Cl^- ion showed similar needle-like crystal shapes and dimensions. The crystals in the presence of NaCl and KCl at pH 8 were similarly needle-like shape.

8.2.3 Growth of struvite crystal studies (Chapter 6)

The supersaturation used in the study was kept in the metastable zone. The growth of struvite crystals was conducted in a stirred seeded batch crystallizer in which

the effects of solution pH, temperature, impurities, crystal size and hydrodynamic condition on the kinetics of struvite crystal growth were investigated. All experimental studies showed that the kinetic rate of the decay of supersaturation followed first order kinetics. The growth rate of struvite crystals increased with increase in seed loading (40 – 100 mg), solution pH (8 – 9), temperature (20 – 35^{O}C), stirrer speed (50 – 120 rpm) and NaCl addition (50 – 200 ppm) but decreases with crystal size (24.3 – 84.8 μm). From the growth rate order data, these values indicate that crystal growth of struvite is predominantly controlled by diffusion.

8.2.4 Dissolution of struvite crystal studies (Chapter 7)

To determine the mechanisms of dissolution process in batch crystallizer system, the dissolution kinetics of struvite was studied at different stirrer speeds, temperatures and crystal loadings. Increasing stirrer speeds consistently increases dissolution of constituent ions of struvite crystals up to 400 rpm and the dissolution rate remained relatively constant above 400 rpm. Diffusion-controlled mechanism occurred at stirrer speeds of 120 - 400 rpm and changed to a surface integration-controlled mechanism at over 400 rpm. Furthermore, the activation energies for both stirrer speeds 200 and 500 rpm indicate that the mechanism of struvite dissolution is controlled by diffusion at 200 rpm and surface integration at 500 rpm with activation energies of 17.92 kJ/mol to 54.56 kJ/mol, respectively.

8.3 Recommendations

As is the nature of research, the present study generated some research questions that could not be addressed within the time allocated or were beyond the scope of this research work. The following recommendations are made for future research and include:

8.3.1 Solubility of struvite crystals

- From experimental solubility data of present study, it could be recommended to be simulated by using Non-random two liquid (NRTL) model. The NRTL model could be used for predicting the activity coefficient of electrolytes in

aqueous system. And this model allows the minimisation of the required experimental work and significantly facilitates interpolation and extrapolation in the range of operating conditions.

- Analysed product crystals by using XRD are require to know characterise the crystallinity. At initial solution pH 11 showed that the shape of product crystal was hexagonal form. According to reaction (Eq. 4.12) shows that initial solution pH 11 may produces brucite ($Mg(OH)_2$). So XRD analysis is needed to answer this question.
- The present study showed that effect of common-ion of Cl^- derived from NaCl, KCl and $CaCl_2$ can increase solubility of struvite. On the other hand, the present common-ions present in water is not only Cl^- but also the others, such as Fe, Mg, etc. So it could be recommended on the future work. Moreover, the combination common-ions mixtures in water are important to studied in understanding ionic equilibrium, ion-solvent and ion-ion interaction in natural waters. Accurate and reliable data on physicochemical properties of aqueous salt systems are necessary for many industrial processes where these systems are used as feed. Further work is recommended for solubility of struvite study with using multicomponent electrolyte mixtures in water.

8.3.2 Spontaneous nucleation of struvite crystals

- Spontaneous nucleation of struvite crystals was influenced by solution pH, temperature and impurities. The raw materials of present study used synthetic solution. Further work is recommended to investigate spontaneous nucleation of struvite by using real wastewater from a wastewater treatment plant.

8.3.3 Growth of struvite crystals

- The growth of struvite crystal study was attempted to explore the effect of solution pH, temperature, impurities, crystal size and hydrodynamic condition on the struvite crystallisation especially on the kinetics of struvite crystal growth. All experimental studies showed that crystal growth of struvite is predominantly controlled by diffusion based on the first order growth rate results obtained. For further investigation, the morphology of the struvite

crystals grown is also observed by in-situ optical microscopy, scanning electron microscopy (SEM) and atomic force microscopy (AFM) to elucidate the crystal growth mechanism to verify if crystal growth is diffusion or surface integration controlled.

- The effect of other impurities present in the waste water such as calcium, potassium and others in a stirred batch crystallizer at different condition (such as temperature, supersaturation and solution pH) should be investigated.

8.3.4 Dissolution of struvite crystals

- Dissolution of struvite crystals has been investigated by using water at different conditions, such as stirrer speed and temperature. Previous dissolution study used hydrochloric acid (HCl) to investigate dissolution of struvite (Bhuiyan et al., 2009). On the other hand, HCl has a high corrosive effect. Further work is recommended by using various ammonium salts of inorganic acid (such as ammonium acetate) or organic acids (acetic acid and citric acid).

References

_____. 2006. Wastewater treatment – onsite domestic systems, Department of Water Government of Western Australia. Available: http://www.water.wa.gov.au/PublicationStore/first/93698.pdf.

AAGE, H. K., ANDERSEN, B. L., BLOM, A. & JENSEN, I. 1997. The solubility of struvite. *Journal of Radio Analytical and Nuclear Chemistry,* 223**,** 213 - 215.

ABBONA, F., LUNDAGER, M. H. & BOISTELLE, R. 1982. Crystallization of two magnesium phosphates, struvite and newberyite: Effects of pH and concentration. *Journal of Crystal Growth,* 57**,** 6 - 14.

ABONNA, F. & BOISTELLE, R. 1979. Growth morphology and crystal habit of structure crystals (MgNH4PO4 -6H20). *Journal of Crystal Growth,* 46**,** 339 - 354.

ADNAN, A., DASTUR, M., MAVINIC, D. S. & KOCH, F. A. 2004. Preliminary investigation into factors affecting controlled struvite crystallization at the bench scale. *Journal of Environmental Engineering and Science,* 3**,** 195 - 202.

AKRAP, M., KUZMANIĆ, N. & PRLIĆ-KARDUM, J. 2010. Effect of mixing on the crystal size distribution of borax decahydrate in a batch cooling crystallizer. *Journal of Crystal Growth,* 312**,** 3603 - 3608.

ALI, M. I., SCHNEIDER, P. A. & HUDSON, N. 2005. Thermodynamic and Solution Chemistry of Struvite. *Journal of The indian Institute of Science* 85**,** 141 - 149.

AMRAM, K. & GANOR, J. 2005. The combined effect of pH and temperature on smectite dissolution rate under acidic conditions. *Geochimica et Cosmochimica Acta,* 69**,** 2535 - 2546.

ANDRADE, A. & SCHUILING, R. D. 2001. The chemistry of struvite crystallization. *Mineral Journal (Ukraine),* 23**,** 37 - 46.

APPELO, C. A. J. & POSTMA, D. 1999. *Geochemistry, Groundwater and Pollution,* A. A. Balkema, Leiden, The Netherlands.

ASAKURA, H., SELENGUT, J. D., JOHNSON, W. H. O. & DRETLER, S. P. 1998. The Effect Of Calprotectin On The Nucleation And Growth Of Struvite Crystals As Assayed By Light Microscopy In Real-Time. *The Journal of Urology,* 159**,** 1384 - 1389.

ASSELBERGS, C. J. & DE JONG, E. J. 1972. *Secondary Nucleation, Discussion of the Working Party on Crystallization,* Baekelo, European Federation of Chemical Engineering.

BABIN, R. E. 2005. *Assesment of factors influencing water reuse opportunities in Western Australia.* Bachelor of Engineering (Environmental), University of Southern Queensland.

BANAKAR, U. V. 1992. *Pharmaceutical Dissolution Testing,* New York, Marcel Dekker, Inc.

BANKS, E., CHIANELLI, R. & KORENSTEIN, R. 1975. Crystal chemistry of struvite analogs of the type $MgMPO_4.6H_2O$ (M+=potassium(1+), rubidium(1+), cesium (1+), thallium(1+), ammonium(1+). *Inorganic Chemistry,* 14**,** 1634-1639.

BARRETT, P. & GLENNON, B. 2002. Characterizing the Metastable Zone Width and Solubility Curve Using Lasentec FBRM and PVM. *Chemical Engineering Research and Design,* 80**,** 799 - 805.

BATTISTONI, P., ANGELIS, A. D., PAVAN, P., PRISCIANDARO, M. & CECCHI, F. 2001. Phosphorus removal from a real anaerobic supernatant by struvite crystallization. *Water Research,* 35**,** 2167 - 2178.

BATTISTONI, P., BOCCADORO, R., FATONE, F. & PAVAN, P. 2005. Auto-nucleation and crystal growth of struvite in a demonstrative fluidised bed reactor (FBR). *Environmental Technology,* 26**,** 975 - 982.

BAVIC-IVANCIC, V., JASMINKA, K., DAMIR, K. & LJERKA, B. 2002. Precipitation diagram of struvite and dissolution kinetics of different struvite morphologies. *Croatica Chemica Acta,* 75**,** 89 - 106.

BEN MOUSSA, S., TLILI, M. M., BATIS, N. & AMOR, M. B. 2011. Influence of tempereature on Struvite precipitation by CO2-deagassing method. *Crystal Research and Technology,* 46**,** 255 - 260.

BHUIYAN, M. I. H., MAVINIC, D. S. & BECKIE, R. D. 2007. A Solubility and Thermodynamic Study of Struvite. *Environmental Technology,* 28**,** 1015 – 1026.

BHUIYAN, M. I. H., MAVINIC, D. S. & BECKIE, R. D. 2008. Nucleation and growth kinetic of struvite in a fluidized bed reactor. *Journal of Crystal Growth,* 310**,** 1187 - 1194.

BHUIYAN, M. I. H., MAVINIC, D. S. & BECKIE, R. D. 2009. Dissolution kinetics of struvite pellets grown in a pilot-scale crystallizer. *Canadian Journal of Civil Engineering,* 36**,** 550 - 558.

BLESA, M. A., MORANDO, P. J. & REGAZZONI, A. E. 1994. *Chemical Dissolution of Metal Oxides,* Boca Raton, CRC Press.

BOISTELLE, R. & ABBONA, F. 1985. Nucleation of struvite ($MgNH_4PO_4 \cdot 6H_2O$) single crystals and aggregates. *Crystal Research and Technology,* 20**,** 133 - 140.

BOOKER, N. A., PRIESTLEY, A. J. & FRASER, I. H. 1999. Struvite formation in wastewater treatment plants: Opportunities for nutrient recovery. *Environmental Technology,* 20**,** 777 - 782.

BORGERDING, J. 1972. Phosphate deposit in digestion system. *Journal of the Water Pollution Control Federation,* 44**,** 813 - 819.

BOUROPOULOS, C., VAGENAS, N., KLEPETSANIS, P., STAVROPOULOS, N. & BOUROPOULOS, N. 2004. Growth of calcium oxalate monohydrate on uric acid crystals at sustained supersaturation. *Crystal Research and Technology,* 39**,** 699 - 704.

BOUROPOULOS, N. C. & KOUTSOUKOS, P. G. 2000. Spontaneous precipitation of struvite from aqueous solutions. *Journal of Crystal Growth,* 213**,** 381 - 388

BRIDGER, G. L., SALUTSKY, M. L. & STAROSTKA, R. W. 1962. Metal Ammonium Phosphates as Fertilizers. *Journal of Agricultural and Food Chemistry,* 10**,** 181 - 188.

BUCHANAN, J., MOTE, C. & ROBINSON, R. 1994. Thermodynamics of struvite formation. *Trans. ASAE,* 37**,** 617 - 621.

BURNS, J. R. & FINLAYSON, B. 1982. Solubility product of magnesium ammonium phosphate hexahydrate at various temperatures. *The Journal of Urology,* 128**,** 426 - 428.

CAPDEVIELLE, A., SÝKOROVÁ, E., BISCANS, B., BÉLINE, F. & DAUMER, M. L. 2013. Optimization of struvite precipitation in synthetic biologically treated swine wastewater--determination of the optimal process parameters. *Journal of Hazardous Materials,* 244 - 245**,** 357 - 369.

CECCHI, F., BATTISTONI, P. & BOCCADORO, R. 2003. Phosphate crystallization process for P recovery applied at Treviso municipal wastewater treatment plant (Italy). Available: http://www.nhm.ac.uk/mineralogy/phos/Treviso2003 pdf [Accessed January 14, 2010].

CELEN, I. & TÜRKER, M. 2001. Recovery of ammonia as struvite from anaerobic digester effluents. *Environmental Technology*, 22**,** 1263 - 1272.

CHANG, M. C. & TAI, C. Y. 2010. Effect of the magnetic field on the growth rate of aragonite and the precipitation of CaCO3 *Chemical Engineering Journal,* 164**,** 1 - 9.

CHAUHAN, C. K., JOSEPH, K. C., PAREKH, B. B. & JOSHI, M. J. 2008. Growth and characterization of struvite crystals. *Indian Journal of Pure & Applied Physics,* 46**,** 507 - 512.

CHENG, W. & LI, Z. 2010. Nucleation kinetics of nesquehonite ($MgCO_3$. $3H_2O$) in the $MgCl_2$ - Na_2CO_3 system. *Journal of Crystal Growth,* 312**,** 1563 - 1571.

CHIEN, W. C., TAI, C. Y. & HSU, J. P. 1999. The induction period of the $CaCl_2$–Na_2CO_3 system: Theory and experiment. *Journal of Chemical Physics* 111**,** 2657 - 2664.

COUPER, J. R., PENNEY, W. R., FAIR, J. R. & WALAS, S. M. 2005. *Chemical Process Equipment: Selection and Design*, Gulf Professional Publishing.

DE JONG, E. 1984. Industrial Crystallization 84. *9th Symposium on Industrial Crystallization.* The Hague, The Netherland.

DE YOREO, J. J., REK, Z. U., ZAITSEVA, N. P. & WOODS, B. W. 1996. Sources of optical distortion in rapidly grown crystals of KH_2PO_4. *Journal of Crystal Growth,* 166**,** 291 - 297.

DEGAN, A. & KOSEC, M. 2000. Effect of pH and Impurities on the Surface Charge of Zinc Oxide in Aquoeous Solution. *Journal of the European Ceramic Society,* 20**,** 667 - 673.

DEMIRKIRAN, N. 2008. A study on dissolution of ulexite in ammonium acetate solutions. *Chemical Engineering Journal,* 141**,** 180 - 186.

DEMIRKIRAN, N. 2009. Dissolution kinetics of ulexite in ammonium nitrate solutions. *Hydrometallurgy,* 95**,** 198 - 202.

DENK JR, E. G. & BOTSARIS, G. D. 1972. Fundamental Studies in Secondary Nucleation from Solution. *Journal of Crystal Growth,* 13**,** 493 - 499.

DOYLE, J. D., OLDRING, K., CHURCHLEY, J. & PARSONS, S. A. 2002. Struvite formation and the fouling propensity of different materials. *Water Research,* 36**,** 3971–3978.

DOYLE, J. D., OLDRING, K., CHURCHLEY, J., PRICE, C. & PARSONS, S. A. 2003. Chemical control of struvite precipitation. *Journal of Environmental Engineering - ASCE,* 129**,** 419 - 426.

DOYLE, J. D. & PARSONS, S. A. 2002. Struvite formation, control and recovery. *Water Research,* 36**,** 3925 - 3940

DURRANT, A. E., SCRIMSHAW, M. D., STRATFUL, I. & LESTER, J. N. 1999. Review of the Feasibility of Recovering Phosphate from Wastewater for Use as a Raw Material by the Phosphate Industry. *Environmental Technology,* 20**,** 749 - 758.

DUTTA, B. K. 2007. *Principles Of Mass Transfer And Separation Processes,* New Delhi, PHI Learning Pvt. Ltd.

EHRLICH, H., KOUTSOUKOS, P. G., DEMADIS, K. D. & POKROVSKY, O. S. 2009. Principles of demineralization: Modern strategies for the isolation of organic frameworks: Part II. Decalcification. *Micron,* 40**,** 169 - 193.

ELWORTHY, P. H., FLORENCE, A. T. & MACFARLANE, C. B. 1968. *Solubilization by surface-active agents and its applications in chemistry and the biological sciences* London, Chapman & Hall.

FAURE, G. 1991. *Principles and Applications of Inorganic Geochemistry,* New York, Macmillan Publishing company.

FEDOROČKOVÁ, A. & RASCHMAN, P. 2008. Effects of pH and acid anions on the dissolution kinetics of MgO. *Chemical Engineering Journal,* 143**,** 265 - 272.

FRANK, F. C. 1949. The influence of dislocations on crystal growth. *Discussions of the Faraday Society,* 5**,** 48 - 54.

FRANK, F. C. 1958. Kinematic theory of crystal growth and dissolution processes. *In Doremus, Roberts and Turnbull***,** 411 - 420.

FRAWLEY, P. J., MITCHELL, N. A., O'CIARDHA, C. T. & HUTTON, K. W. 2012. The effects of supersaturation, temperature, agitation and seed surface area on the secondary nucleation of paracetamol in ethanol solutions. *Chemical Engineering Science* 75 183 - 197.

GALBRAITH, S. C. & SCHNEIDER, P. A. 2009. A review of struvite nucleation studies. *International Conference on Nutrient Recovery from Wastewater Streams.* Vancouver, Canada.

GARSIDE, J., BREČEVIĆ, L. & MULLIN, J. W. 1982. The effect of temperature on the precipitation of calcium oxalate. *Journal of Crystal Growth,* 57**,** 233 - 240.

GIBBS, J. 1948. *The Collected Works. Vol.1. Thermodynamics,* England, Yale University Press.

GIESEN, A. 1999. Crystallization process enables environmental friendly phosphate removal at low cost. *Environmental Technology,* 20**,** 769 - 775.

GIULIETTI, M., SECKLER, M. M., DERENZO, S., RÉ, M. I. & CEKINSKI, E. 2001. Industrial crystallization and precipitation from solution : state of the technique. *Brazilian Journal of Chemical Engineering,* 18**,** 423 - 440.

HAFNER, B. 2013. *Scanning Electron Microscopy (SEM)* [Online]. Available: http://www.microscopy.ethz.ch/sem.htm [Accessed May, 17 2013].

HANSEN, F. K. & UGELSTAD, J. 1978. Particle nucleation in emulsion polymerization. I. A theory for homogeneous nucleation. *Journal of Polymer Science,* 16**,** 1953 - 1979.

HARTEL, R. W. 2001. *Crystallization in Foods,* Maryland, Springer.

HAUSMANNS, S., LAUFENBERG, G. & KUNZ, B. 1996. Rejection of acetic acid and its improvement by combination with organic acids in dilute solutions using reverse osmosis. *Desalination,* 104**,** 95 - 98.

HINTZ, R. J. & JOHNSON, K. C. 1989. The effect of particle size distribution on dissolution rate and oral absorption. *International Journal of Pharmaceutics,* 51**,** 9 - 17.

HUANG, D. C., LIU, W., ZHAO, S. K., SHI, Y. Q., WANG, Z. X. & SUN, Y. M. 2010. Quantitative design of seed load for solution cooling crystallization based on kinetic analysis. *Chemical Engineering Journal,* 156**,** 360 - 365.

HUTNIK, N., KOZIK, A., MAZIENCZUK, A., PIOTROWSKI, K., WIERZBOWSKA, B. & MATYNIA, A. 2013. Phosphates (V) recovery from phosphorus mineral fertilizers industry wastewater by continuous struvite reaction crystallization process. *Water Research,* 47**,** 3635 - 3643.

JANCIC, S. J. & GROOTSCHOLTEN, P. A. M. 1984. *Inductrial Crystallization,* Holland, Delft University Press.

JONES, A. G. 2002. *Crystallization process system,* Oxford, Butterworth-Heinemann.

JUDGE, R. A., JACOBS, R. S., FRAZIER, T., SNELL, E. H. & PUSEY, M. L. 1999. The effect of temperature and solution pH on the nucleation of tetragonal lysozyme crystals. *Biophysical Journal,* 77**,** 1585 - 1593

KABDASLI, I., PARSONS, S. A. & TÜNAY, O. 2006. Effect of Major Ions on Induction Time of Struvite Precipitation. *Croatica Chemica Acta,* 79**,** 234-251.

KAWASHIMA, Y. 2006. Solubility and Dissolution Rate. *In:* MASUDA, H., HIGASHITANI, K. & YOSHIDA, H. (eds.) *Powder Technology Handbook.* Third ed. Boca Raton: CRC Press.

KELLER, K. W. 1986. Hill formation by two-dimensional nucleation as one mode of crystal growth. *Journal of Crystal Growth,* 78**,** 509 - 518.

KIM, D., KIM, J., RYU, H. D. & LEE, S. I. 2009. Effect of mixing on spontaneous struvite precipitation from semiconductor wastewater. *Bioresource Technology,* 100**,** 74 - 78.

KIM, K. J. & RYU, S. K. 1997. Nucleation of thiourea adduct crystal with cyclohexane-methylcyclopentane. *Chemical Engineering Communications,* 159**,** 51 - 66.

KOFINA, A. N. & KOUTSOUKOS, P. G. 2005. Spontaneous precipitation of struvite from synthetic wastewater solutions. *Crystal Gorwth and Design,* 5**,** 489 - 496.

KORALEWSKA, J., PIOTROWSKI, K., WIERZBOWSKA, B. & MATYNIA, A. 2007. Nucleation and Crystal Growth Rates of Struvite in DTM Type Crystallizer with a Jet-Pump of Descending Suspension Flow in a Mixing Chamber. *American Journal of Agricultural and Biological Sciences,* 2**,** 260 - 266.

KORALEWSKA, J., PIOTROWSKI, K., WIERZBOWSKA, B. & MATYNIA, A. 2009. Kinetics of reaction-crystallization of struvite in the continuous draft tube magma type crystallizer - influence of different internal hydrodynamics. *Chinese Journal of Chemical Engineering,* 17**,** 330 - 339.

KOSSEL, W. 1934. Zur energetik von oberflachenvorgangen. *Annalen der Physik,* 21**,** 457 - 480.

KUBOTA, N., YAMADA, M., FUJISAWA, Y. & YOKOTA, M. 1996. Impurity Effect of Chromium(III) on the Growth Rate of Potassium Hydrogen Phthalate Crystals. *JOURNAL OF CHEMICAL ENGINEERING OF JAPAN,* 29**,** 642 - 647.

KUMAR, R. & PAL, P. 2013. Turning hazardous waste into value-added products: production and characterization of struvite from ammoniacal waste with new approaches. *Journal of Cleaner Production,* 43**,** 59 - 70.

LE CORRE, K. S., VALSAMI-JONES, E., HOBBS, P., JEFFERSON, B. & PARSONS, S. A. 2007. Agglomeration of struvite crystals. *Water Research,* 41**,** 419 - 425.

LE CORRE, K. S., VALSAMI-JONES, E., HOBBS, P. & PARSONS, S. A. 2005. Impact of calcium on struvite crystal size, shape and purity. *Journal of Crystal Growth,* 283**,** 514 - 522.

LE CORRE, K. S., VALSAMI-JONES, E., HOBBS, P. & PARSONS, S. A. 2009. Phosphorus recovery from wastewater by struvite crystallization: A review. *Critical Reviews in Environmental Science and Technology,* 39**,** 433 - 477.

LI, X. Z. & ZHAO, Q. L. 2003. Recovery of ammonium-nitrogen from landfill leachate as a multi-nutrient fertilizer. *Ecological Engineering,* 20**,** 171-181.

LINDENBERG, C. & MAZZOTTI, M. 2009. Effect of temperature on the nucleation kinetics of L-glutamic acid. *Journal of Crystal Growth,* 311**,** 1178 - 1184.

LIRI, M., KOIRANEN, T. & AITTAMAA, J. 2002. Secondary nucleation due to crystal–impeller and crystal–vessel collisions by population balances in CFD-modelling. *Journal of Crystal Growth,* 237 - 239.

LOEHE, J. & DONOHUE, M. 1997. Recent Advances in Modelling Thermodynamic Properties of Aqueous Strong Electrolyte System. *AIChE Journal,* 43**,** 180 - 195.

LOEWENTHAL, R. E., KORNMÜLLER, U. R. C. & HEERDEN, E. P. V. 1994. Modelling struvite precipitation in anaerobic treatment systems. *Water Science and Technology,* 30.

MA, Y. F., GAO, Y. H. & FENG, Q. L. 2010. Effects of pH and temperature on CaCO3 crystallization in aqueous solution with water soluble matrix of pearls. *Journal of Crystal Growth,* 312**,** 3165 - 3170.

MAEKAWA, T., LIAO, C. M. & FENG, X. D. 1995. Nitrogen and phosphorus removal for swine wastewater using intermittent aeration batch reactor followed by ammonium crystallization process. *Water Research,* 29**,** 2643 - 2650.

MAIWA, K., NAKAMURA, H., KIMURA, H. & MIYAZAKI, A. 2006. Effect of temperature and supersaturation on the growth of $Sr(No_3)_2$ (1 1 1) face in aqueous solution. *Journal of Crystal Growth,* 289**,** 303 -307.

MAMAIS, D., PITT, P. A., CHENG, Y. W., LOIACONO, J. & JENKINS, D. 1994. Determination of ferric-chloride dose to control struvite precipitation in anaerobic sludge digesters. *Water Environment Research,* 66**,** 912 - 918.

MARTELL, A., SMITH, R. & MOTEKAITIS, R. 1998. NIST Critically Selected Stability Constants of Metal Complexes, Database Version 5.0 NIST Standard Reference Database 46 Texas A&M University .

MASUDA, H., HIGASHITANI, K. & YOSHIDA, H. 2006. *Powder Technology handbook*, CRC Press.

MATYNIA, A., KORALEWSKA, J., WIERZBOWSKA, B. & PIOTROWSKI, K. 2006. The influence of process parameters on struvite continuous crystallization kinetics. *Chemical Engineering Communications,* 193**,** 160 - 176.

MAVINIC, D. S., ADNAN, A. & KOCH, F. A. 2003. Pilot-scale study of phosphorus recovery through struvite crystallization - examining the process feasibility. *Journal of Environmental Engineering & Science,* 2**,** 315 - 324.

MCCABE, W. L., SMITH, J. & HARRIOTT, P. 2005. *Unit Operations of Chemical Engineering*, McGraw-Hill Education.

MD. ALI, I. & SCHNEIDER, P. A. 2005. Crystallization of struvite from metastable region with different types of seed crystal. *Journal of Non-Equilibrium Thermodynamics,* 30**,** 95 -111.

MEHTA, C. M. & BATSTONE, D. J. 2013. Nucleation and growth kinetics of struvite crystallization. *Water Research,* 47**,** 2890 - 2900.

MERGEN, A. & DEMIRHAN, M. H. 2009. Dissolution kinetics of probertite in boric acid solution. *International Journal of Mineral Processing,* 90**,** 16 - 20.

MERSMANN, A. 2001. *Crystallization Technology Handbook,* New York, Marcel Dekker Inc.

MERSMANN, A., BRAUN, B. & LÖFFELMANN, M. 2002. Prediction of crystallization coefficients of the population balance. *Chemical Engineering Science,* 57**,** 4267 - 4275.

METZ, V. & GANOR, J. 2001. Stirring effect on kaolinite dissolution rate. *Geochimica et Cosmochimica Acta,* 65**,** 3475 - 3490.

MIJANGOS, F., KAMEL, M., LESMES, G. & MURAVIEV, D. N. 2004. Synthesis of struvite by ion exchange isothermal supersaturation technique. *Reactive and Functional Polymers,* 60**,** 151 - 161.

MULLIN, J. W. 2001. *Crystallization,* Oxford, Butterworth-Heinemann.

MÜNCH, E. V. & BARR., K. 2001. Controlled struvite crystallisation for removing phosphorus from anaerobic digester sidestreams. *Water Research,* 35**,** 151 - 159.

MUSVOTO, E. V., WENTZEL, M. C. & EKAMA, G. A. 2000. Integrated chemical-physical process modeling-II. Simulation aeration treatment for anaerobic digester supernatant. *Water Research,* 34**,** 1868 - 1880.

MYERSON, A. & TOYOKURA, S. 1990. Crystallization as a Separations Process. *American Chemical Society Symposium Series 438.* Washington.

MYERSON, A. S. 2002. *Handbook of industrial crystallization,* Woburn (USA), Butterworth-Heinemann.

MYERSON, A. S. & JANG, S. M. 1995. A comparison of binding energy and metastable zone width for adipic acid with various additives. *Journal of Crystal Growth,* 156**,** 459 - 466.

NELSON, N. O., MIKKELSEN, R. L. & HESTERBERG, D. L. 2003. Struvite precipitation in anaerobic swine lagoon liquid: effect of pH and Mg:P ratio and determination of rate constant. *Bioresource Technology,* 89**,** 229 - 236

NERNST, W. 1904. Theorie der Reaktionsgeschwindigkeit in heterogenen Systemen. *Zeitschrift für physikalische Chemie,* 47**,** 52 - 55.

NIELSEN, A. E. 1964. *Kinetics of Precipitation,* New York, Pergamon Press.

NIELSEN, A. E. & TOFT, J. M. 1984. Electrolyte crystal growth kinetics. *Journal of Crystal Growth,* 67**,** 278 - 288.

NOYES, A. A. & WHITNEY, W. R. 1897. The Rate Of Solution Of Solid Substances In Their Own Solutions. *Journal of The American Chemical Society,* 19**,** 930 - 934.

NÝVLT, J. 1971. *Industrial Crystallisation from Solutions,* London, Butterworths.

NÝVLT, J. 1992. *Design of crystallizers,* Boca Raton, CRC Press.

NYVLT, J., SOHNEL, O., MATUCHOVA, M. & BROUL, M. 1985. *The Kinetics of Industrial Crystallization* Amsterdam, Elsevier.

O'GRADY, D., BARRETT, M., CASEY, E. & GLENNON, B. 2007. The Effect of Mixing on the Metastable Zone Width and Nucleation Kinetics in the Anti-Solvent Crystallization of Benzoic Acid. *Chemical Engineering Research and Design,* 85**,** 945 - 952.

OHLINGER, K. N., YOUNG, T. M. & SCHROEDER, E. D. 1998. Predicting struvite formation in digestion. *Water Research,* 32**,** 3607 - 3614.

OHLINGER, K. N., YOUNG, T. M. & SCHROEDER, E. D. 1999. Kinetics effects on preferential struvite accumulation in wasterwater. *Journal of Environmental Engineering,* 125**,** 730 - 737.

OHLINGER, K. N., YOUNG, T. M. & SCHROEDER, E. D. 2000. Postdigestion Struvite Precipitation Using a Fluidized Bed Reactor. *Journal of Environmental Engineering,* 126**,** 361 - 368.

OMAR, W. & ULRICH, J. 2003. Influence of crystallization conditions on the mechanism and rate of crystal growth of potassium sulphate. *Crystal Research and Technology,* 34**,** 34 - 41.

PARKHURST, D. L. & APPELO, C. A. J. 1999. *User's Guide To Phreeqc (Version 2) - A Computer Program For Speciation, Batch-Reaction, One-Dimensional Transport, And Inverse Geochemical Calculations,* Denver, Colorado.

PASTOR, L., MANGIN, D., BARAT, R. & SECO, A. 2008. A pilot-scale study of struvite precipitation in a stirred tank reactor: Conditions influencing the process. *Bioresource Technology,* 99**,** 6285 - 691.

PAULIK, J. & PAULIK, F. 1975. TG and EGA investigations of the decomposition of some metal ammonium phosphate monohydrates by means of the Derivatograph under conventional and quasi-isothermal - Quasi-isobaric conditions. *Journal of Thermal Analysis and Calorimetry,* 8**,** 567 - 576.

PEREIRA, J. A. M., SCHWAAB, M., DELL'ORO, E., PINTO, J. C., MONTEIRO, J. L. F. & HENRIQUES, C. A. 2009. The kinetics of gibbsite dissolution in NaOH. *Hydrometallurgy,* 96**,** 6 - 13.

PERERA, P. W. A., WU, W. X., CHEN, Y. X. & HAN, Z. Y. 2009. Struvite recovery from swine waste biogas digester effluent through a stainless steel device under constant pH conditions. *Biomedical and Environemental Sciences* 22**,** 201 - 209.

PHILIPPE, F. X., CABARAUX, J. F. & NICKS, B. 2011. Ammonia emissions from pig houses: Influencing factors and mitigation techniques. *Agriculture, Ecosystems & Environment,* 141**,** 245 - 260.

POKROVSKY, O. S. 1998. Precipitation of calcium and magnesium carbonates from homogeneous supersaturated solutions. *Journal of Crystal Growth,* 186**,** 233 - 239.

QIN, X., LU, A. & ZHANG, L. 2012. Effect of stirring conditions on cellulose dissolution in NaOH/urea aqueous solution at low temperature. *Journal of Applied Polymer Science,* 126**,** E470 - E477.

QUINTANA, M., SANCHEZ, E., COLMENAREJO, M. F., BARRERA, J., GARCIA, G. & BORJA, R. 2005. Kinetics of phosphorus removal and struvite formation by the utilization of by-product of magnesium oxide production. *Chemical Engineering Journal,* 111**,** 45 - 52.

RAHAMAN, M. S., ELLIS, N. & MAVINIC, D. S. 2008. Effects of various process parameters on struvite precipitation kinetics and subsequent determination of rate constants. *Water Science & Technology,* 57**,** 647 - 654.

RAJESH, P., RAMASAMY, P. & BHAGAVANNARAYANA, G. 2009. Effect of ammonium malate on growth rate, crystalline perfection, structural, optical, thermal, mechanical, dielectric and NLO behaviour of ammonium dihydrogen phosphate crystals. *Journal of Crystal Growth,* 311**,** 4069 - 4075.

RANDOLPH, A. D. & LARSON, M. A. 1988. *Theory of Particulate Processes: Analysis and Techniques of Continuous Crystallization,* New York, Academic Press Inc.

RANDOLPH, A. D. & SIKDAR, S. K. 1974. Effect of a soft impeller coating on the net formation of secondary nuclei. *AIChE Journal,* 20**,** 410 - 412.

RONCAL-HERRERO, T. & OELKERS, E. H. 2011. Experimental determination of struvite dissolution and precipitation rates as a function of pH. *Applied Geochemistry,* 26**,** 921 - 928.

RONTELTAP, M., MAURER, M. & GUJER, W. 2007. Struvite precipitation thermodynamics in source-separated urine. *Water Research,* 41**,** 977 - 984.

RONTELTAP, M., MAURER, M., HAUSHERR, R. & GUJER, W. 2010. Struvite precipitation from urine – Influencing factors on particle size. *Water Research,* 44**,** 2038 - 2046.

ROUSSEAU, R. W., LI, K. & MCCABE, W. L. 1976. The Influence of Crystal Size on Nucleation Rate. *AIChE Symposium Series,* 72**,** 48 - 52.

RYU, H. D., KIM, D. & LEE, S. I. 2008. Application of struvite precipitation in treating ammonium nitrogen from semiconductor wastewater. *Journal of Hazardous Materials,* 156**,** 163 - 169.

RYU, H. D., LIM, C. S., KANG, M. K. & LEE, S. I. 2012. Evaluation of struvite obtained from semiconductor wastewater as a fertilizer in cultivating Chinese cabbage. *Journal of Hazardous Materials,* 221**,** 248 - 255.

SAFAEEFAR, P. 2007. *Crystallisation of manganese sulphate from mix solvents.* PhD, Curtin University.

SAYAN, P. & ULRICH, J. 2001. Effect of Various Impurities on the Hardness of NaCl Crystals. *Crystal Research and Technology,* 36**,** 1253 - 1262.

SHAH, B. C., MCCABE, W. L. & ROUSSEAU, R. W. 1973. Polyethylene versus stainless steel impellers for crystallization processes. *AIChE Journal,* 19**,** 194.

SHAN, G., IGARASHI, K. & OOSHIMA, H. 2002. Dissolution kinetics of crystals in suspension and its application to L-aspartic acid crystals. *Chemical Engineering Journal,* 88**,** 53 - 58.

SHIMAMURA, K., TANAKA, T., MIURA, Y. & ISHIKAWA, H. 2003. Development of a high-efficiency phosphorus recovery method using a fluidized-bed crystallised phosphorus removal system. *Water Science and Technology,* 48**,** 163 - 170.

SHUKLA, J., MOHANDAS, V. P. & KUMAR, A. 2008. Effect of pH on the Solubility of CaSO4·2H2O in Aqueous NaCl Solutions and

Physicochemical Solution Properties at 35 °C. *Journal of Chemical & Engineering Data,* 53**,** 2797 - 2800.

SINGH, S. K., KUNDU, A. & KISHORE, N. 2004. Interactions of some amino acids and glycine peptides with aqueous sodium dodecyl sulfate and cetyltrimethylammonium bromide at T=298.15 K: a volumetric approach. *The Journal of Chemical Thermodynamics,* 36**,** 7 - 16.

SNOEYINK, V. L. & JENKINS, D. 1980. *Water chemistry,* New York, John Wiley and Sons.

SÖHNEL, O. & GARSIDE, J. 1992. *Precipitation: basic principles and industrial applications,* Oxford, Butterworth - Heinemann.

SÖHNEL, O. & MULLIN, J. W. 1988. Interpretation of crystallization induction periods. *Journal of Colloid and Interface Science,* 123**,** 43 - 50.

SONG, Z., LI, Q. & GAO, L. 1997. Preparation and properties of nano-TiO_2 Powder. *Journal of Material Science Technology,* 13**,** 321 - 323.

SOTO, A., ARCE, A. & KHOSHKBARCHI, M. K. 2004. Thermodynamics of Diglycine and Triglycine in Aqueous NaCl Solutions: Apparent Molar Volume, Isentropic Compressibility, and Refractive Index. *Journal of Solution Chemistry,* 33**,** 11-21.

STATISTICS, A. B. O. 2009. *Australian Demographic Statistics, March 2009* [Online]. Available: http://www.abs.gov.au/ausstats/abs@.nsf/mf/3101.0 [Accessed April, 24th 2012].

STRATFUL, I., SCRIMSHAW, M. D. & LESTER, J. N. 2001. Conditions influencing the precipitation of magnesium ammonium phosphate. *Water Research,* 35**,** 4191 - 4199.

STRICKLAND-CONSTABLE, R. F. & MASON, R. E. A. 1963. Breeding of Nuclei. *Nature,* 197**,** 897 - 898.

STUBIČAR, N., MARKOVIĆ, B., TONEJC, A. & STUBIČAR, M. 1993. Crystal growth of lead fluoride phases using the constant composition method III. Effect of pH and ionic strength. *Journal of Crystal Growth,* 130**,** 300 - 304.

STUMM, W. & MORGAN, J. J. 1981. *Aquatic Chemistry: An Introduction Emphasizing Chemical Equilibria in Natural Waters* Canada, John Wiley and Sons Ltd.

STUMM, W. & MORGAN, J. J. 1995. *Aquatic Chemistry: Chemical Equilibria and Rates in Natural Waters,* New York, Wiley.

SUGUNA, K., THENMOZHI, M. & SEKAR, C. 2012. Growth, spectral, structural and mechanical properties of struvite crystal grown in presence of sodium fluoride. *Bulletin of Materials Science,* 35**,** 701 - 706.

SUNG, M. H., KIM, J. S., KIM, W. S. & IZUMI HIRASAWA, W. S. K. 2002. Modification of crystal growth mechanism of yttrium oxalate in metastable solution. *Journal of Crystal Growth,* 235**,** 529 - 540.

SUZUKI, K., TANAKA, Y., KURODA, K., HANAJIMA, D., FUKUMOTO, Y., YASUDA, T. & WAKI, M. 2007. Removal and recovery of phosphorous from swine wastewater by demonstration crystallization reactor and struvite accumulation device. *Bioresource Technology,* 98**,** 1573 - 1578.

SÝKORA, V., PITTER, P., BITTNEROVÁ, I. & LEDERER, T. 2001. Biodegradability of ethylenediamine-based complexing agents. *Water Research,* 35**,** 2010 - 2016.

TAI, C. Y. 1997. Crystallization Kinetics Revealed from Experimental Data Analyzed by the Two-Step Growth Model. *Journal of Chemical Engineering of Japan,* 30**,** 373 - 381.

TAI, C. Y., CHANG, M. C., WU, C. K. & LIN, Y. C. 2006a. Interpretation of calcite growth data using the two-step crystal growth model. *Chemical Engineering Science,* 61**,** 5346 - 5354.

TAI, C. Y., CHEN, P. C. & TSAO, T. M. 2006b. Growth kinetics of CaF_2 in a pH-stat fluidized-bed crystallizer. *Journal of Crystal Growth,* 290**,** 576 - 584.

TAI, C. Y., CHIEN, W.-C. & CHEN, C.-Y. 1999. Crystal growth kinetics of calcite in a dense fluidized-bed crystallizer. *AIChE Journal,* 45**,** 1605 - 1614.

TAI, C. Y. & CHIEN, W. C. 2002 Effects of operating variables on the induction period of CaCl2–Na2CO3 system. *Journal of Crystal Growth,* 237 - 239**,** 2142–2147.

TAYLOR, A. W., FRAZIER, A. W. & GURNEY, E. L. 1963. Solubility products of magnesium ammonium and magnesium potassium phosphates. *Trans Faraday Soc,* 59**,** 1580 - 1584.

TING, H. H. & MCCABE, W. L. 1934. Supersaturation and Crystal Formation in Seeded Solutions. *Industrial Engineering Chemistry,* 26**,** 1201 - 1207.

TRIGER, A., PIC, J. S. & CABASSUD, C. 2012. Determination of struvite crystallization mechanisms in urine using turbidity measurement. *Water Research,* 46**,** 6084 - 6094.

UENO, Y. & FUJII, M. 2001. Three years experience of operating and selling recovered struvite from full-scale plant. *Environmental Technology,* 22**,** 1373 - 1381.

ULUDAG-DEMIRER, S., DEMIRER, G. N. & CHEN, S. 2005. Ammonia removal from anaerobically digested dairy manure by struvite precipitation. *Process Biochemistry,* 40**,** 3667 - 3674.

ULUDAG-DEMIRER, S. & OTHMAN, M. 2009. Removal of ammonium and phosphate from the supernatant of anaerobically digested waste activated sludge by chemical precipitation. *Bioresource Technology,* 100**,** 3236 - 3244.

VOLMER, M. 1939. Kinetik der phasenbildung. Steinkopff, Leipzig.

WANG, J., BURKEN, J. G. & ZHANG, X. J. 2006. Effect of seeding materials and mixing strength on struvite precipitation. *Water Environment Research,* 78**,** 125 - 132.

WARMADEWANTHI & LIU, J. C. 2009. Recovery of phosphate and ammonium as struvite from semiconductor wastewater. *Separation and Purification Technology,* 64**,** 368 - 373.

WEBB, K. & HO, G. 1992. Struvite solubility and its application to a piggery effluent problem. *Water Science & Technology,* 26**,** 2229 - 2232.

WEINER, E. R. 2008. *Application of environmental aquatic chemistry; A practical guide,* Boca Raton, CRC Press.

WHITAKER, A. & JEFFERY, J. W. 1970. The Crystal Structure of Struvite, $MgNH_4PO4.6H_20$. *Acta Crystallographica,* B26**,** 1429 -1440.

WILSENACH, J. A., SCHUURBIERS, C. A. H. & LOOSDRECHT, M. C. M. V. 2007. Phosphate and potassium recovery from source separated urine through struvite precipitation. *Water Research,* 41**,** 458 - 466.

ZANG, T., DING, L., REN, H. & XIONG, X. 2009. Ammonium nitrogen removal from cocking wastewater by chemical precipitation recycle technology. *Water Research,* 43**,** 5209 - 5215.

ZHANG, D. M., CHEN, Y. X., JILANI, G., WU, W. X., LIU, W. L. & HAN, Z. Y. 2012. Optimization of struvite crystallization protocol for pretreating the swine wastewater and its impact on subsequent anaerobic biodegradation of pollutants. *Bioresource Technology,* 116**,** 386 - 395.

ZHANG, Y., LI, Y. & ZHANG, Y. 2003. Supersolubility and induction of aluminosilicate nucleation from clear solution. *Journal of Crystal Growth,* 254**,** 156 - 163.

Nomenclature

Greek Notation

γ_i	: ion activity
$\Delta\mu$	: chemical potential difference per solute molecule
$\beta\ \alpha$	: area and volume shape factor
γ_s	: interfacial tension/energy
γhet	: heterogeneous interfacial energy
γhom	: homogeneous interfacial energy
$\emptyset$	**:** wetting angle
$\frac{\delta C}{\delta x}$	: concentration gradient
ϕ_a	: area shape factor
ϕ_v	: volume shape factor
ρ_c	: crystal density
υ_m	: the molecular volume of struvite (= molar volume/(Avogadro's number x density x number of ions in formula unit) = $7.99 \times 10^{-23} \mathrm{cm}^3/\mathrm{mol}$)

General Notation

A	: frequency constant
A	: surface area of suspended crystal (m^2)
A_c	: area of a single crystal
B	: constants according to the nucleation classical theory
B_{hom}	: constants according to the nucleation classical theory (homogeneous nucleation)
B_{het}	: constants according to the nucleation classical theory (heterogeneous nucleation)
C	: bulk solute concentration medium (mol)
C_b	: concentration of drug in solution (dissolution medium) at

time *t*.

C_i : solute concentration in the solution at crystal solution interface

C_S : saturation concentration or solubility in the dissolution

C^* : equilibrium saturation concentration

Cl^- : molar concentration of chlorine in solution

Cl^-_{eqm} : chlorine introduced in solution through the equimolar feed

c : solution concentration

c^* : equilibrium saturation at given temperature T

dL : changing size of crystal

dt : changing time

$\frac{dC}{dt}$: changing concentration per time

E : excess ion

E_{act} : activation energy (J/mol)

G : linear crystal growth velocity (length/time)

g : order of the overall growth process

ΔG : Gibbs free energy

ΔG_V : volume free energy

ΔG_S : surface free energy

ΔG_{hom} : gibbs free energy for homogeneous nucleation

ΔG_{het} : gibbs free energy for heterogeneous nucleation

IAP : ion activity product of the lattice ions in solution

J : rate of nucleation

k : rate constant

k_1 : first-order constant

k_2 : second-order constant

n : order of reaction

K_c : solubility product in term of concentration

K_G : overall growth rate constant

K_{sp} : solubility product in term of ion activity

K_L : overall mass transfer coefficient

K_d	: dissolution rate constant (m/s)
k_d	: coefficient of mass transfer by diffusion
k_N	: nucleation rate constant
k_r	: rate constant for surface reaction (integration) process
m_c	: mass of a single crystal
N_A	: Avogadro number
n	: the kinetic order
R	: gas constant (8.314 J/K.mol)
r_c	: critical size of lattice
S	: supersaturation
SI	: saturation index
S_i	: supersaturation at time t=0
S_{aq}	: solubility of struvite in pure water
S_{salt}	: solubility of struvite in aqueous chloride
S_t	: supersaturation at time t
T	: absolute temperature
t_g	: time required nucleus to grow to a detectable size
t_{ind}	: induction time
t_n	: formation of a stable nucleus time
t_r	: relaxation time
V	: volume of liquid (m^3)
V_c	: volume of singe crystal
V_m	: molar volume
z^+ and z^-	: valencies of the ions
$[Mg^{2+}]$	: magnesium ion concentration
$[NH_4{}^+]$	: ammonium ion concentration
$[PO_4{}^{3-}]$	: phosphate ion concentration
ΔHr^0	: enthalpy energy

Appendix A: Solubility Studies

A1. Solubility data in various solution pH and temperature

Example of Solubility Calculation

Weight of Initial sturvite before solubility process[d)] = 0.0403 g
Weight of filter paper[a)] = 22.0341 g
Struvite crystals were agitated for 24 hours into water of 100 ml. After 24 hours sturvite was filtered and dried.
Weight of crystal and filter paper after drying[b)] = 22.0453 g
Weight of struvite crystal left on filter paper[c)] = 22.0453 g – 22.0341 g
= 0.0112 g
Solubility of struvite = 0.0403 g – 0.0112 g
= 0.0291g/100ml or
= 0.291 mg/ml or
= 291 mg/l

Table A1.1: Solubility data of struvite at $25^{O}C$

Solution pH	Solubility (mg/100ml)	Solubility (mg/l)	Mean of Solubility (mg/l)
3.1	29.2	292	292
	29.1	291	
	29.3	293	
5.0	21.3	213	212
	21.2	212	
	21.1	211	
6.5	18.7	187	185.5
	18.4	184	
7.0	17.2	172	174
	17.8	178	
	17.3	173	
8.5	17.6	176	175
	17.6	176	
	17.3	173	
9.0	18.2	182	180
	17.8	178	
10.0	18.9	189	189
11.0	25.9	259	257
	25.5	255	

Table A1.2: Solubility data of struvite at $30^{O}C$

Solution pH	Solubility (mg/100ml)	Solubility (mg/l)	Mean of Solubility (mg/l)
3.1	31.6	316	315.5
	31.5	315	
5.0	25	250	249
	24.8	248	
7.0	21.8	218	218
	21.8	218	
8.5	21.5	215	215
9.0	22.7	227	227.5
	22.8	228	
10.0	23.8	238	238
11.0	30.7	307	305
	30.3	303	

Table A1.2: Solubility data of struvite at $35^{O}C$

pH	Solubility (mg/100ml)	Solubility (mg/l)	Mean of Solubility (mg/l)
3.1	32.7	327	329.5
	33.2	332	
5.0	29.3	293	290
	28.7	287	
7.0	24.7	247	247
	24.7	247	
8.5	25.6	256	253
	25.0	250	
9.0	26.2	262	261.5
	26.1	261	
10.0	28.6	286	283
	28.0	280	
11	33.5	335	332.5
	33.0	330	

Table A1.3: Solubility data of struvite at $40^{O}C$

Solution pH	Solubility (mg/100ml)	Solubility (mg/l)	Mean of Solubility (mg/l)
3.0	32.1	321	324
	32.7	327	
5.0	26.9	269	266
	26.3	266	
7.0	23.1	231	229
	22.7	227	
8.5	23.6	236	232
	22.8	228	
9.0	24.1	241	237
	23.3	233	
10.0	25.5	255	254
	25.3	253	
11.0	32.0	320	318
	31.6	316	

A2. Solubility product calculation

Solubility Calculation Correcting for Ionic Strength

1. Enter precipitate equilibrium as MaXb <==> aM + bX:
(m+ is charge on the cation and x- is charge on the anion.)

MaXb		a	M	m+		b	X	x-		c	Z	
MgNH4PO4	<==>	1	Mg	2	+	1	NH4	1	+	1	PO4	-3

3. Enter initial guess of ion concentrations:

Ion	C (M)	alpha	z²	z²C	Activity Coeff.			
Mg	0.000120	0.8	4	0.0004806	0.921	1.106E-04	2.13E-12	11.67
PO4	0.000118	0.4	9	0.0010623	0.827	9.759E-05		
NH4	0.000202	0.25	1	0.0002018	0.979	1.975E-04		
					0.9088			

4. Enter any additional ions and concentrations:

Ion	C (M)	alpha	z²	z²C	Activity Coeff.
Na	0.00000	0.4	1	0	0.979
Cl	0	0.3	1	0	0.979
Ca	0.00000	0.6	4	0	0.920
Cl	0.00000	0.3	1	0	0.979
			Ionic Strength:	0.000341	

Figure A2.1 Solubility product and ionic strength calculation by excel program

Table A2.1 Ion concentration of struvite after 24 hour solubility process at 25^{O}C

Solution pH	Mg^{2+} (mg)	Mg^{2+}, (x 10^{-5} Mol)	PO_4^{3-} (mg)	PO_4^{3-}, (x 10^{-5} Mol)	NH_4^{+}, (mg)	NH_4^{+}, (x 10^{-5} Mol)	Ksp, (x 10^{-13})	pKa
3.1	2.45	10.08	12.24	12.89	1.65	9.15	9.24	12.03
5.0	2.00	8.23	8.45	8.90	1.4	7.76	4.52	12.34
7.0	1.78	7.32	6.72	7.08	1.25	6.93	2.89	12.54
8.5	1.81	7.45	6.74	7.10	1.19	6.60	2.81	12.55
9.0	1.73	7.12	6.98	7.35	1.39	7.71	3.25	12.49
10.0	1.68	6.91	7.01	7.38	1.89	10.48	4.28	12.37
11.0	1.85	7.61	9.62	10.13	2.92	16.19	9.77	12.01

Table A2.2 Ion concentration of struvite after 24 hour solubility process at different temperature and pH 7

Temp, C	Solubility, mg/L	Mg^{2+} (mg)	Mg^{2+}, (x 10^{-5} Mol)	PO_4^{3-} (mg)	PO_4^{3-}, (x 10^{-5} Mol)	NH_4^{+}, (mg)	NH_4^{+}, (x 10^{-5} Mol)	Ksp, (x 10^{-13})	pKa
20	145	1.43	5.95	5.66	5.96	1.02	5.65	1.63	12.79
25	174	1.78	7.32	6.72	7.07	1.25	6.93	2.89	12.54
30	218	2.13	8.84	8.40	8.84	1.67	9.26	5.65	12.25
35	247	2.39	9.83	9.55	10.05	1.88	10.42	8.01	12.10
40	229	2.12	8.72	9.1	9.58	1.58	8.74	5.78	12.24
45	189	1.86	7.65	7.2	7.58	1.52	8.43	3.91	12.41
50	173	1.6	6.58	6.74	7.10	1.34	7.43	2.82	12.55

A.3. Effect of common-ion on Solubility

Table A3.1 Solubility product data of struvite crystal in different KCl concentration

KCl (mMol)	Solubility (mg/l)	Ionic Strength	Ion Activity Product (IAP)	Ksp (x 10^{-13})	pKa
0.00	174	0.000177	0.9324	2.88	12.54
0.25	201	0.000455	0.8963	3.92	12.41
0.50	219	0.000727	0.8730	4.91	12.31
0.75	236	0.001001	0.8548	6.15	12.21
1.00	262	0.001267	0.8391	7.01	12.15
1.25	278	0.001533	0.8261	7.95	12.10
1.50	289	0.001789	0.8148	8.10	12.09

Table A3.2 Solubility product data of struvite crystal in different NaCl concentration

NaCl (mMol)	Solubility (mg/l)	Ionic Strength	Ion Activity Product (IAP)	Ksp (x 10^{-13})	pKa
0.00	174	0.000177	0.9324	2.88	12.54
0.25	209	0.000463	0.8955	4.39	12.36
0.50	243	0.000748	0.8711	6.32	12.20
0.75	259	0.001014	0.8533	7.15	12.15
1.00	284	0.001289	0.8379	8.88	12.05
1.25	301	0.001557	0.8250	1.00	12.00
1.50	319	0.001825	0.8135	1.14	11.94

Table A3.3 Solubility product data of struvite crystal in different $CaCl_2$ concentration.

CaCl2 (mMol)	Solubility (mg/l)	Ionic Strength	Ion Activity Product (IAP)	Ksp (x 10^{-13})	pKa
0.00	174	0.000177	0.9324	2.88	12.54
0.25	225	0.000979	0.8555	4.73	12.33
0.50	258	0.001763	0.8161	6.10	12.21
0.75	279	0.002534	0.7881	6.85	12.16
1.00	302	0.003308	0.7659	7.87	12.10
1.25	326	0.004082	0.7474	9.07	12.04
1.50	358	0.004865	0.7313	1.11	11.95

Appendix B: PhreeqC Model

B1. Supersaturation calculation with using Phreeq Model

B1.1. Major equilibria reaction involved in the computation of solution

```
SOLUTION 1
    temp      25
    pH        8
    pe        4
    redox     pe
    units     mmol/l
    density   1
    P         2.63 as PO4+3
    N(-3)     2.63
    Mg        2.63
    -water    1 # kg
SOLUTION_SPECIES
2H+ + HPO4-2 = H3PO4
    log_k     9.37
    delta_h   3.744 kJ
H+ + PO4-3 = HPO4-2
    log_k     12.37
    delta_h   -14.769 kJ
H+ + HPO4-2 = H2PO4-
    log_k     7.2
    delta_h   -4.205 kJ
H2O + Mg+2 = MgOH+ + H+
    log_k     -11.44
    delta_h   66.743 kJ
H+ + OH- = H2O
    log_k     14
    delta_h   -55.906 kJ
H2PO4- + Mg+2 = MgH2PO4+
    log_k     0.45
    delta_h   14.225 kJ
HPO4-2 + Mg+2 = MgHPO4
    log_k     2.87
    delta_h   13.807 kJ
Mg+2 + PO4-3 = MgPO4-
    log_k     4.8
    delta_h   12.97 kJ
H+ + NH3 = NH3H+
    log_k     9.24
    delta_h   -51.92 kJ
Mg+2 + NH3 = MgNH3+2
    log_k     0.24
Mg+2 + 2NH3 = Mg(NH3)2+2
    log_k     0.2
Mg+2 + 3NH3 = Mg(NH3)3+2
    log_k     -0.3
Cl- + Mg+2 = MgCl+
    log_k     -0.135
    delta_h   -0.586 kJ

PHASES
Struvite
    MgNH4PO4:6H2O = 6H2O + Mg+2 + NH3H+ + PO4-3
    delta_h   23.62 kcal
```

```
            -analytical_expression -1157.45 -0.784 -63.86
        556.83 19.54 0
        End
```

B1.2. Output from PhreeqC model

```
------------------
Reading data base.
------------------

      SOLUTION_MASTER_SPECIES
      SOLUTION_SPECIES
      PHASES
      EXCHANGE_MASTER_SPECIES
      EXCHANGE_SPECIES
      SURFACE_MASTER_SPECIES
      SURFACE_SPECIES
      RATES
      END
-----------------------------------
Reading input data for simulation 1.
-----------------------------------

      SOLUTION 1
          temp      25
          pH        8.5
          pe        4
          redox     pe
          units     mmol/l
          density   1
          P         2.63 as PO4+3
          N(-3)     2.63
          Mg        2.63
          water    1 # kg
      SOLUTION_SPECIES
      2H+ + HPO4-2 = H3PO4
          log_k     9.37
          delta_h   3.744 kJ
      H+ + PO4-3 = HPO4-2
          log_k     12.37
          delta_h   -14.769 kJ
      H+ + HPO4-2 = H2PO4-
          log_k     7.2
          delta_h   -4.205 kJ
      H2O + Mg+2 = MgOH+ + H+
          log_k     -11.44
          delta_h   66.743 kJ
      H+ + OH- = H2O
          log_k     14
          delta_h   -55.906 kJ
      H2PO4- + Mg+2 = MgH2PO4+
          log_k     0.45
          delta_h   14.225 kJ
      HPO4-2 + Mg+2 = MgHPO4
          log_k     2.87
          delta_h   13.807 kJ
```

```
      Mg+2 + PO4-3 = MgPO4-
          log_k     4.8
          delta_h   12.97 kJ
      H+ + NH3 = NH3H+
          log_k     9.24
          delta_h   -51.92 kJ
      Mg+2 + NH3 = MgNH3+2
          log_k     0.24
      Mg+2 + 2NH3 = Mg(NH3)2+2
          log_k     0.2
      Mg+2 + 3NH3 = Mg(NH3)3+2
          log_k     -0.3
      Cl- + Mg+2 = MgCl+
          log_k     -0.135
          delta_h   -0.586 kJ
      PHASES
      Struvite
          MgNH4PO4:6H2O = 6H2O + Mg+2 + NH3H+ + PO4-3
          delta_h   23.62 kcal
          analytical_expression -1157.45 -0.784 -63.86 556.83
19.54 0
      End
-------------------------------------------
Beginning of initial solution calculations.
-------------------------------------------

Initial solution 1.

-----------------------------Solution composition------------------
-------------

      Elements           Molality       Moles

      Mg                2.631e-003  2.631e-003
      N(-3)             2.631e-003  2.631e-003
      P                 2.631e-003  2.631e-003

----------------------------Description of solution---------------
-------------

                                       pH  =   8.500
                                       pe  =   4.000
       Specific Conductance (uS/cm, 25 oC) = 238
                            Density (g/cm3)  =   0.99723
                         Activity of water  =   1.000
                            Ionic strength  =  7.782e-003
                        Mass of water (kg)  =  1.000e+000
                 Total alkalinity (eq/kg)   =  2.788e-003
                    Total carbon (mol/kg)   =  0.000e+000
                       Total CO2 (mol/kg)   =  0.000e+000
                     Temperature (deg C)    =  25.000
                  Electrical balance (eq)   =  2.474e-003
 Percent error, 100*(Cat-|An|)/(Cat+|An|)   =  27.38
                                 Iterations  =   6
                                    Total H  = 1.110254e+002
                                    Total O  = 5.551675e+001

----------------------------Distribution of species---------------
-------------
```

Species	Molality	Activity	Log Molality	Log Activity	Log Gamma
OH-	3.477e-006	3.165e-006	-5.459	-5.500	-0.041
H+	3.433e-009	3.162e-009	-8.464	-8.500	-0.036
H2O	5.551e+001	9.999e-001	1.744	0.000	0.000
H(0)	1.413e-028				
H2	7.067e-029	7.079e-029	-28.151	-28.150	0.001
Mg	2.631e-003				
Mg+2	1.661e-003	1.166e-003	-2.780	-2.933	-0.153
MgHPO4	9.557e-004	9.574e-004	-3.020	-3.019	0.001
MgPO4-	1.206e-005	1.099e-005	-4.919	-4.959	-0.040
MgOH+	1.469e-006	1.339e-006	-5.833	-5.873	-0.040
MgNH3+2	5.872e-007	4.059e-007	-6.231	-6.392	-0.160
MgH2PO4+	2.001e-007	1.824e-007	-6.699	-6.739	-0.040
Mg(NH3)2+2	1.072e-010	7.412e-011	-9.970	-10.130	-0.160
Mg(NH3)3+2	6.790e-015	4.694e-015	-14.168	-14.328	-0.160
N(-3)	2.631e-003				
NH4+	1.224e-003	1.111e-003	-2.912	-2.954	-0.042
NH3H+	1.207e-003	1.100e-003	-2.918	-2.958	-0.040
NH3	1.999e-004	2.002e-004	-3.699	-3.698	0.001
MgNH3+2	5.872e-007	4.059e-007	-6.231	-6.392	-0.160
Mg(NH3)2+2	1.072e-010	7.412e-011	-9.970	-10.130	-0.160
Mg(NH3)3+2	6.790e-015	4.694e-015	-14.168	-14.328	-0.160
O(0)	1.660e-036				
O2	8.301e-037	8.316e-037	-36.081	-36.080	0.001
P	2.631e-003				
HPO4-2	1.602e-003	1.107e-003	-2.795	-2.956	-0.160
MgHPO4	9.557e-004	9.574e-004	-3.020	-3.019	0.001
H2PO4-	6.086e-005	5.549e-005	-4.216	-4.256	-0.040
MgPO4-	1.206e-005	1.099e-005	-4.919	-4.959	-0.040
PO4-3	3.440e-007	1.494e-007	-6.463	-6.826	-0.362

```
   MgH2PO4+              2.001e-007  1.824e-007    -6.699    -
6.739    -0.040
   H3PO4                 2.591e-011  2.595e-011   -10.587   -
10.586     0.001

-------------------------------Saturation indices------------------
-------------

      Phase               SI log IAP  log KT

      H2(g)           -25.00  -28.15   -3.15  H2
      H2O(g)           -1.51   -0.00    1.51  H2O
      NH3(g)           -5.47   -3.70    1.77  NH3
      O2(g)           -33.19  -36.08   -2.89  O2
      Struvite          0.86  -12.72  -13.57  MgNH4PO4:6H2O

------------------
End of simulation.
------------------

------------------------------------
Reading input data for simulation 2.
------------------------------------

-----------
End of run.
-----------
```

Appendix C: Crystal Growth Studies

C1. Effect of seed on struvite crystals growth

Table C1.1 Effect of seed loading on the decay of supersaturation. pH 8, temperature 25^{O}C, seed size 24.3 μm and agitator speed 120 rpm.

Time	Concentration (mG/L)			SI	S
	Mg	PO4	NH4		
Seed Loading 100 mg					
0	2.50	2.50	2.50	0.31	2.04
5	2.47	2.48	2.46	0.30	2.00
10	2.43	2.45	2.40	0.28	1.91
15	2.35	2.34	2.35	0.25	1.78
20	2.24	2.25	2.24	0.20	1.58
25	2.14	2.16	2.16	0.16	1.45
30	2.10	2.12	2.11	0.13	1.35
35	2.03	2.03	2.02	0.10	1.26
40	1.97	1.97	1.96	0.07	1.17
45	1.93	1.93	1.93	0.05	1.12
50	1.90	1.90	1.91	0.04	1.10
55	1.90	1.89	1.90	0.04	1.10
60	1.89	1.91	1.89	0.03	1.07
Seed Loading 40 mg					
0	2.50	2.50	2.50	0.31	2.04
5	2.50	2.47	2.40	0.30	2.00
10	2.47	2.48	2.35	0.28	1.91
15	2.40	2.40	2.30	0.27	1.86
20	2.35	2.35	2.30	0.24	1.74
25	2.28	2.27	2.22	0.21	1.62
30	2.32	2.21	2.20	0.18	1.51
35	2.18	2.15	2.14	0.15	1.41
40	2.10	2.12	2.11	0.13	1.35
45	2.05	2.05	2.05	0.11	1.29
50	2.00	1.98	2.00	0.09	1.23
55	1.98	1.98	1.98	0.08	1.20
60	1.95	1.95	1.95	0.06	1.15

Table C2.1 Effect of average seed size on the decay of supersaturation for a solution temperature, pH and seed loading of 25^{O}C and 100 mg, respectively.

Time	Concentration (mMol/L)			SI	S
	Mg	PO4	NH4		
24.3 µm					
0	2.50	2.50	2.50	0.31	2.04
5	2.38	2.38	2.37	0.26	1.82
10	2.25	2.25	2.25	0.21	1.62
15	2.12	2.12	2.12	0.15	1.41
20	2.02	2.02	2.02	0.10	1.26
25	1.95	1.95	1.95	0.06	1.15
30	1.90	1.90	1.90	0.03	1.07
35	1.98	1.98	1.98	0.02	1.05
40	1.85	1.85	1.85	0.01	1.02
45	1.85	1.85	1.85	0.01	1.02
50	1.90	1.90	1.90	0.02	1.05
55	1.85	1.85	1.85	0.01	1.02
60	1.90	1.90	1.90	0.02	1.05
43.5 µm					
0	2.50	2.50	2.50	0.31	2.04
5	2.45	2.45	2.45	0.29	1.95
10	2.38	2.37	2.37	0.26	1.82
15	2.30	2.30	2.30	0.23	1.70
20	2.23	2.23	2.23	0.20	1.58
25	2.15	2.15	2.15	0.16	1.45
30	2.08	2.08	2.08	0.13	1.35
35	2.05	2.05	2.05	0.11	1.29
40	2.00	2.00	2.00	0.09	1.23
45	1.96	1.96	1.96	0.07	1.17
50	1.94	1.94	1.94	0.06	1.15
55	1.93	1.93	1.93	0.05	1.12
60	1.90	1.90	1.90	0.03	1.07
24.3 µm					
0	2.50	2.50	2.50	0.31	2.04
5	2.50	2.47	2.40	0.30	2.00
10	2.45	2.45	2.45	0.29	1.95
15	2.36	2.36	2.36	0.26	1.82
20	2.34	2.34	2.34	0.25	1.78
25	2.25	2.25	2.25	0.21	1.62
30	2.20	2.20	2.20	0.18	1.51

35	2.13	2.13	2.13	0.15	1.41
40	2.08	2.08	2.08	0.13	1.35
45	2.02	2.02	2.02	0.10	1.26
50	2.00	2.00	2.00	0.09	1.23
55	1.96	1.96	1.96	0.07	1.17
60	1.91	1.91	1.91	0.04	1.10

C2. Effect of solution pH on struvite crystal growth kinetic

Table C2.1 Effect of pH on the decay of supersaturation curve for supersaturation, temperature and stirrer speed of 2.04, 25^{O}C and 120 rpm, respectively.

Time	**Concentration (mMol/L)**			**SI**	**S**
	Mg	PO4	NH4		
pH 8.0					
0	2.50	2.50	2.50	0.31	2.04
5	2.50	2.47	2.40	0.30	2.00
10	2.47	2.48	2.35	0.28	1.91
15	2.40	2.40	2.30	0.27	1.86
20	2.35	2.35	2.30	0.24	1.74
25	2.28	2.27	2.22	0.21	1.62
30	2.32	2.21	2.20	0.18	1.51
35	2.18	2.15	2.14	0.15	1.41
40	2.10	2.12	2.11	0.13	1.35
45	2.05	2.05	2.05	0.11	1.29
50	2.00	1.98	2.00	0.09	1.23
55	1.98	1.98	1.98	0.08	1.20
60	1.95	1.95	1.95	0.06	1.15
pH 8.5					
0	1.54	1.54	1.54	0.31	2.04
5	1.49	1.49	1.49	0.28	1.91
10	1.47	1.47	1.47	0.26	1.82
15	1.40	1.40	1.40	0.21	1.62
20	1.32	1.32	1.32	0.15	1.41
25	1.27	1.27	1.27	0.11	1.29
30	1.22	1.22	1.22	0.07	1.17
35	1.20	1.20	1.20	0.05	1.12
40	1.18	1.18	1.18	0.03	1.07
45	1.17	1.17	1.17	0.02	1.05
50	1.17	1.17	1.17	0.02	1.05
55	1.17	1.17	1.17	0.02	1.05
60	1.17	1.17	1.17	0.02	1.05

pH 9.0					
0	1.03	1.03	1.03	0.31	2.04
5	0.97	0.97	0.97	0.26	1.82
10	0.93	0.93	0.93	0.21	1.62
15	0.88	0.88	0.88	0.15	1.41
20	0.84	0.84	0.84	0.10	1.26
25	0.81	0.81	0.81	0.06	1.15
30	0.79	0.79	0.79	0.03	1.07
35	0.78	0.78	0.78	0.02	1.05
40	0.77	0.77	0.77	0.01	1.02
45	0.77	0.77	0.77	0.01	1.02
50	0.77	0.77	0.77	0.02	1.05
55	0.77	0.77	0.77	0.01	1.02
60	0.77	0.77	0.77	0.01	1.02

Table C2.2 Effect of pH on crystal growth at 25^{O}C and 120 rpm

Supersaturation, S	**SI=log S**	**G, (x 10^{-9} m/s)**
pH 8.0		
1.95	0.29	2.07
2.19	0.34	2.80
3.16	0.45	4.29
4.47	0.65	6.05
6.03	0.78	10.04
10	1.00	17.50
pH 8.5		
1.95	0.29	4.10
2.19	0.34	9.12
3.16	0.45	13.05
4.47	0.65	23.19
6.03	0.78	18.03
10	1.00	43.00
pH 9.0		
1.95	0.29	8.11
2.19	0.34	15.20
3.16	0.45	30.05
4.47	0.65	50.19
6.03	0.78	80.75

C3. Effect of stirrer speed on struvite crystal growth kinetic at pH 9

Table C3.1 Decay of supersaturation curves of struvite crystallisation at initial supersaturation 2.04 for different stirrer speeds at pH 9 and 25^{O}C.

Time	Concentration (mMol/L)			SI	S
	Mg	PO4	NH4		
120 rpm					
0	1.03	1.03	1.03	0.31	2.04
5	0.97	0.97	0.97	0.26	1.82
10	0.93	0.93	0.93	0.21	1.62
15	0.88	0.88	0.88	0.15	1.41
20	0.84	0.84	0.84	0.10	1.26
25	0.81	0.81	0.81	0.06	1.15
30	0.79	0.79	0.79	0.03	1.07
35	0.78	0.78	0.78	0.02	1.05
40	0.77	0.77	0.77	0.01	1.02
45	0.77	0.77	0.77	0.01	1.02
50	0.77	0.77	0.77	0.02	1.05
55	0.77	0.77	0.77	0.01	1.02
60	0.77	0.77	0.77	0.01	1.02
100 rpm					
0	1.03	1.03	1.03	0.31	2.04
5	1.01	1.01	1.01	0.30	2.00
10	0.97	0.97	0.97	0.26	1.82
15	0.93	0.92	0.93	0.21	1.62
20	0.89	0.89	0.89	0.17	1.48
25	0.87	0.87	0.87	0.13	1.35
30	0.83	0.83	0.83	0.09	1.23
35	0.81	0.81	0.81	0.06	1.15
40	0.79	0.79	0.79	0.04	1.10
45	0.77	0.77	0.77	0.02	1.05
50	0.77	0.76	0.77	0.01	1.02
55	0.76	0.76	0.77	0.02	1.05
60	0.77	0.76	0.77	0.01	1.02
50 rpm					
0	1.03	1.03	1.03	0.31	2.04
5	1.02	1.02	1.02	0.31	2.04
10	1.00	1.00	1.00	0.29	1.95
15	0.98	0.97	0.97	0.26	1.82
20	0.93	0.93	0.93	0.23	1.70

25	0.90	0.90	0.90	0.18	1.51
30	0.87	0.87	0.88	0.15	1.41
35	0.87	0.87	0.87	0.13	1.35
40	0.84	0.84	0.84	0.10	1.26
45	0.82	0.82	0.82	0.08	1.20
50	0.81	0.81	0.81	0.06	1.15
55	0.79	0.79	0.79	0.04	1.10
60	0.79	0.79	0.79	0.04	1.10

Table C3.2 Effect of stirrer speeds on crystal growth at 25^{O}C and pH 9

Supersaturation, S	**SI=log S**	**G, (x 10^{-9} m/s)**
50 rpm		
1.95	0.29	0.99
3.16	0.50	2.09
4.47	0.65	2.52
6.03	0.78	4.50
8.13	0.91	6.09
10.00	1.00	7.09
100 rpm		
1.95	0.29	3.43
3.16	0.50	6.73
4.47	0.65	9.54
6.03	0.78	12.81
8.13	0.91	22.17
10.00	1.00	29.27
120 rpm		
1.95	0.29	8.10
3.02	0.48	15.14
5.25	0.72	25.02
8.13	0.91	50.12
10.23	1.01	70.17

C4. Effect of temperature on struvite crystal growth kinetic at pH 9 and 120 rpm

Table C4.1 Decay of supersaturation curves of struvite crystallisation at initial supersaturation 2.04 for different temperature at pH 9 and 120 rpm.

Time	Concentration (mMol/L)			SI	S
	Mg	PO4	NH4		
20^{O}C					
0	0.87	0.87	0.87	0.31	2.04
5	0.83	0.83	0.84	0.27	1.86
10	0.81	0.80	0.80	0.23	1.70
15	0.77	0.77	0.77	0.18	1.51
20	0.74	0.74	0.74	0.14	1.38
25	0.71	0.71	0.71	0.09	1.23
30	0.69	0.69	0.69	0.06	1.15
35	0.68	0.67	0.68	0.04	1.10
40	0.68	0.67	0.67	0.02	1.05
45	0.66	0.66	0.66	0.01	1.02
50	0.67	0.66	0.66	0.02	1.05
55	0.66	0.66	0.66	0.01	1.02
60	0.66	0.66	0.66	0.01	1.02
25^{O}C					
0	1.03	1.03	1.03	0.31	2.04
5	0.97	0.97	0.97	0.26	1.82
10	0.93	0.93	0.93	0.21	1.62
15	0.88	0.88	0.88	0.15	1.41
20	0.84	0.84	0.84	0.10	1.26
25	0.81	0.81	0.81	0.06	1.15
30	0.79	0.79	0.79	0.03	1.07
35	0.78	0.78	0.78	0.02	1.05
40	0.77	0.77	0.77	0.01	1.02
45	0.77	0.77	0.77	0.01	1.02
50	0.77	0.77	0.77	0.02	1.05
55	0.77	0.77	0.77	0.01	1.02
60	0.77	0.77	0.77	0.01	1.02
30^{O}C					
0	1.14	1.14	1.14	0.31	2.04
5	1.06	1.06	1.06	0.24	1.74
10	1.00	1.00	1.01	0.18	1.51
15	0.95	0.95	0.95	0.12	1.32
20	0.91	0.91	0.92	0.08	1.20
25	0.89	0.89	0.89	0.05	1.12

30	0.87	0.86	0.87	0.02	1.05
35	0.86	0.86	0.86	0.01	1.02
40	0.86	0.86	0.86	0.01	1.02
45	0.86	0.86	0.86	0.01	1.02
50	0.86	0.86	0.86	0.02	1.05
55	0.86	0.86	0.86	0.01	1.02
60	0.86	0.86	0.86	0.01	1.02

Table C3.2 Effect of temperature on crystal growth at pH 9 and 120 rpm

Supersaturation, S	**SI=log S**	**G', (x 10^{-9} m/s)**
20^{O}C		
1.95	0.29	4.70
3.02	0.48	9.01
5.25	0.72	13.08
8.13	0.91	20.13
10.23	1.01	31.46
25^{O}C		
1.95	0.29	8.10
3.02	0.48	15.07
5.25	0.72	30.17
8.13	0.91	50.24
10.23	1.01	80.47
30^{O}C		
1.95	0.29	16.19
3.02	0.48	23.30
5.25	0.72	60.71
8.13	0.91	100.21
10.23	1.01	190.12

C4. Effect of NaCl addition on crystal growth

Table C4.1 Effect of NaCl addition on crystal growth at pH 8.5, 120 rpm and $25^{O}C$

Supersaturation, S	SI=log S	G', (x 10^{-9} m/s)
0 ppm NaCl		
1.91	0.28	4.10
2.95	0.47	9.01
3.80	0.58	13.18
4.79	0.68	18.17
6.45	0.81	27.21
9.77	0.99	43.95
50 ppm NaCl		
1.91	0.28	10.14
2.95	0.47	18.71
3.80	0.58	29.07
4.79	0.68	32.41
6.45	0.81	56.02
9.77	0.99	80.16
100 ppm NaCl		
1.91	0.28	18.53
2.95	0.47	36.02
3.80	0.58	50.17
4.79	0.68	69.09
6.45	0.81	87.56
9.77	0.99	140.26
200 ppm NaCl		
1.91	0.28	24.09
2.95	0.47	48.16
3.80	0.58	65.71
4.79	0.68	85.07
6.45	0.81	120.16
9.77	0.99	241.04

Appendix D: Dissolution Studies

D1. Dissolution of struvite crystals in deionized water

Table D1.1 Ion concentration in deionized water during dissolution of struvite crystals at 25^{O}C, 120 rpm, loading mass of 1000 mg and crystal size of 24.3 μm (a) 1 hour (3600 s), (b) 50 h

Time, S	PO4, (x 10^{-5} mMol/L)	NH4, (x 10^{-5} mMol/L)	Mg, (x 10^{-5} mMol/L)	Mean Concentration, (x 10^{-5} mMol/L)
0	0.0	0.0	0.0	0.0
10	1.6	0.8	1.1	1.2
15	1.7	1.5	1.2	1.5
20	2.5	2.1	1.9	2.2
25	3.2	3.5	2.9	3.1
30	4.4	3.5	3.5	3.9
35	5.0	4.4	4.5	4.7
40	5.7	5.1	5.5	5.3
45	6.6	5.7	6.1	6.1
50	6.8	6.1	6.4	6.4
55	7.3	6.7	6.8	6.9
60	7.8	7.3	7.5	7.5

Time, hr	PO4, (x 10^{-4} mMol/L)	NH4, (x 10^{-4} mMol/L)	Mg, (x 10^{-4} mMol/L)	Mean Concentration, (x 10^{-4} mMol/L)
0	0.0	0.0	0.0	0.0
1	0.8	0.7	0.8	0.8
2	1.3	0.9	1.1	1.1
4	2.0	1.6	1.6	1.7
5	2.5	2.1	2.4	2.3
6	3.3	3.0	3.1	3.2
8	4.0	3.6	3.8	3.8
10	4.5	4.1	4.1	4.3
15	5.7	5.3	5.5	5.5
24	7.6	7.0	7.1	7.2
36	7.5	7.3	7.6	7.5
50	7.8	7.2	7.4	7.5

Table D1.2 Ion concentration in deionized water during dissolution of struvite crystals on different stirrer speed at 25^{O}C, loading mass of 1000 mg and crystal size of 24.3 μm

time, (min)	PO4, (x 10^{-5} mMol/L)	NH4, (x 10^{-5} mMol/L)	Mg, (x 10^{-5} mMol/L)	Mean Concentration, (x 10^{-5} mMol/L)
200 rpm				
0	0.0	0.0	0.0	0.0
10	2.3	1.7	1.8	1.9
15	2.9	2.8	2.8	2.8
20	4.3	3.6	3.7	3.9
25	5.4	4.9	5.3	5.2
30	6.0	5.4	6.0	5.8
35	6.5	6.4	6.5	6.5
40	7.4	6.9	7.1	7.1
45	8.2	8.1	8.1	8.1
50	8.6	8.5	8.5	8.5
55	8.9	9.3	8.4	8.9
60	9.6	9.4	9.2	9.4
300 rpm				
0	0.0	0.0	0.0	0.0
10	4.2	3.7	3.8	3.9
15	6.3	5.8	5.4	5.8
20	7.9	7.7	7.7	7.8
25	8.4	7.9	8.0	8.1
30	11.6	10.6	10.4	10.9
35	13.7	11.9	12.6	12.8
40	14.2	13.7	13.3	13.7
45	16.7	15.1	14.9	15.6
50	17.3	16.4	16.2	16.4
55	18.2	17.3	17.1	17.5
60	19.9	18.5	18.4	18.9
400 rpm				
0	0.0	0.0	0.0	0.0
10	6.5	4.8	4.4	5.2
15	7.9	6.7	6.6	7.1
20	9.4	8.6	8.7	8.9
25	11.4	9.7	10.6	10.6
30	13.6	13.1	13.0	13.1
35	15.9	15.4	15.7	15.7
40	17.4	16.5	16.4	16.8

45	18.2	17.7	17.6	17.8
50	19.4	18.8	18.6	18.9
55	21.6	20.4	20.5	20.8
60	24.1	23.6	23.4	23.7
500 rpm				
0	0.0	0.0	0.0	0.0
10	5.5	3.8	3.7	4.3
15	6.5	5.3	5.4	5.7
20	9.6	7.9	7.9	8.5
25	11.6	10.4	9.3	10.4
30	13.9	12.9	12.4	13.1
35	15.5	14.3	14.3	14.7
40	16.4	15.7	15.3	15.8
45	18.6	17.8	17.0	17.8
50	22.4	22.6	22.2	22.4
55	23.8	23.4	22.7	23.3
60	24.5	24.7	23.1	24.1
800 rpm				
0	0.0	0.0	0.0	0.0
10	5.3	5.6	5.1	5.2
15	7.5	8.6	7.3	6.7
20	9.8	10.4	9.6	9.7
25	12.4	13.6	12.0	11.5
30	14.1	15.5	13.4	13.4
35	15.7	16.6	15.3	15.3
40	17.8	18.5	17.4	17.5
45	19.4	20.8	18.9	18.6
50	22.3	23.7	21.8	21.4
55	23.9	24.8	23.5	23.4
60	25.1	25.9	24.8	24.7

Table D1.3 The dissolution of struvuite at different temperatures at 200 rpm, loading mass of 1000 mg and crystal size of 24.3 μm.

time, (min)	Mean Concentration, (x 10^{-5} mMol/L)	
	200 RPM	500 RPM
20^{O}C		
0	0.0	0.0
10	1.2	1.9
15	2.1	3.1
20	2.9	4.1
25	3.5	5.6
30	4.1	6.3
35	5.2	7.4
40	5.9	7.9
45	6.5	9.3
50	7.3	10.0
55	7.9	11.5
60	8.3	12.0
25^{O}C		
0	0.0	0.0
10	1.9	4.3
15	2.8	5.7
20	3.9	8.5
25	5.2	10.4
30	5.8	13.1
35	6.5	14.7
40	7.1	15.8
45	8.1	17.8
50	8.5	22.4
55	8.9	23.3
60	9.4	24.1
30^{O}C		
0	0.0	0.0
10	2.9	7.9
15	4.2	10.2
20	3.9	15.1
25	5.9	18.9
30	7.3	20.3

35	8.1	22.3
40	8.9	26.4
45	9.6	28.8
50	10.5	30.0
55	11.5	32.5
60	12.4	35.1
$35^{O}C$		
0	0.0	0.0
10	4.1	9.4
15	5.8	14.2
20	6.9	20.0
25	8.2	23.8
30	9.4	30.3
35	10.2	35.3
40	10.9	39.4
45	12.2	43.8
50	13.1	48.0
55	13.5	51.5
60	14.1	54.5

Table D1.4 Effect of initial crystal size on dissolution of struvite crystals in deionized water at $25^{O}C$, 200 rpm and 1000 mg mass loading.

Time, (min)	**Mean Concentration, (x 10^{-5} mMol/L)**		
	24.3 μm	43.5 μm	84.8 μm
0	0.0	0.0	0.0
10	1.9	1.3	1.2
15	2.8	2.1	1.9
20	3.9	2.9	2.4
25	5.2	3.8	3.1
30	5.8	4.5	3.8
35	6.5	5.2	4.4
40	7.1	6.3	5.2
45	8.1	6.9	6.0
50	8.5	7.7	6.8
55	8.9	8.3	7.2
60	9.4	8.7	7.8